DISSERTATION

MEMBRANE TREATMENT OF WASTEWATER FROM OIL AND GAS PRODUCTION: MOTIVATIONS AND MATERIAL INNOVATION

Submitted by

Xuewei Du

Department of Civil and Environmental Engineering

In partial fulfillment of the requirements

For the Degree of Doctor of Philosophy

Colorado State University

Fort Collins, Colorado

Spring 2022

Doctoral Committee:

Advisor: Tiezheng Tong

Kenneth Carlson
Sybil Sharvelle
Arun Kumar Kota

ABSTRACT

MEMBRANE TREATMENT OF WASTEWATER FROM OIL AND GAS PRODUCTION: MOTIVATIONS AND MATERIAL INNOVATION

The rise of shale oil and gas (O&G) via hydraulic fracturing (HF) has boosted energy production in the United States. Further, many of the U.S. shale plays coincide with water-scarce areas that suffer from prolonged drought periodically. The substantial volumes of water consumption and wastewater generation associated with O&G activities intensify local water stress and create a challenge of wastewater management, rendering treatment and reuse of O&G wastewater an essential strategy to improve water sustainability of O&G-producing regions. Herein, the main goal of this dissertation is to facilitate the reuse and treatment of O&G wastewater in order to promote water sustainability of O&G-producing regions. To achieve this goal, two sets of studies were performed, which pertain to (1) data analysis to investigate the water footprint of O&G production under hydrodynamic variation; and (2) developing novel membrane materials for more efficient O&G wastewater treatment.

First, I investigated the relationship of hydroclimate variation with the activities and water footprint of O&G production in Colorado, one of the major O&G producing states in the U.S. I discovered that hydroclimate variation imposes a negligible impact on well number and water footprint of O&G production. However, the intensive water consumption by HF under arid conditions could escalate competition for water resources at the local scale. Further, I expanded the research scope to estimate the water consumption by HF activities under different hydroclimate conditions in eleven O&G-producing states in the central and western U.S. from 2011 to 2020. The results show that the water consumption under abnormally dry or drought climates accounted

for 49.7% (475.3 billion gallons) of total water usage of HF, with 9% (86.1 billion gallons) of water usage occurred under extreme or exceptional drought conditions. The water usage of HF under arid conditions can translate to high densities of water footprint at the local scale, equivalent to more than 50% of the annual water usage by the irrigation and domestic sectors in 21-47 and 11-51 counties (depending on the specific year), respectively. Such water stress imposed by O&G production, however, could be effectively mitigated by the reuse of flowback and produced water. This renders wastewater reuse necessary to maintain water sustainability of O&G-producing regions in the context of both a rising O&G industry and a changing climate.

Second, I focused on developing novel membrane materials for the treatment of O&G wastewater by membrane distillation (MD), which is an emerging technology showing promise for efficient desalination of high salinity industrial wastewater. I investigated the impacts of membrane surface wettability on the treatment of O&G wastewaters by MD. From this study, omniphobic membranes with high wetting resistance showed more robust performance, but they also required the use of toxic long-chain per- and polyfluoroalkyl substances (PFASs, ≥ 8 fluorinated carbons) during fabrication process and displayed lower water productivity compared to conventional hydrophobic membranes. Then, I developed highly wetting-resistant MD membranes while avoiding the use of long-chain PFASs, which is essential to improve the viability of MD for resilient and sustainable MD desalination. I demonstrated that long-chain PFASs are not required when designing membranes with high wetting resistance. Instead, the combination of hierarchical texture and (ultra)short-chain fluorocarbons are able to create MD membranes with exceptional wetting resistance. Finally, I also elucidated the fundamental relationship between membrane wetting resistance and water vapor permeability in the MD process, which needs to be taken into consideration when designing and selecting appropriate membranes for effective MD

treatment of O&G wastewater. I identified that a trade-off exists between wetting resistance and water vapor permeability of MD membranes, and also unveiled the mechanism of such a trade-off by revealing the importance of water-air interfacial area in regulating water vapor transport through microporous membranes. I envision that the novel insights on omniphobic membrane fabrication and the wetting resistance-vapor permeability trade-off will pave the way for more rational design of MD membranes for sustainable O&G wastewater treatment applications.

ACKNOWLEDGEMENTS

First and foremost, I am highly indebted to my advisor, Dr. Tiezheng Tong. Without his dedicated support, immense knowledge, motivation, and guidance at every step of my research process, I would never have completed this dissertation. I really appreciate his help and understanding during the past four years. I could not have envisioned a better dissertation advisor than Dr. Tiezheng Tong for my Ph.D. study.

Furthermore, I would like to thank the rest of my committee, Dr. Kenneth Carlson, Dr. Sybil Sharvelle and Dr. Arun Kumar Kota, for all of their insightful comments and suggestions throughout this process. I also wish to express my sincere thanks to Dr. Wei Wang for his ideas, encouragement, and knowledge support.

I would like to take this opportunity to express appreciation to all the department faculty members for their help and assistance. My sincere thanks are also due to my fellow friends and research engineers Zuoyou Zhang, Yiming Yin, Nohyeong Jeong, and Robbins Cristian for the discussions and friendship throughout my time at CSU.

I am also very thankful to my boyfriend Liping Wang for his companionship, support and understanding.

Finally, I must express my deepest gratitude to my family, Zhigang Du and Haimei Hui, for providing me with unconditional love, ceaseless support, and continuous encouragement throughout my years of Ph.D. study.

TABLE OF CONTENTS

LIST OF TABLES

LIST OF FIGURES

CHAPTER 1: Introduction

The rise of unconventional oil and gas (UOG) has considerably enhanced the energy security of the United States.[1] The application of novel drilling technologies such as horizontal drilling and hydraulic fracturing (HF) has allowed the production of oil and natural gas (O&G) from unconventional shale formations, thereby contributing to a significant O&G production increase.[2,3] As shown in Figure 1-1, the crude oil and natural gas productions have been climbing steeply since 2008, and then reached record high in 2019 which accounted for 31% and 35% of the total U.S. primary energy production, respectively.[4]

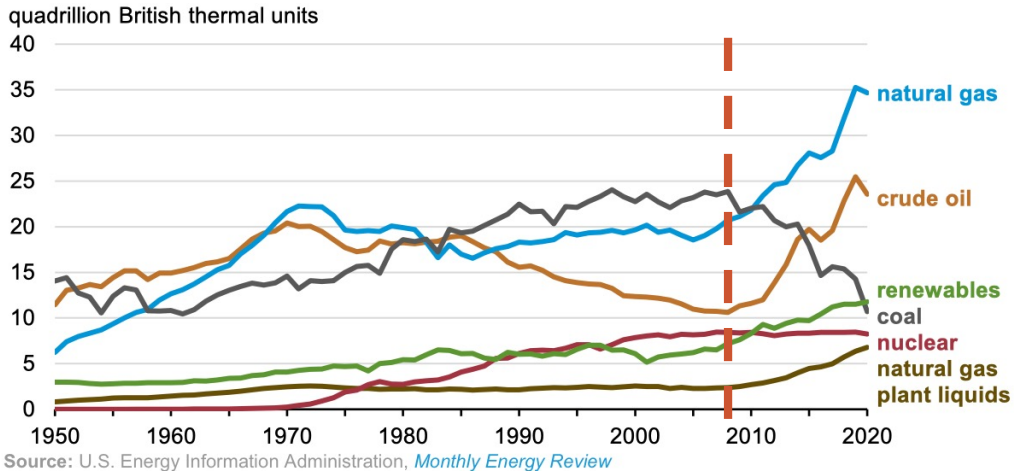

Figure 1-1. U.S. total energy production by different sources from 1950 to 2020. This figure is adopted from Annual Energy Outlook 2020 (U.S. EIA).[4]

However, the rapid expansion of O&G production consumes increasing amounts of freshwater and also generates substantial amounts of hazardous wastewater.[5-12] For example, HF activities total consumed 94 billion m^3 of water in the U.S. during the years from 2005 to 2014, while generating a total of 0.78 billion m^3 O&G wastewater.[7] Furthermore, the water usage per HF well

had continuously increased up to 770% between 2011 and 2016 in major U.S. shale O&G-producing regions, while the volumes of wastewater generated within the first 12 months of O&G production had increased up to 550%.[2]

The major O&G shale plays are located in semiarid or arid regions of the central and western United States where water scarcity has become increasingly frequent.[13] A research paper estimated that 57% of HF water consumption took place in areas experiencing high to extremely high water stress during the years from 2011 to 2016 (Figure 1-2).[14] Meanwhile, over 50% of the HF wells were drilled in high or extremely high water stress areas in Texas, the largest O&G-producing state in the U.S.[14] As a result, the high water consumption intensity of O&G production possesses a great potential to limit local water availability in the arid O&G-producing regions. To date, the geographical coincidence of U.S. shale plays with water-scarce regions has been commonly used in the literature to justify the need of O&G wastewater recycling and beneficial reuse.[14-17] However, relatively little attention has been paid to understand the impacts of O&G production on regional water supplies, which have more implications in understanding on how the augmentation of O&G production might alter local water allocation. Closing these knowledge gaps is essential to motivate the policymakers and O&G producers to transform the water resource management paradigm of the O&G industry towards O&G wastewater treatment and reuse, in order to improve water sustainability of O&G-producing regions.

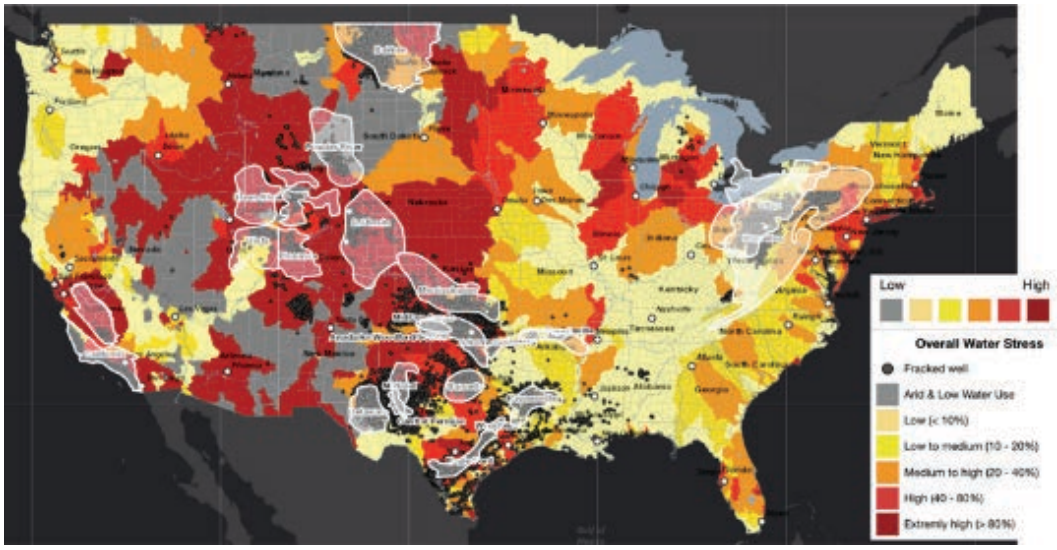

Figure 1-2. Map of water stress and major O&G shale plays in the U.S. from 2011 to 2016. This figure is adopted from Freyman, M. (2014)[14]

In addition to the substantial demands of water by HF, the handling and disposal of the large amounts of O&G wastewater is also becoming a growing concern.[12, 18, 19] Currently, most of the O&G wastewater is disposed by injecting into Class II wells in the U.S.[20] For example, Veil et al. reported that around 90% of wastewater produced from the O&G activities was injected in Class II wells in 2012.[21] However, these practices could lead to seismic events [22, 23] or contaminate the water environment due to the high salinity and toxicity potential of O&G wastewater.[24, 25] Under such scenarios, effective and economically feasible treatment and reuse of O&G wastewater are highly desirable, not only to preserve the water used by the O&G activity within the hydrological cycle but to mitigate environmental pollution.

The O&G wastewater typically contains high levels of total dissolved solids (TDS, up to 300,000 mg/L), oil and grease, various organic and inorganic compounds.[25-27] Membrane distillation (MD) is a hybrid membrane- and thermal-based desalination technology that has been

considered as a promising technology for hypersaline wastewater treatment.[28] MD process utilizes a vapor pressure difference between hot feedwater and cold distilled stream in order to drive the water vapor passing through a microporous, hydrophobic membrane.[29, 30] In addition, MD can be operated at moderate temperatures (60-80°C), and thus it can use low-grade waste heat that is typically available at the O&G well sites to reduce the primary energy cost and carbon footprint.[31] Besides, due to its nature of membrane technology, the modularity of MD results in smaller footprint and renders the treatment system adaptable to fluctuations in both quantity and quality of O&G wastewater.[32] Therefore, MD is a promising and suitable technology for the treatment and reuse of highly saline O&G wastewater.[28]

However, membrane pore wetting caused by low surface tension contaminants leads to the significant penetration of saline feed solution through the membrane pores and failure of the MD process.[30, 33] Membrane wetting is especially problematic for the treatment of the O&G wastewater due to its high concentrations of low surface energy contaminants, such as oil and grease, surfactants, and organic compounds.[34, 35] Recently, it has been demonstrated that omniphobic membranes could resist membrane wetting due to low surface energy contaminants, which holds promise for MD application in the treatment of O&G wastewater.[28, 36] Many approaches have been applied to fabricate omniphobic membranes by introducing both multilevel reentrant structure and low surface energy materials.[37-42] To date, however, the fabrication of omniphobic membranes typically requires the use of long-chain per- and polyfluoroalkyl substances (PFASs, with ≥ 8 fluorinated carbons) because of their ultra-low surface tension.[33, 36, 43-49] Such long-chain PFAS

compounds pose high risks to the environment and human health due to their high bioaccumulation potential, long-lasting persistence, and acute toxicity.[50, 51] Recently, they were listed as persistent organic pollutants and were phased out from emissions and products globally.[52-56] Furthermore, omniphobic membranes typically exhibit lower water vapor fluxes than their hydrophobic counterparts, decreasing the efficiency of MD treatment. These problems have impeded the practical manufacturing and implementation of omniphobic membranes and consequently their applications in treatment and reuse of O&G wastewater. Therefore, it is highly desirable to develop more efficient and sustainable approaches for the fabrication of omniphobic membranes tailored to O&G wastewater treatment.

This dissertation begins with a comprehensive background of current HF water footprint in the U.S., O&G wastewater management paradigm, and the cutting-edge treatment technologies for O&G wastewater (Chapter 2). Chapter 3 listed the primary research objectives. In Chapter 4, I put emphasis on the state of Colorado to elucidate the impacts of hydroclimate variation on the activities and water consumption of O&G production. In Chapter 5, I expanded the scope to analyze the water footprint of O&G production under different hydroclimate conditions for 11 states in the central and western U.S. between 2011 and 2020, demonstrating the motivations of O&G wastewater treatment and reuse. Chapter 6 evaluated the effects of membrane surface wettability on MD desalination of real O&G wastewater. Chapter 7 focused on avoiding the use of long-chain PFASs in the fabrication of highly wetting-resistant membrane. Chapter 8 identified the fundamental relationship between membrane wetting resistance and water vapor permeability

in MD desalination process. Finally, conclusions and future research opportunities are listed in Chapter 9.

References

1. Vidic, R. D.; Brantley, S. L.; Vandenbossche, J. M.; Yoxtheimer, D.; Abad, J. D., Impact of shale gas development on regional water quality. *Science* 2013, 340, (6134).
2. Kondash, A. J.; Lauer, N. E.; Vengosh, A., The intensification of the water footprint of hydraulic fracturing. *Sci Adv* 2018, 4, (8).
3. Chen, H.; Carter, K. E., Water usage for natural gas production through hydraulic fracturing in the United States from 2008 to 2014. *J Environ Manage* 2016, 170, 152-159.
4. U.S. Energy Information Administration. Annual Energy Outlook 2020. Table 14, Oil and Gas Supply. https://www.eia.gov/outlooks/aeo/data/browser/#/?id=14-AEO2020&cases=ref2020&sourcekey=0
5. Clark, C. E.; Horner, R. M.; Harto, C. B., Life cycle water consumption for shale gas and conventional natural gas. *Environ Sci Technol* 2013, 47, (20), 11829-11836.
6. Kondash, A.; Vengosh, A., Water footprint of hydraulic fracturing. *Environ Sci Tech Let* 2015, 2, (10), 276-280.
7. Scanlon, B. R.; Reedy, R. C.; Male, F.; Hove, M., Managing the increasing water footprint of hydraulic fracturing in the Bakken Play, United States. *Environ Sci Technol* 2016, 50, (18), 10273-10281.
8. Brantley, S. L.; Yoxtheimer, D.; Arjmand, S.; Grieve, P.; Vidic, R.; Pollak, J.; Llewellyn, G. T.; Abad, J.; Simon, C., Water resource impacts during unconventional shale gas development: The Pennsylvania experience. *Int J Coal Geol* 2014, 126, 140-156.
9. Nicot, J. P.; Scanlon, B. R., Water use for shale-gas production in Texas, US. *Environ Sci Technol* 2012, 46, (6), 3580-3586.
10. Nicot, J. P.; Scanlon, B. R.; Reedy, R. C.; Costley, R. A., Source and fate of hydraulic fracturing water in the Barnett Shale: A historical perspective. *Environ Sci Technol* 2014, 48, (4), 2464-2471.
11. Gallegos, T. J.; Varela, B. A.; Haines, S. S.; Engle, M. A., Hydraulic fracturing water use variability in the United States and potential environmental implications. *Water Resour Res* 2015, 51, (7), 5839-5845.
12. Gregory, K. B.; Vidic, R. D.; Dzombak, D. A., Water management challenges associated with the production of shale gas by hydraulic fracturing. *Elements* 2011, 7, (3), 181-186.
13. Vengosh, A.; Jackson, R. B.; Warner, N.; Darrah, T. H.; Kondash, A., A critical review of the risks to water resources from unconventional shale gas development and hydraulic fracturing in the United States. *Environ Sci Technol* 2014, 48, (15), 8334-48.
14. Freyman, M., Hydraulic fracturing & water stress: Water demand by the numbers. Ceres Boston, MA: 2014.
15. Scanlon, B. R.; Ikonnikova, S.; Yang, Q.; Reedy, R. C., Will water issues constrain oil and gas production in the United States? *Environ Sci Technol* 2020, 54, (6), 3510-3519.
16. Scanlon, B. R.; Reedy, R. C.; Nicot, J. P., Will water scarcity in semiarid regions limit hydraulic fracturing of shale plays? *Environ Res Lett* 2014, 9, (12), 124011.

17. Scanlon, B. R.; Reedy, R. C.; Xu, P.; Engle, M.; Nicot, J.; Yoxtheimer, D.; Yang, Q.; Ikonnikova, S., Can we beneficially reuse produced water from oil and gas extraction in the US? *Sci Total Environ* 2020, 717, 137085.
18. Lutz, B. D.; Lewis, A. N.; Doyle, M. W., Generation, transport, and disposal of wastewater associated with Marcellus Shale gas development. *Water Resour Res* 2013, 49, (2), 647-656.
19. Getzinger, G. J.; O'Connor, M. P.; Hoelzer, K.; Drollette, B. D.; Karatum, O.; Deshusses, M. A.; Ferguson, P. L.; Elsner, M.; Plata, D. L., Natural gas residual fluids: sources, endpoints, and organic chemical composition after centralized waste treatment in Pennsylvania. *Environ Sci Technol* 2015, 49, (14), 8347-8355.
20. EPA., U. S., Hydraulic Fracturing for Oil and Gas: Impacts from the Hydraulic Fracturing Water Cycle on Drinking Water Resources in the United States (Final Report). U.S. Environmental Protection Agency, Washington, DC, EPA/600/R-16/236F, 2016.
21. Veil, J., US produced water volumes and management practices in 2012. Groundwater Protection Council 2015.
22. Kim, W. Y., Induced seismicity associated with fluid injection into a deep well in Youngstown, Ohio. Journal of Geophysical Research: Solid Earth 2013, 118, (7), 3506-3518.
23. Ellsworth, W. L., Injection-induced earthquakes. *Science* 2013, 341, (6142).
24. He, Y.; Sun, C.; Zhang, Y.; Folkerts, E. J.; Martin, J. W.; Goss, G. G., Developmental toxicity of the organic fraction from hydraulic fracturing flowback and produced waters to early life stages of zebrafish (Danio rerio). *Environ Sci Technol* 2018, 52, (6), 3820-3830.
25. Butkovskyi, A.; Bruning, H.; Kools, S. A.; Rijnaarts, H. H.; Van Wezel, A. P., Organic pollutants in shale gas flowback and produced waters: identification, potential ecological impact, and implications for treatment strategies. *Environ Sci Technol* 2017, 51, (9), 4740-4754.
26. Kim, S.; Omur-Ozbek, P.; Dhanasekar, A.; Prior, A.; Carlson, K., Temporal analysis of flowback and produced water composition from shale oil and gas operations: impact of frac fluid characteristics. *J Petrol Sci Eng* 2016, 147, 202-210.
27. Rosenblum, J.; Thurman, E. M.; Ferrer, I.; Aiken, G.; Linden, K. G., Organic chemical characterization and mass balance of a hydraulically fractured well: from fracturing fluid to produced water over 405 days. *Environ Sci Technol* 2017, 51, (23), 14006-14015.
28. Deshmukh, A.; Boo, C.; Karanikola, V.; Lin, S.; Straub, A. P.; Tong, T.; Warsinger, D. M.; Elimelech, M., Membrane distillation at the water-energy nexus: limits, opportunities, and challenges. *Energ Environ Sci* 2018, 11, (5), 1177-1196.
29. Alklaibi, A. M.; Lior, N., Membrane-distillation desalination: status and potential. *Desalination* 2005, 171, (2), 111-131.
30. Lawson, K. W.; Lloyd, D. R., Membrane distillation. *J Membrane Sci* 1997, 124, (1), 1-25.

31. Shaffer, D. L.; Arias Chavez, L. H.; Ben-Sasson, M.; Romero-Vargas Castrillón, S.; Yip, N. Y.; Elimelech, M., Desalination and reuse of high-salinity shale gas produced water: drivers, technologies, and future directions. *Environ Sci Technol* 2013, 47, (17), 9569-9583.
32. Tong, T.; Elimelech, M., The global rise of zero liquid discharge for wastewater management: drivers, technologies, and future directions. *Environ Sci Technol* 2016, 50, (13), 6846-6855.
33. Lin, S.; Nejati, S.; Boo, C.; Hu, Y.; Osuji, C. O.; Elimelech, M., Omniphobic membrane for robust membrane distillation. *Environ Sci Tech Let* 2014, 1, (11), 443-447.
34. Boo, C.; Lee, J.; Elimelech, M., Omniphobic polyvinylidene fluoride (PVDF) membrane for desalination of shale gas produced water by membrane distillation. *Environ Sci Technol* 2016, 50, (22), 12275-12282.
35. Shaffer, D. L.; Chavez, L. H. A.; Ben-Sasson, M.; Castrillon, S. R. V.; Yip, N. Y.; Elimelech, M., Desalination and reuse of high-salinity shale gas produced water: Drivers, technologies, and future directions. *Environ Sci Technol* 2013, 47, (17), 9569-9583.
36. Lee, J.; Boo, C.; Ryu, W. H.; Taylor, A. D.; Elimelech, M., Development of omniphobic desalination membranes using a charged electrospun nanofiber scaffold. *Acs Appl Mater Inter* 2016, 8, (17), 11154-11161.
37. Wang, Z. X.; Elimelech, M.; Lin, S. H., Environmental applications of interfacial materials with special wettability. *Environ Sci Technol* 2016, 50, (5), 2132-2150.
38. Kota, A. K.; Kwon, G.; Tuteja, A., The design and applications of superomniphobic surfaces. *Npg Asia Mater* 2014, 6, (7), e109-e109.
39. Tuteja, A.; Choi, W.; Mabry, J. M.; McKinley, G. H.; Cohen, R. E., Robust omniphobic surfaces. *P Natl Acad Sci USA* 2008, 105, (47), 18200-18205.
40. Deng, X.; Mammen, L.; Butt, H. J.; Vollmer, D., Candle soot as a template for a transparent robust superamphiphobic coating. *Science* 2012, 335, (6064), 67-70.
41. Tuteja, A.; Choi, W.; Ma, M. L.; Mabry, J. M.; Mazzella, S. A.; Rutledge, G. C.; McKinley, G. H.; Cohen, R. E., Designing superoleophobic surfaces. *Science* 2007, 318, (5856), 1618-1622.
42. Liu, K. S.; Tian, Y.; Jiang, L., Bio-inspired superoleophobic and smart materials: Design, fabrication, and application. *Prog Mater Sci* 2013, 58, (4), 503-564.
43. Boo, C.; Lee, J.; Elimelech, M., Engineering surface energy and nanostructure of microporous films for expanded membrane distillation applications. *Environ Sci Technol* 2016, 50, (15), 8112-8119.
44. Huang, Y. X.; Wang, Z. X.; Jin, J.; Lin, S. H., Novel janus membrane for membrane distillation with simultaneous fouling and wetting resistance. *Environ Sci Technol* 2017, 51, (22), 13304-13310.

45. Lu, X. M.; Peng, Y. L.; Qiu, H. R.; Liu, X. R.; Ge, L., Anti-fouling membranes by manipulating surface wettability and their anti-fouling mechanism. *Desalination* 2017, 413, 127-135.
46. Woo, Y. C.; Kim, Y.; Yao, M. W.; Tijing, L. D.; Cho, J. S.; Lee, S.; Kim, S. H.; Shon, H. K., Hierarchical composite membranes with robust omniphobic surface using layer-by-layer assembly technique. *Environ Sci Technol* 2018, 52, (4), 2186-2196.
47. Zheng, R.; Chen, Y.; Wang, J.; Song, J. F.; Li, X. M.; He, T., Preparation of omniphobic PVDF membrane with hierarchical structure for treating saline oily wastewater using direct contact membrane distillation. *J Membrane Sci* 2018, 555, 197-205.
48. Chen, L. H.; Huang, A.; Chen, Y. R.; Chen, C. H.; Hsu, C. C.; Tsai, F. Y.; Tung, K. L., Omniphobic membranes for direct contact membrane distillation: Effective deposition of zinc oxide nanoparticles. *Desalination* 2018, 428, 255-263.
49. Li, X.; Shan, H.; Cao, M.; Li, B., Facile fabrication of omniphobic PVDF composite membrane via a waterborne coating for anti-wetting and anti-fouling membrane distillation. *J Membrane Sci* 2019, 589, 117262.
50. Dichiarante, V.; Martinez Espinoza, M. I.; Gazzera, L.; Vuckovac, M.; Latikka, M.; Cavallo, G.; Raffaini, G.; Oropesa-Nuñez, R.; Canale, C.; Dante, S., A short-chain multibranched perfluoroalkyl thiol for more sustainable hydrophobic coatings. *Acs Sustain Chem Eng* 2018, 6, (8), 9734-9743.
51. Krafft, M. P.; Riess, J. G., Per-and polyfluorinated substances (PFASs): Environmental challenges. *Current opinion in colloid & interface science* 2015, 20, (3), 192-212.
52. Lu, M.; Cagnetta, G.; Zhang, K.; Huang, J.; Yu, G., Mechanochemical mineralization of "very persistent" fluorocarbon surfactants–6: 2 fluorotelomer sulfonate (6: 2FTS) as an example. *Sci Rep*-Uk 2017, 7, (1), 1-10.
53. Dichiarante, V.; Milani, R.; Metrangolo, P., Natural surfactants towards a more sustainable fluorine chemistry. *Green Chemistry* 2018, 20, (1), 13-27.
54. Wang, Z.; Cousins, I. T.; Scheringer, M.; Hungerbühler, K., Fluorinated alternatives to long-chain perfluoroalkyl carboxylic acids (PFCAs), perfluoroalkane sulfonic acids (PFSAs) and their potential precursors. *Environ Int* 2013, 60, 242-248.
55. Manzetti, S.; van der Spoel, E. R.; van der Spoel, D., Chemical properties, environmental fate, and degradation of seven classes of pollutants. *Chemical research in toxicology* 2014, 27, (5), 713-737.
56. Wang, Z.; Cousins, I. T.; Scheringer, M.; Hungerbuehler, K., Hazard assessment of fluorinated alternatives to long-chain perfluoroalkyl acids (PFAAs) and their precursors: status quo, ongoing challenges and possible solutions. *Environ Int* 2015, 75, 172-179.

CHAPTER 2: Background

2.1 Water footprint of O&G production in the United States

Onshore O&G exploration in the United States has been growing dramatically since the mid-2000s. Meanwhile, technology advances in hydraulic fracturing (HF) and horizontal drilling have allowed the augment of O&G production from low-permeable unconventional reservoirs.[1] However, since the novel drilling technologies (e.g., horizontal drilling and HF) require substantial amounts of freshwater withdrawal,[2-9] the water consumption and wastewater production associated with O&G activities in major O&G production regions have increased steadily in the past decade.[10] For example, the HF water use per well had increased up to 770% from 2011 to 2016 in the U.S., while flowback and produced water (FPW) volumes generated within the first 12 months of production had increased up to 550%.[1] During the years of 2009 and 2017, the water consumption by HF activities totaled 137 billion gallons in the Permian Basin (Figure 2-1),[11] and the O&G production had consumed 145 million m^3 of water in the Barnett shale from 2000 to 2011.[6] On the other hand, the volume of O&G wastewater generated within the first year of well completion had increased from 1,823 m^3 to 2,959 m^3 in the Niobrara shale formation during the period of 2011-2016.[2] In 2014, O&G produced water totaled 9.4 million m^3 in the South Platte basin, which represented 42% of the total water used for HF activities.[12]

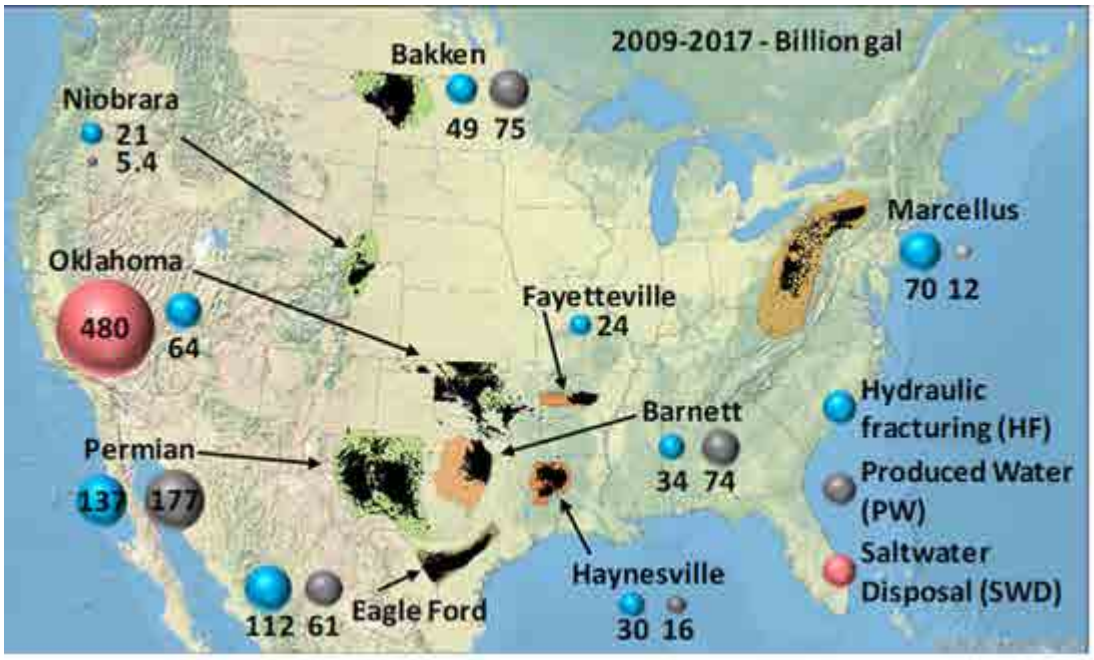

Figure 2-1. Total volumes of water used for hydraulic fracturing (HF) and produced water (PW) (2009–2017) from unconventional horizontal wells in major tight oil (green) and shale gas (orange) plays and Eagle Ford (brown, includes oil and gas). This figure is adopted from Scanlon et al. (2020).[11]

Meanwhile, most of the U.S. shale plays coincide with arid or semiarid regions experiencing high to extremely high water stress (Figure 2-2)[5]. During 2011-2014, about 50% of the HF wells were drilled in areas where water withdrawals account for over 80% of available water resources (i.e., including surface water and groundwater).[13] Although O&G activities typically consume negligible volumes of water when compared to other water users, such as agricultural irrigation sector,[14-16] the intensive water withdrawals by HF activities may reduce regional freshwater availability for other water users, particularly during drought conditions.[11, 17-19] For example, Scanlon et al. reported that regional groundwater resources had been depleted by HF activities in several semiarid regions in western Eagle Ford shale play.[11] Moreover, O&G activities leaded to

intensified conflicts with other water-consuming sectors (e.g., agricultural irrigation and domestic sectors) during extreme to exceptional drought periods in many of O&G-producing regions in the states of Texas and Colorado.[20] Under such scenarios, the water acquisition becomes more challenging and costly to O&G energy producers,[1,21,22] and thus it is a desire to increase the reuse and treatment of O&G wastewater.

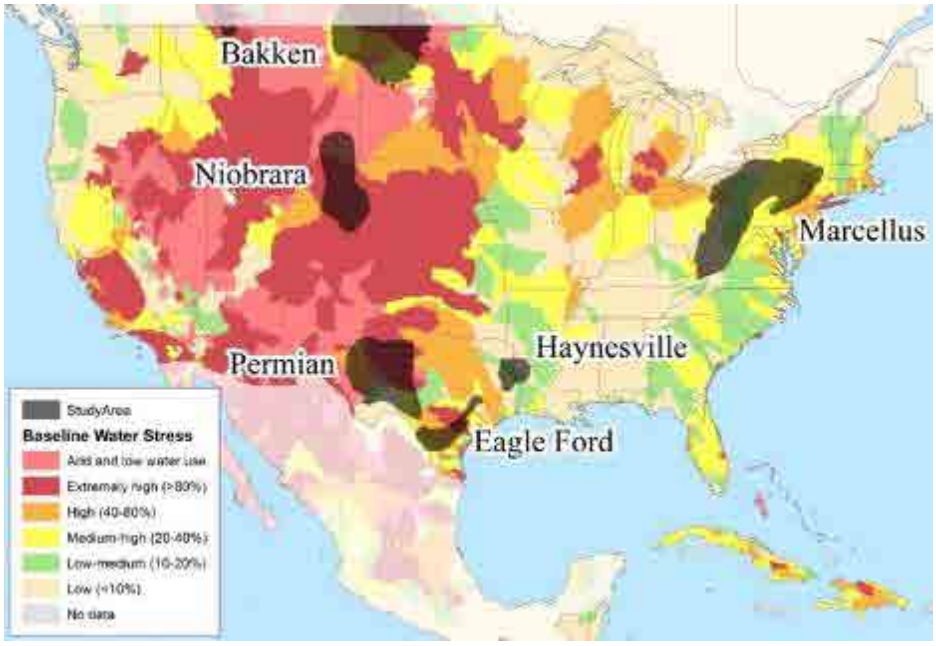

Figure 2-2. Water stress and shale regions in the United States. This figure is adopted from Kondash et al. (2018).[1]

To date, high extents of produced water reuse are not applied to most O&G-producing states in the central and western U.S.[10] O&G activities typically use freshwater taken from nearby groundwater or surface water resources, which are also used for domestic and agricultural irrigation.[10, 23] The proximity of HF activities to water-scare areas could constrain the local water resources, and thus reuse of O&G wastewater is highly desirable.[1, 3, 4, 6] However, we still lack sufficient data needed to quantify the risks of O&G activities imposes on water supplies in water-

stressing areas.[24] It is essential to close this knowledge gap to facilitate the reuse and treatment of O&G wastewater, thereby relieving the local water stress particularly under drought periods. Therefore, understanding the impacts of water footprint of O&G production on the local water availability under hydroclimate variation is critical for water management and regulatory decisions.

2.2 O&G wastewater treatment technologies

The O&G wastewater generated by HF wells are commonly referred to as flowback and produced water (FPW). The treatment of O&G wastewater is extremely challenging because it contains high concentrations of total dissolved solids (TDS, Figure 2-3), chemicals used in HF processes, and various organic contaminants.[25-27] As shown in Figure 2-3, TDS concentrations of O&G wastewater range from 35,000 to 400,000 mg/L in the states of Texas and Oklahoma, and such TDS contents are more than the salinity of seawater.

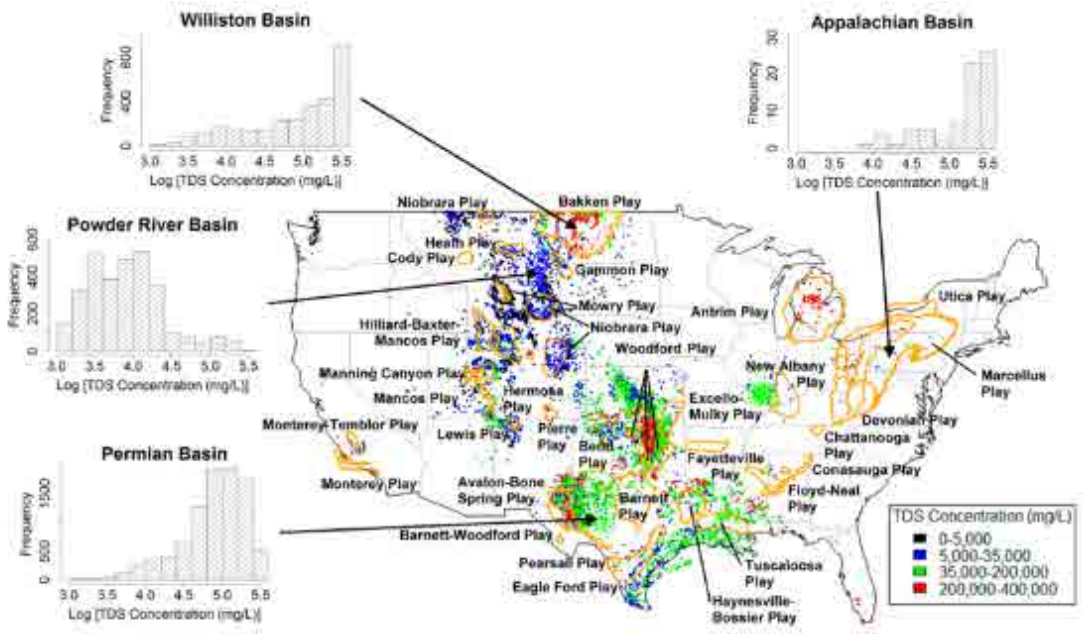

Figure 2-3. The ranges of O&G wastewater TDS concentrations in the U.S. shale plays. Histograms illustrate the range of O&G wastewater TDS concentrations for the Williston Basin, Powder River Basin, Permian Basin, and Appalachian Basin. This figure is adopted from Shaffer et al. (2013).[28]

In recent years, numerous efforts have been invested to develop technologies for the treatment of hypersaline O&G wastewater,[28-30] in order to effectively remove a majority of salts and contaminants. According to previous studies, the treatment technologies typically include thermal-based processes (e.g., mechanical vapor compression, MVC),[31] membrane-based technologies (e.g., reverse osmosis, RO; and forward osmosis, FO),[32,33] as well as hybrid membrane-thermal technology (e.g., membrane distillation, MD).[34]

2.2.1 Mechanical vapor compression

MVC desalination process utilizes electrical energy to power a compressor, in order to supply the thermal energy required to evaporate water from a hypersaline wastewater (Figure 2-4).[28] MVC

is basically a well-designed heat transfer system including an evaporator and a condenser. In the MVC system, the feed solution is preheated by two heat exchangers which use the heat from the permeate and brine stream. The feed solution then flows to the evaporator-condenser and mixes with the brine. Thereafter, the blended brine is then pumped to a nozzle distribution system to form a continuous film on the heat transfer tubes, which improves the energy efficiency of the heat exchange processes.

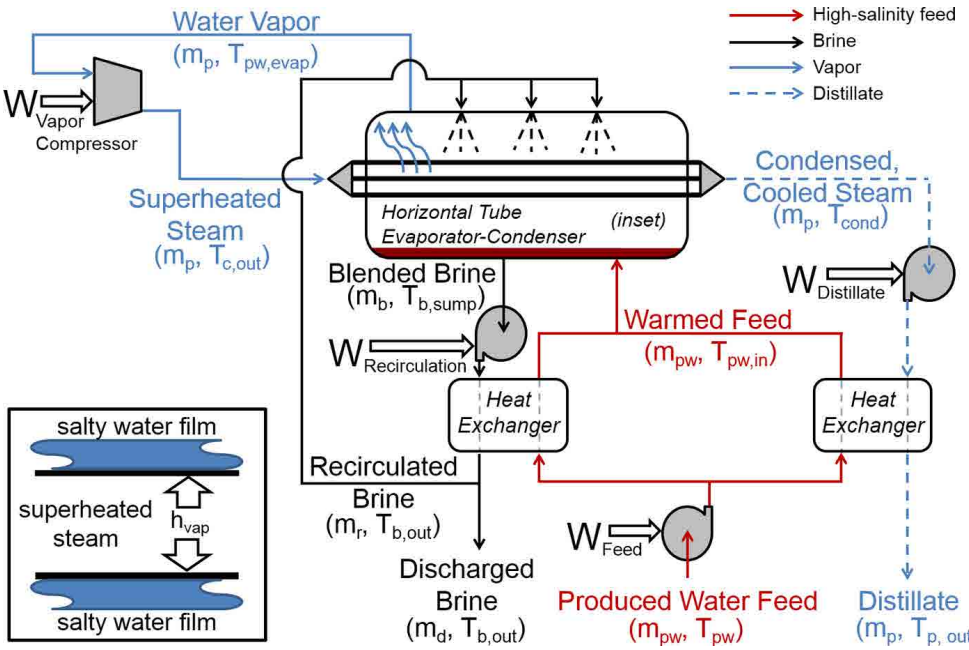

Figure 2-4. Schematic diagram of the MVC process. This figure is adopted from Shaffer et al. (2013).[28]

Although MVC is able to tolerate hypersaline O&G wastewater, the energy consumption is high because of the energy loss associated with evaporation and condensation processes. MVC system generally requires substantial amounts of electric energy for the treatment of wastewater (20-25 kWh_e/m^3 of feed solution)[35]. McGinnis et al. reported that MVC desalination consumes 28-

39 kWh_e/m^3 of O&G wastewater.[36] To date, MVC is the most expensive thermal technology, and the requirements of high temperature and expensive corrosive-resistant materials contribute to its high capital cost.[35] Therefore, it is highly desired to develop novel technologies in order to promote both cost- and energy- efficiency for the treatment of O&G wastewater.

Reverse osmosis

RO, which is the most popular type of membrane-based technology, utilizes an applied hydraulic pressure to force water contained in feed solutions to permeate through a semi-permeable membrane (Figure 2-5). RO process is capable of effectively reducing up to >99% of the dissolved contaminants (e.g., salts, organics, and colloids) from O&G wastewater, thereby producing a concentrate solute stream and a high-quality water permeate.[37] Thus, the water products generated by RO are able to meet the external reuse requirements, such as agricultural irrigation or direct discharge into surface waters.[38, 39] Furthermore, unlike thermal-based technologies, RO desalination process doesn't require phase transition from liquid to vapor for water purification. Thus, RO can avoid the irreversible energy losses related to water evaporation-condensation process within thermal desalination system. So far, although RO is the most energy-efficient technology for treating O&G wastewater, its treatment capacity is limited by the salinity limit (~70,000 mg/L of TDS) which is imposed by the membrane system's maximum hydraulic pressure tolerance.[35,40] Therefore, RO is not suitable for the treatment of hypersaline produced water with salinity higher than such a threshold.

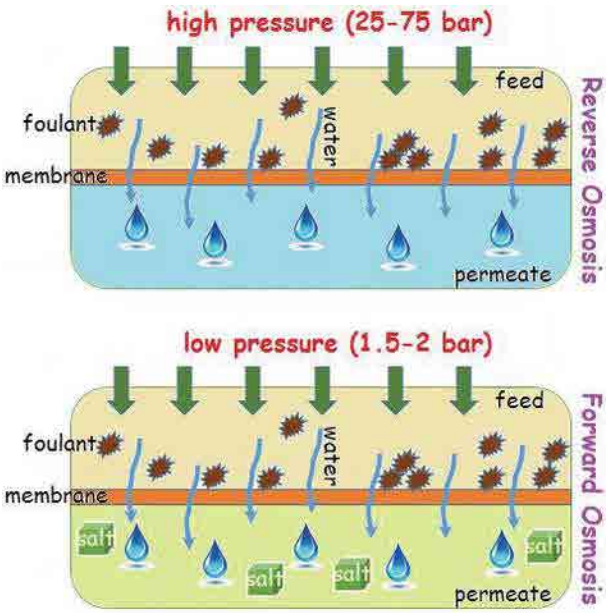

Figure 2-5. Illustration of comparison between FO and RO processes. This figure is adopted from Eyvaz et al. (2017).[41]

2.2.2 Forward osmosis

FO is a robust membrane-based desalination technology, which utilizes an osmotic pressure difference between a feedwater and a higher salinity draw solution to drive the water passing through a semi-permeable membrane (Figure 2-5).[42] Unlike RO process, FO doesn't require an extra hydraulic pressure, and thus the energy cost is negligible for the water transport through the membrane. FO is also capable of rejecting a broad range of contaminants from highly saline feedwaters (up to >200,000 mg/L TDS).[35] Moreover, the fouling propensity of FO membranes is lower when compare to that of RO membranes due to the loosely packed fouling layer formed on FO membrane surfaces without external hydraulic pressure.[42]

Despite its commercial applications in the treatment of wastewaters produced from power plants, thermolytic FO has not been implemented on a large scale in the O&G industry.[35,43] The complexity of the FO configuration, which requires the use of an independent concentrated draw

solution recovery system, may prove to be a significant impediment (i.e., the membrane modules). In addition, the reverse flow of ammonia salts into the feedwater consumes NH_3-CO_2 draw solutes, thereby raising the cost of the FO process.

2.2.3 Membrane distillation

Recently, MD, a hybrid membrane-thermal desalination technology,[36, 44] has emerged as an alternative for the O&G wastewater treatment.[44] In MD process, a hydrophobic, microporous membrane acts as a barrier for the liquid phase, only allowing water vapor to transport through the membrane (Figure 2-6). MD is typically operated at moderate temperatures (60°C–80°C), and the desalination process can achieve 100% retention of TDS and contanminants.[45] Due to its nature of thermal separation technology, MD is considered to be less energy efficient than RO. However, unlike RO, MD process can utilize low-grade waste heat sources (e.g., geothermal or solar energy), which could also significantly reduce the energy cost and carbon footprint. Recently, MD has been applied increasingly for treating O&G wastewater streams with a much higher load of contaminants,[34, 46-49] and the high-quality water products generated from MD process demonstrate the feasibility of its practical implementation in O&G wastewater treatment. However, membrane fouling and wetting can considerably constrain the MD efficiency by reducing both water vapor permeability and salt rejection efficiency,[50, 51] which are especially problematic for the treatment of O&G wastewater with an abundance of salts and low surface tension contaminants.

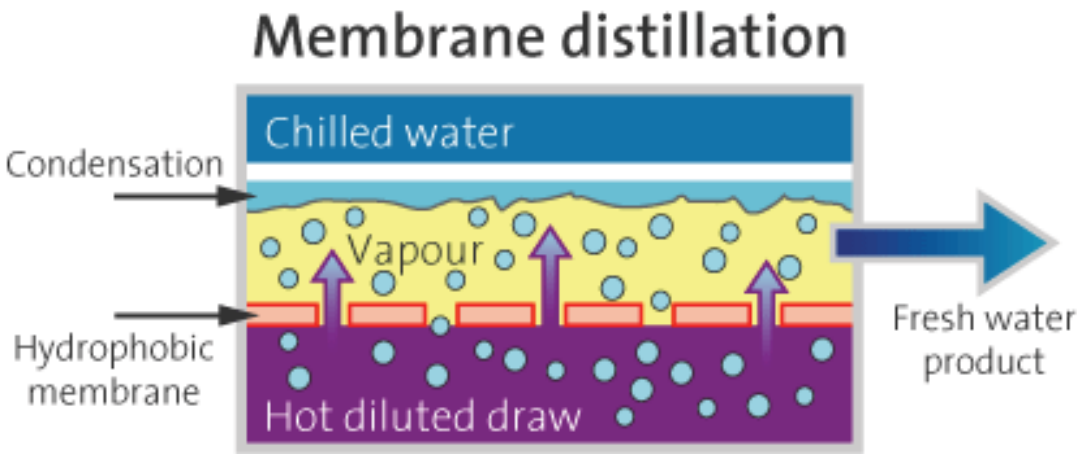

Figure 2-6. Illustration of MD process. This figure is adopted from bluetec.[52]

2.3 Membrane fouling and wetting

Two major problems, namely membrane fouling and wetting, can lead to the consequent failure of MD process. Membrane fouling refers to the deposition of foulants from the feedwater on the hydrophobic membrane surface due to the hydrophobic-hydrophobic interaction (Figure 2-7C), which result in membrane pore blocking and a consequently considerable decline of water permeate flux.[53, 54] Membrane fouling occurs when the hydrophobic membrane is utilized in MD desalination of O&G wastewaters with high concentrations of hydrophobic contaminants, such as oil, grease and various hydrophobic organics.[55] Previous studies have evaluated the performances of the conventional hydrophobic membranes in the MD desalination of hyper salinity wastewaters enriched in hydrophobic pollutions (e.g., oil and organic chemicals) and severe membrane fouling was observed as evidenced by the rapid reduction of water vapor flux.[54, 56, 57]

Further, membrane wetting is also a significant challenge when MD is applied to the treatment of hypersaline feedwater, which contains low surface energy contaminants (e.g., oil and surfactants,

Figure 2-7B).[58] The low surface tension contaminants can reduce the liquid entry pressure (LEP), and then render the feed solution penetrating through the membrane pores into the distillate stream, thereby resulting in a significant reduction of salt rejection.[59, 60]

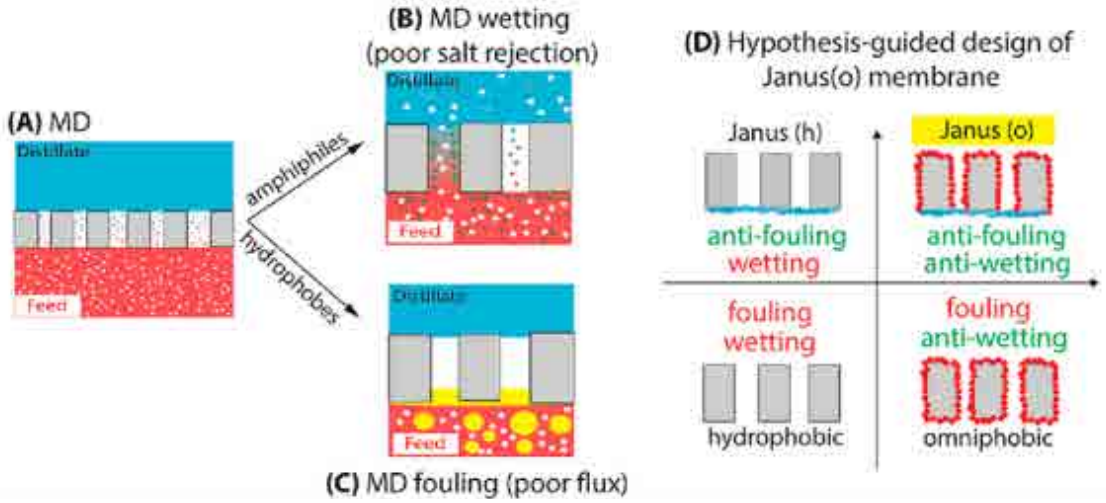

Figure 2-7. (A) Illustration of MD process. (B) Illustration of surfactant-induced wetting in an MD process. (C) Illustration of oil fouling in an MD process. (D) Illustration of the hypothesis that only a Janus membrane with an omniphobic substrate (i.e., a Janus(o) membrane) can achieve simultaneous fouling and wetting resistance. This figure is adopted from Huang et al. (2017).[59]

2.4 Fabrication of wetting- and fouling-resistant membranes with tailored surface wettability

Recently, various effective approaches have been developed to optimize the surface wettability of conventional hydrophobic MD membranes in order to prevent membrane fouling and wetting (Figure 2-7D).[47, 58, 59, 61-67] Firstly, omniphobic membranes have been developed to prevent MD wetting induced by low surface energy contaminants.[44] As elucidated in the field of surface science, the omniphobicity of membranes can be achieved by combining reentrant textures and low surface tension materials.[68-72] Since the reentrant structure via superimposing a layer of nanostructures on the micro-structured PVDF surfaces leads to a heterogeneously rough surfaces

of the composite membranes. When a liquid droplet contacting with such surfaces, it can be supported by the composite interface consisting of solid surface and air trapped inside the grooves of hierarchical structures.[73, 74] Given the intrinsically strong omniphobicity of air, the hierarchically textured surfaces are able to sustain a metastable Cassie-Baxter state thermodynamically and exhibit enhanced liquid repellence.[75, 76] Thus, omniphobic membranes display exceptional wetting resistance to liquids of a wide range of surface tensions. On the other hand, organic fouling can be minimized by coating the membrane surface with a thin in-air hydrophilic layer.[59, 63] Due to its underwater oleophobic property, the hydrophilic layer can deter hydrophobic foulants (e.g., oil droplets) from adhering to the membrane surface and prevent the blocking of membrane pores.[59, 63] Moreover, a Janus membrane, composed of an omniphobic substrate and an in-air hydrophilic layer, could resist both wetting and fouling.[59]

So far, numerous studies have focused on testing the MD performance of novel omniphobic membranes with synthetic feed solutions containing individual surfactants and foulants.[77-81] However, the performance of these membranes in desalinating real complex hypersaline O&G wastewater has not been well understood, which has more implications in promoting the efficiency and feasibility of MD treatment of O&G wastewater.

Moreover, the fabrication of omniphobic membranes typically involves the use of low surface energy substrates like of long-chain per- and polyfluoroalkyl substances (PFASs, with ≥ 8 fluorinated carbons).[47, 58, 61, 62, 66, 67] Such long-chain fluorinated compounds have been phased out globally due to their unintended environmental and health impacts.[82] As a result, the use of long-

chain PFASs is not sustainable and could impede the manufacturing and implementation of omniphobic membranes for MD desalination. The avoidance of long-chain PFASs in the fabrication of omniphobic membranes is thus highly desirable.

Furthermore, omniphobic membranes typically exhibit lower water vapor fluxes than their hydrophobic counterparts, decreasing the efficiency of MD treatment (Figure 2-8).[47, 81, 83-94] The water permeability plays an important role in maintaining the membrane separation efficiency in MD process. However, it has not received sufficient consideration in the design of omniphobic membranes. A fundamental understanding of the relationship between membrane wetting resistance and water permeability is of immense significance to achieve smarter membrane design for MD applications for the treatment of O&G wastewaters.

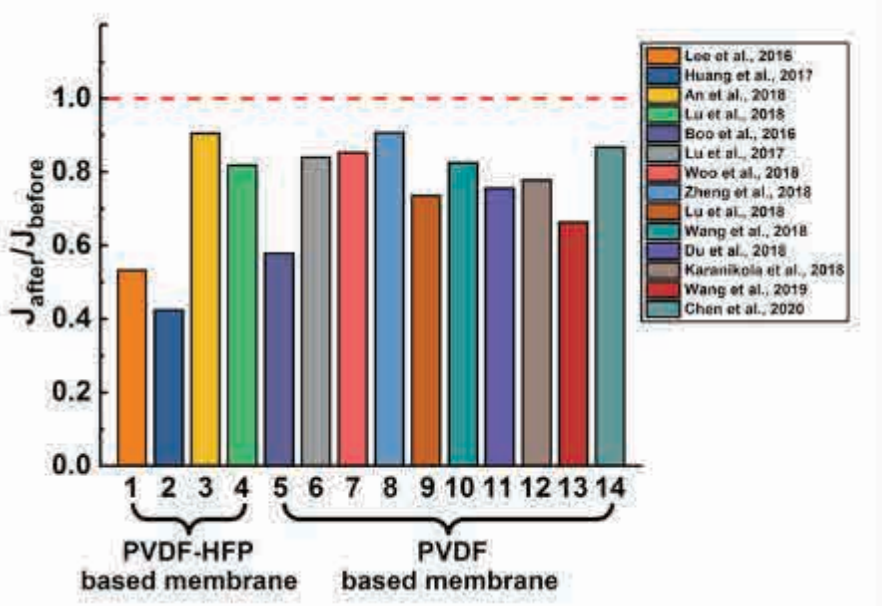

Figure 2-8. Ratios of water flux after the surface modification of pristine hydrophobic membrane with low-surface-energy materials (J_{after}) to water flux before the modification (J_{before}), calculated from the data in the literature of direct-contact membrane distillation (DCMD). PVDF represents poly(vinylidene fluoride) and PVDF-HFP represents poly(vinylidene fluoride-co-hexafluoropropylene). This figure is adopted from Li et al. (2020).[95]

References

1. Kondash, A. J.; Lauer, N. E.; Vengosh, A., The intensification of the water footprint of hydraulic fracturing. *Sci Adv* 2018, 4, (8).
2. Clark, C. E.; Horner, R. M.; Harto, C. B., Life Cycle Water consumption for shale gas and conventional natural gas. *Environ Sci Technol* 2013, 47, (20), 11829-11836.
3. Kondash, A.; Vengosh, A., Water footprint of hydraulic fracturing. *Environmental Science & Technology Letters* 2015, 2, (10), 276-280.
4. Scanlon, B. R.; Reedy, R. C.; Male, F.; Hove, M., Managing the increasing water footprint of hydraulic fracturing in the Bakken Play, United States. *Environ Sci Technol* 2016, 50, (18), 10273-10281.
5. Brantley, S. L.; Yoxtheimer, D.; Arjmand, S.; Grieve, P.; Vidic, R.; Pollak, J.; Llewellyn, G. T.; Abad, J.; Simon, C., Water resource impacts during unconventional shale gas development: The Pennsylvania experience. *Int J Coal Geol* 2014, 126, 140-156.
6. Nicot, J. P.; Scanlon, B. R., Water use for shale-gas production in Texas, US. *Environ Sci Technol* 2012, 46, (6), 3580-3586.
7. Nicot, J. P.; Scanlon, B. R.; Reedy, R. C.; Costley, R. A., Source and fate of hydraulic fracturing water in the Barnett Shale: A historical perspective. *Environ Sci Technol* 2014, 48, (4), 2464-2471.
8. Gallegos, T. J.; Varela, B. A.; Haines, S. S.; Engle, M. A., Hydraulic fracturing water use variability in the United States and potential environmental implications. *Water Resour Res* 2015, 51, (7), 5839-5845.
9. Gregory, K. B.; Vidic, R. D.; Dzombak, D. A., Water management challenges associated with the production of shale gas by hydraulic fracturing. *Elements* 2011, 7, (3), 181-186.
10. EPA., U. S., Hydraulic fracturing for oil and gas: Impacts from the hydraulic fracturing water cycle on drinking water resources in the United States (Final Report). U.S. Environmental Protection Agency, Washington, DC, EPA/600/R-16/236F, 2016.
11. Scanlon, B. R.; Ikonnikova, S.; Yang, Q.; Reedy, R. C., Will water issues constrain oil and gas production in the United States? *Environ Sci Technol* 2020, 54, (6), 3510-3519.
12. Walker, E. L.; Anderson, A. M.; Read, L. K.; Hogue, T. S., Water use for hydraulic fracturing of oil and gas in the South Platte River Basin, Colorado. *JAWRA Journal of the American Water Resources Association* 2017, 53, (4), 839-853.
13. Freyman, M., Hydraulic fracturing & water stress: Water demand by the numbers. Ceres Boston, MA: 2014.
14. Jackson, R. B.; Vengosh, A.; Carey, J. W.; Davies, R. J.; Darrah, T. H.; O'Sullivan, F.; Petron, G., The Environmental costs and benefits of fracking. *Annu Rev Env Resour* 2014, 39, 327-362.
15. Kondash, A. J.; Albright, E.; Vengosh, A., Quantity of flowback and produced waters from unconventional oil and gas exploration. *Sci Total Environ* 2017, 574, 314-321.

16. Vengosh, A.; Jackson, R. B.; Warner, N.; Darrah, T. H.; Kondash, A., A critical review of the risks to water resources from unconventional shale gas development and hydraulic fracturing in the United States. *Environ Sci Technol* 2014, 48, (15), 8334-48.
17. Koba, M., "Not even severe drought can stop fracking," Oil and Gas Exploration, https://www.cnbc.com/2014/06/10/not-even-severe-drought-can-stop-fracking.html (accessed December 9, 2021).
18. Goldenberg, S., "Fracking is depleting water supplies in America's driest areas, report shows," US environment correspondent, https://www.theguardian.com/environment/2014/feb/05/fracking-water-america-drought-oil-gas (accessed December 9, 2021).
19. Lin, Z.; Lin, T.; Lim, S. H.; Hove, M. H.; Schuh, W. M., Impacts of Bakken shale oil development on regional water uses and supply. *JAWRA Journal of the American Water Resources Association* 2018, 54, (1), 225-239.
20. Kenworthy, T., "Fracking can strain U.S. water supplies, ENERGY AND ENVIRONMENT", The Center for American Progress, https://www.americanprogress.org/issues/green/news/2013/06/14/66544/fracking-threatens-u-s-water-supplies/ (assessed December 9, 2020).
21. Shrestha, N.; Chilkoor, G.; Wilder, J.; Gadhamshetty, V.; Stone, J. J., Potential water resource impacts of hydraulic fracturing from unconventional oil production in the Bakken shale. Water Res 2017, 108, 1-24.
22. Cook, M.; Webber, M., Food, fracking, and freshwater: The potential for markets and cross-sectoral investments to enable water conservation. *Water-Sui* 2016, 8, (2).
23. Kuwayama, Y.; Olmstead, S. M.; Krupnick, A., Water resources and unconventional fossil fuel development: linking physical impacts to social costs. *Resources for the Future DP* 2013, 13-34.
24. Kustin, M. E., "U.S. lacks data needed to weigh effects of oil and gas production on western water supply", Center for American Progress https://www.americanprogress.org/issues/green/news/2019/06/27/471512/u-s-lacks-data-needed-weigh-effects-oil-gas-production-western-water-supply/ (assessed December 9, 2021).
25. Butkovskyi, A.; Bruning, H.; Kools, S. A.; Rijnaarts, H. H.; Van Wezel, A. P., Organic pollutants in shale gas flowback and produced waters: identification, potential ecological impact, and implications for treatment strategies. *Environ Sci Technol* 2017, 51, (9), 4740-4754.
26. Kim, S.; Omur-Ozbek, P.; Dhanasekar, A.; Prior, A.; Carlson, K., Temporal analysis of flowback and produced water composition from shale oil and gas operations: impact of frac fluid characteristics. *J Petrol Sci Eng* 2016, 147, 202-210.

27. Rosenblum, J.; Thurman, E. M.; Ferrer, I.; Aiken, G.; Linden, K. G., Organic chemical characterization and mass balance of a hydraulically fractured well: from fracturing fluid to produced water over 405 days. *Environ Sci Technol* 2017, 51, (23), 14006-14015.
28. Shaffer, D. L.; Arias Chavez, L. H.; Ben-Sasson, M.; Romero-Vargas Castrillón, S.; Yip, N. Y.; Elimelech, M., Desalination and reuse of high-salinity shale gas produced water: drivers, technologies, and future directions. *Environ Sci Technol* 2013, 47, (17), 9569-9583.
29. Tong, T.; Carlson, K. H.; Robbins, C. A.; Zhang, Z.; Du, X., Membrane-based treatment of shale oil and gas wastewater: The current state of knowledge. *Frontiers of Environmental Science & Engineering* 2019, 13, (4), 63.
30. Chang, H.; Li, T.; Liu, B.; Vidic, R. D.; Elimelech, M.; Crittenden, J. C., Potential and implemented membrane-based technologies for the treatment and reuse of flowback and produced water from shale gas and oil plays: A review. *Desalination* 2019, 455, 34-57.
31. Koren, A.; Nadav, N., Mechanical vapour compression to treat oil field produced water. *Desalination* 1994, 98, (1-3), 41-48.
32. Riley, S. M.; Ahoor, D. C.; Oetjen, K.; Cath, T. Y., Closed circuit desalination of O&G produced water: An evaluation of NF/RO performance and integrity. *Desalination* 2018, 442, 51-61.
33. Liden, T.; Carlton Jr, D. D.; Miyazaki, S.; Otoyo, T.; Schug, K. A., Forward osmosis remediation of high salinity Permian Basin produced water from unconventional oil and gas development. *Sci Total Environ* 2019, 653, 82-90.
34. Kim, J.; Kwon, H.; Lee, S.; Lee, S.; Hong, S., Membrane distillation (MD) integrated with crystallization (MDC) for shale gas produced water (SGPW) treatment. *Desalination* 2017, 403, 172-178.
35. Tong, T.; Elimelech, M., The global rise of zero liquid discharge for wastewater management: drivers, technologies, and future directions. *Environ Sci Technol* 2016, 50, (13), 6846-6855.
36. McGinnis, R. L.; Hancock, N. T.; Nowosielski-Slepowron, M. S.; McGurgan, G. D., Pilot demonstration of the NH3/CO2 forward osmosis desalination process on high salinity brines. *Desalination* 2013, 312, 67-74.
37. Fritzmann, C.; Löwenberg, J.; Wintgens, T.; Melin, T., State-of-the-art of reverse osmosis desalination. *Desalination* 2007, 216, (1-3), 1-76.
38. Miller, D. J.; Huang, X.; Li, H.; Kasemset, S.; Lee, A.; Agnihotri, D.; Hayes, T.; Paul, D. R.; Freeman, B. D., Fouling-resistant membranes for the treatment of flowback water from hydraulic shale fracturing: A pilot study. *J Membrane Sci* 2013, 437, 265-275.
39. Tong, T.; Carlson, K. H.; Robbins, C. A.; Zhang, Z.; Du, X., Membrane-based treatment of shale oil and gas wastewater: The current state of knowledge. *Frontiers of Environmental Science & Engineering* 2019, 13, (4), 1-17.

40. Elimelech, M.; Phillip, W. A., The future of seawater desalination: energy, technology, and the environment. *Science* 2011, 333, (6043), 712-717.
41. Eyvaz, M.; Arslan, S.; İmer, D.; Yüksel, E.; Koyuncu, İ., Forward Osmosis Membranes–A Review: Part I. In osmotically driven membrane processes-approach, development and current status, IntechOpen: 2018.
42. Shaffer, D. L.; Werber, J. R.; Jaramillo, H.; Lin, S.; Elimelech, M., Forward osmosis: where are we now? *Desalination* 2015, 356, 271-284.
43. Oasys Water Inc (2014). Oasys applies FO to treat wastewater from
57. China's growing power market. *Membrane Technology*, 2014(11):
58. 2–3
44. Deshmukh, A.; Boo, C.; Karanikola, V.; Lin, S.; Straub, A. P.; Tong, T.; Warsinger, D. M.; Elimelech, M., Membrane distillation at the water-energy nexus: limits, opportunities, and challenges. *Energ Environ Sci* 2018, 11, (5), 1177-1196.
45. Lawson, K. W.; Lloyd, D. R., Membrane distillation. *J Membrane Sci* 1997, 124, (1), 1-25.
46. Singh, D.; Sirkar, K. K., Desalination of brine and produced water by direct contact membrane distillation at high temperatures and pressures. *J Membrane Sci* 2012, 389, 380-388.
47. Boo, C.; Lee, J.; Elimelech, M., Omniphobic polyvinylidene fluoride (PVDF) membrane for desalination of shale gas produced water by membrane distillation. *Environ. Sci. Technol.* 2016, 50, (22), 12275-12282.
48. Lokare, O. R.; Tavakkoli, S.; Wadekar, S.; Khanna, V.; Vidic, R. D., Fouling in direct contact membrane distillation of produced water from unconventional gas extraction. *J Membrane Sci* 2017, 524, 493-501.
49. Du, X. W.; Zhang, Z. Y.; Carlson, K. H.; Lee, J.; Tong, T. Z., Membrane fouling and reusability in membrane distillation of shale oil and gas produced water: Effects of membrane surface wettability. *J Membrane Sci* 2018, 567, 199-208.
50. Warsinger, D. M.; Swaminathan, J.; Guillen-Burrieza, E.; Arafat, H. A., Scaling and fouling in membrane distillation for desalination applications: a review. *Desalination* 2015, 356, 294-313.
51. Tijing, L. D.; Woo, Y. C.; Choi, J.-S.; Lee, S.; Kim, S.-H.; Shon, H. K., Fouling and its control in membrane distillation—A review. *J Membrane Sci* 2015, 475, 215-244.
52. Coyote, G. Bureau of reclamation selects twenty-one projects to receive $2.93 million to study water treatment technologies. Retrieved by:https://coyotegulch.blog/2016/07/01/bureau-of-reclamation-selects-twenty-one-projects-to-receive-2-93-million-to-study-water-treatment-technologies/
53. Gryta, M.; Tomaszewska, M.; Grzechulska, J.; Morawski, A., Membrane distillation of NaCl solution containing natural organic matter. *J Membrane Sci* 2001, 181, (2), 279-287.

54. Wang, Z.; Hou, D.; Lin, S., Composite membrane with underwater-oleophobic surface for anti-oil-fouling membrane distillation. *Environ Sci Technol* 2016, 50, (7), 3866-3874.
55. Israelachvili, J.; Pashley, R., The hydrophobic interaction is long range, decaying exponentially with distance. *Nature* 1982, 300, (5890), 341-342.
56. Zuo, G.; Wang, R., Novel membrane surface modification to enhance anti-oil fouling property for membrane distillation application. *J Membrane Sci* 2013, 447, 26-35.
57. Wang, Z.; Jin, J.; Hou, D.; Lin, S., Tailoring surface charge and wetting property for robust oil-fouling mitigation in membrane distillation. *J Membrane Sci 2016*, 516, 113-122.
58. Razmjou, A.; Arifin, E.; Dong, G.; Mansouri, J.; Chen, V., Superhydrophobic modification of TiO2 nanocomposite PVDF membranes for applications in membrane distillation. *J Membrane Sci* 2012, 415, 850-863.
59. Huang, Y. X.; Wang, Z. X.; Jin, J.; Lin, S. H., Novel janus membrane for membrane distillation with simultaneous fouling and wetting resistance. *Environ Sci Technol* 2017, 51, (22), 13304-13310.
60. Deshmukh, A.; Boo, C.; Karanikola, V.; Lin, S. H.; Straub, A. P.; Tong, T. Z.; Warsinger, D. M.; Elimelech, M., Membrane distillation at the water-energy nexus: limits, opportunities, and challenges. *Energ Environ Sci* 2018, 11, (5), 1177-1196.
61. Lin, S.; Nejati, S.; Boo, C.; Hu, Y.; Osuji, C. O.; Elimelech, M., Omniphobic membrane for robust membrane distillation. *Environ Sci Tech Let* 2014, 1, (11), 443-447.
62. Boo, C.; Lee, J.; Elimelech, M., Engineering surface energy and nanostructure of microporous films for expanded membrane distillation applications. *Environ Sci Technol* 2016, 50, (15), 8112-8119.
63. Wang, Z. X.; Jin, J.; Hou, D. Y.; Lin, S. H., Tailoring surface charge and wetting property for robust oil-fouling mitigation in membrane distillation. *J Membrane Sci 2016*, 516, 113-122.
64. Wang, Z. X.; Hou, D. Y.; Lin, S. H., Composite membrane with underwater-oleophobic surface for anti-oil-fouling membrane distillation. *Environ Sci Technol* 2016, 50, (7), 3866-3874.
65. Wang, Z. X.; Lin, S. H., Membrane fouling and wetting in membrane distillation and their mitigation by novel membranes with special wettability. *Water Res* 2017, 112, 38-47.
66. Woo, Y. C.; Kim, Y.; Yao, M.; Tijing, L. D.; Choi, J.-S.; Lee, S.; Kim, S.-H.; Shon, H. K., Hierarchical composite membranes with robust omniphobic surface using layer-by-layer assembly technique. *Environ Sci Technol* 2018, 52, (4), 2186-2196.
67. Lee, E.-J.; Deka, B. J.; Guo, J.; Woo, Y. C.; Shon, H. K.; An, A. K., Engineering the re-entrant hierarchy and surface energy of PDMS-PVDF membrane for membrane distillation using a facile and benign microsphere coating. *Environ Sci Technol* 2017, 51, (17), 10117-10126.
68. Butt, H. J.; Semprebon, C.; Papadopoulos, P.; Vollmer, D.; Brinkmann, M.; Ciccotti, M., Design principles for superamphiphobic surfaces. *Soft Matter* 2013, 9, (2), 418-428.

69. Wang, Z. X.; Elimelech, M.; Lin, S. H., Environmental applications of interfacial materials with special wettability. *Environ Sci Technol* 2016, 50, (5), 2132-2150.
70. Deng, X.; Mammen, L.; Butt, H. J.; Vollmer, D., Candle soot as a template for a transparent robust superamphiphobic coating. *Science* 2012, 335, (6064), 67-70.
71. Tuteja, A.; Choi, W.; Ma, M. L.; Mabry, J. M.; Mazzella, S. A.; Rutledge, G. C.; McKinley, G. H.; Cohen, R. E., Designing superoleophobic surfaces. *Science* 2007, 318, (5856), 1618-1622.
72. Liu, K. S.; Tian, Y.; Jiang, L., Bio-inspired superoleophobic and smart materials: Design, fabrication, and application. *Prog Mater Sci* 2013, 58, (4), 503-564.
73. Gao, N.; Yan, Y.; Chen, X.; Mee, D., Superhydrophobic surfaces with hierarchical structure. *Mater Lett* 2011, 65, (19-20), 2902-2905.
74. Lafuma, A.; Quéré, D., Superhydrophobic states. *Nature materials* 2003, 2, (7), 457-460.
75. Swain, P. S.; Lipowsky, R., Contact angles on heterogeneous surfaces: A new look at Cassie's and Wenzel's laws. *Langmuir* 1998, 14, (23), 6772-6780.
76. Erbil, H. Y.; Cansoy, C. E., Range of applicability of the Wenzel and Cassie− Baxter equations for superhydrophobic surfaces. *Langmuir* 2009, 25, (24), 14135-14145.
77. Woo, Y. C.; Chen, Y.; Tijing, L. D.; Phuntsho, S.; He, T.; Choi, J.-S.; Kim, S.-H.; Shon, H. K., CF_4 plasma-modified omniphobic electrospun nanofiber membrane for produced water brine treatment by membrane distillation. *J Membrane* Sci 2017, 529, 234-242.
78. Kota, A. K.; Kwon, G.; Tuteja, A., The design and applications of superomniphobic surfaces. *Npg Asia Mater* 2014, 6, (7), e109-e109.
79. Lee, J.; Boo, C.; Ryu, W. H.; Taylor, A. D.; Elimelech, M., Development of omniphobic desalination membranes using a charged electrospun nanofiber scaffold. *Acs Appl Mater Inter* 2016, 8, (17), 11154-11161.
80. Zheng, G.; Yao, L.; You, X.; Liao, Y.; Wang, R.; Huang, J. J., Effects of different secondary nano-scaled roughness on the properties of omniphobic membranes for brine treatment using membrane distillation. *J Membrane Sci* 2021, 620, 118918.
81. Lu, C.; Su, C.; Cao, H.; Ma, X.; Duan, F.; Chang, J.; Li, Y., F-POSS based omniphobic membrane for robust membrane distillation. *Mater Lett* 2018, 228, 85-88.
82. Batley, G. E.; Kirby, J. K.; McLaughlin, M. J., Fate and risks of nanomaterials in aquatic and terrestrial environments. *Accounts of chemical research* 2013, 46, (3), 854-862.
83. Huang, Y. X.; Wang, Z.; Jin, J.; Lin, S., Novel Janus membrane for membrane distillation with dimultaneous fouling and wetting resistance. *Environ Sci Technol* 2017, 51, (22), 13304-13310.
84. An, X.; Liu, Z.; Hu, Y., Amphiphobic surface modification of electrospun nanofibrous membranes for anti-wetting performance in membrane distillation. *Desalination* 2018, 432, 23-31.
85. Lu, X.; Peng, Y.; Qiu, H.; Liu, X.; Ge, L., Anti-fouling membranes by manipulating surface wettability and their anti-fouling mechanism. *Desalination* 2017, 413, 127-135.

86. Woo, Y. C.; Kim, Y.; Yao, M.; Tijing, L. D.; Choi, J. S.; Lee, S.; Kim, S. H.; Shon, H. K., Hierarchical composite membranes with robust omniphobic surface using layer-by-layer assembly technique. *Environ. Sci. Technol.* 2018, 52, (4), 2186-2196.
87. Zheng, R.; Chen, Y.; Wang, J.; Song, J.; Li, X.-M.; He, T., Preparation of omniphobic PVDF membrane with hierarchical structure for treating saline oily wastewater using direct contact membrane distillation. *J Membrane Sci* 2018, 555, 197-205.
88. Lu, K. J.; Zuo, J.; Chang, J.; Kuan, H. N.; Chung, T.-S., Omniphobic hollow-fiber membranes for vacuum membrane distillation. *Environ Sci Technol* 2018, 52, (7), 4472-4480.
89. Wang, M.; Liu, G.; Yu, H.; Lee, S.-H.; Wang, L.; Zheng, J.; Wang, T.; Yun, Y.; Lee, J. K., ZnO nanorod array modified PVDF membrane with superhydrophobic surface for vacuum membrane distillation application. *ACS Appl. Mater. Interfaces* 2018, 10, (16), 13452-13461.
90. Du, X.; Zhang, Z.; Carlson, K. H.; Lee, J.; Tong, T., Membrane fouling and reusability in membrane distillation of shale oil and gas produced water: Effects of membrane surface wettability. *J. Membr. Sci.* 2018, 567, 199-208.
91. Karanikola, V.; Boo, C.; Rolf, J.; Elimelech, M., Engineered Slippery Surface to Mitigate Gypsum Scaling in Membrane Distillation for Treatment of Hypersaline Industrial Wastewaters. *Environ. Sci. Technol.* 2018, 52, (24), 14362-14370.
92. Wang, W.; Du, X.; Vahabi, H.; Zhao, S.; Yin, Y.; Kota, A. K.; Tong, T., Trade-off in membrane distillation with monolithic omniphobic membranes. *Nat. Commun.* 2019, 10, (1), 3220.
93. Chen, Y.; Lu, K. J.; Chung, T.-S., An omniphobic slippery membrane with simultaneous anti-wetting and anti-scaling properties for robust membrane distillation. *J. Membr. Sci.* 2020, 595, 117572.
94. Lee, J.; Boo, C.; Ryu, W.-H.; Taylor, A. D.; Elimelech, M., Development of omniphobic desalination membranes using a charged electrospun nanofiber scaffold. *ACS Appl. Mater. Interfaces* 2016, 8, (17), 11154-11161.
95. Li, C.; Li, X.; Du, X.; Zhang, Y.; Wang, W.; Tong, T.; Kota, A. K.; Lee, J., Elucidating the trade-off between membrane wetting resistance and water vapor flux in membrane distillation. *Environ Sci Technol* 2020, 54, (16), 10333-10341.

CHAPTER 3: Research objectives

In this dissertation, I aim at facilitating the treatment and reuse of O&G wastewater to improve water sustainability of O&G-producing regions in the U.S. at the water-energy-climate nexus Based on this objective, I mainly focus on two aspects associated with membrane-based treatment of O&G wastewater: motivations and material innovation.

First, I performed spatiotemporal data analyses on the water footprint of O&G production under different hydroclimate conditions in the U.S., in order to provide quantitative evidence that demonstrates the water stress imposed by O&G activities. Such efforts could benefit policy makers, regulators, and the O&G industry while motivating them to shift the current wastewater management paradigm towards treatment and reuse. Second, I employed membrane desalination for the treatment of O&G wastewater, and develop novel membrane materials for more efficient and sustainable wastewater treatment. Accordingly, my research will answer the following three main questions:

1. What is the water footprint of O&G production under hydroclimate variation?

The high water consumption of O&G production has been used as the main motivation of UOG wastewater treatment and reuse in the literature. However, the O&G water footprint under arid, water-stress conditions (when wastewater reuse is the most desirable) has not been quantified. I investigated the impacts of hydroclimate variation on the activities and water footprint of O&G in Colorado, one of the major O&G-producing states in the U.S. (Chapter 4). Further, I expanded

my research scope to estimate the water footprint of O&G activities under different hydroclimate conditions for 11 states of the central and western United States during the years of 2011-2020 (Chapter 5). These quantitative studies on water consumption and wastewater generation related to O&G activities that take place in water-stressed areas has more implications in understanding the role of O&G production in affecting regional freshwater resources, thereby providing necessary insights that potentially stimulate the reuse and treatment of O&G wastewater.

2. How does membrane surface wettability affect membrane performance in MD treatment of O&G wastewater?

Although membranes with tailored wettability have been developed to mitigate membrane fouling and wetting of MD desalination, they have been rarely tested in the treatment of real O&G wastewater. I evaluated the performance of MD membranes with different membrane surface wettability in MD desalination of industrial O&G wastewater generated from Denver-Julesburg Basin of Colorado in this work (Chapter 6). This work elucidated the potential benefits and limitations of applying membranes with special wettability to improve the performance of MD treatment of O&G wastewater.

3. How to improve the design framework for membranes used in MD treatment of UOG wastewater?

The design of MD membranes for the treatment of hypersaline wastewater, including O&G wastewater, typically aims to improve membrane wetting and fouling resistance, while other factors such as the sustainability of membrane fabrication and water productivity (i.e., water vapor

flux) have been rarely considered. For example, the use of long-chain fluorinated compounds in the fabrication of omniphobic membranes imposes ecological and health concerns, significantly increasing the lifecycle cost of MD treatment. Also, the water productivity of membranes determines the process efficiency of MD treatment, with membranes possessing high water vapor permeability corresponding to lower energy efficiency and membrane cost. Therefore, a rational framework of membrane design tailored to MD treatment needs to take the above two factors into comprehensive consideration. In order to answer this question, I developed novel fabrication approaches that achieve highly wetting-resistant membranes utilizing (ultra)short-chain fluorinated compounds ($\leq$4 CF_2, Chapter 7). I tuned the hierarchical texture of membrane surface and introduce (ultra)short-chain fluorinated compounds as an alternative to the typically used long-chain fluorinated substances. Further, I investigated the relationship between wetting resistance and water vapor permeability of MD membranes, and elucidated the underlying mechanisms (Chapter 8). These efforts provide valuable insights that guide rational membrane design of high-performance, sustainable membrane materials suitable for efficient MD treatment of O&G wastewater.

CHAPTER 4: Activity and water footprint of unconventional energy production under hydroclimate variation in Colorado [1]

4.1 Introduction

Unconventional energy exploitation has improved the national energy security of the United States.[1] The technological advances in horizontal drilling and high-volume hydraulic fracturing (HF) have rendered the extraction of oil and natural gas from tight shale formations commercially feasible.[2,3] According to the U.S. Energy Information Administration (EIA),[4] crude oil and natural gas produced from tight shale resources are responsible for 63% of total oil production and 75% of total natural gas production of the U.S., respectively. However, the rise of the unconventional oil and gas (UOG) industry has also led to an increase of freshwater consumption and wastewater generation.[5-12] It was reported that UOG production in the U.S. had consumed 940 million m^3 (~250 billion gallons) of water from 2005 to 2014,[7] and the major shale plays had witnessed an increase of water usage per production well of up to 770% from 2011 to 2016.[2] Many of the U.S. shale plays are located in arid areas with high to severe water stress.[13] For example, a majority of the Niobrara Shale, which is mainly located in the states of Colorado and Wyoming, resides in areas where water withdrawals comprise > 80% of water availability.[14] As a result, the high water

[1] This chapter has been published as a research article in *ACS ES&T Water* with the following citation:

Du, X.; Li, H.; Robbins, C. A.; Carlson, K. H.; Tong, T., Activity and water footprint of unconventional energy production under hydroclimate variation in Colorado. *ACS ES&T Water* 2020, 1, (2), 281-290.

intensity of the UOG industry creates a challenge that imposes potential threats to water sustainability of the UOG producing regions.

During the past few years, extensive and prolonged droughts have occurred in the western region of North America.[15] The variations in hydroclimate condition amplify the deficit in terrestrial water storage. A significant water depletion of ~240 gigatons, which is in the magnitude of the annual mass depletion from the Greenland Ice Sheet, was reported for March 2014 across the western United States where several major shale plays are located.[16] The varying drought scenarios complicate the mutual interactions between UOG production and water supply. During drought periods, the intensive water consumption of HF within a short timeframe further reduces freshwater availability for other water-consuming sectors that are already under water stress, while water acquisition would become more challenging and costly to energy producers.[2,17,18] However, whether hydroclimate variation imposes a significant effect on the activity and water footprint of UOG production have yet to be revealed. Further, although the total water footprint of UOG production has been reported for major shale plays in the U.S.,[2, 6, 7, 9] the water consumption of UOG activities under drought climates has not been quantified, which has more implications in understanding on how the rise of UOG production might alter local water supply. Closing these knowledge gaps is an essential step for the policymakers and energy producers to formulate wiser strategies of water resource management, in order to promote sustainability at the water-energy-climate nexus.

In this work, we investigate the relationship of hydroclimate variation with the activity and water footprint of UOG production via analyzing of a comprehensive dataset for the state of Colorado, one of the major UOG producing states in the U.S. We perform correlation analyses on the drought intensity with the number and water consumption of newly drilled UOG wells both temporally and spatially on a monthly basis within a 13-year period (i.e., from 2007 to 2019). Further, the total water consumption by UOG production within drought-occurring areas is calculated and compared with regional municipal water usage. We also present a new metric of "drought-escaping distance" to quantify the spatial impact of drought climate on the interactions between UOG production and local water supply. Finally, the potential of wastewater reuse to mitigate local water stress intensified by UOG production in Colorado is evaluated and discussed.

4.2 Materials and methods

4.2.1 Data acquisition

The monthly data for the number and locations of UOG wells drilled from 2007 to 2019 in Colorado were obtained from the Colorado Oil and Gas Conservation Commission (COGCC) database.[19] This database is established upon well survey reports submitted by the oil and gas operators, which include information on detailed well characteristics including the American Petroleum Institute (API) well identification, spud date, as well as well type and location. This database also provides information on the monthly volume of wastewater (including flowback and produced water) generated from UOG production. However, the COGCC database does not

include the information associated with water usage. Thus, the water use data of HF were obtained from the FracFocus Chemical Disclosure Registry (referred to as the FracFocus database in this study).[20] This database, with only available data from 2011 to 2019, is managed by the Groundwater Protection Council and Interstate Oil and Gas Compact Commission, providing a platform of data disclosure associated with UOG production.

The weekly drought maps from 2007 to 2019 are accessible in the database of U.S. Drought Monitor (USDM)[21]. The USDM map is generated from expert combinations of multiple data sources, including surface stream flow, soil moisture, rainfall and temperature anomalies, crop and range conditions, as well as snow coverage. We selected the map in the middle of each month to represent the drought condition of the entire month, because only monthly data of wells are used in this study and drilling activities typically last for several weeks.[22] The data of annual water use and total gross domestic product (GDP) for specific water-consuming sectors (e.g., irrigation and oil and gas production) in Colorado were obtained from the U.S. Geological Survey (USGS)[23] and the Federal Reserve Economic Data (FRED) database (managed by the Federal Reserve Bank of St. Louis),[24] respectively. The historical prices of crude oil in Colorado were taken from the U.S. EIA.[25]

4.2.2 The correlation of UOG activity and water footprint with drought intensity

The COGCC data, which contained 24,614 individual wells fractured between 2007 and 2019, were sorted by the spud date and aligned by well age. The water use data from the FracFocus

database were sorted by the job start date, and the water consumption by UOG wells drilled in each month was calculated. The drought scenarios in Colorado between 2007 and 2019 were classified into five categories according to the USDM, ranging from abnormally dry (D0) to exceptional drought (D4). The description for each drought category could be found on the USDM website.[26] In this study, each category was designated as an integer from 0 to 4 (abnormally dry, D0 = 0; moderate drought, D1 = 1; severe drought, D2 = 2; extreme drought, D3 = 3; and exceptional drought, D4 = 4). The drought severity classification index (DSCI) was accordingly defined to quantify the drought magnitude by converting the drought categories from the USDM map to a single value (Equation 4-1):[27]

$$DSCI=0\times D0\%+1\times D1\%+2\times D2\%+3\times D3\%+4\times D4\% \qquad (4\text{-}1)$$

where the values of D0% to D4% represent the normalized area percentages (to the total Colorado area) of the corresponding drought categories in each drought map of Colorado. This results in a range of DSCI from 0 to 400. Consistent with the selection of drought map, the DSCI calculated in the middle of each month was selected to represent the drought intensity of Colorado in the corresponding month.

Correlation analyses were performed to correlate the number and water use of newly drilled wells with the corresponding DSCI each month using the Origin Lab 9.1 (Origin Lab Corporation) and R Script software. We calculated both liner (Pearson's r) and non-linear (Spearman's r_s and Kendall's τ) correlation coefficients, as well as the statistical significance ($p < 0.05$ indicating statistically significant correlation), in the analyses (Section 1, Appendix A). We also performed

time series analysis in our study in order to better understand their relationship between DSCI and the drilling activity or UOG water consumption (Section 1, Appendix A). The correlation between crude oil price and well number was also obtained for comparison. Further, the locations of UOG wells, based on the latitude and longitude data provided by COGCC database, were overlapped with the USDM drought maps using Geographic Information System (GIS) software (ArcGIS 10.2, ESRI). The number of newly drilled wells located within each drought category was calculated with the "Join" tool embedded in the GIS software. Since the databases of COGCC and USDM employ different coordination systems (the Geographic Coordinate System of North American Datum of 1983 (GCS_NAD83) for COGCC, and World Geodetic System of 1984 (WGS84) for USDM), the latitude and longitude data of both databases were projected to the North American Datum of 1983 (UTM Zone 13N) system, in order to render the well location of the two databases consistent.

4.2.3 The interactions of UOG activity with local water supply under hydroclimate variation

Two approaches were used to investigate the interactions of UOG activity with water supply at the local scale. First, the monthly water consumption by wells drilled in the areas of D1–D4 drought categories was calculated for both Weld County and Garfield County (the dominant UOG producing regions in Colorado) by multiplying the number of wells under each drought category and the average water use per well calculated from the FracFocus database. Drought category D0 indicates abnormally dry rather than drought and is thus not included in the analysis. Within the

drought categories of D1–D4, moderate or more severe drought has occurred, resulting in water-use restrictions and damages to agriculture (defined by USDM,[28] although exception might happen). The corresponding populations that would be sustained by UOG water usage under drought climates were then estimated based on the daily water use per capita (95 gallons and 143 gallons per day for Weld and Garfield Counties, respectively [23]), which were then compared to the total population of each county. Second, we define a new metric of "drought-escaping distance (d_{es})" as the shortest distance between each newly drilled well and the nearest area without any water stress (i.e., with no drought category, or outside D0-D4, as illustrated in Figure A2, Appendix A), in order to indicate the spatial impact of drought on the interactions between UOG production and local water supply. Water acquisition within d_{es} causes strong competition between UOG production and other water-consuming sectors for freshwater due to the concurrent drought climate. In order to avoid intensified water stress, the water used for UOG production needs to be obtained with a transport distance higher than d_{es}.

4.2.4 The potential of wastewater reuse to mitigate water consumption by UOG production

Wastewater reuse is a promising strategy of mitigating local water stress resulting from UOG production[29-32]. Therefore, the wastewater volume generated by all the active UOG wells (obtained from the COGCC database) was compared to the water consumption by UOG activities (obtained from the FracFocus database) on a monthly basis in the period of 2011-2019. The monthly

volumetric ratios of wastewater generation to water consumption were calculated to indicate the potential capacity of wastewater reuse to reduce the water footprint of UOG production.

4.3 Results and discussion

4.3.1 Correlations of hydroclimate condition with UOG activity and water footprint

From 2007 to 2019, the number of newly drilled UOG wells in each month varied between 61 and 287 in Colorado, resulting in an average of 158 wells drilled per month. As shown in Figure 4-1a, two extreme drought events occurred during the years of 2012-2013 and 2018-2019, in which up to 100% of Colorado area was covered by a certain magnitude of dry or drought climate (i.e., D0 category indicates dry or arid climate while D1-D4 categories imply drought climate, as defined by USDM [28]). However, the drought intensity indicated by DSCI displayed no linear correlation with the number of newly drilled wells (Figure 4-1b, Pearson's r = 0.01, p = 0.89). A positive relationship between DSCI and drilling activity was shown by Spearman and Kendall correlations, with the correlation being weak but statistically significant (Figure 4-1b, r_s and $\tau < 0.3$, $p < 0.005$). However, the positive relationship (r_s and $\tau > 0$) indicates that such correlations are mathematically valid but practically meaningless, because enhanced drought condition should not increase the activity of water-consumptive HF in practical. According to the FracFocus database, the water usage of HF in Colorado increased substantially from 0.58 million to 9.38 million gallons/well from 2011 to 2019 (Figure A3, Appendix A), during which 81.7 billion gallons of water had been consumed to fracture 16,109 individual wells in Colorado. The corresponding water consumption

by UOG activities was calculated for each month, which also demonstrated no linear correlation with the drought intensity (Figure 4-1c, r = -0.15, p = 0.12). However, a weakly negative monotonic correlation exists between DSCI and water consumption by HF with high statistical significance, evidenced by both Spearman and Kendall correlations (the absolute values of r_s and $\tau < 0.3$, $p < 0.05$). Therefore, the water consumption by HF is slightly limited under high levels of drought climates, at least mathematically. Such a weak effect could be attributed to the constrained water availability and potentially increased water price during drought periods. We also performed decomposition of time series for the correlation of UOG well number and water footprint with drought intensity (to exclude any potential effects of seasonal cycles), which resulted in consistent conclusions with the above analyses (Section 1, Appendix A). Therefore, hydroclimate variation imposed a negligible or weak effect on the activity and water footprint of UOG production in Colorado, and drought conditions have not significantly prohibited the water consumption by HF.

As shown in Figure 4-1d, the number of newly drilled UOG wells exhibited statistically significant correlation with the crude oil price in all the three correlation analyses (r = 0.62, p < 0.001, r_s =0.60, p <0.001 and τ = 0.44, p <0.001). Hence, economic incentive, rather than hydroclimate condition, plays a dominant role in determining the extent of UOG production activities. We compared the economic efficiencies of water use (i.e., the generation of GDP per unit of water use) between oil and gas production and agricultural irrigation, the largest water consumer in Colorado (Figure 4-1e). With a gallon of water input, the oil and gas industry generates a GDP of ~$1.2 in Colorado, which is more than three orders of magnitude higher than

that of agricultural irrigation (~$0.0009 GDP/gallon of water). On the other hand, the water consumption of agricultural irrigation is ~550 times of that of oil and gas industry in Colorado.

These remarkable discrepancies explain the insensitivity of water-consumptive UOG production to hydrodynamic variation. In Colorado, the distribution of water resources adheres to the water rights system, which is based on the prior appropriation doctrine.[33] Although the oil and gas companies has inferior water right to that of agricultural and municipal users, they are allowed to purchase water from municipalities or landowners with rights to surface water.[13,34] Even under drought conditions, they are still able to acquire water supplies by purchasing and diverting water away from other water-consuming sectors with lower economic efficiencies (e.g., agricultural irrigation due to its highest water consumption).[35-37] In other words, water flows to chase high economic efficiencies, providing adequate water supplies for UOG production regardless of the hydroclimate condition.

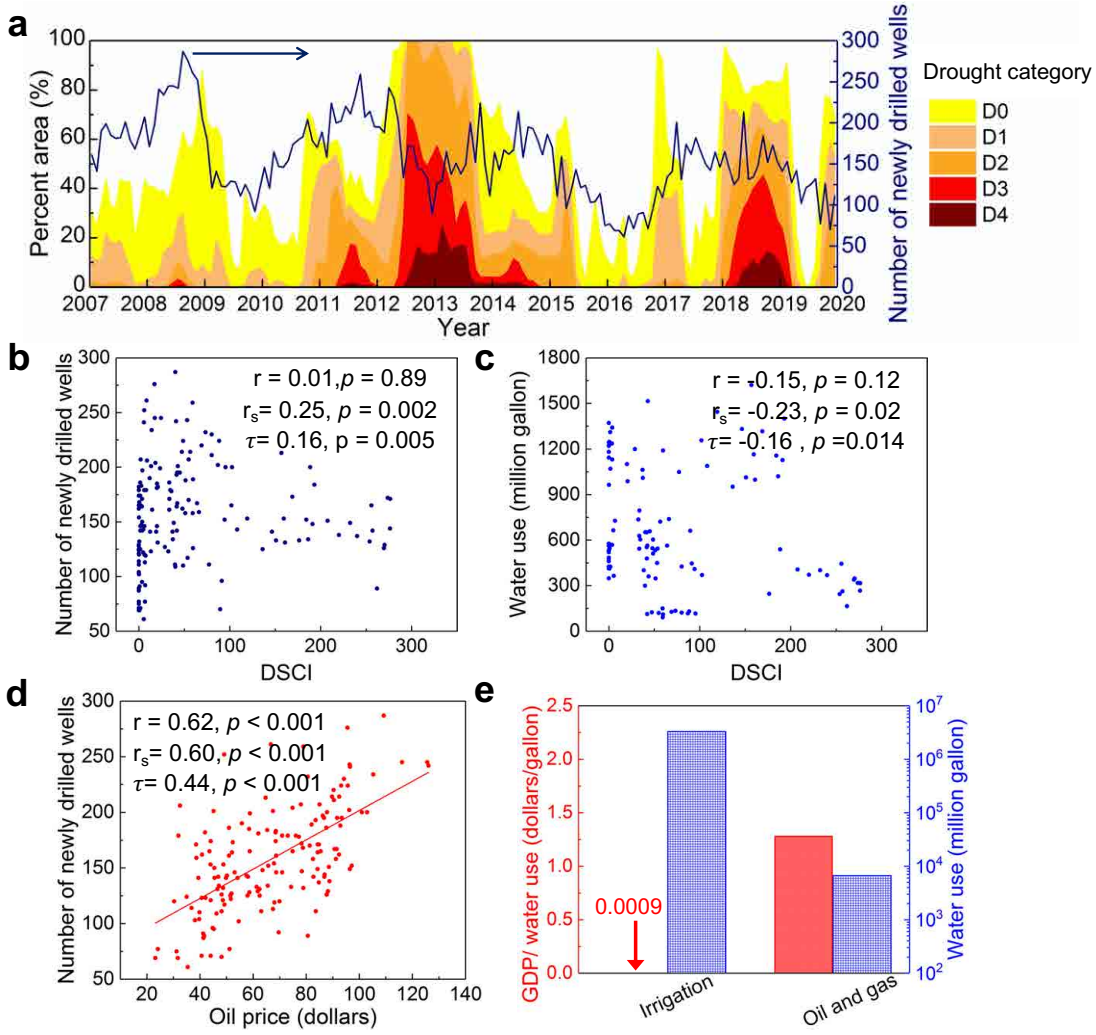

Figure 4-1. (a) Time-series drought severity and coverage data (left y axis) as well as the corresponding UOG production activity (indicated by the number of new wells drilled each month, blue line, right y axis) from 2007-2019 in Colorado. D0 to D4 define the area percentages under different drought categories as defined by the U.S. Drought Monitor. Note that the sum of percentage area of the left y axis is up to 100%. (b) The correlation of UOG activity (as indicated by the number of newly drilled wells each month) with DSCI from 2007 to 2019. (c) The correlation of water consumption by UOG activities with DSCI from 2011 to 2019. (d) The correlation of UOG activity with crude oil price from 2007 to 2019. For (b), (c), and (d), the correlation efficient and statistical significance of Pearson (r), Spearman (r_s), and Kendall (τ) correlations are presented. (e) The histogram plots of water use (blue columns) and GDP generation per unit of water use (red columns) for irrigation and oil and gas sectors in Colorado. Data from the year of 2015 were used because the most recent available data of water usage by irrigation in the USGS database is for 2015. The GDP data are obtained from the FRED database, while the data of water usage by oil and gas industry is from the FracFocus database.

There were 11,421 (46.4% of total) UOG wells drilled in areas experiencing aridity or drought (within D0-D4 drought category) in Colorado between 2007 and 2019. Between 2011 and 2019 when water use data are available, the 7,097 wells drilled under arid or drought climates consumed 31.3 billion gallons of water (Figures 4-2a and 4-2b). Excluding the well drilled under the D0 category (i.e., arid climate but not drought), 16.2 billion gallons of water was consumed by UOG activities under drought climate. As shown in Figure 4-2c, the UOG well sites were mainly located in Weld and Garfield Counties, independent of the hydrodynamic conditions. Therefore, a high fraction of drilling activities and associated water consumption occurred in water-stressed areas when drought covered these two counties. For example, 86.4% of the newly drilled wells (2253 out of 2608) were located in drought areas (i.e., in D1 to D4 categories) during the first extreme drought event from April 2012 to August 2013 (Figure 4-2a). In this water-stressed period, the water consumption by HF under drought climates accounted for 61.4% and 62.3% of total UOG water use in 2012 and 2013, respectively (Figure 4-2b). In particular, 139 (96.5%) and 4 (2.8%) wells were drilled in areas under the categories of extreme (D3) and exceptional (D4) drought in September 2012, respectively. In the second extreme drought event, only 29% of the new wells (630 out of 2148) were drilled in drought areas between January 2018 and February 2019, despite >80% of Colorado area being under drought conditions at the time. This was because Weld County, one of the major UOG producing regions, escaped from this extreme drought event

(Figure 4-2c). In this period, 30.1 % of total UOG water use occurred in drought areas in 2018, when 1.5 billion gallons of water were consumed under D3 and D4 drought categories.

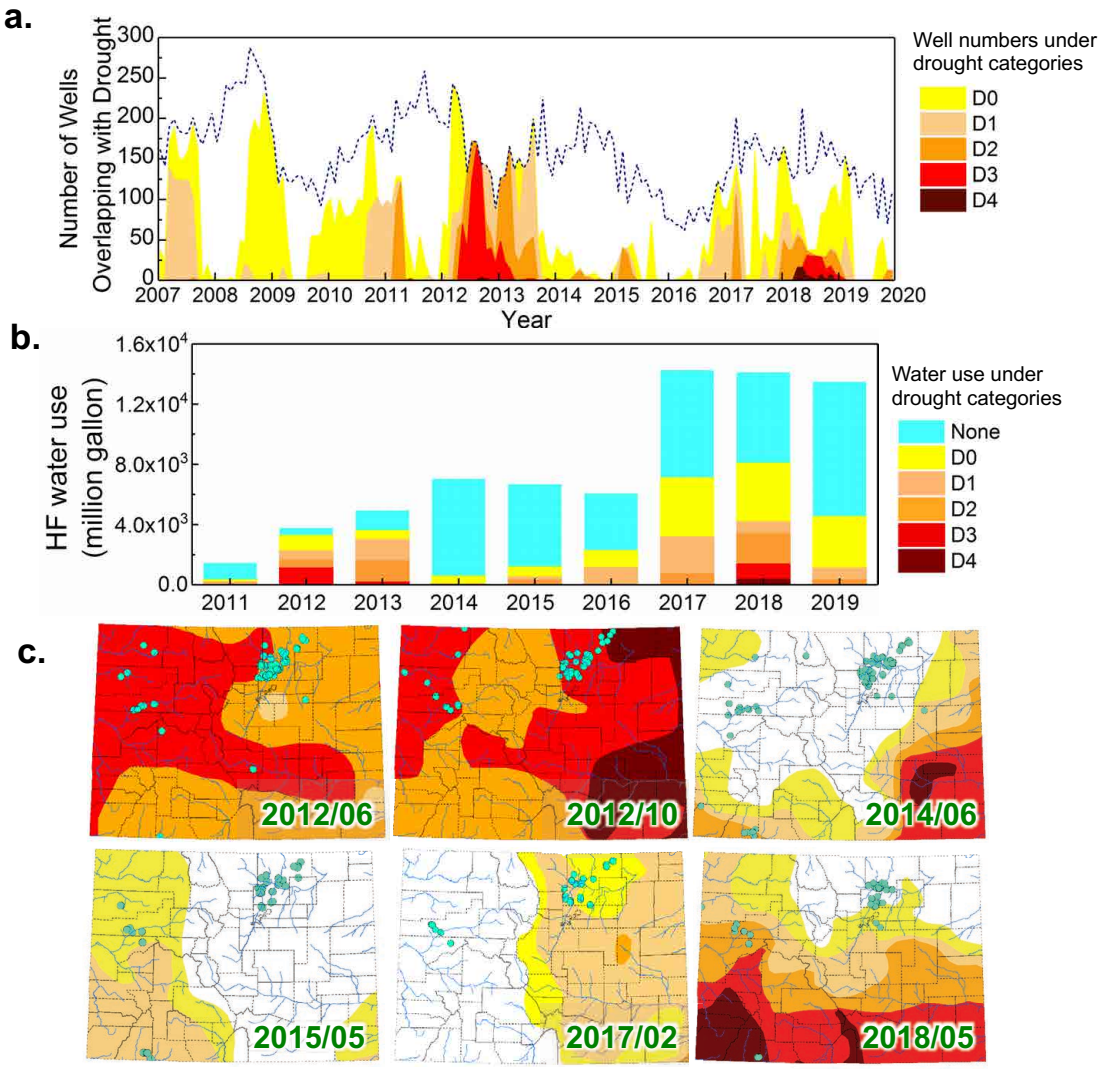

Figure 4-2. (a) Time-series changes of the number of UOG wells drilled in different drought categories for each month from 2007-2019 in Colorado. Top dash blue line indicates the total number of newly drilled wells each month in Colorado. D0 to D4 define the number of newly drilled wells in different drought categories. (b) Annual water consumption by newly drilled UOG wells located in area without any drought categories and area under different drought categories each year from 2011 to 2019 in Colorado. The wells in the area under different drought categories indicate those in areas of D0-D4 drought categories. (c) The maps of drought severity and coverage overlaid with the locations of newly drilled wells (Blue dots) in exemplified months in Colorado.

Note that due to the size of the blue dots, one dot might cover more than one well. The state and county boundaries were obtained from the Colorado department of public Health & Environment (CDPHE). The red and blue insets of Figure 4-2b (in the 2014/06 map) outlines the boundaries of Weld county and Garfield county, respectively, which are the major UOG producing areas in Colorado.

4.3.2 The interactions of UOG activity with local water supply under hydroclimate variation

The total volume of water consumption by newly drilled wells located in drought areas were 9.7 billion and 4.2 billion gallons between 2011 and 2019 for Weld and Garfield Counties, respectively. The water consumption by UOG production under drought climates in Weld County varied from 18.3 million to 990.5 million gallons/month, which would sustain 3% to 114% of the entire county population (Figure 4-3a). As for Garfield County, such water usage was in the range from 51.7 million to 230.8 million gallons/month, which was sufficient for 21%-95% of the county population (Figure 4-3b). The highest water consumption under drought climate occurred in April 2017 for Weld County, when the consumption of 990.5 million gallons of water would sustain a population of 350,246 (Figure A4a, Appendix A). For Garfield county, such peak water usage was 230.8 million gallons in May 2012, which equals the municipal water use by a population of 54,500 (Figure A4b, Appendix A). Therefore, although the water consumption by UOG production was dwarfed by that of agricultural irrigation, it was equivalent to a large proportion of local municipal water usage. Under D1-D4 categories, damages to crops or pasture occur, voluntary or mandatory water-use restriction are imposed according to USDM.[26] The intensive amount of water demand by UOG production, if acquired locally, would intensify water scarcity and adversely affect the distribution of the limited water resources.

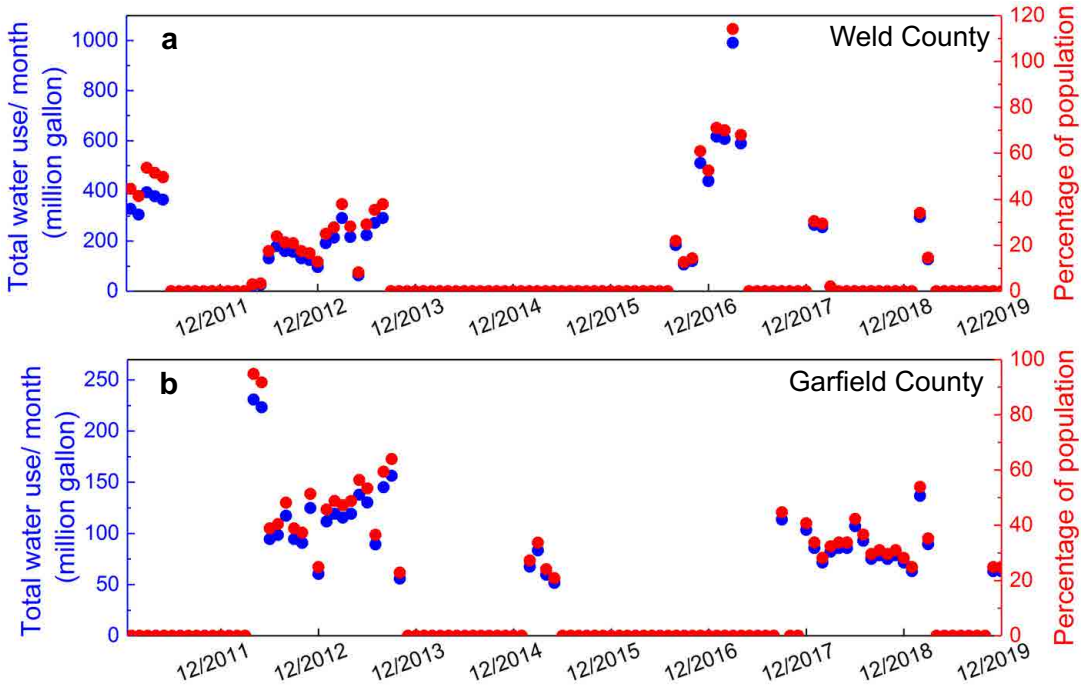

Figure 4-3. Water consumption by the newly drilled UOG wells located in the drought areas (i.e., within drought categories of D1-D4) each month from 2011 to 2019 (Blue) and the corresponding sustained population percentage (Red) for (a) Weld county and (b) Garfield county.

In order to further quantify the effect of hydroclimate condition on the spatial interactions between UOG production and regional water resources, we define a new metric of drought-escaping distance (d_{es}), which refers to the shortest distance between newly drilled wells that located in the drought areas (D1 to D4) to the nearest area without any drought category (Figure A2). As shown in Figures 4-4 a and b, the values of d_{es} significantly increased when drought events occurred. For example, the monthly average d_{es} values ranged from 45 to 590 miles and 78 to 545 miles in Weld and Garfield Counties during the first extreme drought event from April 2012 to August 2013, respectively (the value of d_{es} could be as low as 0 when no drought occurs). In particular, all 109 wells fractured in these two counties displayed high d_{es} values of > 500 miles in

January 2013. In the second extreme drought event from January 2018 to February 2019, the average d_{es} values of newly drilled wells were in the range of 78 to 161 miles in Garfield County, but only 3 to 62 miles in Weld County that was mostly outside the drought area. Therefore, the drought climates could cover tens or hundreds of miles surrounding HF activities in Colorado. In such scenarios, freshwater withdrawal for HF activities is more than likely to occur in areas that are already under water stress due to the expensive cost for water transportation. The intensive water demand of UOG production is likely met by local water resources that are under pressure, thereby decreasing the already scarce water availability and intensifying water competition with agricultural, commercial and municipal water-consuming sectors.

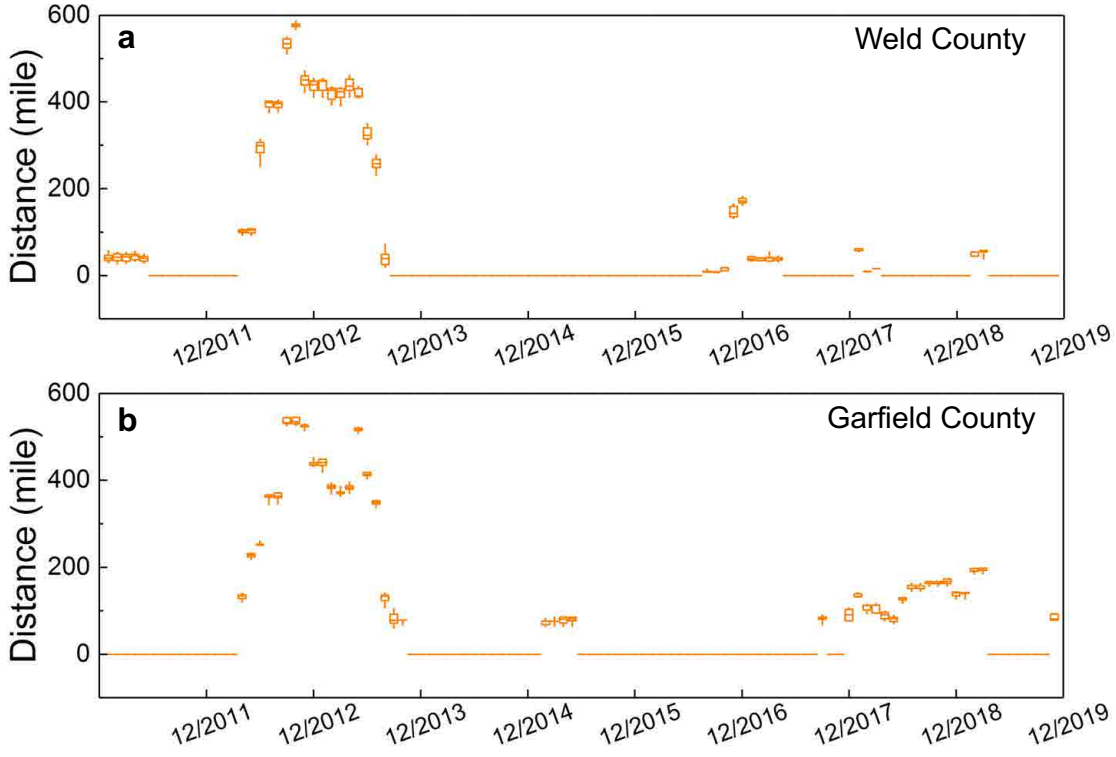

Figure 4-4. Box plots of the drought-escaping distance (d_{es}, the distance from newly drilled UOG wells to the nearest area without water stress) for (a) Weld County and (b) Garfield County from

2011 to 2019. The central line of each box refers to the median value, while the top and bottom lines of each box represent the third and first quartile, respectively. The whiskers of the box plot represent the 95% confidence interval of the calculated d_{es} values.

4.3.3 Potential of UOG wastewater reuse to mitigate water stress

One strategy of mitigating water consumption by the UOG production is wastewater reuse. Between 2011 and 2019, 56.0 billion and 11.9 billion gallons of water were consumed by UOG production in Weld and Garfield Counties, respectively, while generating 14.9 billion and 12.9 billion gallons of flowback and produced water (based on the COGCC and Fracfocus databases). For Weld County, the monthly water consumption by HF was below 780 million gallons/month (with an average of 371 million gallons/month) before 2017, but it increased sharply to ~1000 million gallons/month (with an average of 924 million gallons/month) between 2017 and 2019 (Figure 4-5a). Meanwhile, the volume of UOG wastewater increased steadily from 33 million to 322 million gallons/month during 2011-2019. Correspondingly, the monthly volumetric ratio of wastewater generation to water consumption associated with UOG production varies from 0.09 to 0.68 in Weld County, with an average value of 0.22. Such volumetric ratios are higher in Garfield County (in the range of 0.4 to 3.7, with the average of 1.1, Figure 4-5b). The higher volumetric ratios of wastewater generation to water consumption in Garfield County are probably due to the following reasons. The major targeting products of Weld County and Garfield County are oil and gas, respectively. Garfield County has produced substantial amounts of natural gas from the Piceance Basin since 2007, but Weld County have replaced Garfield County as the largest UOG producing area in Colorado since 2015 due to the boom of Denver-Julesburg Basin.[38] As Garfield

County, which targets at gas that has less value than oil, could not justify profitable drilling for several years, its drilling activities have decreased since 2011[39]. Its water consumption of HF decreased from >200 million gallons/month in 2011 to only ~90 million gallons/month in 2019 (Figure 4-5b), while the existing wells still produce high volume of wastewater. In contrast, Weld County has witnessed an increase of drilling since 2015. Its water consumption by HF increased with time (in particular after 2015, Figure 4-5a) due to the high activities of oil production, resulting in lower ratio of wastewater to water consumption than Garfield County.

In the first extreme drought event (i.e., from April 2012 to August 2013), the volume of UOG wastewater equals to 19%-64% and 65%-229% of the water consumption by HF in Weld and Garfield Counties, respectively. Similarly, such percentages were in the ranges of 17-68% and 60%-220% during the second extreme drought event from January 2018 to February 2019. The above results indicate that wastewater reuse has the potential to meet full or a large proportion of water demand by UOG production, thereby alleviating the intensified water stress in particular during extreme drought conditions. However, the reuse of UOG wastewater, especially outside oil and gas fields (i.e., external reuse), still faces multiple barriers that render such activities difficult to be fully achieved (see detailed discussion below).

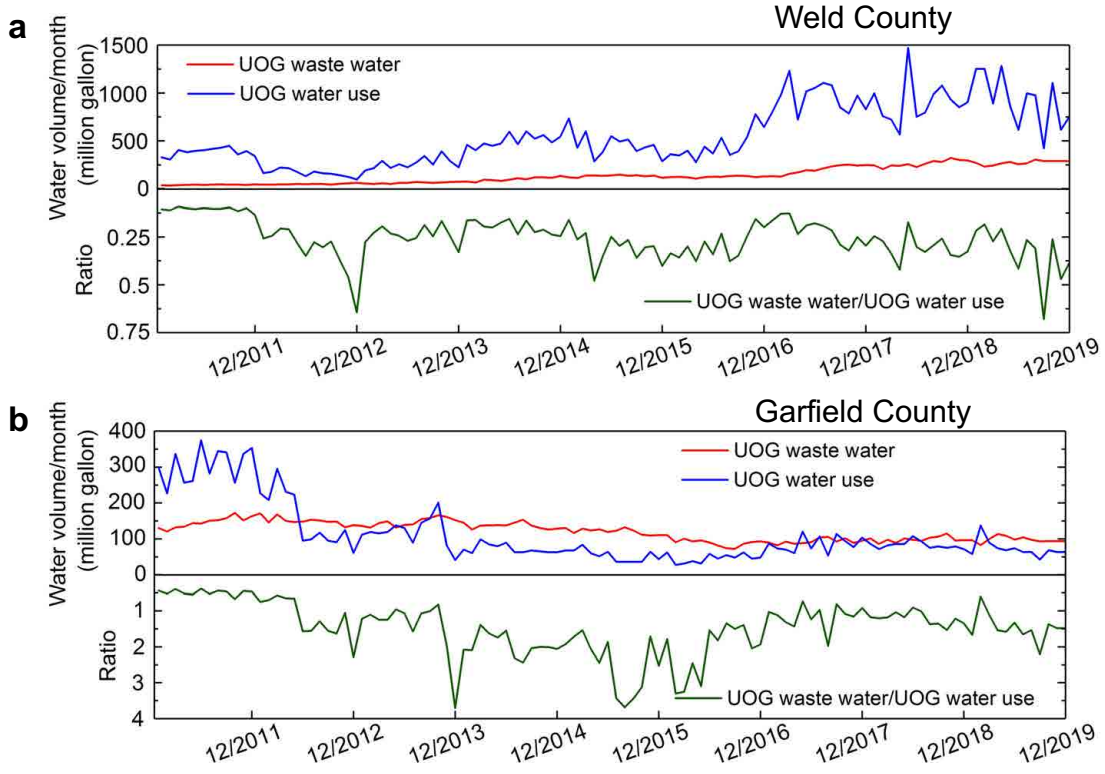

Figure 4-5. Monthly volumetric ratio of wastewater generation to water consumption associated with UOG production from 2011 to 2019 for (a) Weld County and (b) Garfield County.

4.3.4 Environmental implications

In this work, we investigated the temporal and spatial correlation of hydroclimate condition with the activity and water footprint of UOG production in the state of Colorado. Our results demonstrate that hydroclimate variation, which alters freshwater availability, has been posing negligible or weak impacts on the number or water usage of newly drilled wells for UOG production. The sites of these wells, which are determined by the geological locations of oil and gas reservoirs, do not shift away from water-stressed areas, resulting in a large number of wells fractured under drought climate. Especially, we found that high volumes of water were consumed

by UOG production in areas that were already under drought climate (i.e., >16 billion, >9 billion and >4 billion gallons between 2011 and 2019 for the state of Colorado, Weld County, and Garfield County, respectively). This disconnect between hydroclimate condition and water footprint of UOG activities was likely due to the high economic efficiency of water usage by UOG production.

One common perspective on UOG production is that it consumes negligible water compared to agricultural irrigation and other industrial sectors.[13, 40, 41] However, our findings demonstrate that the quantity of water consumption by UOG production is not trivial compared to regional municipal water usage in oil and gas producing areas of Colorado. In the presence of drought climates, which are projected to occur more frequently in the future,[42,43] the water use by UOG activities would sustain up to >110% of the population at the county scale, suggesting that the effects of UOG production on local water supply should not be neglected. Reducing water footprint of the UOG industry will enhance local water security that is being threatened by climate variability. Also, we present a new metric of drought-escaping distance in this study to quantify the spatial impacts of hydrodynamic conditions on the interactions between UOG production and regional water resources. Our results indicate that under extreme drought events, the UOG producers could have to travel greater than 500 miles to acquire water from areas without any water stress. This scenario is essentially infeasible due to the high cost of water transportation. As a result, the withdrawal of water for UOG production was more than likely to take place in areas that were already under water stress, thereby intensifying local water scarcity and competition.

In Colorado the oil and gas companies typically acquire water from other water users that hold water rights (e.g. irrigation, city water, or raw and treated wastewater from water provider), because Colorado's water rights system is based on the prior appropriation doctrine.[33] The UOG industry could obtain water by leasing from the municipalities (surface water from Colorado River Basin),[44] purchasing treated wastewater that would otherwise be discharged into surface water, or leasing agricultural irrigation water from landowners (surface water from a ditch or canal).[33] The oil and gas companies are willing to pay considerably higher prices for water than the agricultural sector.[35] Such an economic incentive motivates the diversion of water from the agricultural and municipal sectors to the UOG industry. Further, most groundwater wells in Colorado do not have water rights of an allowance for oil and gas well construction purposes. Specifically, the limitation on the water volume that is allowed to be withdrawn from groundwater wells in a given period of time would potentially prohibit the permits to well construction.[33] Thus, groundwater is not an appropriate source of sufficient water for the UOG industry in Colorado. Since surface water is also the primary water sources for agricultural irrigation and municipal usage in Colorado,[45,46] the water demand by the UOG industry would cause local water conflicts with other local water users such as the municipal and irrigation sectors, especially during drought periods.

Further, our study establishes a protocol to evaluate the interactions of UOG production with local water supply under hydroclimate variation. This protocol, which couples drought category with water footprint of UOG activities, can be expanded to other arid UOG producing-states (e.g.,

Texas, Oklahoma, and Wyoming). By integrating predictive tools of hydroclimate conditions[47] with the permitting and water use of UOG wells, it is possible to forecast the water consumption by the UOG industry in water-stressed areas, thereby providing value information for policy makers to better manage water resources in UOG-active regions. Such efforts, although are out of the scope of the current study, will be performed in our future work.

Our study also shows the potential of reusing wastewater generated during UOG production to reduce the water footprint and mitigate local water stress. Although our data support that such practice might compensate for a high proportion of water demand required by UOG activities, the prospects of UOG wastewater are still unclear and require more investigations on the associated economics, regulations, and technologies. Internal reuse of UOG wastewater for HF of new wells is the simplest approach that has been applied commonly in the state of Pennsylvania.[1, 31] However, this strategy is economically feasible only if the newly drilled wells are located in proximity with the existing UOG wells. Surface discharge of UOG wastewater into a nearby receiving waterway is another option of wastewater reuse, which supplements local water resources. Such a practice is regulated by the National Pollutant Discharge Elimination System (NPDES), which sets the maximum pollutant concentrations allowed in the discharged UOG wastewater. But it is still unknown whether direct surface discharge of UOG wastewater will pose long-term ecological and health risks, because numerous chemical species present in the UOG wastewater are not regulated by the NPDES permits. Recently, McLaughlin et al.[48] reported that more than 50 unregulated

geogenic and anthropogenic organic chemicals were identified at a discharge site of Wyoming, and that many of these compounds were also detected downstream of the discharge. Due to the increasing public awareness and improved understanding of the health thresholds for such chemicals, the regulations for UOG wastewater discharge are expected to become more stringent. As a result, advanced treatment might be needed to meet the regulatory requirement and ensure the safety of UOG wastewater reuse.

So far, tremendous efforts have been invested to develop technologies for the treatment of UOG wastewater,[29-31] which are able to effectively remove a majority of salts and contaminants. The treated UOG wastewater has the potential to be not only discharged into the surface water, but also utilized for other beneficial purposes such as agricultural irrigation.[49] However, those technologies are typically cost- and energy-consumptive, which are currently unable to compete with existing wastewater management practices such as deep-well injection. For example, reverse osmosis (RO) is the most energy efficient technology for UOG wastewater treatment,[50] but its treatment capability is constrained by the salinity limit (~70,000 mg/L of total dissolved solids, TDS) that is imposed by the maximum hydraulic pressure tolerated by membrane systems.[51] In contrast, thermal technologies such as mechanical vapor compression (MVC) is able to tolerate hypersaline wastewater, but their energy consumption is much higher due to the energy penalty associated with water evaporation and condensation. MVC also requires very high capital cost due to its required high temperature and expensive corrosive-resistant materials.[51] Recently, hybrid membrane-thermal technologies, including thermolytic forward osmosis (FO) and membrane

distillation (MD),[52, 53] have emerged as alternatives for UOG wastewater treatment. Although those technologies have the potential to reduce primary energy cost by utilizing low-grade waste heat, the availability and cost of waste heat usage have not been fully understood. As a result, high energy consumption and cost are still the main barriers to the practical adoption of wastewater treatment and reuse by the UOG industry. The advantages and limitations of current technologies for UOG wastewater treatment have been summarized in detail by several review articles in the literature, and the interested readers are recommended to read the references 29-31 of this article for more information.

As a result, more research is needed to reduce the economic cost and energy consumption of UOG wastewater treatment, and to provide both policymakers and energy producers with sufficient information that would result in incentives for wastewater treatment and reuse in the UOG industry. The results of our study could be indeed utilized by the policy makers to encourage UOG wastewater treatment and reuse, due to the water stress imposed by the UOG production especially under drought conditions. Appropriate treatment and reuse of UOG wastewater could preserve the water consumed by the UOG industry within the hydrological cycle (in contrast to deep-well injection), creating a new water supply to reduce the water footprint of the UOG industry. This will be the key to help us improve the sustainability at the water-energy-climate nexus in the context of rising UOG production and climate variation across the U.S. and the globe.

References

1. Vidic, R. D.; Brantley, S. L.; Vandenbossche, J. M.; Yoxtheimer, D.; Abad, J. D., Impact of shale gas development on regional water quality. *Science* 2013, 340, (6134), 1235009.
2. Kondash, A. J.; Lauer, N. E.; Vengosh, A., The intensification of the water footprint of hydraulic fracturing. *Sci Adv* 2018, 4, (8) , aar5982.
3. Chen, H.; Carter, K. E., Water usage for natural gas production through hydraulic fracturing in the United States from 2008 to 2014. *J Environ Manage* 2016, 170, 152-159.
4. U.S. Energy Information Administration. Annual Energy Outlook 2020. Table 14, Oil and Gas Supply. https://www.eia.gov/outlooks/aeo/data/browser/#/?id=14-AEO2020&cases=ref2020&sourcekey=0 (accessed July 10, 2020).
5. Clark, C. E.; Horner, R. M.; Harto, C. B., Life cycle water consumption for shale gas and conventional natural gas. *Environ Sci Technol* 2013, 47, (20), 11829-11836.
6. Kondash, A.; Vengosh, A., Water footprint of hydraulic fracturing. *Environ Sci Tech Let* 2015, 2, (10), 276-280.
7. Scanlon, B. R.; Reedy, R. C.; Male, F.; Hove, M., Managing the increasing water footprint of hydraulic fracturing in the Bakken Play, United States. *Environ Sci Technol* 2016, 50, (18), 10273-10281.
8. Brantley, S. L.; Yoxtheimer, D.; Arjmand, S.; Grieve, P.; Vidic, R.; Pollak, J.; Llewellyn, G. T.; Abad, J.; Simon, C., Water resource impacts during unconventional shale gas development: The Pennsylvania experience. *Int J Coal Geol* 2014, 126, 140-156.
9. Nicot, J. P.; Scanlon, B. R., Water use for shale-gas production in Texas, US. *Environ Sci Technol* 2012, 46, (6), 3580-3586.
10. Nicot, J. P.; Scanlon, B. R.; Reedy, R. C.; Costley, R. A., Source and fate of hydraulic fracturing water in the Barnett Shale: A historical perspective. *Environ Sci Technol* 2014, 48, (4), 2464-2471.
11. Gallegos, T. J.; Varela, B. A.; Haines, S. S.; Engle, M. A., Hydraulic fracturing water use variability in the United States and potential environmental implications. *Water Resour Res* 2015, 51, (7), 5839-5845.
12. Gregory, K. B.; Vidic, R. D.; Dzombak, D. A., Water management challenges associated with the production of shale gas by hydraulic fracturing. *Elements* 2011, 7, (3), 181-186.
13. Vengosh, A.; Jackson, R. B.; Warner, N.; Darrah, T. H.; Kondash, A., A critical review of the risks to water resources from unconventional shale gas development and hydraulic fracturing in the United States. *Environ Sci Technol* 2014, 48, (15), 8334-48.
14. Freyman, M. Hydraulic fracturing & water stress: Water demand by the numbers; Ceres: Boston, 2014. https://www.ceres.org/resources/reports/hydraulic-fracturing-water-stress-water-demand-numbers (accessed July 10, 2020).
15. Cook, B. I.; Ault, T. R.; Smerdon, J. E., Unprecedented 21st century drought risk in the American Southwest and Central Plains. *Sci Adv* 2015, 1, (1), 1400082.

16. Borsa, A. A.; Agnew, D. C.; Cayan, D. R., Ongoing drought-induced uplift in the western United States. *Science* 2014, 345, (6204), 1587-1590.
17. Shrestha, N.; Chilkoor, G.; Wilder, J.; Gadhamshetty, V.; Stone, J. J., Potential water resource impacts of hydraulic fracturing from unconventional oil production in the Bakken shale. *Water Res* 2017, 108, 1-24.
18. Cook, M.; Webber, M., Food, Fracking, and Freshwater: The potential for markets and cross-sectoral investments to enable water conservation. *Water-Sui* 2016, 8, (2), https://doi.org/10.3390/w8020045.
19. Colorado Oil and Gas Conservation Commission. Data. Downloads. https://cogcc.state.co.us/data2.html#/downloads (accessed July 10, 2020).
20. FracFocus Chemical Disclosure Registry. Data Download. http://fracfocus.org/node/356/done?sid=20159 (accessed July 10, 2020).
21. United State Drought Monitor. Data Download. Comprehensive Statistics. https://droughtmonitor.unl.edu/Data/DataDownloadComprehensiveStatistics.aspx (accessed July 10, 2020).
22. Robert J. Sterrett. Groundwater and wells. Johnson Screens New Brighton.(2007 Published), ISBN-13: 978-0978779306
23. Colorado Water Data Maintainer .USGS Water Use Data for Colorado. Retrieved from https://waterdata.usgs.gov/co/nwis/wu (accessed July 10, 2020)
24. FRED Economic Research. Retrieved from https://fred.stlouisfed.org (accessed July 10, 2020)
25. U.S. Energy Information Administration. Natural Gas Gross Withdrawals and Production. https://www.eia.gov/dnav/pet/hist/LeafHandler.ashxn=PET&s=F004008__3&f=M, (accessed July 10, 2020).
26. United States Drought Monitor, Drought Classification. https://droughtmonitor.unl.edu/About/AbouttheData/DroughtClassification.aspx (accessed July 10, 2020)
27. Abatatzoglou, J. T.; Mcevoy, D. J.; Redmdmond, K. T., The west wide drought tracker: Drought monitoring at fine spatial scales. *B Am Meteorol Soc* 2017, 98, (9), 1815-1820.
28. Svoboda, M.; LeComte, D.; Hayes, M.; Heim, R.; Gleason, K.; Angel, J.; Rippey, B.; Tinker, R.; Palecki, M.; Stooksbury, D.; Miskus, D.; Stephens, S., The drought monitor. *B Am Meteorol Soc* 2002, 83, (8), 1181-1190.
29. Tong, T. Z.; Carlson, K. H.; Robbins, C. A.; Zhang, Z. Y.; Du, X. W., Membrane-based treatment of shale oil and gas wastewater: The current state of knowledge. Front *Env Sci Eng* 2019, 13, (4) ,63 , https://doi.org/10.1007/s11783-019-1147-y.
30. Chang, H. Q.; Li, T.; Liu, B. C.; Vidic, R. D.; Elimelech, M.; Crittenden, J. C., Potential and implemented membrane-based technologies for the treatment and reuse of flowback and produced water from shale gas and oil plays: A review. *Desalination* 2019, 455, 34-57.

31. Shaffer, D. L.; Chavez, L. H. A.; Ben-Sasson, M.; Castrillon, S. R. V.; Yip, N. Y.; Elimelech, M., Desalination and reuse of high-salinity shale gas produced water: Drivers, technologies, and future directions. *Environ Sci Technol* 2013, 47, (17), 9569-9583.
32. Coonrod, C. L.; Yin, Y. B.; Hanna, T.; Atkinson, A. J.; Alvarez, P. J.; Tekavec, T. N.; Reynolds, M. A.; Wong, M. S., Fit-for-purpose treatment goals for produced waters in shale oil and gas fields. *Water Res* 2020, 173, 115467.
33. Colorado Oil and Gas Conservation Commission, Water sources and demand for the hydraulic fracturing of oil and gas wells in Colorado from 2010 through 2015. https://www.colorado.gov/pacific/sites/default/files/13WaterResources1010Water%20Sources%20and%20Demand%20for%20the%20Hydraulic%20Fracturing%20of%20Oil%20and%20Gas%20Wells%20in%20C.pdf (accessed September 13, 2020)
34. Garance, B., "Fracking fuels water fights in nation's dry spots," The Denver Post, https://www.denverpost.com/2013/06/16/fracking-fuels-water-fights-in-nations-dry-spots/ (accessed September 13, 2020)
35. Healy, J., For farms in the west, oil wells are thirsty rivals. The New York Times 2012, 5.https://www.nytimes.com/2012/09/06/us/struggle-for-water-in-colorado-with-rise-in-fracking.html. (accessed September 13, 2020)
36. Hitaj, C.; Boslett, A.; Weber, J. G., Shale development and agriculture. *Choices* 2014, 29, 1-7.
37. Rosa, L.; Rulli, M. C.; Davis, K. F.; D'Odorico, P., The Water-energy nexus of hydraulic fracturing: A global hydrologic analysis for shale oil and gas extraction. *Earths Future* 2018, 6, (5), 745-756.
38. Jessica,L. What the frack is happening in Colorado? A look inside Colorado's hydraulic fracking phenomenon. The 20 Stillwater Associates 7 (accessed September 13, 2020).
39. Aldo, S. Weld County bumps Garfield County as top Colorado gas source. The Denver Post 6 https://stillwaterassociates.com/what-the-frack-is-happening-in-colorado-a-look-inside-colorados-hydraulic-fracking-phenomenon/ (accessed September 13, 2020).
40. Jackson, R. B.; Vengosh, A.; Carey, J. W.; Davies, R. J.; Darrah, T. H.; O'Sullivan, F.; Petron, G., The Environmental Costs and Benefits of Fracking. *Annu Rev Env Resour* 2014, 39, 327-362.
41. Kondash, A. J.; Albright, E.; Vengosh, A., Quantity of flowback and produced waters from unconventional oil and gas exploration. *Sci Total Environ* 2017, 574, 314-321.
42. Vorosmarty, C. J.; Green, P.; Salisbury, J.; Lammers, R. B., Global water resources: Vulnerability from climate change and population growth. *Science* 2000, 289, (5477), 284-288.
43. Cayan, D. R.; Das, T.; Pierce, D. W.; Barnett, T. P.; Tyree, M.; Gershunov, A., Future dryness in the southwest US and the hydrology of the early 21st century drought. *P Natl Acad Sci* USA 2010, 107, (50), 21271-21276.

44. Walker, E. L.; Anderson, A. M.; Read, L. K.; Hogue, T. S., Water use for hydraulic fracturing of oil and gas in the South Platte River Basin, Colorado. *JAWRA Journal of the American Water Resources Association* 2017, 53, (4), 839-853.
45. Colorado Geoogical Survey [CGS]. n.d. Groundwater in Colorado – A primer. Talk, 2002, 5,(4). http://hermes.cde.state.co.us/drupal/islandora/object/co:3267 (accessed September 13, 2020).
46. Neil, G., Citizen's guide to where your water comes from. Colorado Foundation for Water Education 2005. https://www.colorado.gov/pacific/sites/default/files/Citizen%27s%20Guide%20to%20Where%20Your%20Water%20Comes%20From.pdf (accessed September 13, 2020).
47. Hao, Z.; AghaKouchak, A.; Nakhjiri, N.; Farahmand, A., Global integrated drought monitoring and prediction system. *Sci* Data 2014, 1, 140001.
48. McLaughlin, M. C.; Borch, T.; McDevitt, B.; Warner, N.; Blotevogel, J., Water quality assessment downstream of oil and gas produced water discharges intended for beneficial reuse in arid regions. *Sci Total Environ* 2020, 713, 136607.
49. Dolan, F. C.; Cath, T. Y.; Hogue, T. S., Assessing the feasibility of using produced water for irrigation in Colorado. *Sci Total Environ* 2018, 640, 619-628.
50. Elimelech, M.; Phillip, W. A., The future of seawater desalination: energy, technology, and the environment. *Science* 2011, 333, (6043), 712-717.
51. Tong, T.; Elimelech, M., The global rise of zero liquid discharge for wastewater management: drivers, technologies, and future directions. *Environ Sci Technol* 2016, 50, (13), 6846-6855.
52. McGinnis, R. L.; Hancock, N. T.; Nowosielski-Slepowron, M. S.; McGurgan, G. D., Pilot demonstration of the NH3/CO2 forward osmosis desalination process on high salinity brines. *Desalination* 2013, 312, 67-74.
53. Deshmukh, A.; Boo, C.; Karanikola, V.; Lin, S.; Straub, A. P.; Tong, T.; Warsinger, D. M.; Elimelech, M., Membrane distillation at the water-energy nexus: limits, opportunities, and challenges. *Energ Environ Sci* 2018, 11, (5), 1177-1196.

CHAPTER 5: The water footprint of hydraulic fracturing under different hydroclimate conditions in the central and western United States [2]

5.1 Introduction

Onshore oil and gas (O&G) development has contributed to a remarkable increase of energy production in the United States.[1] Technology advances in hydraulic fracturing (HF) and horizontal drilling have allowed for the enhancement of O&G production from low-permeability reservoirs.[2, 3] However, O&G production via HF is accompanied by substantial volumes of freshwater withdrawal and wastewater generation.[4-11] During the years of 2009-2017, the water consumption and wastewater production associated with HF activities totaled ~1.8 billion m^3 (~ 480 billion gallons) and 3.4 billion m^3 (~900 billion gallons) in the U.S.[12] Meanwhile, the water consumption per well had increased by up to 770% from 2011 to 2016 in major U.S. shale plays, and the volumes of flowback and produced water (FPW) generated within the first year of production had increased by up to 550%.[2]

The major shale plays in the U.S. are located in at least 18 states, a majority of which belong to the arid central and western U.S.[13] The geographical coincidence of O&G-producing regions with areas of water scarcity has been commonly used in the literature to demonstrate the potential

[2] This chapter will be submitted as a manuscript under review as

Du, X.; Carlson, K. H.; & Tong, T., The water footprint of hydraulic fracturing under different hydroclimate conditions in the central and western United States, *Sci. Total Environ.* 2022. (Under review).

of O&G activities to alter regional water supply and justify the need of FPW reuse.[12, 14-16] However, the total water use by the O&G industry is equivalent to only a small proportion of those by other more water-demanding sectors such as irrigation at the national or state scale.[15, 17] Although a few public reports have showed intensified water stress due to O&G production in semiarid regions,[8, 15, 18] the influence of O&G production on regional water scarcity is still questionable. For example, Saha et al.[19] suggest that relatively little attention has been paid to quantify and understand the impacts of O&G production on other local water users. Moreover, as pointed out by the Center for American Progress,[20] we still lack sufficient data needed to understand the risks that O&G production imposes on water supplies. Considering the O&G-producing regions experience varying hydrodynamic conditions, the water consumption of HF under dry or drought conditions are more likely to cause intensive competition for local water resources than those under normal or humid conditions. Thus, quantifying the water footprint of HF under different hydrodynamic conditions, which is still lacking in the literature, is essential to better understand the potential impacts imposed by O&G production on water sustainability in the context of a changing climate. Additionally, since the intensive water withdrawal by HF activities typically occur locally (to avoid expensive water transportation costs),[21] the role of O&G production in altering water resource allocation is more profound at the local space. To the best of our knowledge, spatiotemporal analyses of HF water footprint and its potential impact on water stress at the local scale have not been performed.

The main objective of this study is to investigate the water footprint of HF under different hydroclimate conditions for 11 major O&G-producing states located in the arid central and western U.S. We quantify the drilling activities, water consumption of hydraulically fractured wells, and the generation of FPW under various hydroclimate conditions (from abnormally dry to exceptional drought) on a monthly basis within a 10-year period from 2011 to 2020. In order to further understand the effects of O&G production on local water stress, we perform a detailed spatiotemporal analysis that compares the water consumption of HF under abnormally dry or drought conditions with the water usage of irrigation and domestic sectors at the county level. We also calculate the volumetric ratios of FPW generation to HF water usage under each drought category to evaluate the potential of FPW reuse in mitigating the potential water stress imposed by O&G production.

5.2 Materials and Methods

5.2.1 Data acquisition

The drought maps of each week from 2011 to 2020 were obtained from the U.S. Drought Monitor (USDM) database.[22] We chose the drought map in the middle of each month to represent the drought condition of the entire month, because the drought condition does not change significantly within a month and the drilling activities are typically continued for weeks.[23] The number and locations of HF wells drilled within the period of 2011 to 2020, as well as the corresponding water usage data, were downloaded for 11 central and western U.S. states (AR, CO, KS, LA, ND, MT,

NM, OK, TX, UT, WY) from the FracFocus Chemical Disclosure Registry (referred to as the FracFocus database in this study).[24] This database has been commonly used in the literature to quantify the water consumption by HF activities in the U.S.[2, 3, 5, 14, 25, 26] The production volumes of FPW along with the location of each reported well were downloaded from the Enverus DrillingInfo database,[27] in which the data were not available for Oklahoma and Kansas. For Oklahoma, we were able to estimate the volumes of FPW based on the injection volume of saltwater disposal wells (SWD, data obtained from the Enverus DrillingInfo database), according to the analysis performed by Scanlon et al.[12, 16] In addition, the data of irrigation water usage and domestic water usage per capita at the county level for the 11 states were provided by the U.S. Geological Survey (USGS), using the most recent publicly available data of 2015.[28] The annual statistics of population for counties from 2011 to 2020 were downloaded from the U.S. Census Bureau in order to estimate the domestic water usage per county.[29]

5.2.2 Hydroclimate conditions

According to USDM, the drought magnitude is classified into five categories, with D0, D1, D2, D3, and D4 representing abnormally dry, moderate drought, severe drought, extreme drought, and exceptional drought, respectively.[30] Areas not assigned to any drought category indicate those subject to normal or humid hydroclimate conditions. The detailed information for the drought categories could be found on the USDM website.[30] In order to quantify the drought magnitude,

drought severity classification index (DSCI) was used by converting the area percentages under different drought categories to a single value (Equation 5-1):[31]

$$DSCI=0\times S_{D0} + 1\times S_{D1} + 2\times S_{D2} + 3\times S_{D3} + 4\times S_{D4} \qquad (5\text{-}1)$$

where the values of S_{D0} to S_{D4} refer to the area percentages of the corresponding drought category in each state. The DSCI calculated in the middle of each month was used to represent the monthly DSCI value, in accordance with the selection of drought map.

5.2.3 HF water consumption and FPW production under different hydroclimate conditions

In this study, a total of 159,750 individual HF wells recorded in the Fracfocus database were analyzed for the 11 O&G-producing states. These HF wells were sorted by the job start date and grouped into months. The locations of HF wells, which were based on the latitude and longitude data, were overlapped with the drought maps using Geographic Information System (GIS) software (ArcGIS 10.5.1, ESRI). The "Join" tool of ArcGIS was used to calculate the well number and HF water usage under different drought categories. Furthermore, the spatiotemporal distribution of HF water usage under D0−D4 drought categories (i.e., abnormally dry or drought climates) was calculated and compared with the water usage of irrigation and domestic sectors at the county level. As for the irrigation sector, we selected the counties with annual water consumption of irrigation ≥500 million gallons (referred to as the irrigation-active county in this study), in order to avoid the inclusion of counties with no or negligible irrigation activities. We mainly focused on comparing the HF water consumption under arid climates with irrigation water

usage in those counties. In addition, we estimated the FPW production under each hydroclimate condition by combining the FPW data with the USDM drought maps and calculated the volumetric ratio of FPW generation to HF water usage each year for 10 states (except for KS where both FPW and SWD data were not available), in order to investigate the potential of FPW reuse to reduce the water footprint of HF activities.

5.3 Results and Discussion

5.3.1 Hydroclimate variation and HF activities in 11 O&G-producing states of central and western U.S.

All the 11 O&G-producing states in the central and western U.S. had been subject to periods of water scarcity between 2011 and 2020 (Figure 5-1 and Figure B1), with significant portions of the state areas covered by different magnitudes of drought categories (D0 category indicates abnormally dry while D1-D4 categories correspond to moderate to exceptional drought, as defined by USDM)[30]. D0 or higher drought categories occurred more than 80% of the time for all the states (Figure 5-1a). Texas and New Mexico experienced the longest drought periods among the investigated states, with D0 or higher drought categories recorded within the state more than 99% of the time (Figure 5-1a and Figure B1). Extreme drought events were observed periodically for all the states. During such periods, up to ~100% of the state area was affected by drought climates, with the occurrence of extreme (D3) and exceptional (D4) drought conditions (see Figure B1). In particular, D3 and D4 drought categories existed more than 50% of the time in Colorado, Kansas,

New Mexico, Oklahoma, and Texas from 2011 to 2020 (see Figure B2). In those states, D3 and D4 categories were recorded for 67-87 months, covering up to 77.7%-97.0% of the state area on a monthly basis (see Figure B1). According to USDM, drought conditions under D3 and D4 categories cause high levels of crop or pasture losses, accompanied by severe water shortages and restrictions. The prolonged and intense water scarcity witnessed by the O&G-producing states in the central and western U.S. potentially led to HF water consumption under water stress, inducing intensified competition for local water resources between the O&G industry and other water-demanding sectors.

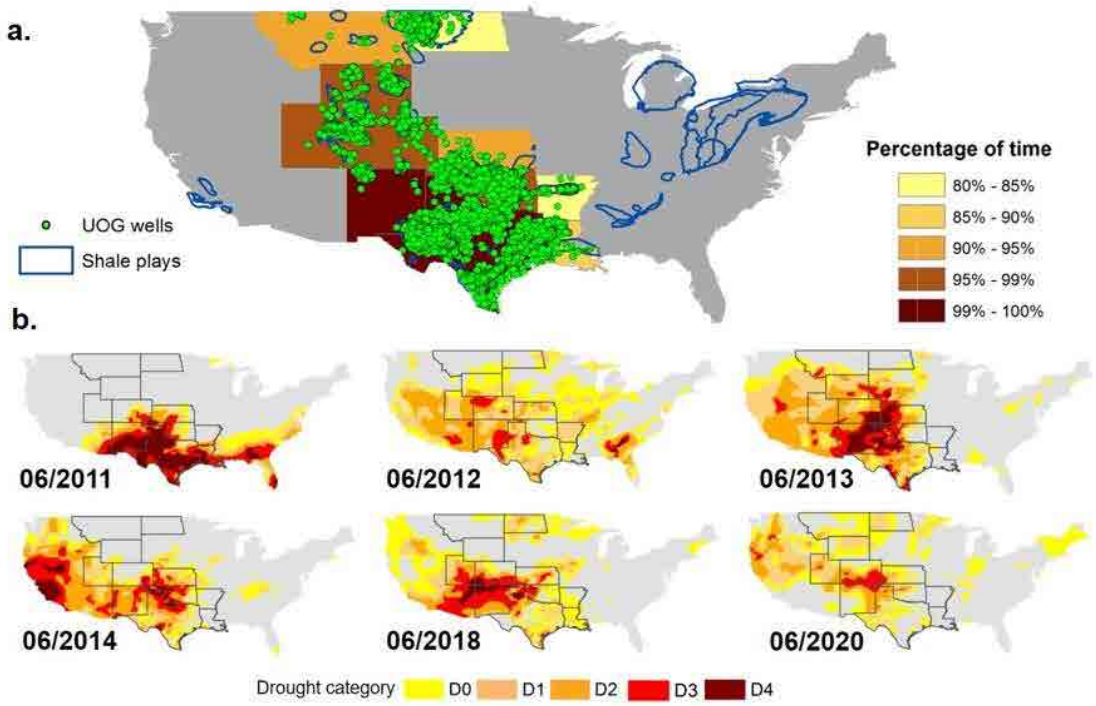

Figure 5-1. (a) Map of O&G well locations across 11 O&G-producing states in the central and western U.S. and the time percentage of each state when D0 or higher drought categories occurred during the period of 2011-2020 in each state. (b) Representative maps of drought severity and coverage in June. Those maps provide evidence that the 11 O&G-producing states investigated in the current study are often under abnormally dry or drought conditions. D0 to D4 refer to different drought categories as defined by the U.S. Drought Monitor.

During the period of 2011 to 2020, HF activities consumed a total of 956.8 billion gallons (3.6 billion m^3) water for 159,750 wells in the 11 central and western states. The statewide water consumption by HF varied from 1 billion gallons (3.8 million m^3) in Kansas to 584.8 billion gallons (2.2 billion m^3) in Texas, with Texas contributing to 61.1% of the total HF water use (Figure B3, Appendix B). The water usage per well climbed with time in eight states (CO, LA, ND, NM, OK, TX, UT, and WY; Figure B4), with a high increase rate ranging from 220% in Oklahoma to 1,904% in New Mexico from 2011 to 2020. Accordingly, a remarkable rise of monthly water consumption was also observed in those states (see Figure B1), even though the number of newly drilled wells did not show a similarly increasing trend (see Figure B5). The increase of water use by HF, which has been also reported by Kondash et al.[2], was likely due to the increase of horizontal drilling[18] and technological evolution (e.g., the change of fracking fluid from gel to slickwater) that requires more water and enables longer lateral length.[18, 32]

We further performed correlation analyses to investigate whether the HF activities were constrained by hydroclimate variation. As shown in Figure B6, hydroclimate condition (as indicated by DSCI) does not exhibit a negative relationship with the number of newly drilled HF wells in all the 11 O&G-producing states. Therefore, hydroclimate variation did not prohibit drilling activities under drought conditions. On the other hand, the number of newly drilled HF wells was correlated positively with the crude oil price in 10 states (Pearson's $r > 0.33$, $p < 0.001$, see Figure B7) except for New Mexico, consistent with the common notion that economic incentives drive O&G companies to increase their drilling activities.

5.3.2 HF activity and water consumption under different hydroclimate conditions

Although hydroclimate variation has posed no significant impact on the HF activities, a substantial portion of HF wells were drilled in areas that were suffering water shortage due to dry or drought conditions. The water consumption by these wells, which has not received sufficient attention so far, has more implications to regional water sustainability than the overall water footprint of O&G production typically reported in the literature. As shown in Figure 5-2, 11.3%-98.2% of newly drilled HF wells in Texas (532-13,694 wells per year) were located under abnormally dry or drought conditions on a yearly basis. These wells were responsible for 11.2%-98.9% of annual HF water consumption (4.6 to 64.2 billion gallons per year, or 17.4 to 243 million m^3 per year, see Figure B8), contributing to 51.9% of the total HF water usage in Texas during 2011-2020 (Figure 5-3). Particularly, more than 80% of the drilling activities and HF water usage in Texas occurred under abnormally dry or drought conditions every year during the period of 2011 to 2014 (Figure 5-2 and Figure B8), when a prolonged and extreme drought event was present (see Figure B1). During this highly water-stressed period, at least 4.7 billion gallons (17.8 million m^3) of water were consumed under extreme and exceptional drought conditions (D3 and D4 drought categories) annually in Texas. The HF drilling activities in the other 10 states also occurred under abnormally dry or drought conditions nearly every year (only MT, AR and ND saw 6 years, 3 years and 1 year when all the HF wells were drilled in areas outside any drought category, respectively) (Figure 5-2). It is worth to mention that for several states (e.g., TX, OK, NM, LA, WY, UT, and KS), up to

(nearly) 100% of annual drilling activities and HF water usage occurred within areas that were covered by D0 or higher drought categories.

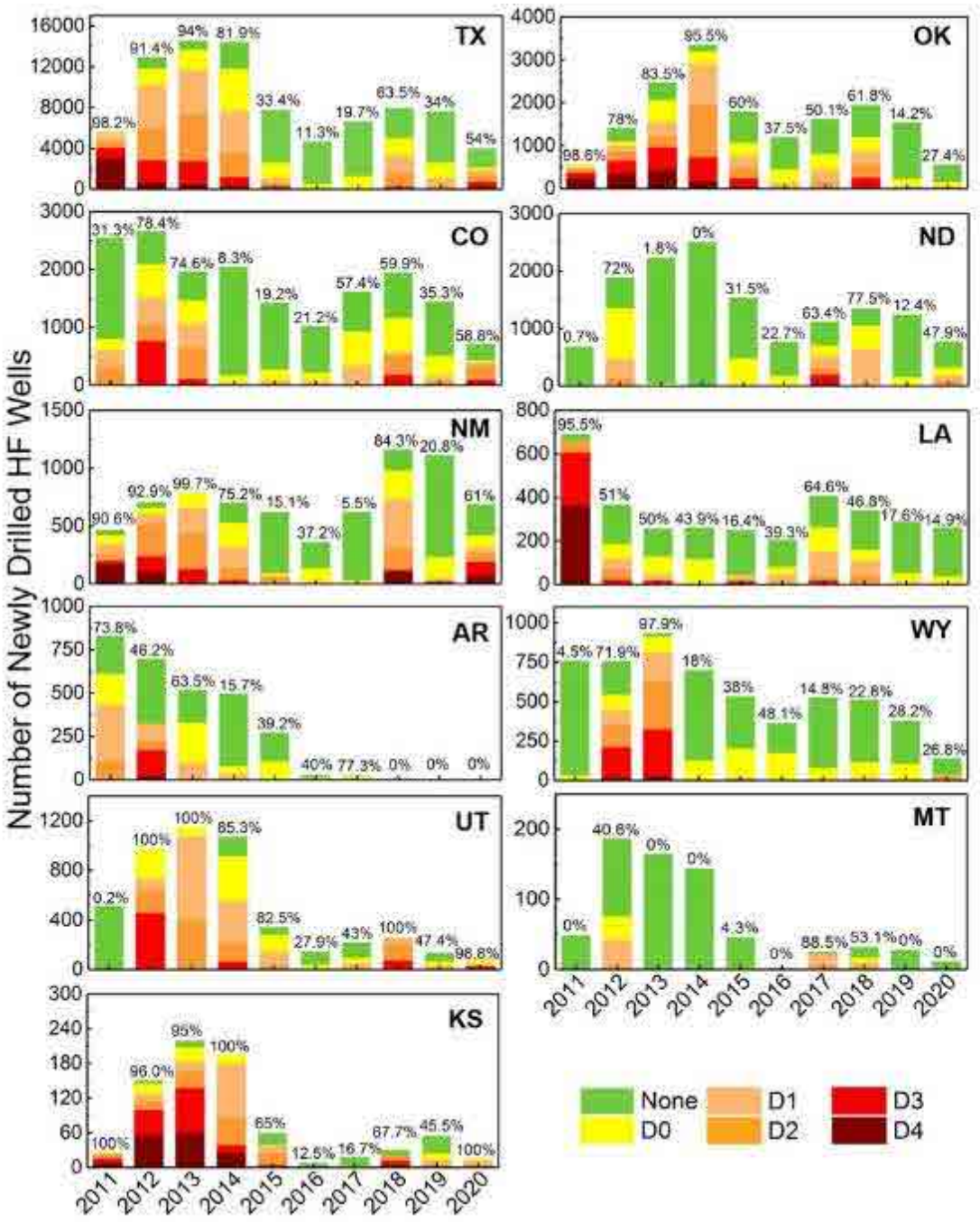

Figure 5-2. Annual number of newly drilled HF wells located in non-arid areas or areas under different drought categories from 2011 to 2020 in 11 O&G-producing states. The value above each

bar indicates the percentage of wells that were located in arid areas under abnormally dry or drought (D0-D4) conditions.

During the period of 2011 to 2020, HF activities under D0 or higher drought categories in the 11 investigated states consumed a total of 475.3 billion gallons (1.8 billion m^3) water, which accounted for 49.7% of the total HF water usage (Figure 5-3). Such a percentage varies from 13.7% (MT) to 92.7% (KS) at the state level. Texas consumed the highest quantity of water under D0 or higher categories (303.3 billion gallons or 1.2 billion m^3), followed by Oklahoma (56.6 billion gallons or 214.3 million m^3), Colorado (35.7 billion gallons or 135.1 million m^3), and North Dakota (26 billion gallons or 98.4 million m^3). Further, HF activities that occurred under extreme (D3) and exceptional (D4) drought conditions consumed a total of 86.1 billion gallons (325.9 million m^3) of water in the 11 states during this 10-year period, contributing to 9% of the total HF water usage.

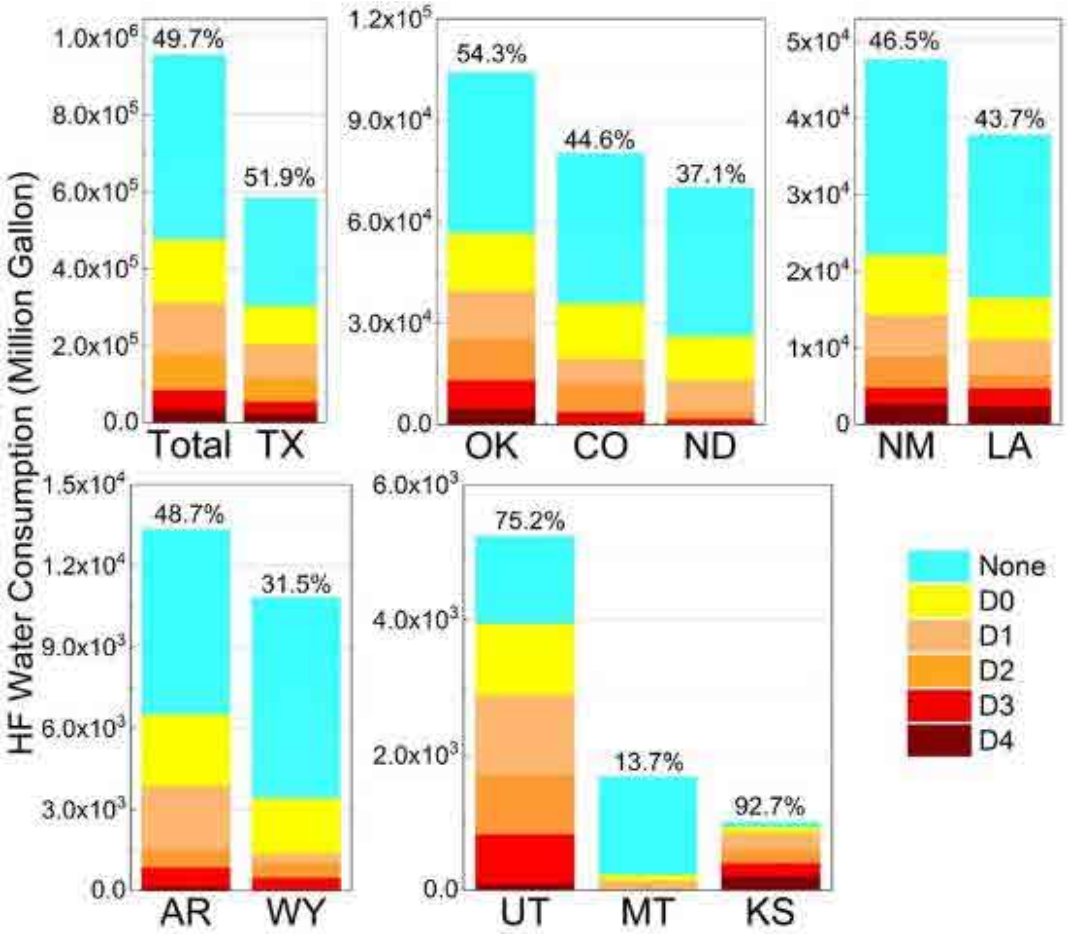

Figure 5-3. Water consumption by newly drilled HF wells located in non-arid areas or areas under different drought categories during 2011 and 2020 in 11 O&G-producing states. The value above each bar indicates the percentage of water consumption in arid areas under abnormally dry or drought (D0-D4) conditions.

According to the USDM, the historical observed impacts of drought on water supplies and water users for different drought categories (D0-D4) vary across states.[33] In Texas, for example, D0 or higher drought categories indicate the decrease of surface water levels while D3 or higher drought categories indicate the occurrences of exceptional water shortages, dryness of surface water sources, as well as the declining of water table.[33] It has been observed that water scarcity, large agricultural economic losses and decrease of the reservoir levels occurred under D3 or higher

drought categories in Oklahoma and Colorado.[33] Under such scenarios, the high volumes of water consumption by HF activities potentially intensify the competition among other local water users (e.g., irrigation and domestic users).

5.3.3 Potential effects of O&G production on local water allocation

Although the above analyses demonstrate high volumes of water consumption by HF activities within areas under water stress in the central and western U.S., the HF water usage is dwarfed statewide by the water consumption of other sectors such as irrigation at the state level (see Figure B9). However, the water use of HF activities under abnormally dry or drought conditions potentially imposes significant impacts on the allocation of water resources at the local level, especially for small rural counties with limited water infrastructure capacity.[34] In order to quantify such effects, we performed spatiotemporal analysis to not only quantify the water footprint of HF with hydroclimate condition at the county level, but also compare HF water usage with regional irrigation and domestic water usage.

During the period of 2011-2020, high densities of water consumption by HF activities occurred under arid conditions in the O&G-active counties. For the 11 states investigated in this study, the annual HF water usage under D0 or higher categories were > 500 million gallons (1.9 million m^3) for 5-39 counties (depending on the specific year), in which 1-31 counties experienced HF water consumption > 1 billion gallons (3.8 million m^3) per year (Figure B10). When compared to the irrigation sector, the HF water usage under D0 or higher drought categories was equivalent

to more than 10% of the total water consumption by irrigation in 6-29 irrigation-active counties (i.e., counties with annual water consumption of irrigation ≥500 million gallons) each year (Figure 5-4 and Figure B11). As shown in Figure B11, the irrigation water use in such counties was up to 4.2-28.7 billion gallons (15.7-108.5 million m^3). This result indicates that the water consumption by HF under arid conditions could equal to a high percentage of irrigation consumption (e.g., ≥10%) in the counties with high extents of agricultural activities. Further, our data also showed that the HF water usage under abnormally dry or drought conditions was able to sustain more than 50% and 100% of domestic water usage in 11-51 and 6-41 counties per year, respectively (Figure 5-5). The high volumetric ratios of HF to irrigation and domestic water usage were mainly observed in the states of Texas, Oklahoma, and North Dakota. In Texas, for example, there were 17 irrigation-active counties and 28 counties where more than 10% of irrigation water usage and 50% of domestic water consumption were satisfied by the water consumed by HF under D0-D4 drought categories in 2018, respectively (Figure 5-4 and Figure 5-5). Within those counties, 14 counties witnessed HF water usage of > 1 billion gallons under D0 or higher drought categories (e.g., HF activities consumed 5.9 billion gallons or 22.3 million m^3 of water under abnormally dry or drought conditions in Martin County, Texas).

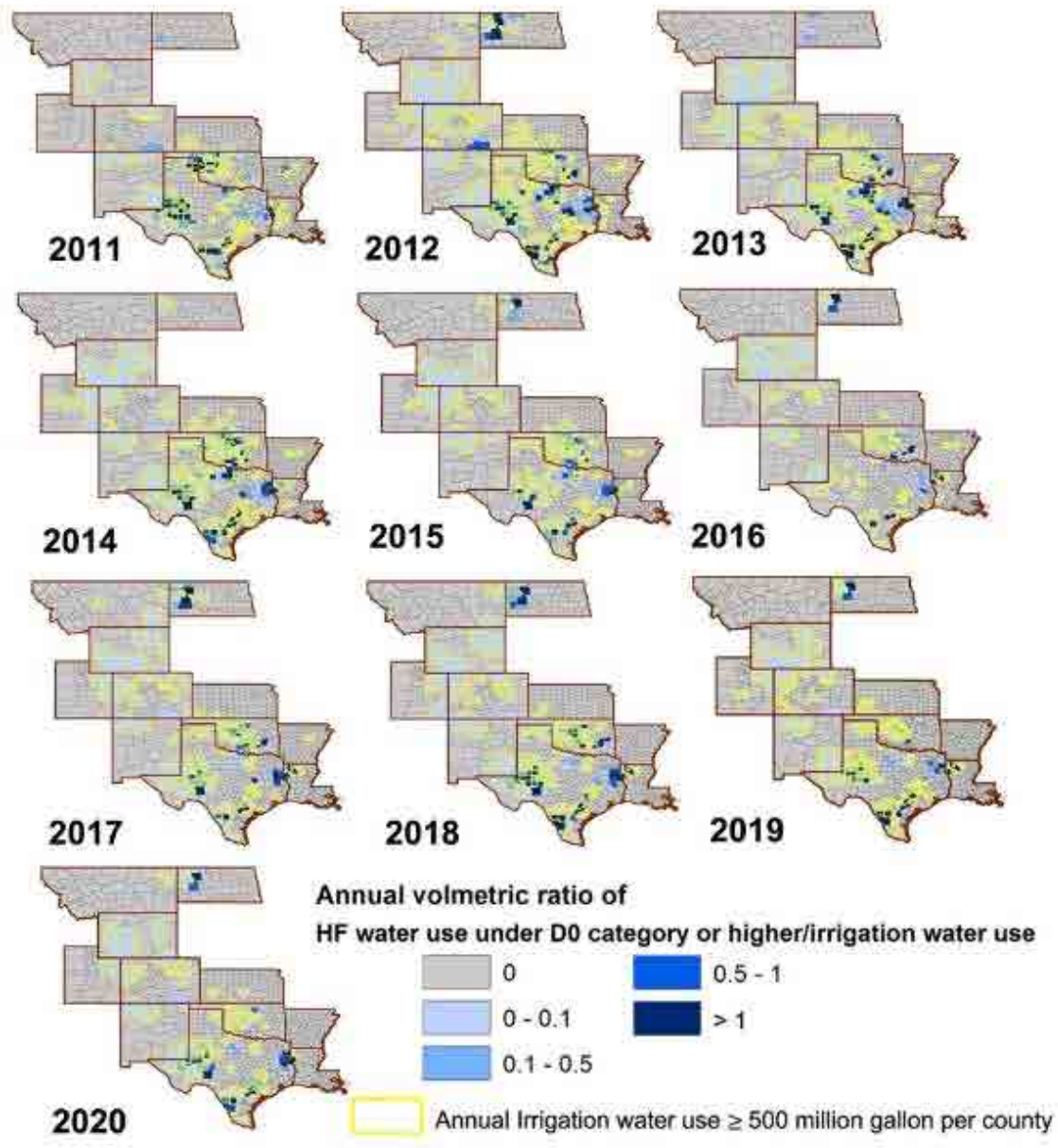

Figure 5-4. Annual volume ratio of HF water usage under abnormally dry or drought (D0-D4) conditions to irrigation water usage at the county level from 2011 to 2020 in 11 O&G-producing states. The annual irrigation water use were ≥ 500 million gallons in the counties with a yellow outline. The most recent available data of irrigation water usage in the year of 2015 were used.

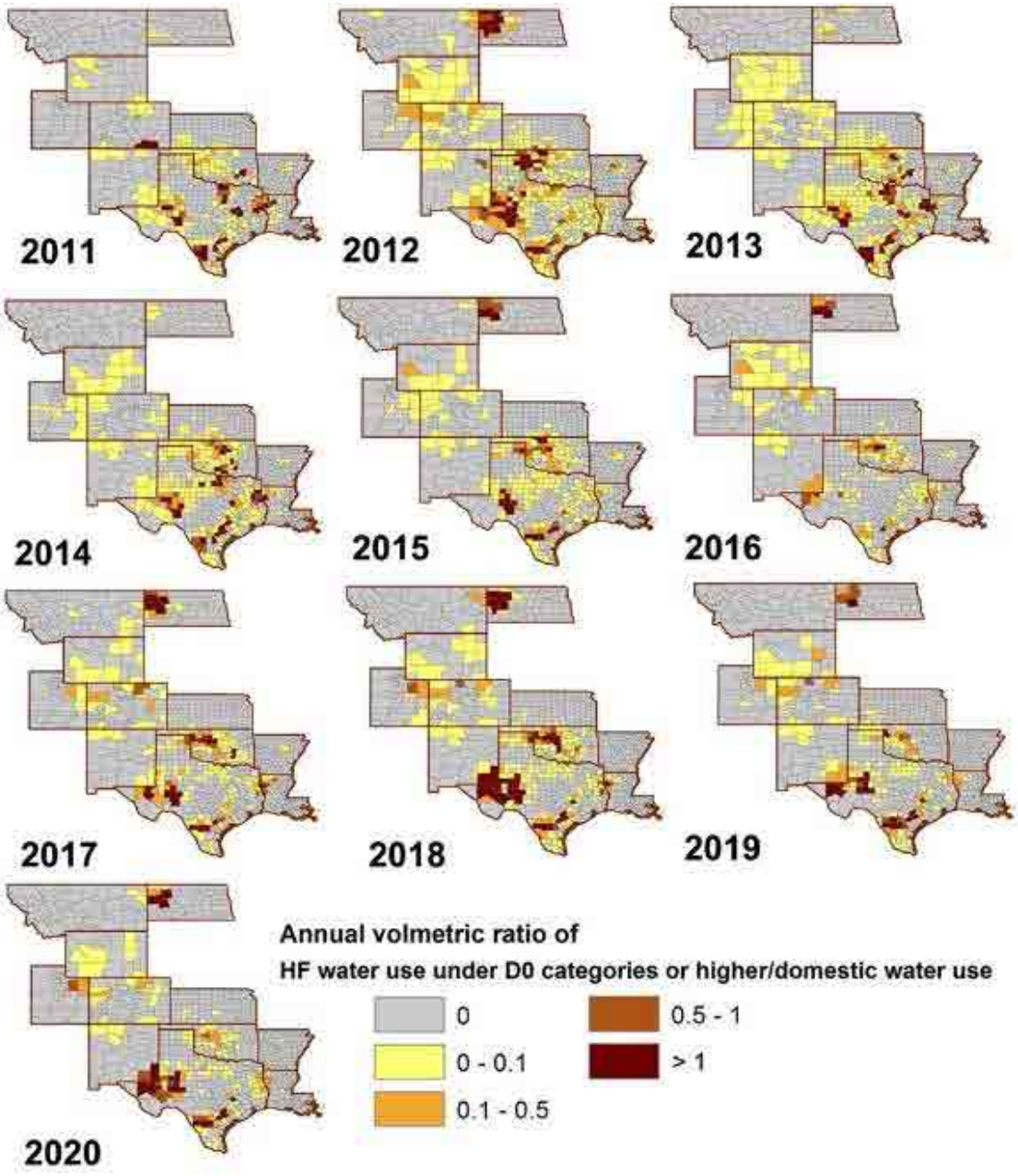

Figure 5-5. Annual volume ratio of HF water usage under abnormally dry or drought (D0-D4) conditions to domestic water usage at the county level from 2011 to 2020 in 11 O&G-producing states.

As a result, the HF water usage under water stress could be equal to a high proportion of irrigation and domestic water usage at the county scale (which is not observed at the national or state scale), thereby playing a significant role in local water allocation. This finding is supported

by several media reports that the water consumption by O&G production had already caused conflicts with other local water users such as farmers under drought conditions in Texas, Oklahoma, Colorado, and North Dakota,[35-36] where counties with high densities of HF water usage under arid conditions were mainly located (Figure 5-4, Figure 5-5, and Figure B10). For example, several small communities had already or nearly run out of water in the O&G-active counties of Texas in 2014 due to the combination of high demand of water by HF and extreme drought.[31]

5.3.4 Comparison of HF water usage with flowback and produced water under arid conditions

Appropriate treatment and reuse of FPW is a promising strategy to mitigate the water footprint of HF and minimize the stress imposed by the O&G industry on local water resources. As shown in Figure 5-6, the volumes of FPW were equivalent to a high proportion or even exceeded the water demand of HF under abnormally dry or drought conditions, especially for states subject to long periods of drought (e.g., TX, OK, and CO). For example, 2.6-32.4 billion gallons (9.8-122.7 million m^3) of FPW were generated under D0 or higher drought categories each year in Texas, accounting for 12.1%-98.9% of its total FPW production (see Figure B12). Correspondingly, the yearly volumetric ratio of FPW to HF water usage under abnormally dry or drought conditions varied from 0.3 to 1.2 in Texas (Figure 5-6). Under extreme and exceptional drought conditions (D3 and D4 categories), the volumes of FPW generated in Texas were equal to up to 130% of the volume of HF water use (with an average of 36% for 2011-2020). For the other states, the yearly volumetric ratio of FPW to HF water use varied from up to 1.4 (for CO) to 76.7 (for MT) under

D0 to D4 categories, and up to 1.4 (for ND) to 65.8 (for UT) under D3 to D4 categories (Figure 5-6). These results indicate that with proper treatment and reuse strategies, FPW is able to serve as a valuable water source that effectively reduces the water footprint by HF activities under water-stressed conditions.

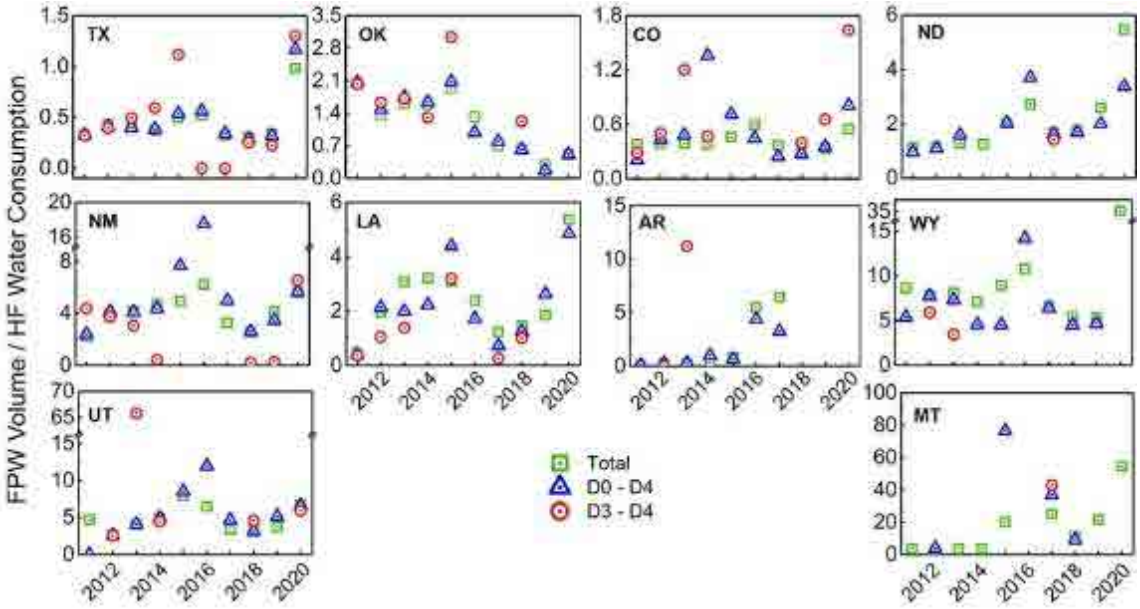

Figure 5-6. Annual volumetric ratio of FPW generation to water consumption by HF under different hydroclimate conditions (total, D0-D4 categories, or D3-D4 categories) from 2011 to 2020 for 10 O&G-producing states. The FPW data for the state of Kansas are not available. The lack of some blue and red scatters in the states of OK, CO, ND, NM, LA, AR, WY, UT and MT is due to no HF water consumption occurred under certain scenarios.

5.3.5 Implications

As reported by the U.S. EPA,[37] the water consumed by HF activities is typically freshwater taken from available groundwater and/or surface water resources located near O&G wells, which are the same water sources for domestic and irrigation water users.[37, 38] In semiarid regions, O&G companies also purchase water from the other local water users (e.g., farmers) with a much higher price.[38-40] The trades of water have already taken place between farmers and O&G companies in Colorado, North Dakota, and Utah.[41] In the City of Greeley, for example, the O&G companies paid $3,300 an acre foot of water in 2012, while the farmers paid only $30 for the same amount of water.[42] Thus, O&G companies are able to obtain sufficient water supplies for HF activities even under drought conditions, resulting the reduction of water availability for other water users.

Several public reports have shown the local impacts of O&G activities on water availability have occurred in the O&G-producing regions, especially under drought conditions.[12, 34, 43, 44] For example, Lin et al.[44] reported that groundwater levels decreased in three aquifers that are the primary water resources for HF activities in the Bakken shale play. Moreover, Scanlon et al.[12] found that HF activities had depleted the groundwater resources in several semiarid regions in western Eagle Ford shale play. In most O&G-producing regions in Texas and Colorado, HF activities created intensified competition and conflicts between other local water users such as farmers and domestic users during extreme drought periods.[45] As water restrictions or emergencies have been occurring at increasing frequencies due to a changing climate,[46] the competition of O&G production with other water users for local water resources under water scarcity does not only

compromise environmental justice but results in an increase of public resistance.[47] Such significant implications could not be reflected by the total water footprint of HF at the national or state levels but are unveiled by quantifying HF water usage under various hydroclimate conditions at the local scale as demonstrated in the current study.

Furthermore, the reuse of FPW has a promising potential to mitigate the water footprint of HF activities. The treatment and beneficial reuse of FPW, either for internal (i.e., drilling of new wells) or external (e.g., surface discharge and irrigation) purposes,[16, 48-50] could play a key role in alleviating the local water stress caused by O&G production. Indeed, the O&G industry has been recently attempting to increase the reuse FPW especially for internal reuse for HF activities.[48, 51] However, the treatment of O&G wastewater for external reuse requires more cost than deep-well injection[37] (the current business-as-usual practice for O&G wastewater management[16]) and thus has not been widely adopted in the industry. The efforts of FPW reuse have the potential to effectively reduce the water footprint of O&G production, but this factor could not be considered in this study due to the lack of data. If the data pertaining to FPW reuse are reported and available from publicly accessible database (similar to the water use data of the FracFocus database) in the future, additional work will be performed to adjust the values of HF water footprint reported by this study and others.[2, 12, 52-54]

Along with the needs of technology innovation to improve the economic viability, the incentives from the policy level or the public are important to practical implementation of O&G wastewater treatment and reuse. Hannibal et al.[47] reported that individuals who live in counties

experiencing drought conditions recognize the effects of HF activities on local water supplies, and thus are willing to support regulatory aspects of HF activities. The data provided in our study can be used to motivate policy makers, regulators, and O&G producers to transform the water resource management paradigm of the O&G industry towards FPW treatment and reuse, in order to improve water sustainability of the O&G-producing regions with both a rising O&G industry and climate change.

5.4 Conclusion

We quantified the water consumption of HF under various hydroclimate conditions in the central and western U.S during a 10-year period of 2011-2020. Our results show that high volumes of water had been consumed by HF activities within areas that were already under water stress. For the 11 O&G-producing states investigated in this study, a total of 475.3 billion gallons (1.8 billion m^3) of water was consumed by HF activities under abnormally dry or drought categories, with 86.1 billion gallons (325.9 million m^3) of water consumed under extreme and exceptional drought conditions. We also demonstrate that the water footprint of HF activities under abnormally dry or drought conditions could translate to high densities of local water consumption, equivalent to more than 10% and 50% of the water demand by irrigation and domestic sectors in 6-29 irrigation-active counties and 11-51 counties per year during 2011-2020, respectively. These results provide quantitative evidence that O&G activities under arid hydroclimate conditions are likely to alter water supply threatened by climate variability and intensify local competition for water resources.

Furthermore, we reveal that the volumes of FPW generated from O&G production exceeded or were equivalent to a high proportion of water consumption by HF under abnormally dry or drought conditions. Appropriate treatment and beneficial reuse of FPW, therefore, is a promising strategy to mitigate the water footprint of HF and improve regional water sustainability in the context of climate change.

References

1. Vidic, R. D.; Brantley, S. L.; Vandenbossche, J. M.; Yoxtheimer, D.; Abad, J. D., Impact of shale gas development on regional water quality. *Science*, 2013, 340, 1235009.
2. Kondash, A. J.; Lauer, N. E.; Vengosh, A., The intensification of the water footprint of hydraulic fracturing. *Sci. Adv.,* 2018, 4, DOI: 10.1126/sciadv.aar5982.
3. Chen, H.; Carter, K. E., Water usage for natural gas production through hydraulic fracturing in the United States from 2008 to 2014. *J. Environ. Manage.,* 2016, 170, 152-159.
4. Clark, C. E.; Horner, R. M.; Harto, C. B., Life Cycle Water consumption for shale gas and conventional natural gas. *Environ. Sci. Technol.,* 2013, 47, 11829-11836.
5. Kondash, A.; Vengosh, A., Water footprint of hydraulic fracturing. *Environ. Sci. Tech. Let.*, 2015, 2, 276-280.
6. Scanlon, B. R.; Reedy, R. C.; Male, F.; Hove, M., Managing the increasing water footprint of hydraulic fracturing in the Bakken Play, United States. *Environ. Sci. Technol.*, 2016, 50, 10273-10281.
7. Brantley, S. L.; Yoxtheimer, D.; Arjmand, S.; Grieve, P.; Vidic, R.; Pollak, J.; Llewellyn, G. T.; Abad, J.; Simon, C., Water resource impacts during unconventional shale gas development: The pennsylvania experience. *Int. J. Coal Geol.,* 2014, 126, 140-156.
8. Nicot, J. P.; Scanlon, B. R., Water use for shale-gas production in Texas, US. *Environ. Sci. Technol.,* 2012, 46, 3580-3586.
9. Nicot, J. P.; Scanlon, B. R.; Reedy, R. C.; Costley, R. A., Source and fate of hydraulic fracturing water in the Barnett Shale: A historical perspective. *Environ. Sci. Technol*., 2014, 48, 2464-2471.
10. Gallegos, T. J.; Varela, B. A.; Haines, S. S.; Engle, M. A., Hydraulic fracturing water use variability in the United States and potential environmental implications. *Water Resour. Res.*, 2015, 51, 5839-5845.
11. Gregory, K. B.; Vidic, R. D.; Dzombak, D. A., Water management challenges associated with the production of shale gas by hydraulic fracturing. *Elements*, 2011, 7, 181-186.
12. Scanlon, B. R.; Ikonnikova, S.; Yang, Q.; Reedy, R. C., Will water issues constrain oil and gas production in the United States? *Environ. Sci. Technol.,* 2020, 54, 3510-3519.
13. Vengosh, A.; Jackson, R. B.; Warner, N.; Darrah, T. H.; Kondash, A., A critical review of the risks to water resources from unconventional shale gas development and hydraulic fracturing in the United States. *Environ. Sci. Technol.,* 2014, 48, 8334-8348.
14. Freyman, M., Hydraulic fracturing & water stress: Water demand by the numbers. Ceres Boston, MA: 2014.
15. Scanlon, B. R.; Reedy, R. C.; Nicot, J. P., Will water scarcity in semiarid regions limit hydraulic fracturing of shale plays? *Environ. Res. Lett.,* 2014, 9, 124011.

16. Scanlon, B. R.; Reedy, R. C.; Xu, P.; Engle, M.; Nicot, J.; Yoxtheimer, D.; Yang, Q.; Ikonnikova, S., Can we beneficially reuse produced water from oil and gas extraction in the US? *Sci. Total. Environ.,* 2020, 717, 137085.
17. Guerra, K.; Dahm, K.; Dundorf, S., Oil and gas produced water management and beneficial use in the Western United States. *US Department of the Interior*, Bureau of Reclamation: 2011.
18. Scanlon, B. R.; Reedy, R. C.; Male, F.; Walsh, M., Water issues related to transitioning from conventional to unconventional oil production in the Permian Basin. *Environ. Sci. Technol.,* 2017, 51, 10903-10912.
19. Saha, G. C.; Quinn, M., Assessing the effects of water withdrawal for hydraulic fracturing on surface water and groundwater-A review. *Meteorology Hydrology and Water Management.* Research and Operational Applications 2020, 8, 52-59.
20. Kustin, M. E., "U.S. lacks data needed to weigh effects of oil and gas production on western water supply", Center for American Progress https://www.americanprogress.org/issues/green/news/2019/06/27/471512/u-s-lacks-data-needed-weigh-effects-oil-gas-production-western-water-supply/ (assessed July 10, 2021).
21. Buono, R. M.; Gunn, E. L.; McKay, J.; Staddon, C., Regulating water security in unconventional oil and gas. *Springer:* 2020.
22. United State Drought Monitor. Data Download. Comprehensive Statistics. https://droughtmonitor.unl.edu/Data/DataDownloadComprehensiveStatistics.aspx (accessed July 10, 2021).
23. Sterrett, R. J., Groundwater and wells. Johnson Screens: 2007.
24. FracFocus Chemical Disclosure Registry. Data Download. http://fracfocus.org/node/356/done?sid=20159 (accessed July 10, 2021).
25. Jackson, R. B.; Lowry, E. R.; Pickle, A.; Kang, M.; DiGiulio, D.; Zhao, K., The depths of hydraulic fracturing and accompanying water use across the United States. *Environ. Sci. Technol.,* 2015, 49, 8969-8976.
26. Oikonomou, P. D.; Kallenberger, J. A.; Waskom, R. M.; Boone, K. K.; Plombon, E. N.; Ryan, J. N., Water acquisition and use during unconventional oil and gas development and the existing data challenges: Weld and Garfield Counties, CO. *J. Environ. Manage.,* 2016, 181, 36-47.
27. DrillingInfo, DrillingInfo Desktop Application (DrillingInfo, 2017); www.didesktop.com/ (accessed July 10, 2021).
28. Water Resources. USGS Water Use Data. Retrieved from https://www.usgs.gov/mission-areas/waterresources (accessed July 10, 2021).
29. U.S. Census Bureau. Retrieved from https://www.census.gov/data/datasets/time-series/demo/popest/2010s-counties-total.html (accessed July 10, 2020)

30. United States Drought Monitor, Drought Classification. https://droughtmonitor.unl.edu/About/AbouttheData/DroughtClassification.aspx (accessed July 10, 2020).
31. Abatatzoglou, J. T.; Mcevoy, D. J.; Redmdmond, K. T., The west wide drought tracker: Drought monitoring at fine spatial scales. *B. Am. Meteorol. Soc.,* 2017, 98, 1815-1820.
32. Scanlon, B. R.; Reedy, R. C.; Nicot, J.-P., Comparison of water use for hydraulic fracturing for unconventional oil and gas versus conventional oil. *Environ. Sci. Technol.*, 2014, 48, 12386-12393.
33. United State Drought Monitor, Data, State Impacts, https://droughtmonitor.unl.edu/DmData/StateImpacts.aspx, (assessed July 10, 2021).
34. Goldenberg, S., "Fracking is depleting water supplies in America's driest areas, report shows," US Environment Correspondent, https://www.theguardian.com/environment/2014/feb/05/fracking-water-america-drought-oil-gas (accessed July 10, 2021).
35. Mark Jaffe, "When drought occurs, fracking and farming collide", The Denver Post (Feb 7, 2014), https://www.denverpost.com/2014/02/07/when-drought-occurs-fracking-and-farming-collide/
36. Valerie Volcovici, "Drilling boom adds stress to U.S. Western water supplies: report" Reuters (Nov 12, 2019), https://www.reuters.com/article/us-usa-oil-water/drilling-boom-adds-stress-to-u-s-western-water-supplies-report-idUSKBN1XM1EF
37. EPA., U. S., Hydraulic fracturing for oil and gas: Impacts from the hydraulic fracturing water cycle on drinking water resources in the United States (Final Report). *U.S. Environmental Protection Agency*, Washington, DC, EPA/600/R-16/236F, 2016.
38. Kuwayama, Y.; Olmstead, S. M.; Krupnick, A., Water resources and unconventional fossil fuel development: Linking physical impacts to social costs. *Resources for the Future*, 2013, DP 13-34.
39. Hitaj, C.; Boslett, A. J.; Weber, J. G., Fracking, farming, and water. *Energ. Policy*, 2020, 146, 111799.
40. Gaudet, G.; Moreaux, M.; Withagen, C., The Alberta Dilemma: Optimal sharing of a water resource by an agricultural and an oil sector. *J. of Environ. Econ. Manag.* 2006, 52, 548-566.
41. Smith, R., Water transfers in the West: Projects, trends, and leading practices in voluntary water trading. Western Governors' Assocation: 2012.
42. Healy, J., "For farms in the West, oil wells are thirsty rivals." The New York Times 2012, 5. https://www.nytimes.com/2012/09/06/us/struggle-for-water-in-colorado-with-rise-in-fracking.html (accessed November 13, 2021).
43. Koba, M., "Not even severe drought can stop fracking," Oil and Gas Exploration, https://www.cnbc.com/2014/06/10/not-even-severe-drought-can-stop-fracking.html (accessed December 9, 2021).

44. Lin, Z.; Lin, T.; Lim, S. H.; Hove, M. H.; Schuh, W. M., Impacts of Bakken Shale oil development on regional water uses and supply. *J. Am. Water Resour. Assoc.,* 2018, 54, 225-239.
45. Kenworthy, T., "Fracking can strain U.S. water supplies, ENERGY AND ENVIRONMENT", The Center for American Progress, https://www.americanprogress.org/issues/green/news/2013/06/14/66544/fracking-threatens-u-s-water-supplies/ (assessed December 9, 2021).
46. Gosling, S. N.; Arnell, N. W., A global assessment of the impact of climate change on water scarcity. *Clim. Change,* 2016, 134, 371-385.
47. Hannibal, B.; Portney, K., The impact of water scarcity on support for hydraulic fracturing regulation: A water-energy nexus study. *Energ. Policy*, 2020, 146, 111718.
48. Al-Ghouti, M. A.; Al-Kaabi, M. A.; Ashfaq, M. Y.; Da'na, D. A., Produced water characteristics, treatment and reuse: A review. *J. Water Process. Eng.,* 2019, 28, 222-239.
49. Echchelh, A.; Hess, T.; Sakrabani, R., Reusing oil and gas produced water for irrigation of food crops in drylands. *Agr. Water Manage*, 2018, 206, 124-134.
50. Sedlacko, E. M.; Jahn, C. E.; Heuberger, A. L.; Sindt, N. M.; Miller, H. M.; Borch, T.; Blaine, A. C.; Cath, T. Y.; Higgins, C. P., Potential for beneficial reuse of oil and gas–derived produced water in agriculture: Physiological and morphological responses in spring wheat (Triticum aestivum). *Environ. Toxicol. Chem*., 2019, 38, 1756-1769.
51. Cooper, C. M.; McCall, J.; Stokes, S. C.; McKay, C.; Bentley, M. J.; Rosenblum, J. S.; Blewett, T. A.; Huang, Z.; Miara, A.; Talmadge, M., Oil and gas produced water reuse: Opportunities, treatment needs, and challenges. *ACS EST Engg.,* 2021, DOI: https://doi.org/10.1021/acsestengg.1c00248
52. Horner, R. M.; Harto, C. B.; Jackson, R. B.; Lowry, E. R.; Brandt, A. R.; Yeskoo, T.; Murphy, D.; Clark, C., Water use and management in the Bakken Shale oil play in North Dakota. *Environ. Sci. Technol*., 2016, 50, 3275-3282.
53. Ellingson, N.; Hargiss, C. L.; Norland, J., Understanding municipal water use and data availability: A case study across North Dakota, USA. *Water Resour. Manag.,* 2019, 33, 4895-4907.
54. Du, X.; Li, H.; Robbins, C. A.; Carlson, K. H.; Tong, T., Activity and water footprint of unconventional energy production under hydroclimate variation in Colorado. *ACS EST Water*, 2020, 1, 281-290.

CHAPTER 6 Membrane fouling and reusability in membrane distillation of shale oil and gas produced water [3]

6.1 Introduction

Shale oil and gas is an unconventional energy resource that is found in relatively impermeable rock and requires hydraulic fracturing to recover the hydrocarbons [1]. The shale oil and gas industry has significantly improved the energy security of the United States, and has disrupted the oil and gas markets by driving down prices worldwide [2]. However, shale oil and gas production consumes substantial amounts of freshwater and produces vast quantities of wastewater [3-5]. For example, shale oil and gas production in the U.S. has led to a total water usage of 940 billion liters from 2005 to 2014, and has produced 775 billion liters of hazardous wastewater [3]. There are growing concerns associated with the handling and disposal of shale oil and gas wastewater. The majority of this wastewater is currently injected underground into deep and isolated formations, but this technology may induce seismic events and is constrained by geological and legal restrictions [1, 6, 7]. Also, the discharge of shale oil and gas wastewater into publicly owned treatment works (POTWs)

[3] This chapter has been published as a research article in *Journal of Membrane Science* with the following citation:

Du, X.; Zhang, Z. Y.; Carlson, K. H.; Lee, J.; Tong, T. Z., Membrane fouling and reusability in membrane distillation of shale oil and gas produced water: Effects of membrane surface wettability. *J Membrane Sci* 2018, 567, 199-208.

pollutes the water environment due to its high salinity and toxicity [1, 8, 9]. Furthermore, many of the western shale plays in the U.S. coincide with areas suffering high to severe water stress [5]. Therefore, effective treatment and reuse of shale oil and gas wastewater as an additional source for beneficial purposes will address the dual challenges of water scarcity and pollution associated with the shale oil and gas industry, thereby promoting sustainability at the water-energy nexus.

Shale oil and gas wastewater, including flowback and produced water, contains high concentrations of total dissolved solids (TDS) and complex organic and inorganic components [9-11]. Hence, the treatment of such complicated wastewater is an extremely challenging task. Although reverse osmosis (RO) is the most energy efficient desalination technology [12], the TDS of shale oil and gas wastewater (up to 360,000 mg/L) typically approaches or exceeds the salinity limit of RO (~70,000 mg/L TDS) [13], rendering RO an inappropriate technology for shale oil and gas wastewater treatment. Membrane distillation (MD) is a hybrid thermal, membrane-based desalination technology, which utilizes a partial vapor pressure difference to drive the transport of water vapor across a hydrophobic, microporous membrane [14, 15]. Like other thermal desalination processes, MD is able to desalinate hypersaline feedwater beyond the salinity limit of RO [16]. The capability of MD to utilize low-grade heat (e.g., geothermal energy), which is commonly contained in shale oil and gas wastewater [13], reduces primary energy consumption and operational costs of the treatment system [16]. Further, the modular configuration of a MD system renders it adaptable to the fluctuation in both quantity and quality of shale oil and gas wastewater [16]. Thus, MD is a

promising technology that is potentially suitable to the desalination of shale oil and gas wastewater [17].

Since MD is typically used in the desalination of concentrated feedwater with high salinities, MD membranes are facing high concentrations of foulants and scalants. As a result, membrane fouling and scaling significantly constrain the efficiency of MD [18, 19]. Also, pore wetting, which is caused by low surface tension foulants, results in significant salt passage and may eliminate the desalination function of the MD process [15, 20]. Accordingly, various modification approaches have been applied to MD membranes to hinder fouling and wetting, primarily by optimizing the wetting properties of membrane surface [20-29]. For example, superhydrophobic or omniphobic membranes with high wetting resistance have been fabricated by introducing both a re-entrant structure and low surface tension materials [20-22, 24, 28, 29]. Recently, a thin in-air hydrophilic layer has been coated on MD membrane surface to reduce organic fouling [23, 25, 26]. The underwater oleophobic property of the hydrophilic layer deters the attachment of hydrophobic foulants (e.g., oil droplets) to the membrane surface and prevents pore blocking [25, 26]. To date, novel MD membranes developed by means of the above approaches have been dominantly tested with synthetic feed solutions containing individual foulants. However, the performance of these MD membranes in desalinating real industrial wastewater with complex and variable chemical compositions has not been systematically understood.

In this work, we performed a comparative study of the effects of membrane surface wettability on MD desalination of shale oil and gas produced water generated from the Wattenberg field in northeast Colorado. The performance of three membranes with different surface wettability, including a commercial hydrophobic PVDF membrane, a superhydrophobic PVDF membrane, and a composite PVDF membrane with hydrophilic coating, was tested and compared in a laboratory-scale, custom-built direct contact MD (DCMD) unit. Produced waters collected from two sampling dates were used as the feedwater, and their varied chemical components enabled us to evaluate the influence of feedwater composition on membrane performance. The fouling layers formed during produced water treatment were characterized in detail by scanning electron microscopy (SEM), energy-dispersive X-ray (EDX) spectroscopy, and attenuated total reflectance-Fourier transform infrared (ATR-FTIR) spectroscopy, in order to understand the mechanisms underlying membrane fouling. After a single treatment cycle, MD membranes were subjected to physical cleaning followed by the treatment of new produced water in multiple cycles, thereby assessing fouling reversibility and membrane reusability. Our results demonstrate that surface wettability influenced both fouling resistance and reusability of MD membranes in produced water treatment, but its impacts could be altered by feedwater composition. The corresponding implications in the design and selection of appropriate MD membranes for efficient treatment of complex industrial wastewater are also discussed.

6.2 Materials and methods

6.2.1 Materials, chemicals, and shale oil and gas produced water

Polyvinyl alcohol (PVA, Mw 13,000−23,000, 98% hydrolyzed), glutaraldehyde (50 wt% in H_2O), (3-aminopropyl)triethoxysilane (APTES, ≥98%), LUDOX HS-30 colloidal silica (30 wt% suspension in H_2O) were purchased from Sigma-Aldrich. (Heptadecafluoro-1,1,2,2-tetrahydrodecyl)triethoxysilane (FAS) was purchased from Gelest Inc. Sodium chloride (NaCl) and sodium hydroxide (NaOH) were purchased from VWR BDH Chemicals. Hydrochloric acid (HCl, 36.5-38%) was provided by Fisher Chemical. Anhydrous ethanol (200 proof) was supplied by Decon Laboratories. Flat sheet polyvinylidene fluoride (PVDF) membranes (HVHP, Durapore) were provided by Millipore Sigma. According to the manufacturer, these hydrophobic, microporous membranes have a nominal pore size of 0.45 μm and an average thickness of 125 μm. Deionized (DI) water was produced from an ultrapure water purification system (>18 MΩ·cm, Millipore).

Shale oil and gas produced water samples were collected from a production site located in the Wattenberg field of northeast Colorado on December 5th, 2017 (designated as Sample 1) and January 22nd, 2018 (designated as Sample 2). The well was drilled and hydraulically fractured during October 2017 (flowback began on October 24th), initially with a slickwater type fluid and then at the toe of the lateral with a gel fluid. The produced water was transported to our laboratory, located at Colorado State University (Fort Collins, CO), within two hours after collection, and

stored at 4 °C to minimize biological activity. The produced waters were pre-filtered through an 8-μm qualitative filter (Grade 2, GE Whatman, PA) to remove large particles before the DCMD tests. The chemical composition of the pre-filtered produced water was analyzed by a third-party certified laboratory (Technology Laboratory, Inc., Fort Collins, CO), and the corresponding results are presented in Table C1 in the Appendix C.

6.2.2 Membrane modification approaches

Two membrane modification approaches were employed to alter the surface wetting property of PVDF membrane. In the first approach, PVA was used to provide a thin, hydrophilic layer on the top of PVDF membranes [30]. Briefly, 1 wt% PVA solution was prepared by dissolving 1 g PVA in 100 mL DI water overnight at a temperature >90 °C. Once PVA was fully dissolved, the resulting solution was cooled down to room temperature, followed by adjusting the solution pH to ~2 using HCl. Then 0.3 mL of 50 wt% glutaraldehyde (GA) solution (as cross-linking agent [31]) was added into 30 mL of PVA solution. After quick stirring, the PVA-GA mixture was poured onto the PVDF membrane surface. The PVDF membrane was then incubated in a vacuum oven at 60 °C for one hour, after which the PVA-modified membrane (designated as PVDF-PVA membrane) was rinsed thoroughly with DI water and dried in air until use. Since water was used as the solvent in the membrane modification process, the PVA solution was unable to wet the pores of hydrophobic PVDF membrane. As a result, PVA modification only altered the top surface of PVDF membrane, but did not compromise the hydrophobicity of the entire membrane.

In the second approach, silica nanoparticles functionalized with FAS were incorporated into the PVDF membrane, following the protocol reported by Boo et al. [21] with slight modification. The low surface energy imparted by FAS and a re-entrant structure introduced by silica nanoparticles render the PVDF membrane omniphobic [21]. Briefly, the PVDF membrane was pre-wetted by ethanol and immersed in 7.5 M NaOH solution at 70 °C for three hours, in order to generate hydroxyl functionality on the membrane surface. The color of PVDF membranes turned brown after the alkaline treatment. Then the membrane was soaked in 1% v/v APTES in ethanol for one hour to functionalize the membrane surface with positively charged amine groups. The APTES-functionalized PVDF membrane was rinsed with ethanol and dried in a vacuum oven at 50 °C for one hour. The membrane was then pre-wetted by ethanol and immersed in an aqueous solution containing silica nanoparticles (0.03 wt%, with 10 mM NaCl) for 30 minutes. The silica nanoparticle-incorporated membrane was rinsed with DI water and dried in the oven. Then the membrane was immersed in 0.4% v/v FAS in hexane and incubated overnight using an orbital shaker at room temperature. The resulting PVDF membrane incorporated with silica nanoparticles functionalized with FAS (designated as PVDF-SiO_2-FAS membrane) was rinsed with hexane and dried on a hot plate (> 80°C) overnight.

6.2.3 Membrane characterization

Surface morphologies of pristine and modified PVDF membranes were investigated by scanning electron microscopy (SEM, Hitachi SU-70). The membrane samples were dried and coated with a

thin layer of iridium using a sputter coater (Denton Desk IV) prior to imaging. The contact angles of each membrane with water (γ = 72.8 mN/m) and hexadecane (γ = 27 mN/m) were measured using the sessile drop method [32], in order to compare membrane surface wettability. The contact angles with the produced water samples were also measured. Further, the underwater contact angles with oil extracted from the production site (ρ = 0.77g/mL) were measured to evaluate potential membrane oil fouling [27]. The zeta potential of the membranes was calculated from streaming potentials measured by a streaming potential analyzer equipped with an asymmetric clamping cell (EKA, Brookhaven Instruments). The measurements were performed with a solution containing 1 mM KCl and 0.1 mM $KHCO_3$, with eight measurements for each membrane. The details of the procedure used to calculate the zeta potential from the measured streaming potential have been described by Walker et al. [33]

6.2.4 Desalination of shale oil and gas produced water by membrane distillation

Desalination of shale oil and gas produced water was performed in a laboratory-scale, custom-built DCMD unit with a transparent acrylic cell, and the performance of three membranes with different surface wettability (i.e., PVDF, PVDF-PVA, and PVDF-SiO_2-FAS membranes) was compared. The feedwater and distillate channels of the acrylic cell had an identical dimension of 77 mm × 26 mm × 3 mm, resulting in an effective membrane area of 20.02 cm^2. Shale oil and gas produced water (1500 mL) was added to the reservoir of feed solution, while DI water (600 mL) was added to the reservoir of distillate. The modified surface of the membranes was facing the hot

feed solution, while the unmodified surface contacted the cold distillate. The temperatures of the feed solution and deionized distillate were kept at 60 °C and 20 °C, respectively. The crossflow velocities of the feed and distillate streams were 8.5 cm/s (0.4 L/min) and 7.4 cm/s (0.35 L/min), respectively. A slightly higher crossflow velocity of the feed stream was used to enable the detection of possible membrane wetting [21, 25]. The weight and conductivity of the solution in the distillate reservoir were monitored continuously to calculate the water (vapor) flux and assess membrane wetting. The DCMD tests were terminated when 800 mL of distillate was collected.

The membrane coupon was taken out of the acrylic cell after the DCMD tests and rinsed gently with DI water. Then the air-dried membranes were analyzed by SEM coupled with energy-dispersive X-ray (EDX) spectroscopy (JEOL JSM-6500F) and attenuated total reflectance-Fourier transform infrared (ATR-FTIR, Nicolet iS-50), in order to investigate the morphology and chemical composition of the foulant layers formed on the MD membrane surface.

6.2.5 Fouling reversibility and membrane reusability after physical cleaning

Fouling reversibility and membrane reusability during MD desalination of shale oil and gas produced water were evaluated with the same DCMD unit and experimental procedure as described above. After collecting 800 mL of distillate, the DCMD test was terminated. The membrane coupon was taken out of the acrylic cell and rinsed thoroughly with DI water (2 L/min, for 20 seconds) on both sides, in order to remove all the inorganic and organic foulants that were not firmly attached to the membrane surface. After being dried in air, the membrane coupon was

re-inserted into the DCMD unit, and 1500 mL of new shale oil and gas produced water was added into the feed reservoir to start a new cycle of DCMD desalination. Three cycles of desalination tests were performed to evaluate membrane reusability after physical cleaning with DI water, and the flux decline rates in different treatment cycles were compared. Also, the permeate flux recovery rate (R) was calculated by using Equation 6-1 as below.

$$R = \frac{J_{0,i}}{J_{0,1}} \qquad (6\text{-}1)$$

where $J_{0,1}$ refers to the initial water (vapor) flux of the membrane in the first cycle of DCMD desalination, and $J_{0,i}$ refers to the initial flux of the membrane in Cycle i (i = 2, 3) of DCMD desalination.

The cross-section of MD membranes after three cycles of produced water treatment were analyzed by SEM coupled with EDX spectroscopy (JEOL JSM-6500F). The membranes were freeze-fractured using liquid nitrogen prior to imaging[34]. SEM-EDX line-scan analysis was then performed to measure the depth of foulant penetration into the membrane. The change of iron (Fe) kα1 signal was used as an indicator of foulant location, due to the ubiquitous presence of Fe in the foulant layer (as shown in subsection 6.3.3).

6.3 Results and Discussion

6.3.1 Surface Properties of Pristine and Modified PVDF Membranes

Two approaches were employed to modify the surface wettability of a commercial hydrophobic PVDF membrane. A combination of various techniques was used to characterize key surface properties of the modified membranes, including membrane morphology, surface wettability, and surface charge.

The first modification approach provided a composite hydrophobic PVDF membrane with a hydrophilic PVA top layer (Figure 6-1A). SEM observation shows that PVA modification did not alter the surface morphology of the PVDF membrane (Figures 6-1B and C1), indicating that the introduced PVA polymer layer was ultrathin. Although the pristine PVDF membrane was in-air hydrophobic with a water contact angle of 119±4°, the PVDF-PVA membrane became in-air hydrophilic as its water contact angle decreased dramatically to 50±2° (Figure 6-1C). Also, both membranes were instantly wicked by hexadecane with low surface tension (γ = 27 mN/m, Figure C2A). We measured the underwater oil contact angles using the oil extracted from the shale oil and gas production site, in order to evaluate potential membrane oil fouling (Figure C3) [27]. The PVDF-PVA membrane was highly underwater oleophobic with an oil contact angle of 160±2°. In contrast, the pristine PVDF membrane was underwater oleophilic due to the strong attractive interaction between its hydrophobic surface and a non-polar oil droplet. Furthermore, as shown in Figure 6-2, PVA coating imposed negligible impacts on the surface charge of the PVDF membrane, as indicated by the unaffected membrane zeta potential. At near-neutral pH, both PVDF and

PVDF-PVA membranes were negatively charged, which was consistent with what has been reported in the literature [25, 28, 30].

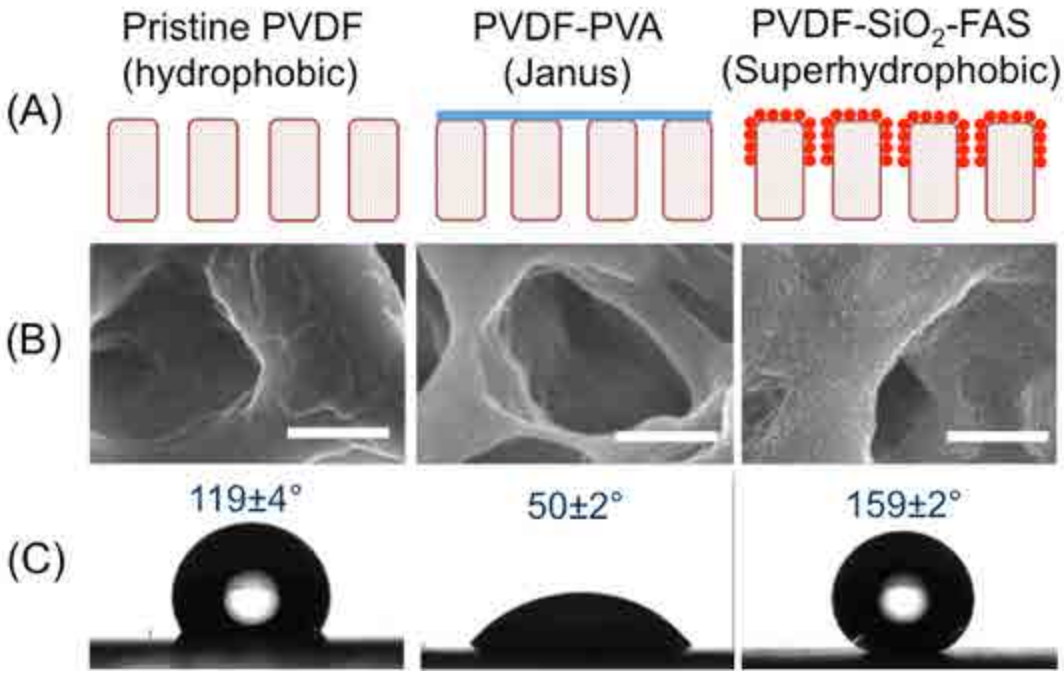

Figure 6-1. MD membranes with different surface wettability used in this study. (A) Schematic illustration of membrane modification approaches that tailor surface wettability. The incorporation of a thin PVA layer into the PVDF membrane surface results in a composite membrane with enhanced hydrophilicity. Grafting of SiO_2 nanoparticles functionalized with FAS introduces both low surface energy and a re-entrant structure, rendering the modified membrane superhydrophobic. (B) Top-view SEM observation of pristine and modified PVDF membranes (with magnification of 80000×). The scale bars represent 500 nm. Note that PVA modification did not alter the surface morphology of the PVDF membrane, while SiO_2 nanoparticles could be clearly observed on the PVDF-SiO_2-FAS membrane. (C) Water contact angles of pristine and modified PVDF membranes. The data are presented as average ± standard deviation (n = 5).

The second modification approach introduced both low surface energy materials (i.e., FAS) and a re-entrant structure (by grafting with silica nanoparticles) to the PVDF membrane. Silica nanoparticles with sizes of ~20 nm were found to cover the PVDF membrane surface, and the re-entrant structure developed by the spherical geometry of silica nanoparticles was clearly observed

(Figure 6-1B). The resultant PVDF-SiO_2-FAS membrane showed superhydrophobicity with a high water contact angle of 159±2°. In contrast to pristine PVDF and PVA-PVDF membranes, the PVDF-SiO_2-FAS membrane was not wicked by hexadecane, with a static contact angle of > 100° (Figure B2A). The combination of low interfacial energy and a re-entrant structure results in a metastable Cassie−Baxter state at the liquid-vapor-solid interface, thereby preventing the membrane from wetting even by liquids with low surface tension [21, 25]. Also, the contact angles with two produced water samples were found identical to those with DI water for all the tested membranes (Figure C2), suggesting that organic substances contained in these samples were insufficient to lower the liquid surface tension significantly. As shown in Figure C3, the PVDF-SiO_2-FAS membrane was underwater oleophilic due to its in-air superhydrophobic nature. Similar to pristine PVDF and PVDF-PVA membranes, the PVDF-SiO_2-FAS membrane exhibited negative surface charge when pH was above 4 (Figure 6-2). As a result, the different treatment performance observed among the tested membranes, as described in the following sections, was primarily due to the variation in membrane surface wettability.

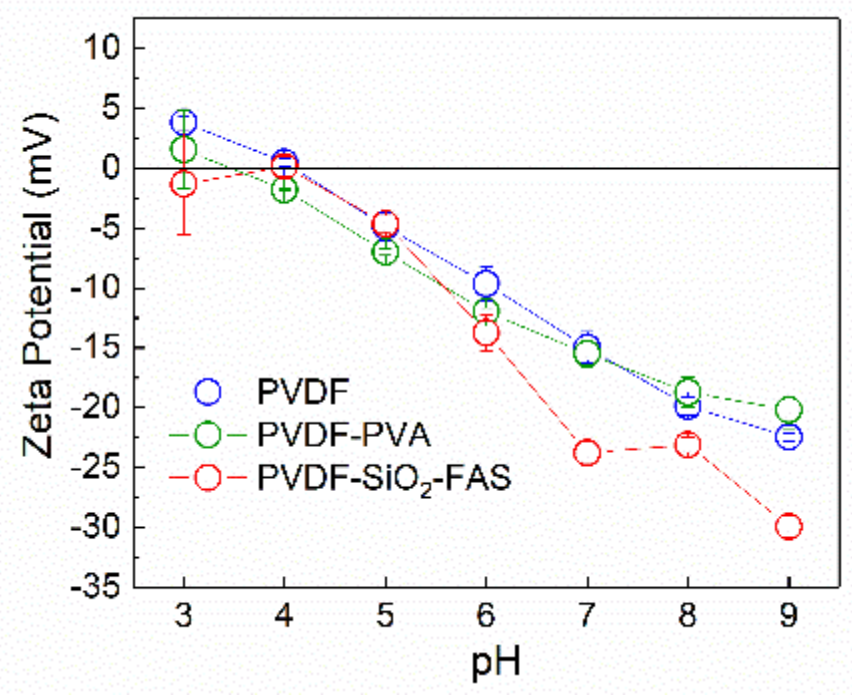

Figure 6-2. Zeta potential of different membranes tested in this study. The error bars represent standard deviation and were calculated from eight measurements.

6.3.2 Membrane performance of treating shale oil and gas produced water by membrane distillation in a single cycle

The pristine and modified PVDF membranes were used to treat real shale oil and gas produced water generated from a Colorado production site in a custom-built DCMD system. Since the chemical composition of shale oil and gas produced water changes with well age [10], produced waters collected at two sampling dates (with a 1.5 month interval) were used to evaluate the response of membranes to feedwater with varied chemical components. As shown in Table C1, the two produced water samples contained similar salinities (TDS of ~40,000 mg/L). However, Sample 1 (collected on December 5th 2017) contained higher concentrations of total organic carbon

(TOC), metal ions (e.g., dissolved calcium, iron, and magnesium), and sulfate (SO_4^{2-}) than Sample 2 (collected on January 22nd, 2018).

Figure 6-3 presents normalized water (vapor) fluxes of the pristine and modified PVDF membranes when treating shale oil and gas produced water in a single cycle. PVA coating did not decrease the initial water flux of PVDF membrane, due to the ultrathin thickness of the PVA layer. However, the initial water fluxes of PVDF-SiO_2-FAS membrane (23.4±0.2 and 26.2±0.2 L m^{-2} h^{-1} for Samples 1 and 2, respectively) were lower than those of pristine PVDF membrane (30.9± 1.7 and 29.4±1.3 L m^{-2} h^{-1} for Samples 1 and 2, respectively) and PVDF-PVA membrane (30.3 ±0.4 and 31.5±2.0 L m^{-2} h^{-1} for Samples 1 and 2, respectively). Therefore, normalized water fluxes are presented as a function of cumulative distillate volume, rendering the treatment performance of the tested membranes comparable. [21]

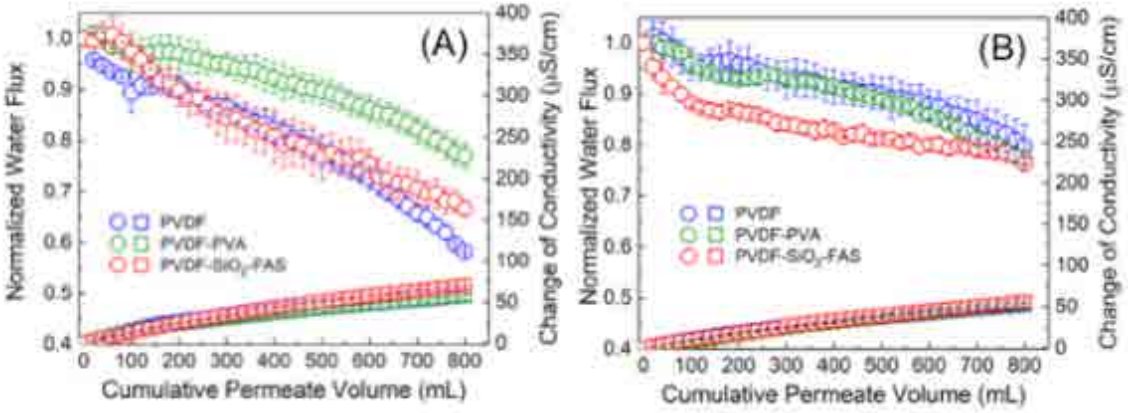

Figure 6-3. Normalized water (vapor) flux during DCMD desalination of shale gas produced water collected on (A) December 5th, 2017 (Sample 1) and (B) January 22nd, 2018 (Sample 2) in a single cycle. The performance of three membranes was compared, including pristine PVDF, PVDF modified with PVA (PVDF-PVA), and PVDF modified with fluorosilanized SiO_2 nanoparticles (PVDF-SiO_2-FAS). The crossflow velocities in the feed and distillate streams were 8.5 cm/s and 7.4 cm/s, respectively. The feed and distillate temperatures were 60 °C and 20 °C, respectively.

The feed volume was 1500 mL. In Figure 6-3A, the initial water fluxes were 30.9±1.7 L m^{-2} h^{-1}, 30.3±0.4 L m^{-2} h^{-1}, and 23.4±0.2 L m^{-2} h^{-1} for pristine PVDF, PVDF-PVA, and PVDF-SiO_2-FAS membranes, respectively. In Figure 6-3B, the initial water fluxes were 29.4±1.3 L m^{-2} h^{-1}, 31.5±2.0 L m^{-2} h^{-1}, and 26.2±0.2 L m^{-2} h^{-1} for pristine PVDF, PVDF-PVA, and PVDF-SiO_2-FAS membranes, respectively. The error bars were calculated from duplicate independent DCMD experiments.

As shown in Figure 6-3, different membranes showed varied extents of flux decline during the DCMD tests, suggesting that surface wettability influenced fouling resistance of the tested membranes. In the treatment of Sample 1, the PVDF-PVA membrane exhibited the best fouling resistance (Figure 6-3A). When collecting 800 mL of distillate, the water flux of the PVDF-PVA membrane dropped by only 23% compared to the initial value, while the pristine PVDF and PVDF-SiO_2-FAS membranes experienced higher flux decline ratios (defined as the percentage of flux decline as compared to the initial water flux) of 42% and 33%, respectively. In the treatment of Sample 2 (Figure 6-3B), however, the three tested membranes showed similar flux decline ratios (22±2%) at the end of the DCMD tests, despite a faster flux decline observed for the PVDF-SiO_2-FAS membrane at the initial stage of produced water treatment. Due to its lower initial water flux, the PVDF-SiO_2-FAS membrane required longer time (21.1±1.6 hours and 18.1±0.8 hours for Samples 1 and 2, respectively) than the pristine PVDF membrane (16.4±0.9 hours and 14.9±0.2 hours for Samples 1 and 2, respectively) and the PVDF-PVA membrane (14.6±0.9 hours and 14.3±1.5 hours for Samples 1 and 2, respectively) to produce 800 mL of distillate. Therefore, the superhydrophobic PVDF-SiO_2-FAS membrane was not advantageous compared to the other two membranes in a single treatment cycle.

The conductivity of the solutions in the distillate reservoir was increased by < 75 μS/cm at the end of the DCMD tests for all the membranes treating both produced water samples (Figure 6-3). This corresponded to an increase of salinity < 35 mg/L NaCl (calculated from Figure C4) and salt removal efficiencies > 99.9% (calculated using the methods of Boo et al. [21] and an initial feedwater salinity of 40,000 mg/L). Therefore, no significant membrane wetting was observed during a single cycle of produced water treatment. This slight increase of distillate conductivity was likely due to intrinsic membrane defects [21]. Although low surface energy contaminants, such as surfactants that are commonly used in hydraulic fracturing [35], are able to wet the hydrophobic pores of MD membranes [22], their concentrations in shale oil and gas wastewater decrease significantly as the well ages [11]. Thus, the amount of low surface energy substances possibly present in the shale oil and gas produced waters, which were collected after 42 and 90 days after flowback began, were insufficient to cause membrane wetting in the current study. This effect was in accordance with the identical contact angles with produced waters to those with DI water as observed in Figure C2. Membrane wetting, therefore, was not a primary limiting factor of membrane performance in our study.

We observed that our results differed from the finding by Boo et al. that omniphobic membrane showed better fouling and wetting resistance than hydrophobic PVDF membrane when desalinating shale gas produced water from the Permian Basin in Texas [21]. Hence, additional DCMD tests with 1 M NaCl solution containing varying concentrations of surfactant sodium

dodecyl sulfate (SDS) as the feed solution were performed on the pristine PVDF and PVDF-SiO_2-FAS membranes in our study (detailed experimental procedure is described in the Appendix C). As shown in Figure C5, the PVDF-SiO_2-FAS membrane exhibited improved wetting resistance against SDS compared to the pristine PVDF membrane. However, this superhydrophobic membrane was partially wetted by 0.2 mM SDS, which did not affect desalination performance of the omniphobic membrane in Boo et al. [21] This difference in membrane wetting property, which was likely due to different membrane modification procedures (see explanation in the Appendix C), could contribute to the discrepancy of membrane performance as described above. Furthermore, superhydrophobic or omniphobic membranes have strong hydrophobic-hydrophobic interaction between membrane surface and non-polar foulants such as oil in the produced water [23, 27]. This effect was consistent with our results that the superhydrophobic membrane exhibited a faster or comparable membrane fouling comparing to hydrophobic membrane, but contrary to the findings of Boo et al. [21] Therefore, smaller amounts of hydrophobic organic compounds were likely present in the produced water used in Boo et al. than ours. Due to the chemical complexity of produced water, a more explicit explanation could not be achieved at this point and requires more investigation.

6.3.3 Characterization of fouling layers formed during MD treatment of shale oil and gas produced water

SEM was employed to investigate the morphologies of membrane surfaces after DCMD treatment of shale oil and gas produced water. As shown in Figure 6-4, no significant difference

was observed among MD membranes with varied surface wettability. However, different produced water samples resulted in contrasting membrane surface morphologies. A rough foulant layer was found to fully cover the membrane surface after the treatment of Sample 1 (Figure 6-4 A-C). However, the MD membranes after treating Sample 2 appeared to be cleaner, and intact PVDF membrane structure was still visible with particulate foulants embedded in the membrane pores (Figure 6-4 D-F).

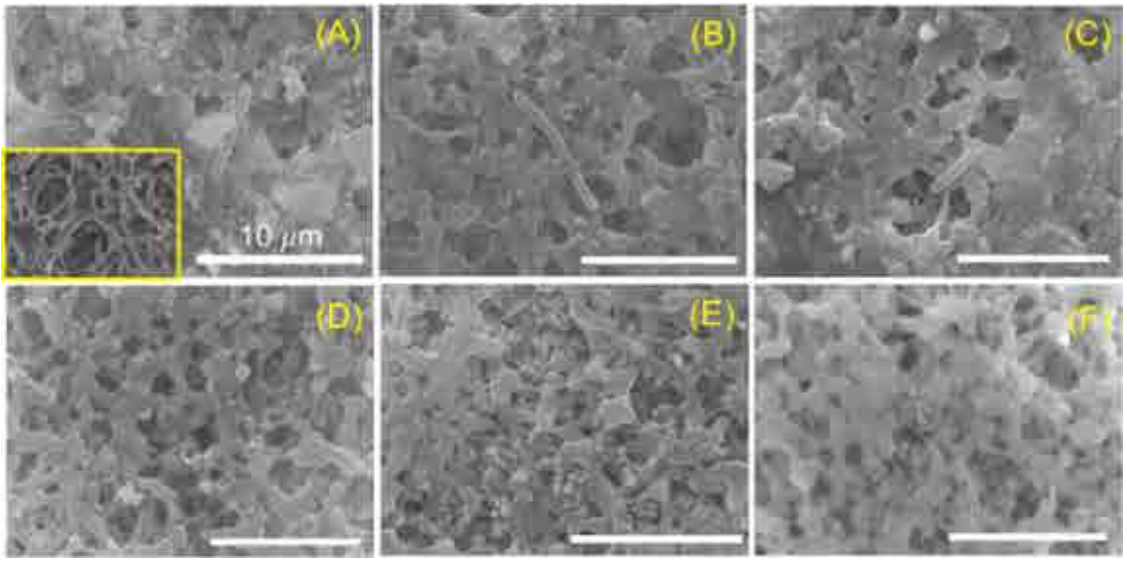

Figure 6-4. SEM micrographs of pristine PVDF (A and D), PVDF-PVA (B and D), and PVDF-SiO_2-FAS membranes (C and F) after DCMD desalination of shale oil and gas produced water in a single cycle. The produced water was collected on (A-C) December 5th, 2017 and (D-F) January 22nd, 2018. The scale bars represent 10 μm. The inset of Figure 6-4A shows a SEM micrograph of virgin (unfouled) PVDF membrane before DCMD desalination.

EDX spectroscopy was used to analyze the chemical composition of foulant layers (Figures 6-5 and C6). Since PVDF membranes contain a high content of carbon, the EDX results only provided information relevant to inorganic fouling (i.e., scaling). The inorganic foulants present on the membrane surfaces after produced water treatment were mainly composed of silica (SiO_2)

and/or silicate precipitates (indicated by the overlapping and strong signals of elements Si and O), which was associated with the element iron (Fe). The coexistence of Fe and silica/silicate has been commonly detected on RO membranes in the literature [36], likely due to the reaction of Fe(III) ions with silicic acid monomers to form sparingly soluble iron silicates and/or the high tendency of Fe(III) ions to adsorb on the silica surface [37, 38]. After the treatment of Sample 2, the silica or silicate particles embedded in the membrane pores exhibited a spherical morphology with sizes of 200-500 nm (Figure C7). Similar colloidal silica particles were also observed by Gilron et al. [39] in membrane pores due to silica scaling in DCMD. However, such spherical morphology of silica/silicate scales was not clearly distinguishable on the membranes after the treatment of Sample 1, which led to a more homogeneous and denser silica fouling layer (Figures 6-4, 6-5, and C6). In addition, barium sulfate (barite), whose precipitation has been reported in shale oil and gas produced water [40], was also observed after the treatment of Sample 1 (Figure C8). Sample 2 contained a very low concentration of sulfate (<0.05 mg/L, Table C1), and thus barite formation was not found on the surface of membranes after the DCMD treatment.

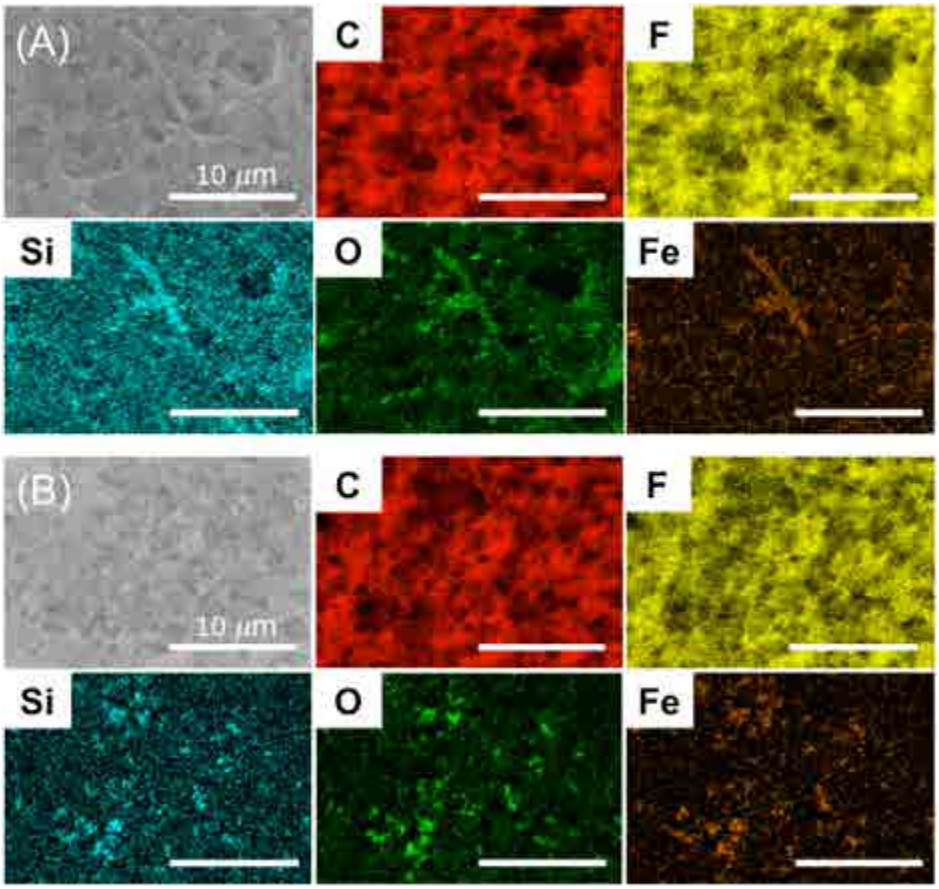

Figure 6-5. The elemental maps obtained by energy-dispersive X-ray spectroscopy for the PVDF-PVA membranes after the desalination of shale oil and gas produced water (A) Sample 1 and (B) Sample 2 in a single cycle. The scale bars represent 10 μm. The elemental maps for other membrane samples are presented in Figure C6 of the Appendix C.

ATR-FTIR was used to characterize organic components of the fouling layers (Figure 6-6). Similar to membrane morphology revealed by SEM observation (Figure 6-4), the FTIR spectra were similar among the tested membranes, whereas different produced water samples led to distinct FTIR features. As compared to the virgin membranes, six new peaks were mainly discovered for the fouled membranes after the treatment of Sample 1. These peaks, which were located at 1540 cm^{-1}, 1650 cm^{-1}, 2853 cm^{-1}, 2923 cm^{-1}, 2954 cm^{-1}, and 3200-3550 cm^{-1}, originated from amide II and amide I bands, symmetric $–CH_2$ stretch, asymmetric $–CH_2$ stretch, asymmetric

–CH_3 stretch, and O–H stretch, respectively [41-43], which represented proteins [42], aliphatic hydrocarbon [43], and humic substances [44, 45] that are common components of shale oil and gas wastewaters [43, 46, 47]. In contrast, those peaks were either smaller or negligible on the fouled membranes after the treatment of Sample 2, indicating fewer organic foulants present on the membrane surfaces. This difference was in accordance with the lower content of TOC (Table C1), cleaner membrane surface (Figure 6-4), and less water flux decline (Figure 6-3) associated with the treatment of produced water Sample 2.

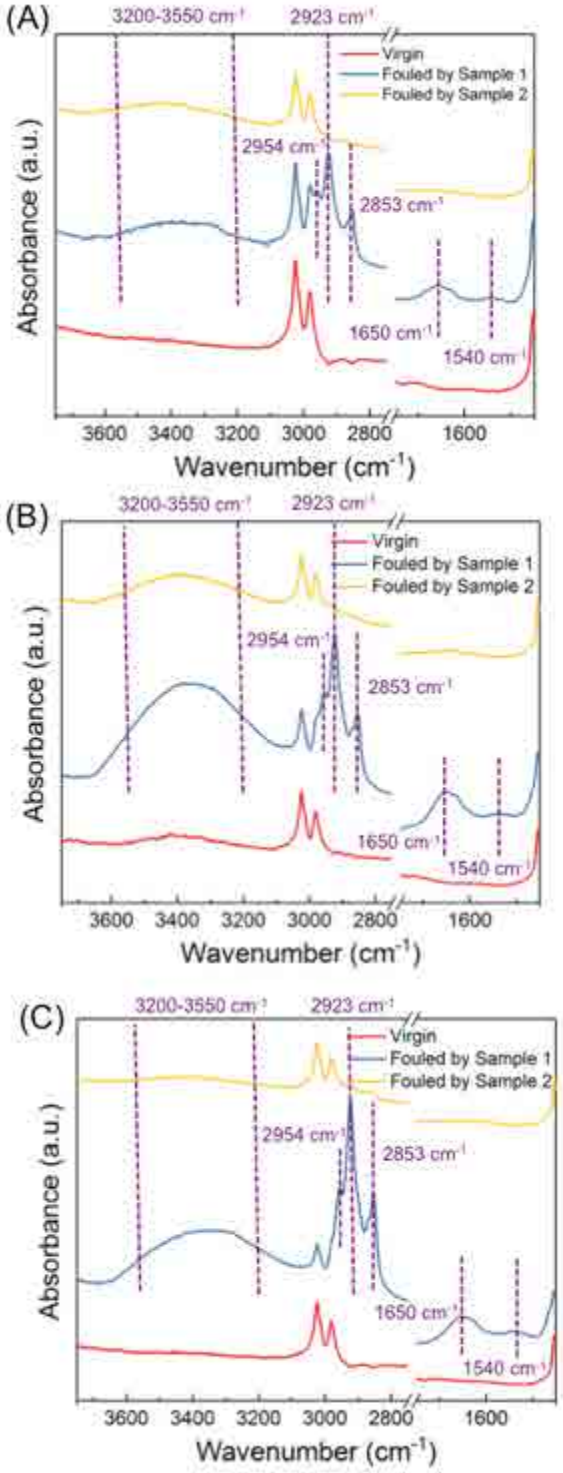

Figure 6-6. ATR-FTIR spectra of (A) pristine PVDF membrane, (B) PVDF-PVA membrane, and (C) PVDF-SiO_2-FAS membrane before and after the desalination of shale oil and gas produced water in a single cycle. New peaks discovered on the fouled membranes are labeled.

The results described above demonstrated that the flux decline observed in the DCMD desalination of shale oil and gas produced water was caused by a combined effect of inorganic scaling and organic fouling. The two produced water samples created distinctive characteristics of fouling layers (Figure 6-6), reflecting their different chemical compositions. This difference partially explained the varied performance of the tested membranes when treating different produced water samples (Figure 6-3). As compared to Sample 2, Sample 1 contained more organic foulants that were able to deposit on the membrane surface. The hydration layer formed by PVA coating rendered the PVDF-PVA membrane underwater oleophobic (Figure C3) and reduced the attachment of organic foulants (hydrophobic foulants in particular) to the membrane surface. This favorable feature contributed to a better fouling resistance of the PVDF-PVA membrane (Figure 6-3A), especially at the initial stage of DCMD desalination when membrane fouling was controlled by membrane-foulant interactions. However, this effect was minimal in the treatment of Sample 2 (Figure 6-3B), due to the small amount of organic foulants on all the membranes after treatment (as indicated by ATR-FTIR in Figure 6-6). Furthermore, the EDX analysis demonstrated the occurrence of silica/silicate scaling on membrane surfaces. It is well known that metal ions, such as Ca^{2+}, Mg^{2+}, and Fe^{3+}, promote silica/silicate scaling by catalyzing silica polymerization or forming silicate precipitates [36, 48, 49]. As shown in Table C1, the concentrations of dissolved calcium, iron, and magnesium were higher in Sample 1 than Sample 2, contributing to the denser silica/silicate layer on the membrane surface after the treatment of Sample 1. Therefore, the lesser extent of organic fouling and silica/silicate scaling caused by Sample 2, along with the lack of

barite scaling (Figure C8), were likely responsible for the generally better membrane performance in the DCMD treatment of Sample 2 (Figure 6-3).

However, we acknowledge that the above explanation does not represent a thorough understanding of the performance difference among the tested membranes, due to the complex organic and inorganic compositions of the produced waters. Alternative techniques to ATR-FTIR, such as liquid chromatography (LC) coupled with organic carbon detection (OCD) or high-resolution mass spectrometry (HRMS), enable a more detailed characterization of organic components [50], thereby deepening our understanding of the foulant-membrane interactions. Also, we still lack sufficient knowledge of how membrane surface properties influence inorganic scaling in the MD process, let alone under more complicated scenarios of combined fouling and scaling [51]. This knowledge gap, although beyond the scope of the current study, supports the need for our future research investigating the behaviors of MD membranes exposed to a mixture of varying organic and inorganic foulants.

6.3.4 Fouling Reversibility and Membrane Reusability After Physical Cleaning

The performance of MD membranes has been evaluated primarily by their fouling and wetting propensity in a single treatment cycle. However, fouling reversibility and membrane reusability after cleaning, which could be only examined in multiple treatment cycles, are also important performance criteria, especially in the assessment of long-term membrane performance. Therefore, physical membrane cleaning was performed after each cycle of produced water treatment (i.e.,

collecting 800 mL of permeate). After cleaning, the MD membranes were air dried and re-inserted into the DCMD unit to start another treatment cycle with newly added produced water. The water vapor fluxes of the tested membranes in three consecutive treatment cycles are presented in Figures 6-7 and C9, with the corresponding flux recovery rates (*R*, as calculated using Equation 6-1) shown in Figure C10.

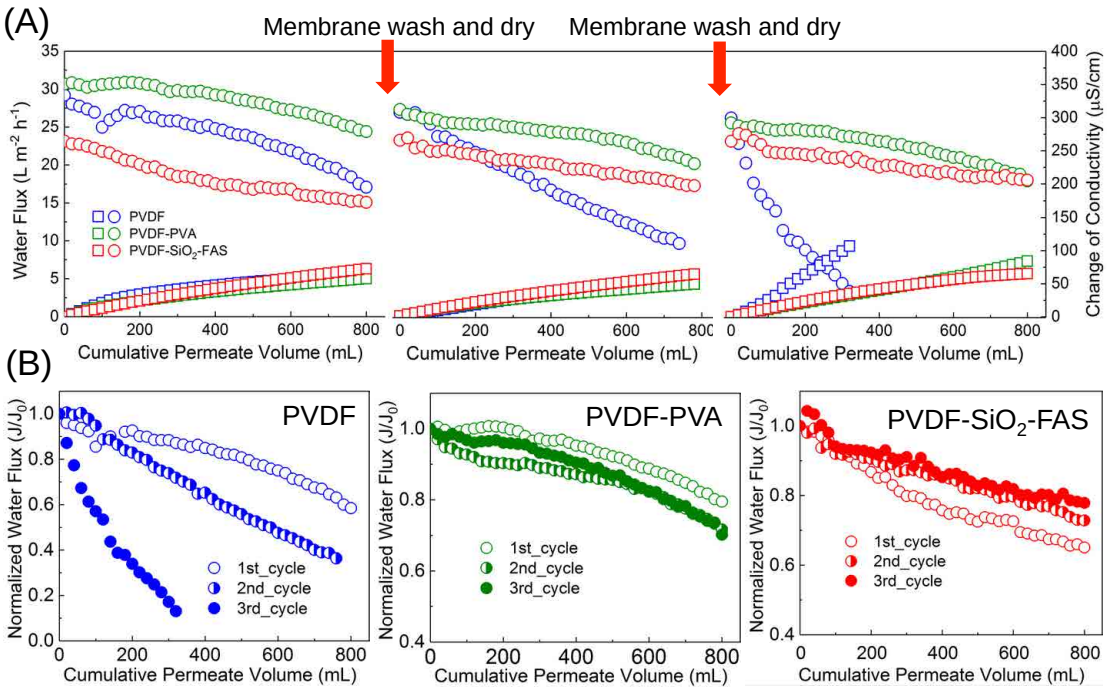

Figure 6-7. Fouling reversibility and membrane reusability during DCMD desalination of shale oil and gas produced water Sample 1 in three treatment cycles. (A) Absolute and (B) normalized water (vapor) fluxes for different tested membranes. The experimental condition of DCMD desalination was identical to that described in Figure 6-3. The red arrows indicate the time when DCMD tests were terminated and the membrane coupons were subjected to physical cleaning followed by in-air drying. The dried membrane was then re-inserted into the DCMD unit to start another cycle of desalination with new shale oil and gas produced water. Note that as the number of treatment cycles increased, the performance of pristine PVDF membrane degraded significantly, whereas a decelerated water flux decline was observed for the PVDF-SiO_2-FAS membrane. The performance of MD membranes in treating produced water Sample 2 is presented in Figure C9 of the Appendix C.

The flux recovery rates after physical cleaning were ≥ 80% for all the tested membranes regardless of treatment cycles (Figure C10). This relatively high fouling reversibility could be attributed to the low operational pressure applied to the MD process. The initial water fluxes of the membranes decreased after each treatment cycle (Figure C10, except for the PVDF-SiO_2-FAS membrane treating Sample 1). Similar phenomena were also observed due to membrane scaling by $CaCO_3$ [52] and membrane fouling by humic substances [53] in MD desalination.

However, membrane reusability, which was evaluated by comparing flux decline rates in different treatment cycles, varied among the tested membranes. In general, the flux decline rates were facilitated for both pristine PVDF and PVDF-PVA membranes as the cycle number increased, whereas the flux decline of the PVDF-SiO_2-FAS membrane was decelerated within three cycles of produced water treatment (Figures 6-7 and C9). When collecting 800 mL distillate from Sample 1 (Figure 6-7), the pristine PVDF membrane experienced increasing flux decline ratios of 42%, 64%, and 87% in Cycles 1, 2, and 3, respectively, and flux decline of the PVDF-PVA membrane increased from 21% in Cycle 1 to 30% in Cycle 3. In contrast, the PVDF-SiO_2-FAS membrane showed less flux decline in Cycles 2 and 3 (27% and 22% of water flux decline for Cycles 2 and 3, respectively) than in Cycle 1 (35% of water flux decline). DCMD treatment of Sample 2 followed the same trend that the PVDF-SiO_2-FAS membrane outperformed the other two membranes in terms of membrane reusability (Figure C9), indicating that the PVDF-SiO_2-FAS membrane was more robust regardless of feedwater composition. In addition, except for pristine

PVDF membrane treating Sample 1 in Cycle 3, all the membranes did not suffer from membrane wetting, as indicated by the consistently low conductivity of the DCMD distillate (Figures 6-7A and C9A).

The better reusability of the PVDF-SiO_2-FAS membrane could be explained by the following reasons. The accelerated flux decline observed for PVDF and PVDF-PVA membranes was likely due to the penetration of produced water into interior membrane pores. As a result, membrane fouling and scaling were not limited to the membrane surface but also occurred at a certain depth within the membranes. The organic foulants or inorganic scalants attached to the membrane pores could attract new foulants or serve as nucleation sites to facilitate membrane fouling and scaling [54]. In contrast, the omniphobicity of the PVDF-SiO_2-FAS membrane retarded the intrusion of feedwater, thereby constraining membrane fouling and scaling to a shallow depth near the membrane surface. Our hypothesis was supported by SEM-EDX line-scan analysis of the cross-section of the fouled membranes after three treatment cycles (Figures 6-8 and C11). The change of Fe kα1 signal was used as an indicator of foulant penetration due to the ubiquitous presence of Fe in the fouling layers (Figures 6-5 and C6, the Si signal was not used because fabrication of the PVDF-SiO_2-FAS membrane involved the use of silica nanoparticles). As shown in Figure 6-8, the penetration depths of foulants for PVDF and PVDF-PVA membranes after the treatment of Sample 1 were ~9 μm, whereas a narrower depth of only ~4 μm was found for the PVDF-SiO_2-FAS membrane. A similar result was observed for the membranes after the treatment of Sample 2

(Figure C10). The confinement of foulants and scalants helped prevent performance degradation of the PVDF-SiO_2-FAS membrane. The hydration layer formed on the PVDF-PVA membrane surface hindered the attachment and deposition of foulants and scalants onto the membrane, which explained the less accelerated flux reduction of the PVDF-PVA membrane compared to the pristine PVDF membrane. It should also be noted that the intrusion of feedwater into the MD membranes (i.e., partial pore wetting) did not cause membrane wetting, which requires the penetration of feedwater through the entire membrane substrate. Further, the initial water flux of PVDF-SiO_2-FAS membrane was lower than the other two membranes, which led to a smaller extent of concentration polarization. The resulting similar elevation of foulant/scalant concentrations at the membrane surface mitigated membrane fouling/scaling and the corresponding flux decline [54]. In addition, the decreased hydrophobicity of the PVDF-SiO_2-FAS membrane after produced water treatment (Figure C12) reduced hydrophobic-hydrophobic interactions between the membrane surface and non-polar foulants, contributing to the decelerated flux decline observed in Cycles 2 and 3 compared to Cycle 1.

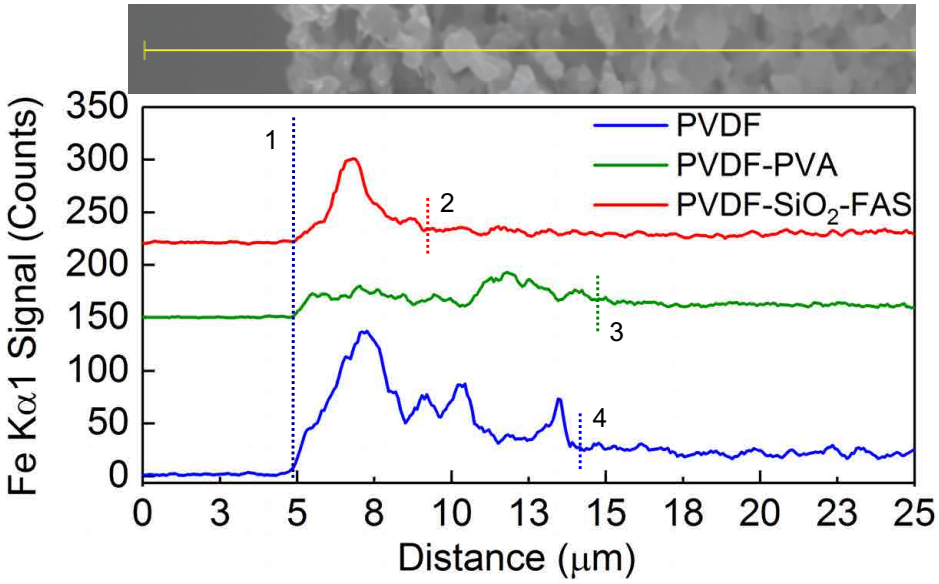

Figure 6-8. SEM-EDS line analysis of the cross-section of MD membranes after three treatment cycles for produced water Sample 1. The SEM image (only showing that of PVDF-FAS-SiO_2 membrane as similar images were obtained for the other two membranes) indicates where the EDS line-scan was performed (yellow line). Fe kα1 signal was used as an indicator of foulant location due to the ubiquitous presence of Fe in the foulant layers. The associated results for produced water Sample 2 are presented in Figure C11 of the Appendix C.

Therefore, although the PVDF-SiO_2-FAS membrane was not advantageous in a single cycle of produced water treatment, it demonstrated robust membrane reusability in multiple treatment cycles integrated with physical membrane cleaning. To the best of our knowledge, our study provides the first set of comparative data on the reusability, not only anti-fouling and anti-wetting properties of MD membranes, in the treatment of complex industrial wastewater like shale oil and gas produced water. The implications of our findings in MD membrane design and selection are discussed in the following subsection.

6.3.5 Environmental implications in membrane design and selection for MD treatment of shale oil and gas produced water

We have demonstrated that membrane performance in MD treatment of shale oil and gas produced water was influenced by not only surface wettability but also feedwater composition. Previous studies establishing relationships between membrane surface properties (in particular surface wettability) and MD performance have been based primarily on using synthetic feedwater with defined chemistry and individual organic foulants [20, 25-27, 45]. However, the performance of MD membranes in treating shale oil and gas wastewater, as shown in our study, was comprehensively regulated by organic fouling and inorganic scaling, which were caused by diverse foulants and scalants present in the feedwater. The variation in chemical composition of wastewater, which commonly occurs in shale oil and gas production activities [10, 55], could further alter MD membrane performance. Therefore, although an increasing number of new membrane materials have been recently fabricated to improve fouling and wetting resistance in MD [23, 28, 29, 56-60], additional efforts are needed to challenge these membranes with feedwater carrying complicated and variable chemical components (e.g., industrial wastewater or synthetic feed solutions with mixed foulants and scalants). This approach will serve as a critical step prior to the commercialization and large-scale applications of anti-fouling/wetting MD membranes.

Furthermore, the comparative performance among the tested membranes differed between a single treatment cycle and multiple treatment cycles. In a single treatment cycle, the superhydrophobic PVDF-SiO_2-FAS membrane did not benefit from its improved wetting resistance, due to the lack of abundant low surface energy substances in the produced waters.

Instead, the PVDF-PVA membrane with a hydrophilic top layer displayed better fouling resistance and water flux (Figure 6-3). When multiple treatment cycles were performed with physical membrane cleaning, however, the PVDF-SiO_2-FAS membrane exhibited better reusability than the pristine PVDF and PVDF-PVA membranes (Figures 6-7 and C8), suggesting its superior durability in long-term MD operation. Therefore, in order to achieve a more comprehensive evaluation of MD membrane performance, MD tests with multiple treatment cycles should be employed as a complementary means to the single-cycle approach typically employed in the literature. In addition, the lower initial water flux of the PVDF-SiO_2-FAS membrane compromised water productivity, which is closely associated with the cost efficiency of MD desalination systems. Therefore, one should consider, comprehensively, fouling and wetting resistance, water productivity, and reusability of MD membranes in the design and selection of appropriate membranes for efficient treatment of complicated, hypersaline wastewater such as shale oil and gas produced water.

6.4 Conclusions

MD membranes with different surface wettability, including a hydrophobic PVDF membrane, a superhydrophobic PVDF membrane, and a composite PVDF membrane with a thin hydrophilic top layer, were fabricated and tested in a DCMD process to treat shale oil and gas produced water generated from the Wattenberg field in northeast Colorado. In a single treatment cycle, the composite membrane showed better fouling resistance than the pristine PVDF membrane and the

superhydrophobic membrane in the treatment of the first produced water sample, but all the tested membranes experienced similar flux decline with a second sample collected at a different sampling date. This difference was caused by varied chemical compositions of the two produced water samples, which resulted in distinct features of inorganic and organic fouling layers formed on the membrane surface. We conclude that the relationship between membrane surface wettability and MD performance was influenced by feedwater composition during the treatment of shale oil and gas produced water.

The fouling reversibility and membrane reusability were evaluated in multiple treatment cycles, each including physical membrane cleaning. Membrane fouling by shale oil and gas produced water was reversible regardless of membrane type, but membrane reusability in long-term operation varied among the tested membranes. Compared to the pristine and composite PVDF membranes, the superhydrophobic membrane exhibited better reusability in three consecutive treatment cycles, while its robustness was achieved at the expense of water productivity. Our study demonstrates the importance of performing multiple cycles in the assessment of membrane performance during MD desalination, as well as the necessity of considering fouling/wetting resistance, water productivity, and reusability in the design and selection of appropriate MD membranes for the treatment of complex industrial wastewater such as shale oil and gas produced water. In addition, future research efforts need to challenge anti-fouling/wetting MD membranes with feedwater possessing complicated and diverse chemical components, in order to evaluate the

performance and reliability of these membranes more accurately prior to their commercialization and large-scale applications.

References

1. Vidic, R. D.; Brantley, S. L.; Vandenbossche, J. M.; Yoxtheimer, D.; Abad, J. D., Impact of shale gas development on regional water quality. *Science* 2013, 340, (6134).
2. Baffes, J.; Kose, M. A.; Ohnsorge, F.; Stocker, M. The great plunge in oil prices: Causes, consequences, and policy pesponses; *Work Bank*: 2015.
3. Kondash, A.; Vengosh, A., Water footprint of hydraulic fracturing. *Environ Sci Tech Let* 2015, 2, (10), 276-280.
4. Shrestha, N.; Chilkoor, G.; Wilder, J.; Gadhamshetty, V.; Stone, J. J., Potential water resource impacts of hydraulic fracturing from unconventional oil production in the Bakken shale. *Water Res* 2017, 108, 1-24.
5. Vengosh, A.; Jackson, R. B.; Warner, N.; Darrah, T. H.; Kondash, A., A critical review of the risks to water resources from unconventional shale gas development and hydraulic fracturing in the United States. *Environ Sci Technol* 2014, 48, (15), 8334-8348.
6. Kim, W. Y., Induced seismicity associated with fluid injection into a deep well in Youngstown, Ohio. *J Geophys Res-Sol Ea* 2013, 118, (7), 3506-3518.
7. Ellsworth, W. L., Injection-induced earthquakes. *Science* 2013, 341, (6142), 142-+.
8. He, Y.; Sun, C.; Zhang, Y.; Folkerts, E. J.; Martin, J. W.; Goss, G. G., Developmental toxicity of the organic fraction from hydraulic fracturing flowback and produced waters to early life stages of Zebrafish (Danio rerio). *Environ Sci Technol* 2018, In press.
9. Butkovskyi, A.; Bruning, H.; Kools, S. A. E.; Rijnaarts, H. H. M.; Van Wezel, A. P., Organic pollutants in shale gas flowback and produced waters: Identification, potential ecological impact, and implications for treatment strategies. *Environ Sci Technol* 2017, 51, (9), 4740-4754.
10. Kim, S. Y.; Omur-Ozbek, P.; Dhanasekar, A.; Prior, A.; Carlson, K., Temporal analysis of flowback and produced water composition from shale oil and gas operations: Impact of frac fluid characteristics. *J Petrol Sci Eng* 2016, 147, 202-210.
11. Rosenblum, J.; Thurman, E. M.; Ferrer, I.; Aiken, G.; Linden, K. G., Organic chemical characterization and mass balance of a hydraulically fractured well: From fracturing fluid to produced water over 405 days. *Environ Sci Technol* 2017, 51, (23), 14006-14015.
12. Elimelech, M.; Phillip, W. A., The future of seawater desalination: Energy, technology, and the environment. *Science* 2011, 333, (6043), 712-717.
13. Shaffer, D. L.; Chavez, L. H. A.; Ben-Sasson, M.; Castrillon, S. R. V.; Yip, N. Y.; Elimelech, M., Desalination and reuse of high-salinity shale gas produced water: Drivers, technologies, and future directions. *Environ Sci Technol* 2013, 47, (17), 9569-9583.
14. Alklaibi, A. M.; Lior, N., Membrane-distillation desalination: status and potential. *Desalination* 2005, 171, (2), 111-131.
15. Lawson, K. W.; Lloyd, D. R., Membrane distillation. *J Membrane Sci* 1997, 124, (1), 1-25.

16. Tong, T. Z.; Elimelech, M., The global rise of zero liquid discharge for wastewater management: Drivers, technologies, and future directions. *Environ Sci Technol* 2016, 50, (13), 6846-6855.
17. Deshmukh, A.; Boo, C.; Karanikola, V.; Lin, S. H.; Straub, A. P.; Tong, T. Z.; Warsinger, D. M.; Elimelech, M., Membrane distillation at the water-energy nexus: limits, opportunities, and challenges. *Energy & Environmental Science* 2018, 11, 1177-1196.
18. Warsinger, D. M.; Swarninathan, J.; Guillen-Burrieza, E.; Arafat, H. A.; Lienhard, J. H., Scaling and fouling in membrane distillation for desalination applications: A review. *Desalination* 2015, 356, 294-313.
19. Tijing, L. D.; Woo, Y. C.; Choi, J. S.; Lee, S.; Kim, S. H.; Shon, H. K., Fouling and its control in membrane distillation-A review. *J Membrane Sci* 2015, 475, 215-244.
20. Lin, S. H.; Nejati, S.; Boo, C.; Hu, Y. X.; Osuji, C. O.; Ehmelech, M., Omniphobic membrane for robust membrane distillation. *Environ Sci Tech Let* 2014, 1, (11), 443-447.
21. Boo, C.; Lee, J.; Elimelech, M., Omniphobic polyvinylidene fluoride (PVDF) membrane for desalination of shale gas produced water by membrane distillation. *Environ Sci Technol* 2016, 50, (22), 12275-12282.
22. Boo, C.; Lee, J.; Elimelech, M., Engineering surface energy and nanostructure of microporous films for expanded membrane distillation applications. *Environ Sci Technol* 2016, 50, (15), 8112-8119.
23. Huang, Y. X.; Wang, Z. X.; Jin, J.; Lin, S. H., Novel Janus membrane for membrane distillation with simultaneous fouling and wetting resistance. *Environ Sci Technol* 2017, 51, (22), 13304-13310.
24. Razmjou, A.; Arifin, E.; Dong, G. X.; Mansouri, J.; Chen, V., Superhydrophobic modification of TiO_2 nanocomposite PVDF membranes for applications in membrane distillation. *J Membrane Sci* 2012, 415, 850-863.
25. Wang, Z. X.; Jin, J.; Hou, D. Y.; Lin, S. H., Tailoring surface charge and wetting property for robust oil-fouling mitigation in membrane distillation. *J Membrane Sci* 2016, 516, 113-122.
26. Wang, Z. X.; Hou, D. Y.; Lin, S. H., Composite membrane with underwater-oleophobic surface for anti-oil-fouling membrane distillation. *Environ Sci Technol* 2016, 50, (7), 3866-3874.
27. Wang, Z. X.; Lin, S. H., Membrane fouling and wetting in membrane distillation and their mitigation by novel membranes with special wettability. *Water Res* 2017, 112, 38-47.
28. Woo, Y. C.; Kim, Y.; Yao, M.; Tijing, L. D.; Choi, J. S.; Lee, S.; Kim, S. H.; Shon, H. K., Hierarchical composite membranes with robust omniphobic surface using layer-by-layer assembly technique. *Environ Sci Technol* 2018, 52, (4), 2186-2196.
29. Lee, E. J.; Deka, B. J.; Guo, J. X.; Woo, Y. C.; Shon, H. K.; An, A. K., Engineering the re-entrant hierarchy and surface energy of PDMS-PVDF membrane for membrane distillation

using a facile and benign microsphere coating. *Environ Sci Technol* 2017, 51, (17), 10117-10126.

30. Du, J. R.; Peldszus, S.; Huck, P. M.; Feng, X. S., Modification of poly(vinylidene fluoride) ultrafiltration membranes with poly(vinyl alcohol) for fouling control in drinking water treatment. *Water Res* 2009, 43, (18), 4559-4568.
31. Zhang, C. H.; Yang, F. L.; Wang, W. J.; Chen, B., Preparation and characterization of hydrophilic modification of polypropylene non-woven fabric by dip-coating PVA (polyvinyl alcohol). *Sep Purif Technol* 2008, 61, (3), 276-286.
32. Lu, X. L.; Castrillon, S. R. V.; Shaffer, D. L.; Ma, J.; Elimelech, M., In situ surface chemical modification of thin-film composite forward osmosis membranes for enhanced organic fouling resistance. *Environ Sci Technol* 2013, 47, (21), 12219-12228.
33. Walker, S. L.; Bhattacharjee, S.; Hoek, E. M. V.; Elimelech, M., A novel asymmetric clamping cell for measuring streaming potential of flat surfaces. *Langmuir* 2002, 18, (6), 2193-2198.
34. Qin, W. L.; Zhang, J. H.; Xie, Z. L.; Ng, D.; Ye, Y.; Gray, S. R.; Xie, M., Synergistic effect of combined colloidal and organic fouling in membrane distillation: Measurements and mechanisms. *Environ Sci-Wat Res* 2017, 3, (1), 119-127.
35. Heyob, K. M.; Blotevogel, J.; Brooker, M.; Evans, M. V.; Lenhart, J. J.; Wright, J.; Lamendella, R.; Borch, T.; Mouser, P. J., Natural attenuation of nonionic surfactants used in hydraulic fracturing fluids: Degradation rates, pathways, and mechanisms. *Environ Sci Technol* 2017, 51, (23), 13985-13994.
36. Bremere, I.; Kennedy, M.; Mhyio, S.; Jaljuli, A.; Witkamp, G. J.; Schippers, J., Prevention of silica scale in membrane systems: removal of monomer and polymer silica. *Desalination* 2000, 132, (1-3), 89-100.
37. Gallup, D. L., Aluminum silicate scale formation and inhibition (2): Scale solubilities and laboratory and field inhibition tests. *Geothermics* 1998, 27, (4), 485-501.
38. Sjoberg, S., Silica in aqueous environments. *J Non-Cryst Solids* 1996, 196, 51-57.
39. Gilron, J.; Ladizansky, Y.; Korin, E., Silica fouling in direct contact membrane distillation. *Ind Eng Chem Res* 2013, 52, (31), 10521-10529.
40. Vankeuren, A. N. P.; Hakala, J. A.; Jarvis, K.; Moore, J. E., Mineral reactions in shale gas reservoirs: Barite Scale formation from reusing produced water as hydraulic fracturing fluid. *Environ Sci Technol* 2017, 51, (16), 9391-9402.
41. Li, N.; Xiao, C. F.; An, S. L.; Hu, X. Y., Preparation and properties of PVDF/PVA hollow fiber membranes. *Desalination* 2010, 250, (2), 530-537.
42. Belfer, S.; Fainchtain, R.; Purinson, Y.; Kedem, O., Surface characterization by FTIR-ATR spectroscopy of polyethersulfone membranes-unmodified, modified and protein fouled. *J Membrane Sci* 2000, 172, (1-2), 113-124.

43. Bell, E. A.; Poynor, T. E.; Newhart, K. B.; Regnery, J.; Coday, B. D.; Cath, T. Y., Produced water treatment using forward osmosis membranes: Evaluation of extended-time performance and fouling. *J Membrane Sci* 2017, 525, 77-88.
44. Zularisam, A. W.; Ismail, A. F.; Salim, R., Behaviours of natural organic matter in membrane filtration for surface water treatment - a review. *Desalination* 2006, 194, (1-3), 211-231.
45. Lu, X. M.; Peng, Y. L.; Qiu, H. R.; Liu, X. R.; Ge, L., Anti-fouling membranes by manipulating surface wettability and their anti-fouling mechanism. *Desalination* 2017, 413, 127-135.
46. Hickenbottom, K. L.; Hancock, N. T.; Hutchings, N. R.; Appleton, E. W.; Beaudry, E. G.; Xu, P.; Cath, T. Y., Forward osmosis treatment of drilling mud and fracturing wastewater from oil and gas operations. *Desalination* 2013, 312, 60-66.
47. Alzahrani, S.; Mohammad, A. W.; Hilal, N.; Abdullah, P.; Jaafar, O., Identification of foulants, fouling mechanisms and cleaning efficiency for NF and RO treatment of produced water. *Sep Purif Technol* 2013, 118, 324-341.
48. Sheikholeslami, R.; Zhou, S., Performance of RO membranes in silica bearing waters. *Desalination* 2000, 132, (1-3), 337-344.
49. Milne, N. A.; O'Reilly, T.; Sanciolo, P.; Ostarcevic, E.; Beighton, M.; Taylor, K.; Mullett, M.; Tarquin, A. J.; Gray, S. R., Chemistry of silica scale mitigation for RO desalination with particular reference to remote operations. *Water Res* 2014, 65, 107-133.
50. Riley, S. M.; Ahoor, D. C.; Regnery, J.; Cath, T. Y., Tracking oil and gas wastewater-derived organic matter in a hybrid biofilter membrane treatment system: A multi-analytical approach. *Sci Total Environ* 2018, 613, 208-217.
51. Quay, A. N.; Tong, T. Z.; Hashmi, S. M.; Zhou, Y.; Zhao, S.; Elimelech, M., Combined organic fouling and inorganic scaling in reverse osmosis: Role of protein-silica interactions. *Environ Sci Technol* 2018, In press.
52. Gryta, M., Fouling in direct contact membrane distillation process. *J Membrane Sci* 2008, 325, (1), 383-394.
53. Naidu, G.; Jeong, S.; Vigneswaran, S., Interaction of humic substances on fouling in membrane distillation for seawater desalination. *Chem Eng J* 2015, 262, 946-957.
54. Martinetti, C. R.; Childress, A. E.; Cath, T. Y., High recovery of concentrated RO brines using forward osmosis and membrane distillation. *J Membrane Sci* 2009, 331, (1-2), 31-39.
55. Rosenblum, J.; Nelson, A. W.; Ruyle, B.; Schultz, M. K.; Ryan, J. N.; Linden, K. G., Temporal characterization of flowback and produced water quality from a hydraulically fractured oil and gas well. *Sci Total Environ* 2017, 596, 369-377.
56. Woo, Y. C.; Chen, Y.; Tijing, L. D.; Phuntsho, S.; He, T.; Choi, J. S.; Kim, S. H.; Shon, H. K., CF4 plasma-modified omniphobic electrospun nanofiber membrane for produced water brine treatment by membrane distillation. *J Membrane Sci* 2017, 529, 234-242.

57. Chen, Y.; Tian, M. M.; Li, X. M.; Wang, Y. Q.; An, A. K.; Fang, J. H.; He, T., Anti-wetting behavior of negatively charged superhydrophobic PVDF membranes in direct contact membrane distillation of emulsified wastewaters. *J Membrane Sci* 2017, 535, 230-238.
58. Zhang, R.; Chen, Y.; Wang, J.; Song, J.; Li, X.; He, T., Preparation of omniphobic PVDF membrane with hierarchical structure for treating saline oily wastewater using direct contact membrane distillation. *J Membrane Sci* 2018, In press.
59. Zhong, W. W.; Hou, J. W.; Yang, H. C.; Chen, V., Superhydrophobic membranes via facile bio-inspired mineralization for vacuum membrane distillation. *J Membrane Sci* 2017, 540, 98-107.
60. Efome, J. E.; Rana, D.; Matsuura, T.; Lan, C. Q., Enhanced performance of PVDF nanocomposite membrane by nanofiber coating: A membrane for sustainable desalination through MD. *Water Res* 2016, 89, 39-49.

CHAPTER 7: Long-chain PFASs-free omniphobic membranes for sustained membrane distillation [4]

7.1 Introduction

Membrane distillation (MD) has emerged as a promising thermal-based membrane technology for the treatment of hypersaline brines.[1-3] Due to its significant potential of promoting water sustainability as well as unique advantages over other desalination technologies, MD has attracted tremendous efforts that aim to improve its efficiency and resiliency. In MD, a partial vapor pressure difference between hot saline and cold distilled streams drives the transport of water vapor across a hydrophobic, microporous membrane.[4, 5] This hybrid membrane-thermal process displays extremely high tolerance to the feed salinity and has a theoretical 100% rejection to non-volatile dissolved solutes.[6, 7] Additionally, MD can be operated at moderate temperatures (e.g., 60-80°C), rendering it uniquely capable of leveraging low-grade thermal energy to reduce the energy cost and carbon footprint.[8-11]

However, membrane pore wetting (i.e., permeation of feed solution through membrane pores into the distillate, leading to failure of MD desalination) poses a significant challenge to sustained MD process, which has drastically impeded the application of MD technology for the treatment of

[4] This chapter will be submitted as a manuscript under review as

Du, X.; Alipanahrostam, M; Wang, W.; Tong, T., Long-chain PFASs-free omniphobic membranes for sustained membrane distillation. *ACS Appl. Mater. Interfaces*. 2022. (Under review).

feed solutions with low surface tensions.[12, 13] Previous studies have shown that low surface energy surfactants, which are commonly present in hypersaline wastewater (e.g., produced water generated from the oil and gas industry),[14, 15] can cause pore wetting of hydrophobic membranes.[16-19] To overcome this obstacle, novel omniphobic MD membranes that possess high wetting resistance against both high surface tension liquids and low surface tension liquids have recently been developed to dramatically enhance the adaptability and resilience of MD technology.[20-24]

The omniphobic membranes can be engineered by combining re-entrant surface textures (i.e., multi-valued or convex texture) and materials with low solid surface energy.[25-29] To date, virtually all omniphobic MD membranes were fabricated using long-chain per- and polyfluoroalkyl substances (PFASs), which consist of fluorinated carbon chains with at least 8 fluorinated carbons, due to their ultra-low surface energy.[16, 30-34] The long-chain PFASs, however, notoriously pose severe risks to humans, wildlife, and the environment due to their long-lasting persistence, high tendency of bioaccumulation, and high toxicity.[35, 36] Therefore, long-chain PFASs have been considered emerging contaminants and being phased out by environmental agencies globally.[37-40] Consequently, there is a dire need for innovative strategy, which leads to omniphobic membranes using alternatives that display lower bioaccumulation potential and less acute toxicity.

In this work, we demonstrate that MD membranes with exceptional wetting resistance can be achieved through the combination of hierarchically structured membranes consisting of re-entrant texture at different length scales and (ultra)short-chain fluorocarbons. It must be noted that the short-chain (i.e., fluorinated chain with 4-6 fluorinated carbons) and ultrashort-chain (i.e.,

fluorinated chain with less than 4 fluorinated carbons) fluorocarbons are less bioaccumulative and more biosafe than the long-chain PFASs.[39, 41] Therefore, they have been increasingly used as alternatives to replace long-chain PFASs.[39, 42] With our long-chain PFASs-free omniphobic membranes, we demonstrate stable MD process in direct contact membrane distillation (DCMD) under various surfactant concentrations, achieving wetting resistance comparable to that of long-chain PFASs-based membranes. Further, based on the exceptional performance of our novel membranes as well as an evaluation of the toxicities of the short- and ultrashort-chain fluorocarbons used in this study, we elucidate the design and sustainability of omniphobic membranes for MD applications. Our results indicate that long-chain PFASs-free membranes with high wetting resistance can be designed by tailoring the hierarchical structures of the membranes. Additionally, the balance between sustainability and wetting resistance of MD systems should be tailored to the wetting potential of the feedwater. We envision that the results and insights obtained from our work will pave the way towards the development of more sustainable MD technology for mitigating environmental impact of hypersaline wastewater and water scarcity.

7.2 Materials and methods

7.2.1 Materials and chemicals

Microporous PVDF membranes with a nominal pore size of 0.45 μm (HVHP, Durapore) were purchased from Millipore Sigma. (3-aminopropyl)triethoxysilane (APTES) and 15 nm silica particles (30 wt% suspension in water) were provided by Sigma-Aldrich, and 120 nm silica

particles (10 mg/mL in water) were supplied by NanoComposix. Nonafluorohexyltriethoxysilane (FC-4, i.e., fluorinated chain consisting of 4 fluorinated carbons) was purchased from Gelest Inc. 3-(heptafluoroisopropoxy)propyltriethoxysilane (i.e., FC-B3, branched ultrashort-chain fluorocarbon compound with 3 fluorinated carbons) was obtained from Santa Cruz Biotechnology Inc. (3,3,3-trifluoropropyl)triethoxysilane (FC-1) was synthesized by Synquest Laboratories. Sodium chloride (NaCl), sodium hydroxide (NaOH), and sodium dodecyl sulfate (SDS) were all obtained from VWR BDH Chemicals. Anhydrous ethanol was purchased from Decon Laboratories. Deionized (DI) water was generated from a Milli-Q ultrapure water purification system (>18 MΩ·cm, Millipore).

7.2.2 Membrane fabrication

Hierarchically micro/nano-structured membranes with different levels of hierarchy (i.e., dual-tier micro/nano-structures and three-tier micro/nano-structures) were fabricated by decorating the microporous pristine PVDF membranes using spherical silica particles with re-entrant texture (see Figure 7-1). To create strong bonding between the membrane surface and the silica particles, hydroxyl groups were first created on the pristine membrane by immersing ethanol-wetted membrane in a 7.5 M NaOH solution for 3 h at 70 °C. The NaOH-modified membrane was washed with DI water and dried in an oven at 70 °C for 1 h. Then the membrane was immerged in a 1% v/v APTES ethanol solution at room temperature for 1 h to functionalize the membrane surface with positively charged amine groups. The APTES-modified membrane was thoroughly rinsed

with ethanol and dried by heating at 60 °C for 1 h. To create dual-tier micro/nano-structure (i.e., microporous membrane decorated with one layer of spherical silica particles), the APTES-modified membrane was prewetted using ethanol and then soaked in an aqueous solution of silica nanoparticles with a certain size. Two different dual-tier micro/nano-structures were fabricated using 120 nm (0.06% w/w in acetic buffer solution of pH 4 in which the membrane was soaked for 3 h) or 15 nm (0.03% w/w in acetic buffer solution of pH 4 in which the membrane was soaked for 1 h) silica particles, respectively. The dual-tier micro/nano-structured membrane was then washed with DI water and dried by heating at 80 °C for 1 h. To create the three-tier micro/nano-structure (i.e., microporous membrane decorated with two layers of spherical silica particles with different sizes), the membrane decorated with the 120 nm silica particles was subsequently modified with APTES under the same condition as described above. The APTES-modified membrane with dual-tier structure was then immersed in the aqueous solution of 15 nm silica particles (0.03% w/w in acetic buffer solution of pH 4) for 1 h, leading to superimposing of finer particles (i.e., 15 nm) on the coarser particles (i.e., 120 nm) and consequently the three-tier micro/nano-structure. The membrane with three-tier micro/nano-structure was washed with DI water and dried at 80 °C for 1 h.

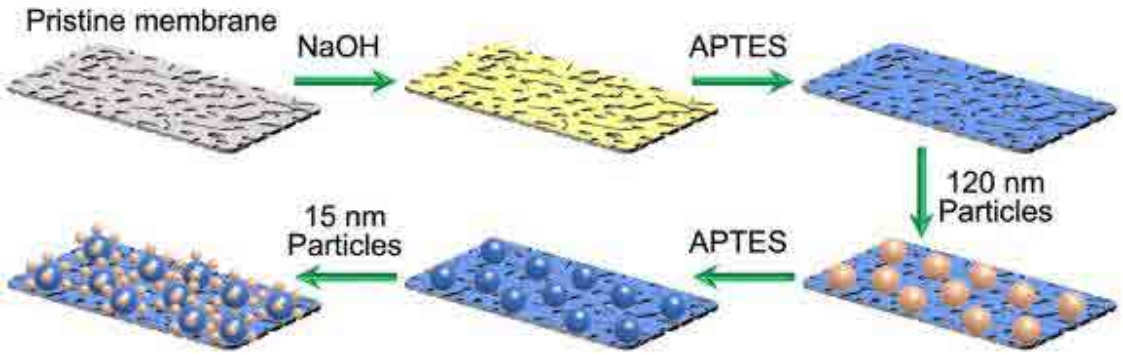

Figure 7-1. Fabrication processes of the hierarchically structured membrane with three-tier micro/nano-structure.

Subsequently, the hierarchically micro/nano-structured membranes with different levels of hierarchy were modified via liquid phase silanization (1% v/v silane in hexane) using fluorinated silanes of different chain lengths (i.e., FC-1, FC-B3, FC-4, or FC-8) for 2 days to impart low solid surface energy. The membranes were then rinsed thoroughly with hexane and dried overnight in an oven at 80 °C. The membranes with dual-tier micro/nano-structures, which were modified with FC-4, are referred to as PVDF-120-FC4 and PVDF-15-FC4, respectively. Similarly, the silane-modified membranes with three-tier micro/nano-structures are referred to as PVDF-120/15-FC1, PVDF-120/15-FCB3, and PVDF-120/15-FC4, respectively.

7.2.3 Membrane characterization

The surface morphologies of the pristine and hierarchically structured membranes were characterized using scanning electron microscopy (SEM, JEOL JSM-6500F) at 10 kV. X-ray photoelectron spectroscopy (XPS, PHI-5800 spectrometer) was used to analyze the surface chemical composition of the membranes. Further, the surface wettability of membranes was

evaluated by measuring contact angles of various liquids with different surface tensions, including 60% ethanol in water (γ_{lv} = 28.7 mN/m), 30% ethanol in water (γ_{lv} = 37.2 mN/m), 20% ethanol in water (γ_{lv} = 43.7 mN/m), 10% ethanol in water (γ_{lv} = 53.4 mN/m), 1.5 mM sodium dodecyl sulfate (SDS) in water (γ_{lv} = 61 mN/m), and water (γ_{lv} = 72.5 mN/m).[30]

7.2.4 Evaluation of membrane wetting resistance in MD

The wetting resistance of the membranes was evaluated using a custom-built, cross-flow DCMD system with an effective membrane area of 20.02 cm^2. The temperatures of the feed and distillate streams were maintained at 60 °C and 20 °C, respectively. The flow rate of the feed stream (9.6 cm/s) was higher than that of the distillate stream (5.3 cm/s) to facilitate the detection of membrane pore wetting.[16, 43] During the initial 1 h of the DCMD experiment, 1 M NaCl was used as the feed solution. SDS, a common amphiphilic surfactant used to evaluate membrane wetting,[16, 44, 45] was then added to the feed stream every 60 min to progressively reduce the surface tension of the feed solution. The SDS concentrations of the feed solution after sequential addition were 0.1, 0.2, 0.3, 0.4, and 0.5 mM, which correspond to surface tensions of ~42, ~33, ~31, ~29 and ~27 mN/m, respectively.[46] The weight and conductivity of the distillate stream were monitored continuously to calculate the water (vapor) fluxes and salt rejections to assess membrane wetting.

7.2.5 Evaluation of bioaccumulation potentials of fluorocarbons of different chain lengths

The bioaccumulation potentials of fluoroalkylsilanes with different chain lengths which were used for membrane fabrication were quantitatively evaluated in the context of regulatory criteria using

three parameters, including octanol-water partition coefficient (K_{ow}, indicating the lipophilicity of compounds), bioconcentration factor (BCF, indicating the chemical uptake from ambient environment only through respiratory surfaces), and bioaccumulation factor (BAF, indicating the chemical uptake from multiple exposure routes in the ambient environment).[47] These parameters were calculated using the Estimations Programs Interface (EPI) Suite software provided by U.S. Environmental Protection Agency (USEPA, Version 4.11).[48] The EPI Suite software is a well-accepted tool utilizing various quantitative structure-activity relationships (QSARs) to estimate physicochemical properties of chemicals based on the chemical structure.[49, 50] The K_{ow}, BCF and BAF values were calculated with the input of a simplified molecular-input line-entry system (SMILES) string in the EPI Suite software.

7.3 Results and discussions

7.3.1 Wettability of hierarchically micro/nano-structured membranes fabricated with short-chain fluorocarbon

Design rationale. Omniphobic MD membranes that display high wetting resistance toward feedwater with low surface tension are typically designed by modifying microporous membranes with re-entrant textures using low surface energy materials (e.g., long-chain PFASs). Upon contact with a texture surface (e.g., microporous membranes), a liquid droplet adopts either the fully wetted Wenzel state [51] or the non-wetting Cassie-Baxter state [52] to minimize its overall free energy, leading to an apparent contact angle θ^*. In the Wenzel state, the liquid droplet completely permeates into the surface texture. Therefore, the Cassie-Baxter state in which air pockets are

trapped in the surface texture underneath the liquid droplet is preferred for designing MD membranes with high wetting resistance. Further, the re-entrant texture is essential for forming the Cassie-Baxter state for liquids with low surface tensions.[53] Additionally, low solid surface energy is typically required to achieve stable Cassie-Baxter state with high apparent contact angles and high wetting resistance.[54] Consequently, virtually all omniphobic MD membranes are designed by combining re-entrant texture and long-chain PFASs, which possess very low surface energy. Due to the high environmental and health concerns on long-chain PFASs,[36, 37, 40] it is of critical importance to develop alternative design strategy for omniphobic MD membranes.

It is worth noting that many biological surfaces (e.g., termite wing), which display high wetting resistance, do not possess very low surface energy.[55, 56] These bio-species achieve this by developing hierarchically micro/nano-structured surfaces through billions of years of evolution. Prior theoretical work has indicated that the recursive form of the Cassie-Baxter relation can be used to predict the apparent contact angles θ_n^* on a hierarchically structured surfaces, which has *n* length scales of textures,[26, 55]

$$\cos\theta_n^* = \left(1 - f_{lv,n}\right)\cos\theta_{n-1}^* - f_{lv,n} \qquad (7\text{-}1)$$

Here, $f_{lv,n}$ is the liquid-air area fraction at the *n*th scale, and θ_{n-1}^* is the apparent contact angle at the *n*-1 length scale. When *n* = 1, Equation 7-1 becomes the classical Cassie-Baxter relation. It is evident from Equation 7-1 that the apparent contact angle θ_n^* can be increased by increasing the number of length scales of the surface texture. In other words, when *n* is sufficiently high, the Cassie-Baxter state with high apparent contact angles can be theoretically formed on hierarchically

structured surfaces with high surface energy and consequently low Young's contact angle (i.e., the equilibrium contact angle on a smooth surface). This suggests that ultra-low surface energy induced by long-chain PFASs is perhaps not required for designing omniphobic MD membranes when the membrane surfaces possess sufficiently high number of length scales of re-entrant textures.

Membrane wettability. Based on the theoretical consideration above, we fabricated hierarchically structured membranes with different levels of hierarchy using fluorinated silanes with short-chain length (FC-4, see Materials and methods), which are less bioaccumulative and more biosafe than long-chain PFASs.[39, 41] The pristine membrane with single-tier structure consisted of interconnected micro-sized granules with re-entrant texture (see Figures 7-2a, 7-2d, and 7-2h). In contrast, for the membranes with dual-tier micro/nano-structures (i.e., PVDF-120-FC4 and PVDF-15-FC4 membranes), the nano-sized spherical silica particles with re-entrant texture were superimposed on the micro-sized granules (see Figures 7-2b, 7-2e, 7-2f, 7-2i, and 7-2j). For the membrane with three-tier micro/nano-structure (i.e., PVDF-120/15-FC4 membrane), smaller spherical particles (i.e., 15 nm, see Figure D1) were superimposed on the larger spherical particles (i.e., 120 nm), which were decorated on the granules of the membrane (see Figures 7-2c, 7-2g, and 7-2k). Therefore, the hierarchically structured membranes with dual-tier and three-tier micro/nano-structures possess re-entrant textures at all length scales. The surface chemical compositions of the membranes with different levels of hierarchy were characterized with XPS. Based on the high-resolution C1*s* XPS spectra (see Figure 7-3a), the pristine membrane with single-tier structure

possessed the characteristic -CH_2 and -CF_2 groups of PVDF. In contrast, the characteristic -CF_3 group of short-chain fluoroalkyl silane (i.e., FC-4 silane) was observed on the membranes with dual-tier and three-tier micro/nano-structures, which indicated successful grafting of FC-4 silane on the membrane surfaces.

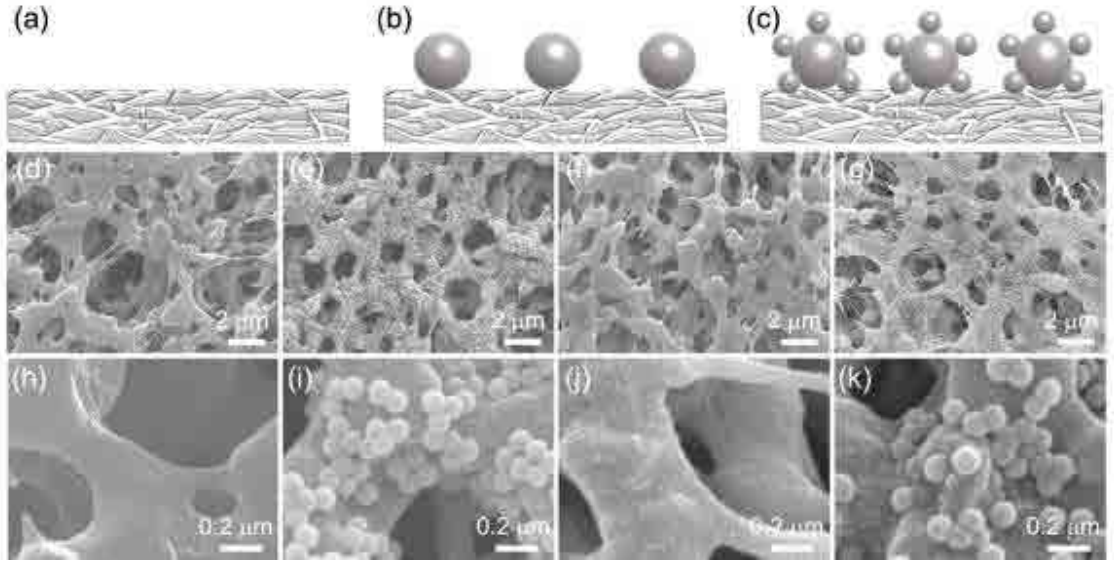

Figure 7-2. Schematics (not to scale) showing (a) single-tier structure, (b) dual-tier micro/nano-structure, and (c) three-tier micro/nano-structure of membrane surface. The top-view SEM images of (d, h) pristine PVDF membrane, (e, i) PVDF-120-FC4 membrane, (f, j) PVDF-15-FC4 membrane, and (g, k) PVDF-120/15-FC4 membrane.

The wettability of hierarchically structured membranes modified with FC-4 and the pristine membrane was investigated by measuring the apparent contact angle θ^* of liquids with different surface tensions on the membranes (see Figure 7-3b). The membranes with hierarchical micro/nano-structures (i.e., PVDF-120-FC4, PVDF-15-FC4, and PVDF-120/15-FC4 membranes) possessing re-entrant textures at all length scales displayed higher liquid repellency compared to the pristine membrane, which is evident from the higher apparent θ^* of different liquids. Further,

the membrane with three-tier micro/nano-structure (i.e., PVDF-120/15-FC4 membrane) possessed significantly enhanced liquid repellency compared to the membranes with dual-tier structures (i.e., PVDF-120-FC4 and PVDF-15-FC4 membranes). This leads to very high apparent θ^* of liquids with a wide range of surface tensions (including water + 60% ethanol with a low surface tension $\gamma_{lv} \approx 28.7$ mN/m displaying $\theta^* \approx 90.4°$) on the PVDF-120/15-FC4 membrane, which indicates the omniphobicity of the hierarchically structured membranes with three-tier micro/nano-structures. In contrast, the membranes with dual-tier structures as well as the pristine membrane were instantly wetted by water + 60% ethanol. The different liquid repellency of the membranes is also demonstrated by different arrays of liquids beading up on or wetting the membrane surfaces (see Figures 7-3 c-f). Further, due to the poor liquid repellency of pristine membrane and membranes with dual-tier structures, water droplets remained stuck to the surfaces upon impacting the membranes (see Figures 7-4 a-c). In contrast, the extreme repellency of the PVDF-120/15-FC4 membrane led to complete rebound of the droplet (see Figure 7-4d). These results indicate that long-chain PFASs-free omniphobic membranes can indeed be designed by increasing the number of length scales of re-entrant textures.

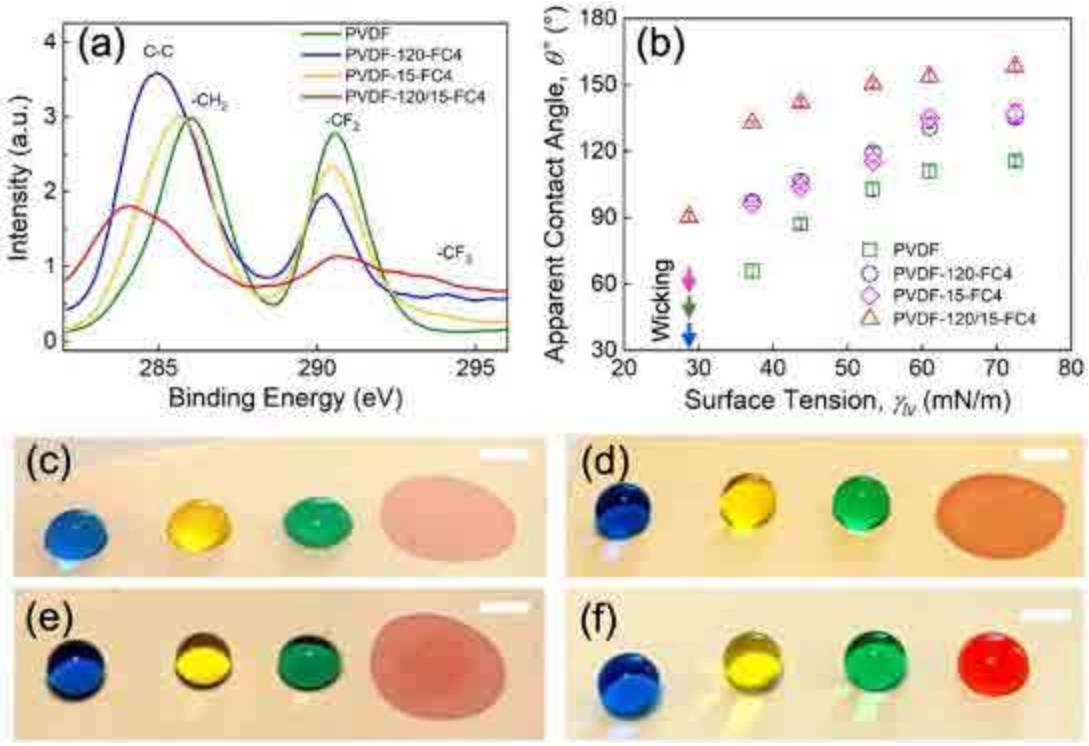

Figure 7-3. (a) High resolution C1s XPS spectra of the membranes. (b) Apparent contact angles of liquids with different surface tensions on the membranes. Error bars represent standard deviation from three independent measurements. The arrows point to the surface tension at which liquid instantly wicked into pristine and composite PVDF membranes. Images showing different liquids beading up on or wetting (c) pristine PVDF membrane, (d) PVDF-120-FC4 membrane, (e) PVDF-15-FC4 membrane, and (f) PVDF-120/15-FC4 membrane. The droplets from left to right: deionized water, 10% ethanol in water, 30% ethanol in water, 60% ethanol in water. The scale bars represent 2 mm.

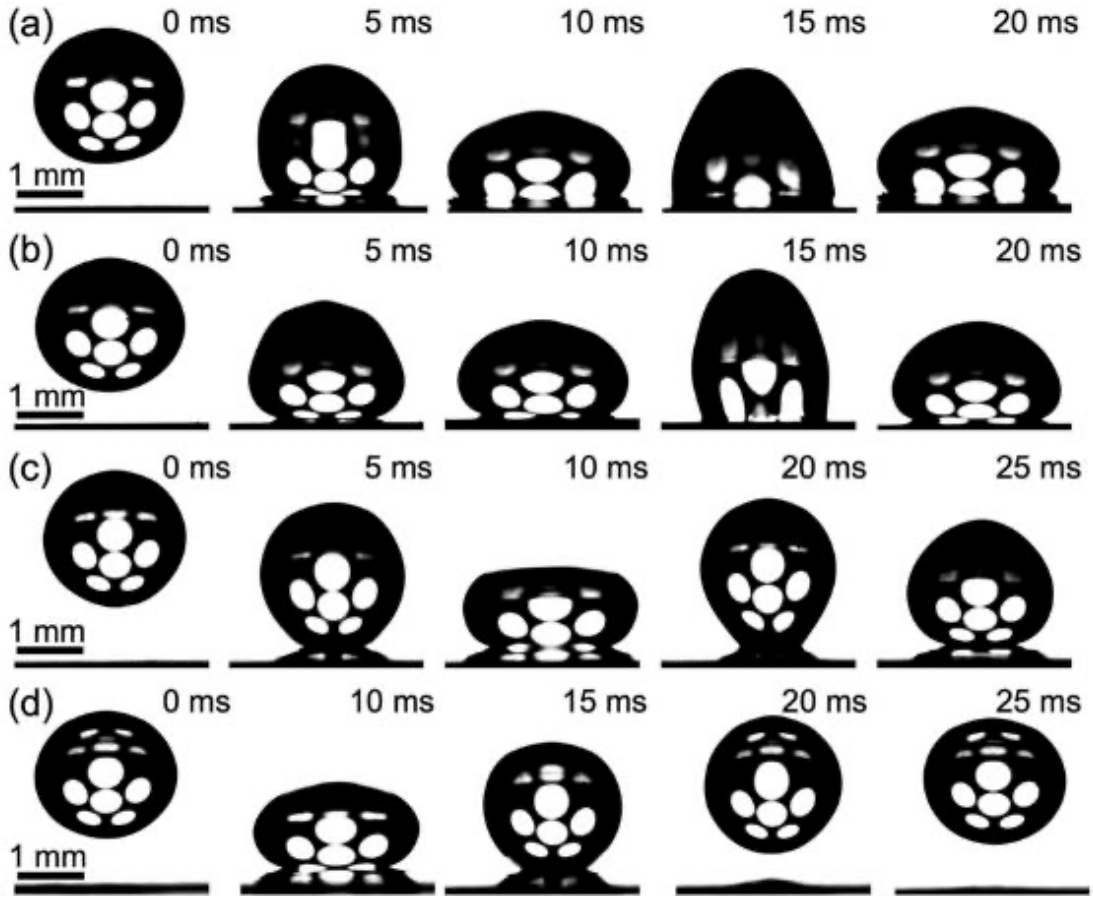

Figure 7-4.Series of snapshots showing water droplets impacting (a) pristine PVDF membrane, (b) PVDF-120-FC4 membrane, (c) PVDF-15-FC4 membrane, and (d) PVDF-120/15-FC4 membrane.

7.3.2 Wetting resistance of hierarchically micro/nano-structured membranes fabricated with short-chain fluorocarbon

The wetting resistances of the hierarchically structured membranes and pristine membrane were evaluated in DCMD experiments, in which the concentration of surfactants (i.e., SDS) was progressively increased to lower the surface tension of feedwater. In the first 1 h without the addition of SDS, all the membranes showed constant fluxes and perfect salt rejections (100%, see Figure 7-5). However, when the SDS concentration increased to 0.1 mM, the pristine membrane was completely wetted, as indicated by the dramatic increase of water vapor flux and decrease of

salt rejection (see Figure 7-5a). The PVDF-120-FC4 and PVDF-15-FC4 membranes experienced a degraded desalination performance at 0.1 mM SDS (see Figures 7-5b and c, although to a less extent than the pristine PVDF membrane) and were completely wetted at 0.2 mM SDS, indicating that the FC-4 modified membranes with dual-tier micro/nano-structures were still prone to wetting by low surface tension feed solutions (~42 mN/m at 0.1 mM SDS). In contrast, the omniphobic PVDF-120/15-FC4 membrane with three-tier micro/nano-structure exhibited exceptional wetting resistance and robust MD desalination performance even in the presence of a very high SDS concentration of 0.5 mM, which corresponds to a surface tension of only ~27 mN/m (see Figure 7-5d). Therefore, the FC-4 modified membrane with three-tier micro/nano-structure (i.e., PVDF-120/15-FC4 membrane) showed superior wetting resistance compared to the PVDF-120-FC4 and PVDF-15-FC4 membranes with dual-tier micro/nano-structures, indicating that the three-tier micro/nano-structure is critical to impart the membrane with high wetting resistance.

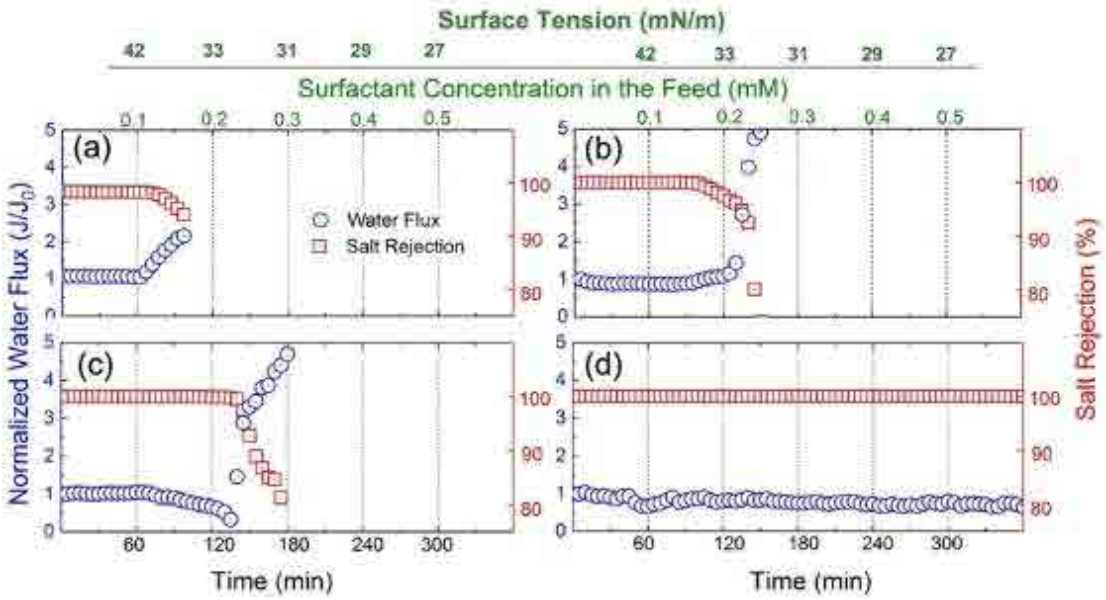

Figure 7-5. Membrane distillation (MD) performance of different PVDF membranes. (a) pristine PVDF membrane, (b) PVDF-120-FC4 membrane, (c) PVDF-15-FC4 membrane, and (d) PVDF-120/15-FC4 membrane. The initial water vapor fluxes for (a), (b), (c), and (d) are 27 L m^{-2} h^{-1}, 26 L m^{-2} h^{-1}, 24 L m^{-2} h^{-1} and 18 L m^{-2} h^{-1}, respectively. The crossflow velocities for the feed and distillate streams were 9.6 cm/s and 5.3 cm/s, respectively. The feed solution contained 1 M NaCl, supplemented with various concentrations of SDS. The feed and distillate temperatures were maintained at 60 °C and 20 °C, respectively. The corresponding surface tensions of the feed solution are indicated. The surface tension values are estimated according to Matijevic et al. and Hou et al.[46, 69]

Furthermore, a thorough literature search indicates that our long-chain PFASs-free omniphobic membrane (i.e., PVDF-120/15-FC4 membrane) possesses comparable or higher wetting resistance than the long-chain PFASs-based omniphobic membranes reported in prior work (see Table D1). This indicates that long-chain PFASs are not necessary for the fabrication of membranes with exceptional wetting resistance when an appropriate surface texture is applied.

7.3.3 Wetting resistance of hierarchically micro/nano-structured membranes fabricated with ultrashort-chain fluorocarbons

We further investigated the wetting resistance of hierarchically structured membranes with three-tier micro/nano-structures, which were modified with ultrashort-chain fluoroalkylsilanes (i.e., FC-B3 and FC-1). It should be noted that the ultrashort-chain fluoroalkylsilanes are less bioaccumulative and more biosafe than the short-chain fluoroalkylsilane (see detailed discussion in the next section). The membranes modified with FC-B3 and FC-1 (i.e., PVDF-120/15-FCB3 and PVDF-120/15-FC1 membranes) displayed higher liquid repellency (i.e., higher contact angles for all the tested liquids) than the pristine PVDF membrane (see Figure D3). For example, the PVDF-120/15-FCB3 and PVDF-120/15-FC1 membranes exhibited much higher contact angles of water + 30% ethanol ($\gamma_{lv} \approx 37.2$ mN/m, $\theta^* \approx 102.4°$ and 93.6°, respectively) than the pristine PVDF membrane ($\theta^* \approx 65.9°$), even though all the tested membranes were wetted by water + 60% ethanol with low surface tension ($\gamma_{lv} \approx 28.7$ mN/m). These results indicate that membrane wetting resistance could still be significantly improved through the combination of three-tier micro/nano-structure and ultrashort-chain fluoroalkylsilanes (i.e., FC-B3 and FC-1).

The anti-wetting performances of the PVDF-120/15-FCB3 and PVDF-120/15-FC1 membranes in DCMD are shown in Figures 7-6a and 7-6b. The PVDF-120/15-FC1 membrane maintained stable water flux and excellent salt rejection (~100%) for SDS concentration up to 0.1 mM and was completely wetted after the addition of 0.2 mM SDS (see Figure 7-6b). Thus, this membrane was able to resist membrane wetting by feedwater of surface tension as low as ~42 mN/m (correspond to 1M NaCl supplemented with 0.1 mM SDS). In contrast, the PVDF-120/15-FCB3 membrane exhibited a stable desalination performance (i.e., constant flux and complete salt

rejection) at 0.2 mM SDS (see Figure 7-6a). While the water flux increased slightly after the addition of 0.3 mM, the salt rejection was still maintained at 99.5%, indicating that only limited membrane pores were wetted. These results indicated the PVDF-120/15-FCB3 membrane was able to tolerate the feedwater surface tension of between 31-33 mN/m (corresponding to 1M NaCl supplemented with 0.2-0.3 mM SDS, see Figure 7-6a). It is worth mentioning that such high wetting resistance was comparable to that of several omniphobic membranes modified with long-chain PFASs as reported in the literature. (see Table D1 and Figure 7-6c).

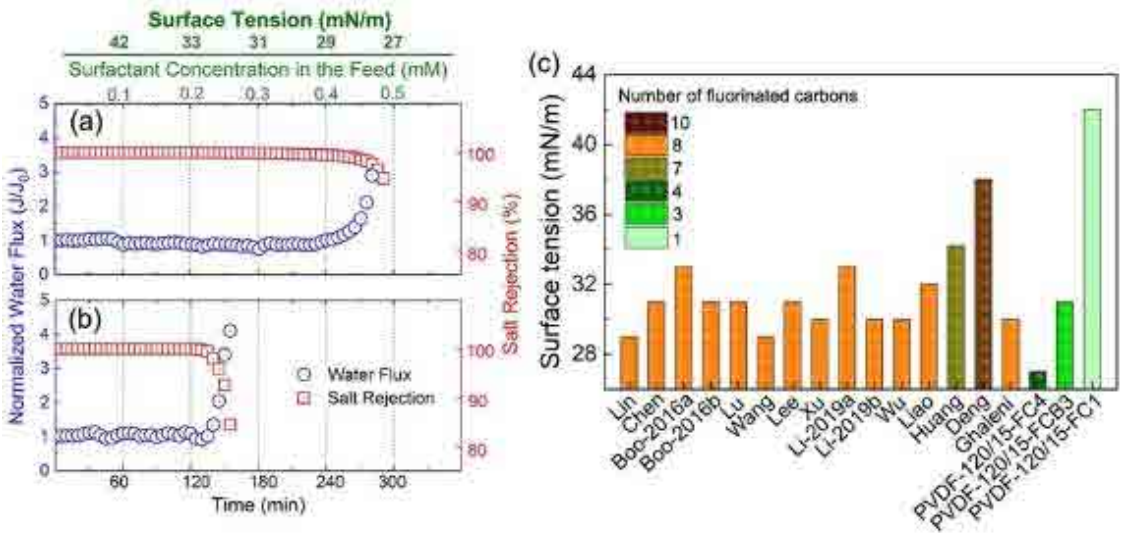

Figure 7-6. Membrane distillation (MD) performance of (a) PVDF-120/15-FCB3 membrane and (b) PVDF-120/15-FC1 membrane. The initial water vapor fluxes for (a) and (b) are 25 L m^{-2} h^{-1} and 24 L m^{-2} h^{-1}, respectively. The crossflow velocities for the feed and distillate streams were 9.6 cm/s and 5.3 cm/s, respectively. The feed solution contained 1 M NaCl, supplemented with various concentrations of SDS. The feed and distillate temperatures were maintained at 60 °C and 20 °C, respectively. The corresponding surface tensions of the feed solution are indicated. (c) Comparison of the lowest surface tension of feedwaters tolerated by wetting-resistant membranes for MD application reported in this study and the literature.[16, 18, 24, 30, 32, 34, 44, 45, 70-76] The surface tension values are estimated according to Matijevic et al. and Hou et al.[46, 69]

7.3.4 Environmental implications

Long-chain PFASs, which are currently being used in the fabrication of omniphobic MD membranes, have exhibited very high tendency to accumulate in wildlife via direct uptake from ambient environment by gills or dietary (bioconcentration or bioaccumulation).[57] The high bioaccumulation potential of long-chain PFASs, along with their acute toxicity,[36, 58, 59] has generated global concerns and controls that ban their use in various industries and commodities.[37-40] On the other hand, short-chain and ultrashort-chain fluorocarbon compounds have shown less acute toxicity and more biosafe compared to the long-chain PFASs.[40, 41, 60-62]

Using the EPI Suite software of USEPA, we evaluated the bioaccumulation potentials of short-chain and ultrashort-chain fluorocarbons using BAF, BCF and K_{ow} (Table 7-1). As shown in Table 7-1, the bioaccumulation potential increases with the length of fluorinated carbon chain, as indicated by the increased values of BAF, BCF, and K_{ow}. Compared to those of FC-8, the values of BAF and K_{ow} of FC-4 decrease by 2 and 3 orders of magnitude, respectively, indicating the much lower bioaccumulation potential of FC-4. Further, the ultrashort-chain fluorocarbons (i.e., FC-B3 and FC-1) have even lower bioaccumulation potentials than FC-4 and are not "bioaccumulative" (the log BAF, log BCF, or log K_{ow} values are lower than 3.7, 3 or 5, respectively [47, 63]). In this work, although hierarchically structured membranes modified with FC-B3 and FC-1 showed enhanced wetting resistance compared to the pristine PVDF membrane, the omniphobic membrane, which possessed exceptional wetting resistant against low surface tension feedwaters (e.g., surface tension < 27 mN/m), needs to be fabricated using FC-4. These results indicate that a

trade-off exists between the wetting resistance and environmental considerations for membranes used for MD desalination.

Table 7-1. Estimated log K_{ow}, log BCF and log BAF values for different fluorocarbon compounds.

Fluorocarbon Compounds	**log K_{ow}**	**log *BCF* (L/kg)[a]**	**log *BAF* (L/kg)[b]**
FC-8	8.4	3.5	6.7
FC-4	5.7	3.4	4.7
FC-B3	4.6	2.7	3.3
FC-1	3.4	1.9	2.3

[a] Predicted log BCF values are calculated by regression-based method.[77]

[b] Predicted log BAF values are calculated by Arnot-Gobas method (upper trophic).[63]

Therefore, one should consider the wetting resistance and the potential environmental risks comprehensively in the design and selection of membrane materials for robust MD desalination. Omniphobic membranes have been proposed to be suitable for the treatment of shale oil and gas produced water,[16, 24, 34] which is well known to contain various surfactants.[64] According to the prior reports,[65, 66] the surface tensions of produced water from oil and gas fields worldwide mainly range from 43 mN/m to 78 mN/m. Under such scenarios, the three-tier micro/nano-structured membranes modified with ultrashort-chain fluorocarbons (i.e., resistant to feed waters with surface tensions < 43 mN/m, as shown in Figures 7-6a, b, and c) could possess sufficient wetting resistance to achieve robust MD desalination of most produced water. However, for applications involving solutions with very low surface tensions (e.g., desalination of water-alcohol mixtures such as wastewater from the brewery industry, resource recovery by membrane contactor using organic solvent),[67, 68] the three-tier micro/nano-structured omniphobic membranes modified with short-chain fluorocarbons may be desired. This requires the tailoring of membrane wetting resistance to the wetting potential (or surface tension) of the feedwater, in order to minimize the environmental risks of fluorocarbons used in MD systems.

7.4 Conclusions

In summary, we demonstrated that MD membranes with exceptional wetting resistance can be designed through the combination of hierarchically structures consisting of re-entrant texture at different length scales and (ultra)short-chain fluorocarbons. Our results indicated that omniphobic

membrane with three-tier micro/nano-structure fabricated with short-chain fluorocarbon exhibited superior wetting resistance against low surface tension liquids and stable MD performance in the desalination of surfactant-containing feed solutions with surface tensions < 27 mN/m. Such high wetting resistance is comparable to or higher than current omniphobic membranes modified with long-chain PFASs. Additionally, the three-tier micro/nano-structured membranes modified with ultrashort-chain fluorocarbons displayed enhanced wetting resistance compared to the pristine membrane. The wetting resistance of the three-tier micro/nano-structured membrane fabricated with FC-B3 was comparable to some omniphobic membranes modified with long-chain PFASs in the literature. Further, our results suggest that the wetting resistance and potential environmental risks of MD membranes need to be comprehensively considered when designing MD membranes. The membrane wetting resistance must be tailored to the wetting potential of the feedwater to minimize the environmental risks of fluorocarbons used in MD systems. We envision that the long-chain PFASs-free omniphobic membranes developed in our work will pave the way towards the development of more sustainable MD technology for mitigating environmental impact of hypersaline wastewater and water scarcity.

References

1. Deshmukh, A.; Boo, C.; Karanikola, V.; Lin, S.; Straub, A. P.; Tong, T.; Warsinger, D. M.; Elimelech, M., Membrane distillation at the water-energy nexus: limits, opportunities, and challenges. *Energ Environ Sci* 2018, 11, (5), 1177-1196.
2. Tong, T.; Elimelech, M., The global rise of zero liquid discharge for wastewater management: drivers, technologies, and future directions. *Environ Sci Technol* 2016, 50, (13), 6846-6855.
3. Al-Obaidani, S.; Curcio, E.; Macedonio, F.; Di Profio, G.; Ai-Hinai, H.; Drioli, E., Potential of membrane distillation in seawater desalination: Thermal efficiency, sensitivity study and cost estimation. *J Membrane Sci* 2008, 323, (1), 85-98.
4. Lawson, K. W.; Lloyd, D. R., Membrane distillation. *J Membrane Sci* 1997, 124, (1), 1-25.
5. Alkhudhiri, A.; Darwish, N.; Hilal, N., Membrane distillation: A comprehensive review. *Desalination* 2012, 287, 2-18.
6. Xu, P.; Cath, T. Y.; Robertson, A. P.; Reinhard, M.; Leckie, J. O.; Drewes, J. E., Critical review of desalination concentrate management, treatment and beneficial use. *Environ Eng Sci* 2013, 30, (8), 502-514.
7. Francis, L.; Ghaffour, N.; Alsaadi, A. A.; Amy, G. L., Material gap membrane distillation: A new design for water vapor flux enhancement. *J Membrane Sci* 2013, 448, 240-247.
8. Alklaibi, A. M.; Lior, N., Membrane-distillation desalination: status and potential. *Desalination* 2005, 171, (2), 111-131.
9. El-Bourawi, M.; Ding, Z.; Ma, R.; Khayet, M., A framework for better understanding membrane distillation separation process. *J Membrane Sci* 2006, 285, (1-2), 4-29.
10. Al-Obaidani, S.; Curcio, E.; Macedonio, F.; Di Profio, G.; Al-Hinai, H.; Drioli, E., Potential of membrane distillation in seawater desalination: thermal efficiency, sensitivity study and cost estimation. *J Membrane Sci* 2008, 323, (1), 85-98.
11. Kim, Y.-D.; Thu, K.; Ghaffour, N.; Ng, K. C., Performance investigation of a solar-assisted direct contact membrane distillation system. *J Membrane Sci* 2013, 427, 345-364.
12. Horseman, T.; Yin, Y.; Christie, K. S.; Wang, Z.; Tong, T.; Lin, S., Wetting, scaling, and fouling in membrane distillation: State-of-the-art insights on fundamental mechanisms and mitigation strategies. *ACS ES&T Engineering* 2020, 1, (1), 117-140.
13. Shaffer, D. L.; Arias Chavez, L. H.; Ben-Sasson, M.; Romero-Vargas Castrillón, S.; Yip, N. Y.; Elimelech, M., Desalination and reuse of high-salinity shale gas produced water: drivers, technologies, and future directions. *Environ Sci Technol* 2013, 47, (17), 9569-9583.
14. Kargbo, D. M.; Wilhelm, R. G.; Campbell, D. J., Natural Gas Plays in the Marcellus Shale: Challenges and Potential Opportunities. *Environ Sci Technol* 2010, 44, (15), 5679-5684.
15. Vidic, R. D.; Brantley, S. L.; Vandenbossche, J. M.; Yoxtheimer, D.; Abad, J. D., Impact of Shale Gas Development on Regional Water Quality. *Science* 2013, 340, (6134).

16. Boo, C.; Lee, J.; Elimelech, M., Omniphobic polyvinylidene fluoride (PVDF) membrane for desalination of shale gas produced water by membrane distillation. *Environ Sci Technol* 2016, 50, (22), 12275-12282.
17. Woo, Y. C.; Kim, Y.; Yao, M. W.; Tijing, L. D.; Cho, J. S.; Lee, S.; Kim, S. H.; Shon, H. K., Hierarchical Composite Membranes with Robust Omniphobic Surface Using Layer-By-Layer Assembly Technique. *Environ Sci Technol* 2018, 52, (4), 2186-2196.
18. Boo, C.; Lee, J.; Elimelech, M., Engineering Surface Energy and Nanostructure of Microporous Films for Expanded Membrane Distillation Applications. *Environ Sci Technol* 2016, 50, (15), 8112-8119.
19. Liao, Y.; Loh, C.-H.; Wang, R.; Fane, A. G., Electrospun superhydrophobic membranes with unique structures for membrane distillation. *Acs Appl Mater Inter* 2014, 6, (18), 16035-16048.
20. Zheng, R.; Chen, Y.; Wang, J.; Song, J. F.; Li, X. M.; He, T., Preparation of omniphobic PVDF membrane with hierarchical structure for treating saline oily wastewater using direct contact membrane distillation. *J Membrane Sci* 2018, 555, 197-205.
21. Lee, J.; Boo, C.; Ryu, W. H.; Taylor, A. D.; Elimelech, M., Development of Omniphobic Desalination Membranes Using a Charged Electrospun Nanofiber Scaffold. *Acs Appl Mater Inter* 2016, 8, (17), 11154-11161.
22. Chen, L. H.; Huang, A.; Chen, Y. R.; Chen, C. H.; Hsu, C. C.; Tsai, F. Y.; Tung, K. L., Omniphobic membranes for direct contact membrane distillation: Effective deposition of zinc oxide nanoparticles. *Desalination* 2018, 428, 255-263.
23. Hou, D. Y.; Ding, C. L.; Fu, C. C.; Wang, D. W.; Zhao, C. W.; Wang, J., Electrospun nanofibrous omniphobic membrane for anti-surfactant-wetting membrane distillation desalination. *Desalination* 2019, 468.
24. Lin, S.; Nejati, S.; Boo, C.; Hu, Y.; Osuji, C. O.; Elimelech, M., Omniphobic membrane for robust membrane distillation. *Environ Sci Tech Let* 2014, 1, (11), 443-447.
25. Wang, Z. X.; Elimelech, M.; Lin, S. H., Environmental Applications of Interfacial Materials with Special Wettability. *Environ Sci Technol* 2016, 50, (5), 2132-2150.
26. Kota, A. K.; Kwon, G.; Tuteja, A., The design and applications of superomniphobic surfaces. *Npg Asia Mater* 2014, 6, (7), e109-e109.
27. Tuteja, A.; Choi, W.; Mabry, J. M.; McKinley, G. H.; Cohen, R. E., Robust omniphobic surfaces. *P Natl Acad Sci* USA 2008, 105, (47), 18200-18205.
28. Deng, X.; Mammen, L.; Butt, H. J.; Vollmer, D., Candle Soot as a Template for a Transparent Robust Superamphiphobic Coating. *Science* 2012, 335, (6064), 67-70.
29. Tuteja, A.; Choi, W.; Ma, M. L.; Mabry, J. M.; Mazzella, S. A.; Rutledge, G. C.; McKinley, G. H.; Cohen, R. E., Designing superoleophobic surfaces. *Science* 2007, 318, (5856), 1618-1622.

30. Wang, W.; Du, X.; Vahabi, H.; Zhao, S.; Yin, Y.; Kota, A. K.; Tong, T., Trade-off in membrane distillation with monolithic omniphobic membranes. *Nat Commun* 2019, 10, (1), 1-9.
31. Zhu, Z.; Zhong, L.; Horseman, T.; Liu, Z.; Zeng, G.; Li, Z.; Lin, S.; Wang, W., Superhydrophobic-omniphobic membrane with anti-deformable pores for membrane distillation with excellent wetting resistance. *J Membrane Sci* 2021, 620, 118768.
32. Chen, L.-H.; Huang, A.; Chen, Y.-R.; Chen, C.-H.; Hsu, C.-C.; Tsai, F.-Y.; Tung, K.-L., Omniphobic membranes for direct contact membrane distillation: effective deposition of zinc oxide nanoparticles. *Desalination* 2018, 428, 255-263.
33. Li, X.; Qing, W.; Wu, Y.; Shao, S.; Peng, L. E.; Yang, Y.; Wang, P.; Liu, F.; Tang, C. Y., Omniphobic nanofibrous membrane with pine-needle-like hierarchical nanostructures: toward enhanced performance for membrane distillation. *Acs Appl Mater Inter* 2019, 11, (51), 47963-47971.
34. Lee, J.; Boo, C.; Ryu, W.-H.; Taylor, A. D.; Elimelech, M., Development of omniphobic desalination membranes using a charged electrospun nanofiber scaffold. *Acs Appl Mater Inter* 2016, 8, (17), 11154-11161.
35. Dichiarante, V.; Martinez Espinoza, M. I.; Gazzera, L.; Vuckovac, M.; Latikka, M.; Cavallo, G.; Raffaini, G.; Oropesa-Nuñez, R.; Canale, C.; Dante, S., A short-chain multibranched perfluoroalkyl thiol for more sustainable hydrophobic coatings. *Acs Sustain Chem Eng* 2018, 6, (8), 9734-9743.
36. Krafft, M. P.; Riess, J. G., Per-and polyfluorinated substances (PFASs): Environmental challenges. *Current opinion in colloid & interface* science 2015, 20, (3), 192-212.
37. Dichiarante, V.; Milani, R.; Metrangolo, P., Natural surfactants towards a more sustainable fluorine chemistry. *Green Chemistry* 2018, 20, (1), 13-27.
38. Lu, M.; Cagnetta, G.; Zhang, K.; Huang, J.; Yu, G., Mechanochemical mineralization of "very persistent" fluorocarbon surfactants–6: 2 fluorotelomer sulfonate (6: 2FTS) as an example. *Sci Rep-Uk* 2017, 7, (1), 1-10.
39. Wang, Z.; Cousins, I. T.; Scheringer, M.; Hungerbühler, K., Fluorinated alternatives to long-chain perfluoroalkyl carboxylic acids (PFCAs), perfluoroalkane sulfonic acids (PFSAs) and their potential precursors. *Environ Int* 2013, 60, 242-248.
40. Wang, Z.; Cousins, I. T.; Scheringer, M.; Hungerbuehler, K., Hazard assessment of fluorinated alternatives to long-chain perfluoroalkyl acids (PFAAs) and their precursors: status quo, ongoing challenges and possible solutions. *Environ Int* 2015, 75, 172-179.
41. Renner, R., The long and the short of perfluorinated replacements. In ACS Publications: 2006.
42. Ritter, S. K., Fluorochemicals go short. *Chem. Eng. News* 2010, 88, 5, 12-17; https://doi.org/10.1021/cen-v088n005.p012.

43. Du, X. W.; Zhang, Z. Y.; Carlson, K. H.; Lee, J.; Tong, T. Z., Membrane fouling and reusability in membrane distillation of shale oil and gas produced water: Effects of membrane surface wettability. *J Membrane Sci* 2018, 567, 199-208.
44. Xu, Y.; Yang, Y.; Fan, X.; Liu, Z.; Song, Y.; Wang, Y.; Tao, P.; Song, C.; Shao, M., In-situ silica nanoparticle assembly technique to develop an omniphobic membrane for durable membrane distillation. *Desalination* 2021, 499, 114832.
45. Lu, C.; Su, C.; Cao, H.; Ma, X.; Duan, F.; Chang, J.; Li, Y., F-POSS based omniphobic membrane for robust membrane distillation. *Mater Lett* 2018, 228, 85-88.
46. Matijević, E.; Pethica, B., The properties of ionized monolayers. Part 1.—Sodium dodecyl sulphate at the air/water interface. *Transactions of the Faraday Society* 1958, 54, 1382-1389.
47. Conder, J. M.; Hoke, R. A.; Wolf, W. d.; Russell, M. H.; Buck, R. C., Are PFCAs bioaccumulative? A critical review and comparison with regulatory criteria and persistent lipophilic compounds. *Environ Sci Technol* 2008, 42, (4), 995-1003.
48. USEPA. EPI (Estimation Programs Interface) Suite version 4.11. US Environmental Protection Agency, Office of Pollution Prevention Toxics and Syracuse Research Corporation, Washington, D.C.,USA. Available from https://www.epa.gov/tsca-screening-tools/download-epi-suitetm-estimation-program-interface-v411 [accessed 1 September 2021].
49. Arp, H. P. H.; Niederer, C.; Goss, K.-U., Predicting the partitioning behavior of various highly fluorinated compounds. *Environ Sci Technol* 2006, 40, (23), 7298-7304.
50. Card, M. L.; Gomez-Alvarez, V.; Lee, W.-H.; Lynch, D. G.; Orentas, N. S.; Lee, M. T.; Wong, E. M.; Boethling, R. S., History of EPI Suite™ and future perspectives on chemical property estimation in US Toxic Substances Control Act new chemical risk assessments. *Environmental Science: Processes & Impacts* 2017, 19, (3), 203-212.
51. Wenzel, R. N., Resistance of solid surfaces to wetting by water. *Industrial & Engineering Chemistry* 1936, 28, (8), 988-994.
52. Cassie, A.; Baxter, S., Wettability of porous surfaces. *Transactions of the Faraday society* 1944, 40, 546-551.
53. Nosonovsky, M.; Bhushan, B., Why re-entrant surface topography is needed for robust oleophobicity. Philosophical Transactions of the Royal Society A: Mathematical, *Physical and Engineering Sciences* 2016, 374, (2073), 20160185.
54. Chunglok, A.; Muensit, N.; Daengngam, C., Extreme wetting-resistant multiscale nano-/microstructured surfaces for viscoelastic liquid repellence. *Journal of Nanomaterials* 2016, 2016.
55. Herminghaus, S., Roughness-induced non-wetting. EPL (Europhysics Letters) 2000, 52, (2), 165.
56. Teisala, H.; Butt, H.-J. r., Hierarchical structures for superhydrophobic and superoleophobic surfaces. *Langmuir* 2018, 35, (33), 10689-10703.

57. Franke, C.; Studinger, G.; Berger, G.; Böhling, S.; Bruckmann, U.; Cohors-Fresenborg, D.; Jöhncke, U., The assessment of bioaccumulation. *Chemosphere* 1994, 29, (7), 1501-1514.
58. Goodrum, P. E.; Anderson, J. K.; Luz, A. L.; Ansell, G. K., Application of a framework for grouping and mixtures toxicity assessment of PFAS: A closer examination of dose-additivity approaches. *Toxicological Sciences* 2021, 179, (2), 262-278.
59. Peshoria, S.; Nandini, D.; Tanwar, R.; Narang, R., Short-chain and long-chain fluorosurfactants in firefighting foam: a review. *Environmental Chemistry Letters* 2020, 18, (4).
60. Li, F.; Duan, J.; Tian, S.; Ji, H.; Zhu, Y.; Wei, Z.; Zhao, D., Short-chain per-and polyfluoroalkyl substances in aquatic systems: Occurrence, impacts and treatment. *Chem Eng J* 2020, 380, 122506.
61. Buck, R. C.; Franklin, J.; Berger, U.; Conder, J. M.; Cousins, I. T.; De Voogt, P.; Jensen, A. A.; Kannan, K.; Mabury, S. A.; van Leeuwen, S. P., Perfluoroalkyl and polyfluoroalkyl substances in the environment: terminology, classification, and origins. *Integrated environmental assessment and management* 2011, 7, (4), 513-541.
62. Brendel, S.; Fetter, É.; Staude, C.; Vierke, L.; Biegel-Engler, A., Short-chain perfluoroalkyl acids: environmental concerns and a regulatory strategy under REACH. *Environmental Sciences Europe* 2018, 30, (1), 1-11.
63. Arnot, J. A.; Gobas, F. A., A review of bioconcentration factor (BCF) and bioaccumulation factor (BAF) assessments for organic chemicals in aquatic organisms. *Environmental Reviews* 2006, 14, (4), 257-297.
64. Shih, J.-S.; Saiers, J. E.; Anisfeld, S. C.; Chu, Z.; Muehlenbachs, L. A.; Olmstead, S. M., Characterization and analysis of liquid waste from Marcellus Shale gas development. *Environ Sci Technol* 2015, 49, (16), 9557-9565.
65. Fakhru'l-Razi, A.; Pendashteh, A.; Abdullah, L. C.; Biak, D. R. A.; Madaeni, S. S.; Abidin, Z. Z., Review of technologies for oil and gas produced water treatment. *J Hazard Mater* 2009, 170, (2-3), 530-551.
66. Tibbetts, P.; Buchanan, I.; Gawel, L.; Large, R., A comprehensive determination of produced water composition. In Produced water, Springer: 1992; pp 97-112.
67. Li, X.; Dutta, A.; Saha, S.; Lee, H.-S.; Lee, J., Recovery of dissolved methane from anaerobically treated food waste leachate using solvent-based membrane contactor. *Water Res* 2020, 175, 115693.
68. Li, X.; Dutta, A.; Dong, Q.; Rollings-Scattergood, S.; Lee, J., Dissolved methane harvesting using omniphobic membranes for anaerobically treated wastewaters. *Environ Sci Tech Let* 2019, 6, (4), 228-234.
69. Hou, D. Y.; Yuan, Z. Y.; Tang, M.; Wang, K. P.; Wang, J., Effect and mechanism of an anionic surfactant on membrane performance during direct contact membrane distillation. *J Membrane Sci* 2020, 595.

70. Li, C.; Li, X.; Du, X.; Tong, T.; Cath, T. Y.; Lee, J., Antiwetting and antifouling Janus membrane for desalination of saline oily wastewater by membrane distillation. *Acs Appl Mater Inter* 2019, 11, (20), 18456-18465.
71. Li, X.; Shan, H.; Cao, M.; Li, B., Facile fabrication of omniphobic PVDF composite membrane via a waterborne coating for anti-wetting and anti-fouling membrane distillation. *J Membrane Sci* 2019, 589, 117262.
72. Wu, X.-Q.; Wu, X.; Wang, T.-Y.; Zhao, L.; Truong, Y. B.; Ng, D.; Zheng, Y.-M.; Xie, Z., Omniphobic surface modification of electrospun nanofiber membrane via vapor deposition for enhanced anti-wetting property in membrane distillation. *J Membrane Sci* 2020, 606, 118075.
73. Liao, X.; Wang, Y.; Liao, Y.; You, X.; Yao, L.; Razaqpur, A. G., Effects of different surfactant properties on anti-wetting behaviours of an omniphobic membrane in membrane distillation. *J Membrane Sci* 2021, 634, 119433.
74. Huang, Y. X.; Wang, Z. X.; Jin, J.; Lin, S. H., Novel Janus Membrane for Membrane Distillation with Simultaneous Fouling and Wetting Resistance. *Environ Sci Technol* 2017, 51, (22), 13304-13310.
75. Mohammadi Ghaleni, M.; Al Balushi, A.; Bavarian, M.; Nejati, S., Omniphobic hollow fiber membranes for water recovery and desalination. *ACS Applied Polymer Materials* 2020, 2, (8), 3034-3038.
76. Deng, L.; Ye, H.; Li, X.; Li, P.; Zhang, J.; Wang, X.; Zhu, M.; Hsiao, B. S., Self-roughened omniphobic coatings on nanofibrous membrane for membrane distillation. *Sep Purif Technol* 2018, 206, 14-25.
77. Garg, R.; Smith, C. J., Predicting the bioconcentration factor of highly hydrophobic organic chemicals. *Food and chemical toxicology* 2014, 69, 252-259.

CHAPTER 8: Trade-off in membrane distillation with monolithic omniphobic membranes [5]

8.1 Introduction

Water scarcity is one of the most critical challenges of our time, posing a major threat to the global economy, regional stability, and ecosystem health.[1-3] The recent water crisis in the Southwest U.S.[4] has caused enormous economic damage, and it is projected that 4-5 billion people will suffer from water stress globally by 2050.[5] To address this grand challenge, innovative technologies that enable the harvesting of purified water from unconventional water resources such as seawater, brackish water, and wastewater are indispensable.[6, 7] Among others, membrane distillation (MD) has recently attracted great attention as an emerging desalination technology for water purification, due to its superior characteristics such as moderate operational temperature, high tolerance to salinity, and unique capability of utilizing low-grade thermal energy.[8-10] As a hybrid membrane-thermal process, MD utilizes the partial pressure gradient between hotter saline feedwater and colder permeate stream to drive the transport of water vapor across a microporous, hydrophobic membrane.[11, 12] Maintaining membrane hydrophobicity is critical in MD, because it prevents salty feedwater from permeating through the membrane into the distilled water product (a phenomenon referred to as membrane wetting).

---

[5] This chapter has been published as a research article in *Nature Communications,* in which I am a co-first author, with the following citation:

Wang, W.; Du, X.; Vahabi, H.; Zhao, S.; Yin, Y.; Kota, A. K.; Tong, T., Trade-off in membrane distillation with monolithic omniphobic membranes. *Nat Commun* 2019 10, (3220) doi: https://doi.org/10.1038/s41467-019-11209-6 (Co-first author).

Conventional hydrophobic MD membranes (i.e., membranes that display apparent contact angle $\theta^* > 90°$ with high surface tension liquids such as water) suffer from membrane wetting in desalination of feedwater containing low surface energy contaminants (e.g., shale gas produced water[13, 14] and coal seam gas produced water[15, 16]). Very recently, it has been demonstrated that membrane wetting induced by low surface energy contaminants can be significantly mitigated in MD by imparting omniphobicity to the membranes.[8] Unlike hydrophobic membranes, omniphobic membranes (i.e., membranes that display apparent contact angle $\theta^* > 90°$ with both high and low surface tension liquids) possess superior wetting resistance to liquids with a wide range of surface tensions. Omniphobic membranes are typically fabricated by combining re-entrant texture and materials of low solid surface energy.[17-22] To date, the fabrication of omniphobic membranes involves complex and/or time-consuming processes, which typically require incorporation of micro- or nano-sized particles onto the membrane surface to create a hierarchical surface texture.[13, 16, 23-29] Also, the unintended environmental and health impacts of such particles, especially those with nano-scale sizes, continue to be an active area of research.[30-32] These concerns can potentially impede large-scale manufacturing of omniphobic membranes and consequently their applications in water purification. Further, water vapor permeability, a key parameter that characterizes the performance of membrane separation, has not received sufficient attention in the design of omniphobic MD membranes. A decrease in membrane water vapor permeability would increase both the cost and the energy consumption of desalination. However, little guidance exists on the relationship between membrane wetting resistance and water vapor permeability in the MD

process. A fundamental understanding of such relationship, therefore, is of great significance to develop a design framework for smart MD membranes.

In this work, we present a particle-free approach that enables rapid fabrication (< 1.5 h) of monolithic omniphobic polyvinylidene difluoride (PVDF) membranes for MD desalination. Our monolithic omniphobic membranes display excellent wetting resistance against liquids with low surface tensions (e.g., ethanol), as well as excellent water purification performance in direct contact MD of hypersaline solutions containing the surfactant sodium dodecyl sulfate (SDS). Further, we identify a trade-off between wetting resistance and water vapor permeability of our monolithic MD membranes and elucidate the underlying mechanisms. Analogous to the classic permeability-selectivity trade-off of synthetic membranes, which has directed the design criteria for membranes in desalination technologies including nanofiltration (NF), reverse osmosis (RO), and forward osmosis (FO),[33-35] the trade-off we identified has the potential to profoundly impact the membrane design for MD process. We envision that our simple and rapid fabrication technique as well as our elucidation of the underlying mechanism of wetting resistance-vapor permeability trade-off will facilitate the practical use and smart design of omniphobic membranes in MD desalination and therefore contribute to the mitigation of water scarcity.

8.2 Materials and Methods

8.2.1 Fabrication of monolithic omniphobic membranes

A sodium/naphthalene-based etching solution with 2-methoxyethyl ether as the solvent (FluoroEtch, Acton Technologies) was used to etch flat sheet polyvinylidene fluoride (PVDF) membranes with a nominal pore size of 0.45 μm (HVHP, Durapore). The PVDF membranes were immersed in the etching solution for approximately 1 s. It should be noted that the membranes were completely wetted by the etching solution upon immersion. Immediately after the membranes were taken out of the etching solution, the etched membranes were thoroughly washed with isopropanol, 0.1 mM acetic acid aqueous solution (~65°C), and deionized water in sequence. The entire process of immersing and washing took approximately 1.5 min. The membranes were dried using nitrogen gas and by heating at 80°C for 20 min. Subsequently, the processed PVDF membranes were modified via vapor phase silanization at 90°C using heptadecafluoro-1,1,2,2-tetrahydrodecyl trichlorosilane (FAS, Gelest) to impart low solid surface energy. The membranes were then thoroughly rinsed with n-hexane. Different durations of silanization (i.e., 5 min and 60 min) were employed to impart different degrees of wetting resistance to the PVDF membrane.

8.2.2 Characterization of membrane surface morphology

The surface morphology of the pristine and processed PVDF membranes was characterized using a scanning electron microscope (SEM; JEOL JSM-6500F) at 10 kV. The surface pore sizes were analyzed with ImageJ (National Institutes of Health). The grayscale SEM image was first converted to a binary (i.e., black and white) image (see Note E3). The apparent surface pores with irregular shapes were then automatically identified with ImageJ. For each apparent surface pore,

the Feret's diameter (i.e., the longest distance between any two points on the boundary of the surface pore) was measured as the apparent surface pore size. We used Feret's diameter to characterize the apparent surface pore because the permeation of liquid into a pore with irregular shape depends on the largest dimension of the surface pore.[52, 58-60] For each membrane, approximately 2000 individual pores obtained from 3 different SEM images were analyzed to obtain the apparent surface pore size distribution.

8.2.3 Characterization of membrane with capillary flow porometry

The pristine and processed PVDF membranes were characterized with a capillary flow porometer (Model CFP-1100A) at Porous Materials Inc. to measure the membrane pore size and the air permeability (see Note E4). Wet/dry flow method was used to measure the membrane pore diameter and dry flow method was used to measure the permeability of air at different pressures. Galwick fluid with a surface tension of 15.9 mN m^{-1} was used as the wetting liquid to completely wet all tested membranes (i.e., the contact angles of Galwick on all our membranes were 0°).

8.2.4 Measurement of liquid entry pressure

The liquid entry pressure of each membrane was measured by placing the membrane in a dead end filtration cell (UHP-43, Sterlitech);[15, 49] the cell was then filled with 50 ml DI water and tightly sealed. Subsequently, the cell was pressurized with compressed air in a step-wise manner (increment of 5±1 kPa and ~5 min for stabilization after each increment). The pressure at which the first water droplet completely permeated through the membrane and flowed out of the cell was

measured as the liquid entry pressure. Three independent measurements were conducted for each membrane.

8.2.5 Characterization of surface chemical composition

X-ray photo-electron spectroscopy (XPS) analysis was performed on the membrane surface using a PHI-5800 spectrometer (Physical Electronics) with a monochromatic Al-K X-ray source operated at 15 kV. The photoelectrons were collected at a takeoff angle of 45° relative to the membrane surface. Fourier-transform infrared (FTIR) spectroscopy was performed with a Nicolet iS-50 spectrometer (Thermo Fisher Scientific).

8.2.6 Measurement of contact angles

The apparent contact angles of liquids with a wide range of surface tensions (21–72.5 mN m^{-1}) were measured using a contact angle goniometer (Ramé-Hart 200-F1). By mixing DI water (72.5 mN m^{-1}) with different concentrations of pure ethanol (22.2 mN m^{-1}), we were able to create an array of polar liquids with gradually decreasing surface tension (see Table E1). For each liquid, three independent measurements with ~8 μL droplets were performed on each membrane.

8.2.7 Membrane distillation of feed solutions with surfactants

The membrane wetting resistance against surfactant sodium dodecyl sulfate (SDS) was evaluated with a custom-built direct contact membrane distillation (DCMD) system with a transparent acrylic cell. SDS is a representative substance that has been typically used to assess membrane wetting resistance in the MD process in the literature.[16, 27, 28] The feedwater and distillate channels

of the acrylic cell had an identical dimension of 77 mm × 26 mm × 3 mm, corresponding to an effective membrane area of 20.02 cm^2. The temperatures of the feed solution and deionized distillate were kept at 60°C and 20°C, respectively, using two recirculating water baths (Polystat, Cole-Parmer). The crossflow velocities of the feed and distillate streams were 9.6 cm s^{-1} (0.45 L min^{-1}) and 5.3 cm s^{-1} (0.25 L min^{-1}) in a concurrent mode, respectively. During the initial 90 min of MD desalination, 1 M NaCl solution at 60 °C was used as the feedwater. SDS was then introduced to the feed reservoir every 90 min to progressively increase the SDS concentration and consequently lower the surface tension of the feed solution. The SDS concentrations after sequential additions were 0.05, 0.1, 0.2, 0.3, and 0.4 mM. Water vapor flux across the membrane (J_w) was measured by monitoring the weight of the solution in the distillate reservoir using a digital balance (EW-10001-05, Cole-Parmer). The salt rejection efficiency was calculated from NaCl concentration in the permeate measured by a calibrated conductivity meter (Oakton Instruments).

8.2.8 Numerical simulations

Two-dimensional numerical simulations with an incompressible, laminar flow model were conducted to reveal the evolution of water-air interface upon water contacting the membrane under an applied pressure (i.e., the transmembrane pressure of 1.2 kPa in the MD experiment, as measured by a low-pressure gauge). The membrane was modeled as a two-layer porous structure consisting of spherical features. The inter-feature spacing of the spherical features was set to represent the critical pore size of the pristine PVDF membrane. The contact angle hysteresis was

ignored on the membrane surface in the simulation. We solved the governing equations with computational fluid dynamics (CFD) software ANSYS Fluent using a pressure-based solver. The geometric reconstruction scheme was used in the volume of fluid model to represent the liquid-air interface. The continuum surface force method was employed in the momentum equation. The SIMPLE (semi-implicit, explicit) algorithm was used for pressure-velocity coupling. A variable time step scheme was used to ensure Courant-Friedrich-Levy number < 1.0 in each time step. Iterations at each time step were terminated when the convergence criteria of all equations was smaller than 10^{-6}.

8.3 Results

8.3.1 Fabrication and characterization of omniphobic membrane.

PVDF membrane is one of the most commonly used membranes in MD process because of its inherent hydrophobicity, low thermal conductivity, and mechanical robustness.[36] However, hydrophobic PVDF membrane is prone to wetting, and surface engineering of PVDF membrane to improve its wetting resistance is a challenging task due to the chemical inertness of fluorocarbon materials. So far, complex and/or time-consuming processes [13, 16, 26, 37] have been used to activate PVDF membrane surface, followed by deposition of particles and surface fluorination, to render it omniphobic. In our approach to fabricate omniphobic PVDF membrane, ultra-fast etching of a commercial PVDF membrane (HVHP, Durapore) by immersing it in a sodium/naphthalene-based solution[38-40] for approximately 1 s was combined with surface chemistry modification using a

fluoroalkyl silane[41-44] (heptadecafluoro-1,1,2,2-tetrahydrodecyl trichlorosilane, FAS) to impart low solid surface energy (see Figure 8-1a). During the etching process, fluorine was stripped from the backbone of PVDF, while oxygen-containing functional groups such as hydroxyl and carboxyl groups were created to provide active sites for the subsequent grafting of fluoroalkyl silane via vapor phase silanization.[45, 46] This chemical transition was evident from the X-ray photon-electron spectroscopy (XPS) survey scans and high-resolution O1*s* spectra of pristine and etched PVDF membranes (see Appendix E, Note E1; Figure E1). Different silanization durations (i.e., 5 min and 1 h) were applied to fabricate PVDF membranes with different wettability. The etched membranes after 5 min- and 1 h-silanization are designated as PVDF-FAS-5 and PVDF-FAS-60 membranes hereafter, respectively. The surface chemical compositions of these membranes were characterized with XPS and Fourier-transform infrared spectroscopy (FTIR) (see Figure 8-1e; Note E2; Figure E2, Appendix E). The high-resolution C1*s* XPS spectra (see Figure 8-1e) indicated the presence of the characteristic $–CH_2$ and $–CF_2$ groups on the pristine PVDF membranes.[47, 48] In contrast, the characteristic $–CF_3$ group of fluoroalkyl silane was observed on the FAS-silanized PVDF membranes. Additionally, PVDF-FAS-60 membrane possessed higher CF_3/CF_2 peak intensity ratio (0.236) than PVDF-FAS-5 membrane (0.227), indicating higher coverage of FAS on the surface and consequently lower solid surface energy.

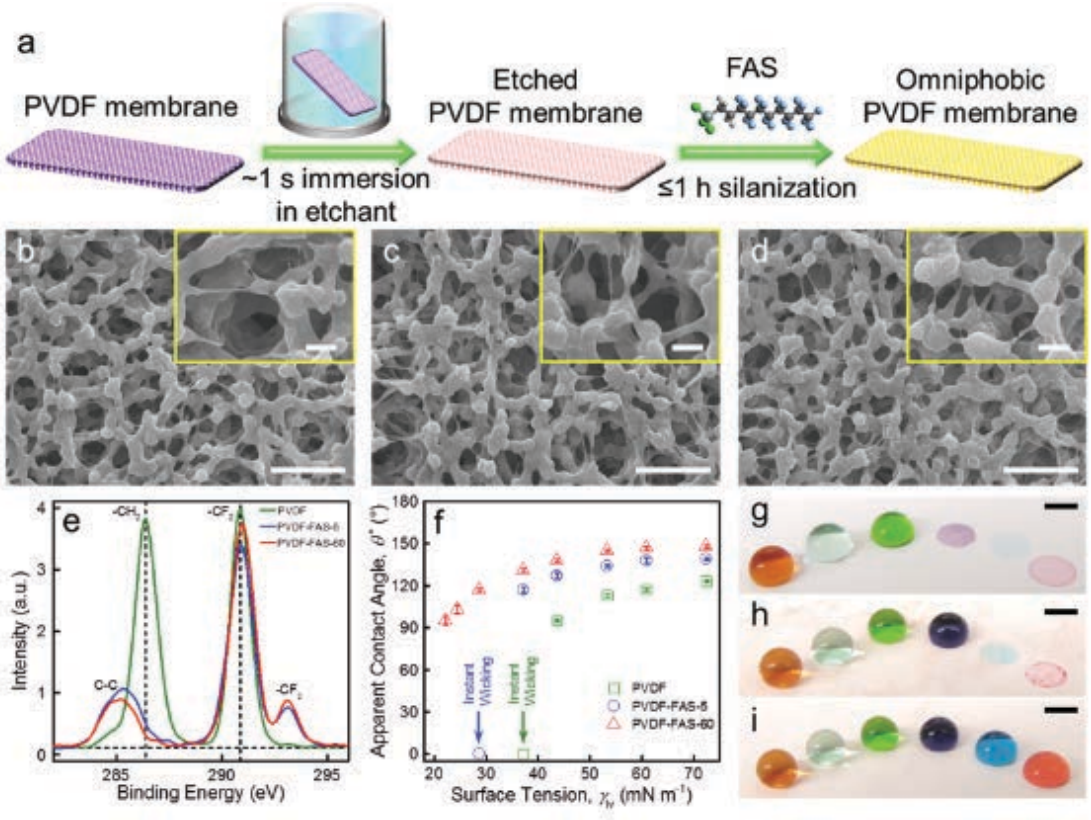

Figure 8-1. Fabrication and characterization of monolithic omniphobic membranes. (a) Schematic depicting the fabrication of omniphobic membranes. Scanning electron microscope (SEM) images of (b) pristine polyvinylidene difluoride (PVDF) membrane, (c) PVDF-FAS-5 membrane, and (d) PVDF-FAS-60 membrane. FAS refers to heptadecafluoro-1,1,2,2-tetrahydrodecyl trichlorosilane. The scale bars represent 5 μm and 1 μm (inset), respectively. (e) High resolution C1s XPS spectra of the membranes. (f) Apparent contact angles of liquids with different surface tensions on the membranes. Error bars represent standard deviation from three independent measurements. The green and blue arrows point to the surface tension at which liquid instantly wicked into pristine PVDF and PVDF-FAS-5 membranes, respectively. (g-i) Images showing different liquids beading up on or wetting (g) pristine PVDF membrane, (h) PVDF-FAS-5 membrane, and (i) PVDF-FAS-60 membrane. The droplets from left to right: water (γ_{lv} = 72.5 mN m^{-1}), 1.5 mM sodium dodecyl sulfate (SDS) in water (γ_{lv} = 61 mN m^{-1}), 20% ethanol in water (γ_{lv} = 43.7 mN m^{-1}), 30% ethanol in water (γ_{lv} = 37.2 mN m^{-1}), 60% ethanol in water (γ_{lv} = 28.7 mN m^{-1}), 100% ethanol (γ_{lv} = 22.2 mN m^{-1}). The scale bars represent 2 mm.

Further, the pristine and processed membranes (see Figure 8-1 b-d) consisted of similar interconnected micro-sized PVDF granules with a re-entrant texture and similar apparent surface pore size distributions obtained from SEM image analysis (see Methods section; Note E3; Figure E3). The membrane pore size distributions were measured with a capillary flow porometer (see Methods section; Note E4; Figure E4a-E4c), and similar membrane pore size distributions were also observed among the membranes. The mean membrane pore sizes were 0.452 μm, 0.462 μm, and 0.456 μm for the pristine PVDF, PVDF-FAS-5, and PVDF-FAS-60 membranes, respectively. These results indicate that the morphology of the processed PVDF membranes remains virtually unaltered compared to the pristine PVDF membrane. In addition, the air permeability of all the tested membranes was measured as an indicator of mass transfer resistance.[49] As shown in Figure E4d, the pristine and processed PVDF membranes displayed similar air permeability, indicating that the membrane modification employed in the current study did not result in additional mass transfer resistance.

The combination of the inherent re-entrant texture of PVDF membrane with sufficient coverage of FAS possessing low solid surface energy rendered the PVDF-FAS-60 membrane omniphobic. Liquids with a wide range of surface tensions displayed high apparent θ^* on the omniphobic PVDF-FAS-60 membrane, including ethanol with an ultra-low surface tension (γ_{lv} = 22.2 mN m^{-1}) demonstrating $\theta^* > 90°$ (see Figure 8-1f and Table E1). In contrast, the pristine PVDF membrane and PVDF-FAS-5 membrane were instantly wetted by water + 30% ethanol (γ_{lv} = 37.2 mN m^{-1}) and water + 60% ethanol (γ_{lv} = 28.7 mN m^{-1}), respectively. The different liquid

repellency of the three PVDF membranes is evident from different arrays of liquids beading up on or wetting the membrane surfaces (see Figure 8-1 g-i). Further, PVDF-FAS-60 membrane possesses higher liquid entry pressure (~175±5 kPa) than that of PVDF-FAS-5 membrane (~146±2 kPa) and pristine PVDF membrane (~114±2 kPa) (see Methods section). Therefore, these results indicate that the order of wetting resistance was PVDF-FAS-60 membrane > PVDF-FAS-5 membrane > pristine PVDF membrane. It is worth noting that although PVDF-FAS-5 membrane was completely wetted by water + 60% ethanol, it was able to resist wetting of non-polar liquids with even lower surface tensions, such as hexadecane (γ_{lv} = 27.5 mN m^{-1}) and silicone oil (γ_{lv} = 21 mN m^{-1}) (see Table E1). This phenomenon highlights the importance of using polar liquids with low surface tensions to characterize membrane liquid repellency.

8.3.2 Membrane wetting resistance in MD desalination.

To evaluate desalination performance of the membranes with different surface wettability, we performed direct contact membrane distillation (DCMD) tests using hypersaline feed solution (1 M NaCl) supplemented with progressively increasing concentrations of surfactant sodium dodecyl sulfate (SDS) (see Methods section). The increase of SDS concentration lowered the surface tension of feed solutions, which would cause wetting of membranes with insufficient wetting resistance.

All the membranes exhibited stable water vapor fluxes and perfect salt rejection prior to the addition of SDS (see Figure 8-2; Figure E5), indicating successful desalination by allowing the

transport of water vapor only. However, the water vapor flux of pristine PVDF membrane increased dramatically at 0.1 mM SDS (see Figure 8-2a and Figure E5a), along with a substantial decrease of salt removal efficiency. This was because a large portion of the membrane pores was completely wetted by the feed solution, resulting in the penetration of dissolved salt into the distillate. The PVDF-FAS-5 membrane showed improved wetting resistance against 0.2 mM SDS, but still lost its desalination function at 0.3 mM SDS (see Figure 8-2b and Figure E5b). In contrast, the omniphobic PVDF-FAS-60 membrane demonstrated remarkable wetting resistance and stable desalination performance even at 0.4 mM SDS (see Figure 8-2c and Figure E5c). This was because the omniphobicity of the PVDF-FAS-60 membrane prevented complete penetration of saline feed solution with surfactants into the porous membrane structure. It should be noted that the highest SDS concentration resisted by our omniphobic membrane is comparable or higher than that reported in prior work with particle-incorporated, hierarchically structured omniphobic membranes,[23, 24, 27-29] indicating that a monolithic membrane with re-entrant texture is sufficient to achieve omniphobicity in MD desalination.

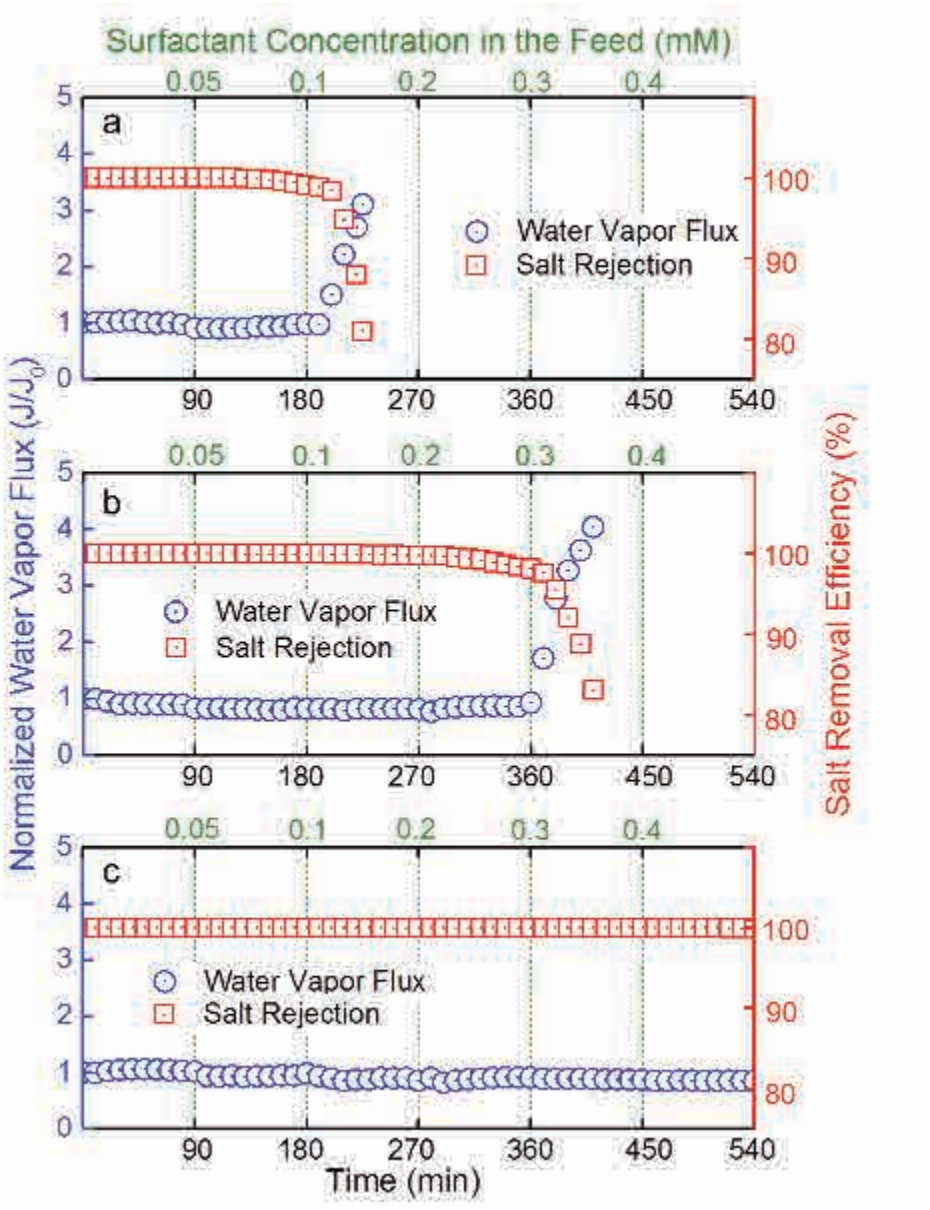

Figure 8-2. Membrane distillation (MD) performance of different PVDF membranes. Normalized water vapor flux (blue) and salt rejection (red) of (a) pristine PVDF membrane, (b) PVDF-FAS-5 membrane, and (c) PVDF-FAS-60 membrane in direct contact membrane distillation (DCMD) desalination, based on sequentially increasing doses of SDS. The feed solution contained 1 M NaCl, supplemented with various concentrations of SDS. The feed and distillate temperatures were maintained at 60°C and 20°C, respectively. Replicate results under identical experimental conditions are presented in the Figure E5, Appendix E.

8.3.3 Wetting resistance and water vapor permeability trade-off.

Ideally, membranes possessing both robust wetting resistance and high water vapor permeability are desirable in the MD process. However, our pristine PVDF, PVDF-FAS-5 and PVDF-FAS-60 membranes displayed decreasing water vapor permeability with increasing wetting resistance (see Figure 8-3). A thorough literature search indicates a similar phenomenon – omniphobic MD membranes with higher wetting resistance typically possess lower water vapor permeability compared to hydrophobic MD membranes with lower wetting resistance (see Table E2).[13, 16, 24-26, 28, 29, 50, 51] This phenomenon is intriguing because wetting resistance (an inverse measure of ease of liquid permeation) and water vapor permeability (a measure of ease of water vapor permeation) are distinct properties. The mechanism of this phenomenon is rarely addressed in the literature. While a few studies qualitatively attributed it to altered membrane morphology (e.g., increased membrane thickness and decreased pore sizes),[16, 26] such arguments cannot explain our results because no morphological difference was observed for our membranes (see Figure 8-1 b-d), regardless of their wetting resistance and water vapor permeability. Additionally, the results of air permeability measured at a wide range of pressures (see Figure E4d) indicate that our PVDF-FAS-5 and PVDF-FAS-60 membranes with higher wetting resistance do not possess additional mass transfer resistance compared to the pristine PVDF membrane. So, there is a need to understand the relationship between wetting resistance and water vapor permeability of MD membranes mechanistically.

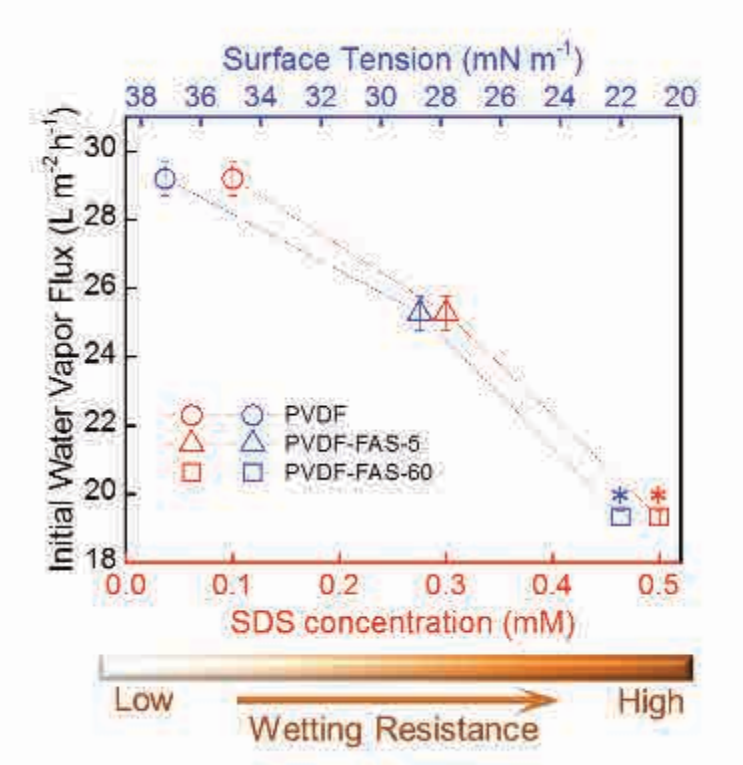

Figure 8-3. The relationship between initial water vapor flux and wetting resistance of different MD membranes tested in this study. The blue and red symbols refer to the critical surface tension and the critical SDS concentration, respectively, at which each membrane was completely wetted. Membranes with enhanced wetting resistance tolerate liquids with lower surface tensions and higher concentrations of SDS. The asterisks indicate that our omniphobic membrane was indeed not fully wetted by ethanol (in contact angle measurement) or 0.4 mM SDS (in DCMD desalination). Error bars represent standard deviation from three independent measurements.

In order to elucidate the mechanisms underlying the wetting resistance-water vapor permeability trade-off of our monolithic membranes, let us first consider the breakthrough pressure P_b[52] (i.e., the pressure at which liquid transitions from the non-wetting Cassie-Baxter state[53] to the wetted Wenzel state[54]) of individual pores with different sizes for PVDF membranes. Assuming that the membranes are composed of hexagonally arranged spherical features with diameters $2R$ and pore sizes (i.e., inter-feature spacing) $2D$ (see Note E6), the breakthrough pressure P_b of each pore can be determined from a force balance at the liquid–air interface:[55]

$$P_b \approx \frac{4\pi\gamma_{lv}(1-\cos\theta)}{R(2\sqrt{3}D^* - \pi)(\sqrt{D^*} - 1 + 2\sin\theta)} \quad (8\text{-}1)$$

Here, θ is the Young's contact angle, and the dimensionless parameter, $D^* = [(R+D)/R]^2$, is a measure of the air trapped underneath a liquid droplet when it forms a composite interface with a textured surface. It is evident from Equation 8-1 that the breakthrough pressure decreases with increasing the pore sizes of the membrane. When the membrane pore size exceeds a certain threshold, the corresponding P_b becomes lower than the transmembrane pressure, leading to the wetting of these pores due to the permeation of liquid water. Therefore, for a membrane with non-uniform pore size distribution (such as the PVDF membranes considered in this work), larger pores with breakthrough pressure less than transmembrane pressure become wetted in the MD process, while smaller pores with breakthrough pressure larger than transmembrane pressure remain non-wetted. More importantly, for a given pore size, the breakthrough pressure decreases with increasing the wettability (i.e., decreasing Young's contact angle). Consequently, for membranes with the same pore size distribution but different wettability, the hydrophobic membrane with lower wetting resistance (e.g., the pristine PVDF membrane) possesses more wetted pores compared to the omniphobic membrane with higher wetting resistance (e.g., the PVDF-FAS-60 membrane) in MD desalination. Compared to non-wetted pores with smaller water-air interfacial area (leading to one-dimensional evaporation, see Figure 8-4a), the water-filled wetted pores provide larger water-air interfacial area (leading to more effective three-dimensional evaporation,

see Figure 8-4b). Therefore, the hydrophobic membrane with more wetted pores is expected to display higher water vapor flux than the omniphobic membrane.

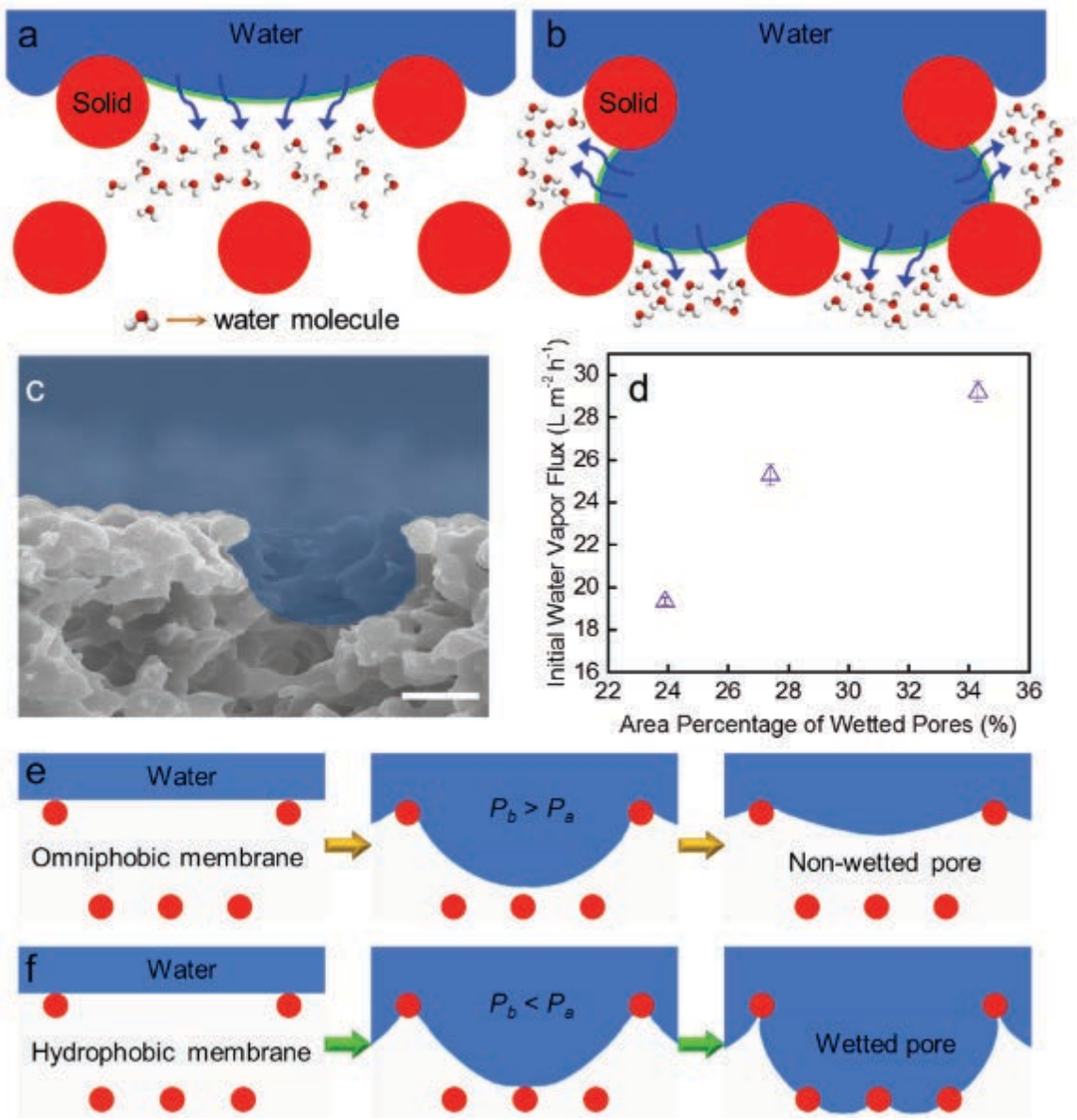

Figure 8-4. Mechanism underlying wetting resistance-water vapor permeability trade-off in MD desalination with monolithic omniphobic membranes. (a and b) Schematics (not drawn to scale) showing that the effective water-air interfacial area for evaporation (solid green line) increases when feedwater wets the pores. (c) Cross-sectional view of PVDF membrane surface, with the pore larger than the critical pore size for wetting (i.e., wetted pore depicted in blue). The scale bar represents 2 μm. (d) The positive correlation observed between area fraction of wetted pores and the initial water vapor flux of the membranes. Error bars represent standard deviation from three

independent measurements. (e and f) A series of snapshots from numerical simulations, showing dynamic formation of (e) non-wetted and (f) wetted pores on omniphobic membrane ($P_b \approx 1.8$ kPa $> P_a \approx 1.2$ kPa for the first layer) and hydrophobic membrane ($P_b \approx 1.19$ kPa $< P_a \approx 1.2$ kPa for the first layer), respectively. Water cannot permeate through the second layer because P_b (~29.4 kPa and ~19.5 kPa for the second layer of omniphobic and hydrophobic membranes, respectively) was greater than P_a. Note that P_a refers to applied pressure. P_b refers to breakthrough pressure, which can be estimated using Equation 8-1.

Based on Equation 8-1, for the transmembrane pressure of 1.2 kPa in our DCMD system, we estimated the critical pore sizes for wetting (beyond which the pores become wetted due to permeation of liquid water; see Figure 8-4c) of pristine PVDF, PVDF-FAS-5, and PVDF-FAS-60 membranes to be 3.35 μm, 3.65 μm, and 3.88 μm, respectively. Correspondingly, we estimated the wetted pore area fractions (obtained from the apparent surface pore size distribution in Figure E3; see Methods section; Note E3) of pristine PVDF, PVDF-FAS-5, and PVDF-FAS-60 membranes to be approximately 34.3%, 27.4%, and 23.9%, respectively (see Figure 8-4d). Lower wetted pore area fraction implies smaller water-air interfacial area for evaporation, which in turn results in lower water vapor flux. Consequently, for pristine PVDF, PVDF-FAS-5 and PVDF-FAS-60 membranes, while the wetting resistance increased (see Figure 8-1f), the water vapor flux decreased (see Figure 8-4d).

To further elucidate the dynamic formation of non-wetted and wetted pores on membranes with different wetting resistance, we performed numerical simulations to reveal the evolution of water-air interface upon water contacting membrane surface under an applied pressure (see Methods section). A two-layer porous structure consisting of spherical features was used to represent the membrane structure (see Figure 8-4e and 8-4f). When an applied pressure P_a (i.e.,

transmembrane pressure of 1.2 kPa) was exerted on water at rest on the first layer, the water-air interface deformed and moved towards the second layer. When P_b of the membrane pore was greater than P_a (e.g., PVDF-FAS-60 omniphobic membrane), our numerical simulations indicate that water cannot completely permeate through the first layer of the membrane, and a stable water-air interface is eventually formed (see Figure 8-4e). This leads to the formation of a non-wetted pore on the omniphobic membrane. In contrast, when P_b of the membrane pore, with same geometry, was less than P_a (e.g., PVDF hydrophobic membrane), our numerical simulations indicate that water permeates through the first layer of the membrane, and forms wetted pores with larger water-air interfacial area (see Figure 8-4f). These numerical simulation results are consistent with our schematic explanation depicted in Figures 8-4a and 8-4b, which indicate that membrane wettability regulates water vapor permeability through the effective evaporation area. In other words, hydrophobic membrane with more wetted pores is expected to display higher water vapor flux than the omniphobic membrane with less wetted pores.

8.4 Discussion

In this work, we fabricated monolithic omniphobic membranes, which displayed both excellent repellency to low surface tension liquids (including ethanol) and robust wetting resistance against surfactants in MD desalination. Compared to the fabrication of particle-incorporated omniphobic membranes, which typically require multiple steps and lengthy preparation duration (e.g., from hours to days), our facile and particle-free approach enables rapid

(<1.5 h) and scalable processing of omniphobic membranes. The monolithic feature of our membranes avoids potential detachment of particles, and thus improves membrane reliability in the MD process. Therefore, our fabrication approach has great potential to achieve large-scale manufacturing of omniphobic membranes for MD desalination.

More importantly, a trade-off between wetting resistance and water vapor permeability of MD membranes was identified in our study (see Figure 8-3; and Note E7; Figure E7). Such a trade-off has important implications that influence the membrane design and selection for MD desalination. Although omniphobic membranes demonstrate superior wetting resistance in MD process, this performance gain is offset by their reduced water vapor permeability that hinders process efficiency. On the other hand, MD membranes with high water vapor permeability tend to have inferior wetting resistance, rendering those membranes inappropriate for the treatment of wastewater with low surface tension. This dilemma is analogous to the classic permeability-selectivity trade-off in membrane desalination, in which an increase of water permeability typically leads to lower membrane selectivity (i.e., reduced salt removal efficiency[33-35]). Both trade-offs suggest that the design of appropriate membranes for desalination requires balance and optimization among different membrane properties. Current research efforts are investing heavily in fabrication of novel omniphobic membranes for MD.[8] However, achieving membrane omniphobicity at the expense of water vapor permeability might not be beneficial in MD desalination, particularly when relatively low concentrations of low surface energy contaminants are present in the feedwater. The practical impacts of membrane wettability on MD performance

should, therefore, be re-evaluated by taking membrane water production into consideration. In other words, one needs to consider membrane wetting resistance and water vapor permeability comprehensively[15, 49, 56, 57] in designing membrane materials for MD desalination of different feedwaters.

In summary, we developed a simple, scalable, and particle-free approach that enables rapid processing (< 1.5 h) of monolithic omniphobic PVDF membranes, and demonstrated a wetting resistance-vapor permeability trade-off for our monolithic membranes in MD desalination. We believe that our fabrication method has promising potential to simplify the manufacturing and scale-up of omniphobic MD membranes. Further, we envision that the wetting resistance-permeability trade-off as well as the mechanistic insight conveyed in our work will pave the way for smarter design strategies for high-performance MD membranes, thereby promoting the cost- and energy-efficiencies of MD desalination for water purification.

References

1 Grant, S. B.; Saphores, J. D.; Feldman, D. L.; Hamilton, A. J.; Fletcher, T. D.; Cook, P. L. M.; Stewardson, M.; Sanders, B. F.; Levin, L. A.; Ambrose, R. F.; Deletic, A.; Brown, R.; Jiang, S. C.; Rosso, D.; Cooper, W. J.; Marusic, I., Taking the "waste" out of "wastewater" for human water security and ecosystem sustainability. *Science* 2012, 337, (6095), 681-686.

2 Hoekstra, A. Y., Water scarcity challenges to business. *Nat. Clim. Change* 2014, 4, (5), 318-320.

3 Vorosmarty, C. J.; McIntyre, P. B.; Gessner, M. O.; Dudgeon, D.; Prusevich, A.; Green, P.; Glidden, S.; Bunn, S. E.; Sullivan, C. A.; Liermann, C. R.; Davies, P. M., Global threats to human water security and river biodiversity. *Nature* 2010, 467, (7315), 555-561.

4 Cook, B. I.; Ault, T. R.; Smerdon, J. E., Unprecedented 21st century drought risk in the american southwest and central plains. *Sci. Adv.* 2015, 1, (1), e1400082.

5 UNESCO Nature-based solutions for water; UNESCO: Paris, 2018.

6 Elimelech, M.; Phillip, W. A., The future of seawater desalination: energy, technology, and the environment. *Science* 2011, 333, (6043), 712-717.

7 Shannon, M. A.; Bohn, P. W.; Elimelech, M.; Georgiadis, J. G.; Marinas, B. J.; Mayes, A. M., Science and technology for water purification in the coming decades. *Nature* 2008, 452, (7185), 301-310.

8 Deshmukh, A.; Boo, C.; Karanikola, V.; Lin, S. H.; Straub, A. P.; Tong, T. Z.; Warsinger, D. M.; Elimelech, M., Membrane distillation at the water-energy nexus: limits, opportunities, and challenges. *Energy Environ. Sci.* 2018, 11, 1177-1196.

9 Tong, T. Z.; Elimelech, M., The global rise of zero liquid discharge for wastewater management: drivers, technologies, and future directions. *Environ. Sci. Technol.* 2016, 50, (13), 6846-6855.

10 Dongare, P. D.; Alabastri, A.; Pedersen, S.; Zodrow, K. R.; Hogan, N. J.; Neumann, O.; Wu, J. J.; Wang, T. X.; Deshmukh, A.; Elimelech, M.; Li, Q. L.; Nordlander, P.; Halas, N. J., Nanophotonics-enabled solar membrane distillation for off-grid water purification. *Proc. Natl. Acad. Sci. U.S.A.* 2017, 114, (27), 6936-6941.

11 Lawson, K. W.; Lloyd, D. R., Membrane distillation. *J. Memb. Sci.* 1997, 124, (1), 1-25.

12 Alkhudhiri, A.; Darwish, N.; Hilal, N., Membrane distillation: a comprehensive review. *Desalination* 2012, 287, 2-18.

13 Boo, C.; Lee, J.; Elimelech, M., Omniphobic polyvinylidene fluoride (PVDF) membrane for desalination of shale gas produced water by membrane distillation. *Environ. Sci. Technol.* 2016, 50, (22), 12275-12282.

14 Shaffer, D. L.; Chavez, L. H. A.; Ben-Sasson, M.; Castrillon, S. R. V.; Yip, N. Y.; Elimelech, M., Desalination and reuse of high-salinity shale gas produced water: drivers, technologies, and future directions. *Environ. Sci. Technol.* 2013, 47, (17), 9569-9583.

15 Woo, Y. C.; Chen, Y.; Tijing, L. D.; Phuntsho, S.; He, T.; Choi, J. S.; Kim, S. H.; Shon, H. K., CF4 plasma-modified omniphobic electrospun nanofiber membrane for produced water brine treatment by membrane distillation. *J. Memb. Sci.* 2017, 529, 234-242.

16 Woo, Y. C.; Kim, Y.; Yao, M.; Tijing, L. D.; Choi, J. S.; Lee, S.; Kim, S. H.; Shon, H. K., Hierarchical composite membranes with robust omniphobic surface using layer-by-layer assembly technique. *Environ. Sci. Technol.* 2018, 52, (4), 2186-2196.

17 Wang, Z. X.; Elimelech, M.; Lin, S. H., Environmental applications of interfacial materials with special wettability. *Environ. Sci. Technol.* 2016, 50, (5), 2132-2150.

18 Kota, A. K.; Kwon, G.; Tuteja, A., The design and applications of superomniphobic surfaces. *NPG Asia Mater.* 2014, 6, e109.

19 Tuteja, A.; Choi, W.; Mabry, J. M.; McKinley, G. H.; Cohen, R. E., Robust omniphobic surfaces. *Proc. Natl. Acad. Sci.* U.S.A. 2008, 105, (47), 18200-18205.

20 Deng, X.; Mammen, L.; Butt, H. J.; Vollmer, D., Candle soot as a template for a transparent robust superamphiphobic coating. *Science* 2012, 335, (6064), 67-70.

21 Tuteja, A.; Choi, W.; Ma, M.; Mabry, J. M.; Mazzella, S. A.; Rutledge, G. C.; McKinley, G. H.; Cohen, R. E., Designing superoleophobic surfaces. *Science* 2007, 318, (5856), 1618-1622.

22 Liu, K.; Tian, Y.; Jiang, L., Bio-inspired superoleophobic and smart materials: design, fabrication, and application. *Prog. Mater. Sci.* 2013, 58, (4), 503-564.

23 Boo, C.; Lee, J.; Elimelech, M., Engineering surface energy and nanostructure of microporous films for expanded membrane distillation applications. *Environ. Sci. Technol. 2016*, 50, (15), 8112-8119.

24 Huang, Y. X.; Wang, Z. X.; Jin, J.; Lin, S. H., Novel janus membrane for membrane distillation with simultaneous fouling and wetting resistance. *Environ. Sci. Technol.* 2017, 51, (22), 13304-13310.

25 Lu, X. M.; Peng, Y. L.; Qiu, H. R.; Liu, X. R.; Ge, L., Anti-fouling membranes by manipulating surface wettability and their anti-fouling mechanism. *Desalination* 2017, 413, 127-135.

26 Zheng, R.; Chen, Y.; Wang, J.; Song, J. F.; Li, X. M.; He, T., Preparation of omniphobic PVDF membrane with hierarchical structure for treating saline oily wastewater using direct contact membrane distillation. *J. Memb. Sci.* 2018, 555, 197-205.

27 Lin, S. H.; Nejati, S.; Boo, C.; Hu, Y. X.; Osuji, C. O.; Ehmelech, M., Omniphobic membrane for robust membrane distillation. *Environ. Sci. Technol. Lett.* 2014, 1, (11), 443-447.

28 Lee, J.; Boo, C.; Ryu, W. H.; Taylor, A. D.; Elimelech, M., Development of omniphobic desalination membranes using a charged electrospun nanofiber scaffold. ACS Appl. Mater. *Interfaces* 2016, 8, (17), 11154-11161.

29 Chen, L. H.; Huang, A.; Chen, Y. R.; Chen, C. H.; Hsu, C. C.; Tsai, F. Y.; Tung, K. L., Omniphobic membranes for direct contact membrane distillation: Effective deposition of zinc oxide nanoparticles. *Desalination* 2018, 428, 255-263.

30 Malysheva, A.; Lombi, E.; Voelcker, N. H., Bridging the divide between human and environmental nanotoxicology. *Nat. Nanotechnol.* 2015, 10, (10), 835.

31 Auffan, M.; Rose, J.; Bottero, J.-Y.; Lowry, G. V.; Jolivet, J.-P.; Wiesner, M. R., Towards a definition of inorganic nanoparticles from an environmental, health and safety perspective. *Nat. Nanotechnol.* 2009, 4, (10), 634.

32 Batley, G. E.; Kirby, J. K.; McLaughlin, M. J., Fate and risks of nanomaterials in aquatic and terrestrial environments. *Acc. Chem. Res.* 2012, 46, (3), 854-862.

33 Werber, J. R.; Deshmukh, A.; Elimelech, M., The critical need for increased selectivity, not increased water permeability, for desalination membranes. *Environ. Sci. Technol. Lett.* 2016, 3, (4), 112-120.

34 Park, H. B.; Kamcev, J.; Robeson, L. M.; Elimelech, M.; Freeman, B. D., Maximizing the right stuff: The trade-off between membrane permeability and selectivity. *Science* 2017, 356, (6343), 1137.

35 Werber, J. R.; Osuji, C. O.; Elimelech, M., Materials for next-generation desalination and water purification membranes. *Nat. Rev. Mater.* 2016, 1, (5), 16018.

36 Thomas, N.; Mavukkandy, M. O.; Loutatidou, S.; Arafat, H. A., Membrane distillation research & implementation: lessons from the past five decades. *Sep. Purif. Technol.* 2017, 189, 108-127.

37 Lu, K. J.; Zuo, J.; Chang, J.; Kuan, H. N.; Chung, T. S., Omniphobic hollow-fiber membranes for vacuum membrane distillation. *Environ. Sci. Technol.* 2018, 52, (7), 4472-4480.

38 Nelson, E.; Kilduff, T. J.; Benderly, A., Bonding of teflon. *Ind. Eng. Chem.* 1958, 50, (3), 329-330.

39 Haridoss, S.; Perlman, M., Chemical modification of near-surface charge trapping in polymers. *J. Appl. Phys.* 1984, 55, (5), 1332-1338.

40 Gabriel, M.; Dahm, M.; Vahl, C.-F., Wet-chemical approach for the cell-adhesive modification of polytetrafluoroethylene. *Biomed. Mater.* 2011, 6, (3), 035007.

41 Deng, L.; Ye, H.; Li, X.; Li, P.; Zhang, J.; Wang, X.; Zhu, M.; Hsiao, B. S., Self-roughened omniphobic coatings on nanofibrous membrane for membrane distillation. *Sep. Purif. Technol.* 2018, 206, 14-25.

42 Li, L.; Li, B.; Dong, J.; Zhang, J., Roles of silanes and silicones in forming superhydrophobic and superoleophobic materials. *J. Mater. Chem.* A 2016, 4, (36), 13677-13725.

43 Movafaghi, S.; Wang, W.; Metzger, A.; Williams, D. D.; Williams, J. D.; Kota, A. K., Tunable superomniphobic surfaces for sorting droplets by surface tension. *Lab Chip* 2016, 16, (17), 3204-3209.

44 Pendurthi, A.; Movafaghi, S.; Wang, W.; Shadman, S.; Yalin, A. P.; Kota, A. K., Fabrication of Nanostructured Omniphobic and Superomniphobic Surfaces with Inexpensive CO2 Laser Engraver. *ACS Appl. Mater. Interfaces* 2017, 9, (31), 25656-25661.

45 Bart, J.; Tiggelaar, R.; Yang, M. L.; Schlautmann, S.; Zuilhof, H.; Gardeniers, H., Room-temperature intermediate layer bonding for microfluidic devices. *Lab Chip* 2009, 9, (24), 3481-3488.

46 Catala-Icardo, M.; Torres-Cartas, S.; Meseguer-Lloret, S.; Gomez-Benito, C.; Carrasco-Correa, E.; Simo-Alfonso, E. F.; Ramis-Ramos, G.; Herrero-Martinez, J. M., Preparation of organic monolithic columns in polytetrafluoroethylene tubes for reversed-phase liquid chromatography. *Anal. Chim. Acta* 2017, 960, 160-167.

47 Zhu, L. P.; Yu, J. Z.; Xu, Y. Y.; Xi, Z. Y.; Zhu, B. K., Surface modification of PVDF porous membranes via poly (DOPA) coating and heparin immobilization. *Colloids Surf. B* 2009, 69, (1), 152-155.

48 Duca, M. D.; Plosceanu, C. L.; Pop, T., Surface modifications of polyvinylidene fluoride (PVDF) under RF Ar plasma. *Polym. Degrad. Stab.* 1998, 61, (1), 65-72.

49 Yang, C.; Li, X.-M.; Gilron, J.; Kong, D.-f.; Yin, Y.; Oren, Y.; Linder, C.; He, T., CF4 plasma-modified superhydrophobic PVDF membranes for direct contact membrane distillation. *J. Memb. Sci.* 2014, 456, 155-161.

50 Lu, C.; Su, C.; Cao, H.; Ma, X.; Duan, F.; Chang, J.; Li, Y., F-POSS based omniphobic membrane for robust membrane distillation. *Mater. Lett.* 2018, 228, 85.

51 Du, X.; Zhang, Z.; Carlson, K. H.; Lee, J.; Tong, T., Membrane fouling and reusability in membrane distillation of shale oil and gas produced water: effects of membrane surface wettability. *J. Memb. Sci.* 2018, 567, 199.

52 Wang, W.; Salazar, J.; Vahabi, H.; Joshi-Imre, A.; Voit, W. E.; Kota, A. K., Metamorphic superomniphobic surfaces. *Adv. Mater.* 2017, 29, (27), 1700295.

53 Cassie, A.; Baxter, S., Wettability of porous surfaces. *Trans. Faraday Soc.* 1944, 40, 546-551.

54 Wenzel, R. N., Resistance of solid surfaces to wetting by water. *Ind. Eng. Chem.* 1936, 28, (8), 988-994.

55 Kota, A. K.; Li, Y.; Mabry, J. M.; Tuteja, A., Hierarchically structured superoleophobic surfaces with ultralow contact angle hysteresis. *Adv. Mater.* 2012, 24, (43), 5838-5843.

56 Hammami, M. A.; Croissant, J. G.; Francis, L.; Alsaiari, S. K.; Anjum, D. H.; Ghaffour, N.; Khashab, N. M., Engineering hydrophobic organosilica nanoparticle-doped nanofibers for enhanced and fouling resistant membrane distillation. *ACS Appl. Mater. Interfaces* 2017, 9, (2), 1737-1745.

57 Yang, C.; Tian, M.; Xie, Y.; Li, X.-M.; Zhao, B.; He, T.; Liu, J., Effective evaporation of CF4 plasma modified PVDF membranes in direct contact membrane distillation. *J. Memb. Sci.* 2015, 482, 25-32.

58 Bielinski, A. R.; Boban, M.; He, Y.; Kazyak, E.; Lee, D. H.; Wang, C.; Tuteja, A.; Dasgupta, N. P., Rational design of hyperbranched nanowire systems for tunable superomniphobic surfaces enabled by atomic layer deposition. *ACS Nano* 2016, 11, (1), 478-489.

59 Liu, T.; Kim, C.-J., Turning a surface superrepellent even to completely wetting liquids. *Science* 2014, 346, (6213), 1096-1100.

60 Papadopoulos, P.; Mammen, L.; Deng, X.; Vollmer, D.; Butt, H.-J., How superhydrophobicity breaks down. *Proc. Natl. Acad. Sci. U.S.A.* 2013, 110, (9), 3254-3258.

CHAPTER 9: Conclusions and recommendations

9.1 Conclusions

Recently, there has been a growing interest in the treatment and reuse of oil and gas (O&G) wastewater in the U.S. due to the rise of hydraulic fracturing activities, water shortage, and environmental concerns. However, most of O&G wastewater has not been widely recycled and reused in the central and western U.S. due to the regulatory, environmental, and technical challenges. Thus, this research work aimed to facilitate the reuse and treatment of O&G wastewater in order to improve the sustainability at water-energy-climate nexus. Regarding this major objective, two sets of studies were performed, including motivation and material innovation, with the following conclusions.

Firstly, spatiotemporal correlation analyses were performed to investigate the impacts of drought intensity on the number and water consumption of newly drilled O&G wells in Colorado, a major O&G producing states in the U.S. The results demonstrate that hydroclimate variation imposes a negligible impact on well number, location, and water footprint of O&G production, and that monthly O&G water consumption in areas under drought climate would sustain up to >110% of municipal water usage at the county scale. Moreover, the O&G producers might have to travel more than 500 miles to acquire water from areas without water stress, resulting in local water withdrawal that intensifies water scarcity and competition. Then, I expanded my research scope and investigated the water consumption and wastewater generation by O&G production

under different hydroclimate conditions in eleven O&G-producing states across the central and western U.S. for a 10-year period from 2011 to 2020. The results show that the water consumed under abnormally dry and drought conditions accounted for nearly half (49.7%, 475.3 billion gallons) of total water usage of HF, with 9% (86.1 billion gallons) of water consumption occurred under extreme or exceptional droughts. The water usage of HF under arid conditions can translate to high densities of water footprint at the local scale, equivalent to more than 10% and 50% of the annual water usage by the irrigation and domestic sectors in 6-29 irrigation-active counties and 11-51 counties (depending on the specific year), respectively. This study also quantified the potential of recycling O&G wastewater to mitigate the water stress imposed by HF activities under drought conditions. These two studies provide quantitative information for both policy makers and O&G operators to formulate wiser strategies of water resource management in the O&G-producing areas of the U.S.

Secondly, I compared three membranes with different surface wettability (a commercial PVDF membrane, an omniphobic membrane, and a composite membrane with hydrophilic coating) in MD treatment of O&G produced water from the Wattenberg field in northeast Colorado. Results show that the comparative performance of these membranes was influenced by not only surface wettability but also produced water composition. Produced waters with varied chemical components led to distinct features of fouling layers, as revealed by detailed microscopic and spectroscopic characterization. Despite its interior fouling resistance in a single treatment cycle,

the omniphobic membrane exhibited the best reusability after physical cleaning among the tested membranes in three consecutive treatment cycles. This robustness, however, was achieved at the expense of initial water flux, and the fabrication of omniphobic membrane typically involves the use of long-chain PFASs. Thereafter, I investigated the feasibility of achieving exceptional wetting resistance of MD membranes by avoiding the use of long-chain PFASs. In this study, I demonstrated that MD membranes with exceptional wetting resistance can be achieved through the combination of hierarchically structured membranes with (ultra)short-chain fluorocarbons, which have much lower acute toxicity and bioaccumulation potentials than long-chain PFASs. The hierarchically structured membrane with three-tier micro/nano-structure modified with short-chain fluorocarbon achieves excellent wetting resistance comparable to or higher than the long-chain PFASs-based omniphobic membranes reported in the literature. Moreover, the similarly structured membranes fabricated with ultrashort-chain fluorocarbons display sufficient wetting resistance against low surface tension O&G wastewaters. Finally, I elucidated the relationship between the wetting resistance and water vapor permeability of MD membranes. This study demonstrated that a trade-off between water vapor permeability and membrane wetting resistance exists in the MD process. The results from these studies indicate that the design and selection of appropriate MD membranes for O&G wastewater treatment should consider wetting resistance, water productivity, and environmental risks comprehensively. Additionally, the novel fabrication method developed in these studies, as well as the elucidation of the vapor permeability-wetting resistance trade-off,

may facilitate the practical use of omniphobic membranes for more efficient and sustainable MD desalination.

9.2 Recommendations for future work

9.2.1 Interactions between O&G activities and other local water users

The two studies performed Chapters 4 and 5 quantified the water footprint of HF under hydroclimate variation, in order to understand the impacts of O&G production on regional water sustainability. These studies demonstrated that water consumption by O&G activities was found to occur in several drought-prone counties. Local water users (e.g., irrigation and domestic sectors) in those counties can face intense competition for water resources due to O&G operations. According to our findings, future research should focus on those counties to better understand the interactions between O&G activity and other local water users. In the future, detailed quantitative analysis should be conducted to determine the extent to which water shortages or price increase for other users have occurred as a result of water consumption by HF activities. These in-depth studies will improve our understanding of the effects of O&G water withdrawals on local water availability, allowing for the development of sustainable water resource management strategies in the O&G-producing regions.

9.2.2 Innovation of omniphobic membrane materials

The study of Chapter 7 created an omniphobic membrane using short-chain fluorocarbon compounds rather than long-chain PFASs. Despite the fact that short-chain fluorocarbon compounds are considered better substitutes due to their lower bioaccumulation potential and lower acute toxicity, I have not achieved membrane omniphobicity by using ultrashort-chain fluorocarbon compounds. Thus, more research should focus on further improving membrane wetting resistance by utilizing ultrashort-chain fluorocarbon compounds in the future. For example, we could optimize and increase the number of layers of hierarchical textures on the membrane surface to further improve surface wetting resistance (i.e., coating three layers of SiNPs on the membrane surface or changing the sizes of SiNPs). The application of omniphobic membranes in the treatment of O&G wastewater will be further bolstered by the use of more environmentally friendly materials.

9.2.3 Breaking the trade-off between the water vapor permeability and membrane wetting resistance

The trade-off between wetting resistance and water vapor permeability of MD membranes can significantly impede the efficiency of omniphobic membranes. According to the study of Chapter 8, due to the interconnected micro-sized granular structure of pristine membrane, increasing wetting resistance can reduce the water-air interfacial area, resulting in a reduction in water vapor flux. Accordingly, further research should be directed toward minimizing the change in the water-

air interfacial area by optimizing the structure of pristine membranes (e.g., applying cylindrical nanoporous structure, or membranes with narrow pore size distribution), in order to break such a trade-off. Omniphobic membranes with high water permeability have the potential to significantly improve the efficiency of MD process for the treatment of O&G wastewater.

9.2.4 Tailoring the membrane wetting resistance to the O&G wastewater

The results of Chapters 7 and 8 suggest that the balance of wetting resistance, sustainability, and water permeability should be considered comprehensively when designing MD membranes for real O&G wastewaters. We should investigate the MD performance and durability of highly wetting resistant membranes modified with (ultra)short-chain flurocarbons for the treatment of real O&G wastewaters in the future. Wetting resistance and fabrication materials should be optimized and tailored to the wetting potential of the O&G wastewater, in order to maximize the efficiency of the MD process in the treatment of O&G wastewater.

APPENDIX A

Section 1. Correlation analyses of UOG activities and water footprint with hydroclimate condition We performed different correlation analyses to evaluate the relationship of the unconventional oil and gas (UOG) activities with hydroclimate condition and crude oil price, including both linear (Pearson correlation) and non-linear (Spearman and Kendall correlations) analyses. Specifically, Pearson's r is the most commonly used correlation coefficient and measures the linear relationship between two continuous variables;[1] Spearman's correlation coefficient (r_s) and Kendall's coefficients (τ) assesses the monotonic relationship (whether linear or not) between two variables;[2,3] For all those correlations, week or negligible relationships exists when the absolute values of correlation coefficients are less than 0.3.[4, 5]

As shown in Table A1, hydroclimate condition (as indicated by the drought severity classification index, DSCI) exhibited no linear relationship with the number of newly drilled wells (evidenced by Pearson's r = 0.01 and $p > 0.1$). Also, a positive relationship was shown by Spearman and Kendall correlations, with the correlation being weak but statistically significant (r_s and $\tau < 0.3$, $p < 0.005$). However, the positive relationship (r_s and $\tau > 0$) indicates that such correlations are mathematically valid but practically meaningless, because enhanced drought condition should not increase the activity of water-consumptive hydraulic fracturing in practical. In contrast, the crude oil price showed strongly positive and statistically significant relationship

with the UOG activity (Table A1) in all the three analyses. Therefore, hydroclimate condition imposes a negligible impact on the drilling activity, which is mainly driven by the market.

Table A1. Correlations of DSCI and oil price with the number of newly drilled wells

Variable	**Raw data**					
	Pearson		**Spearman**		**Kendall**	
	r	***p***	**r_s**	***p***	***τ***	***p***
DSCI	0.01	0.89	0.25	0.002	0.16	0.005
Oil price	0.62	<0.001	0.60	<0.001	0.44	<0.001

Further, hydroclimate condition, crude oil price, drilling activity, and UOG water consumption might be all subject to seasonal cycles. Therefore, we removed the seasonal components of time series in order to better understand the relationship of hydroclimate condition with activity/water consumption of UOG production. Additive decomposition of time series was performed in our analysis because the seasonal variations appears to be constant over time.[6] The additive decomposition assumes that a time series is composed of three additive terms:

$$y_t = S_t + T_t + R_t \tag{A1}$$

where y_t is the raw data, S_t is the seasonal variation, T_t is the trend component, and R_t is the error (or irregular component).

The decompositions of time series of DSCI, crude oil price, number of newly drilled wells, and water consumption by hydraulic fracturing (HF) were performed using the Rstudio software in order to estimate the seasonal trend for each dataset (Figure A1). Adjusted datasets without seasonal components of time series were obtained by subtracting the seasonal trend from each

dataset. Then the correlation analyses were re-calculated for the adjusted datasets and the results are shown in Table A2.

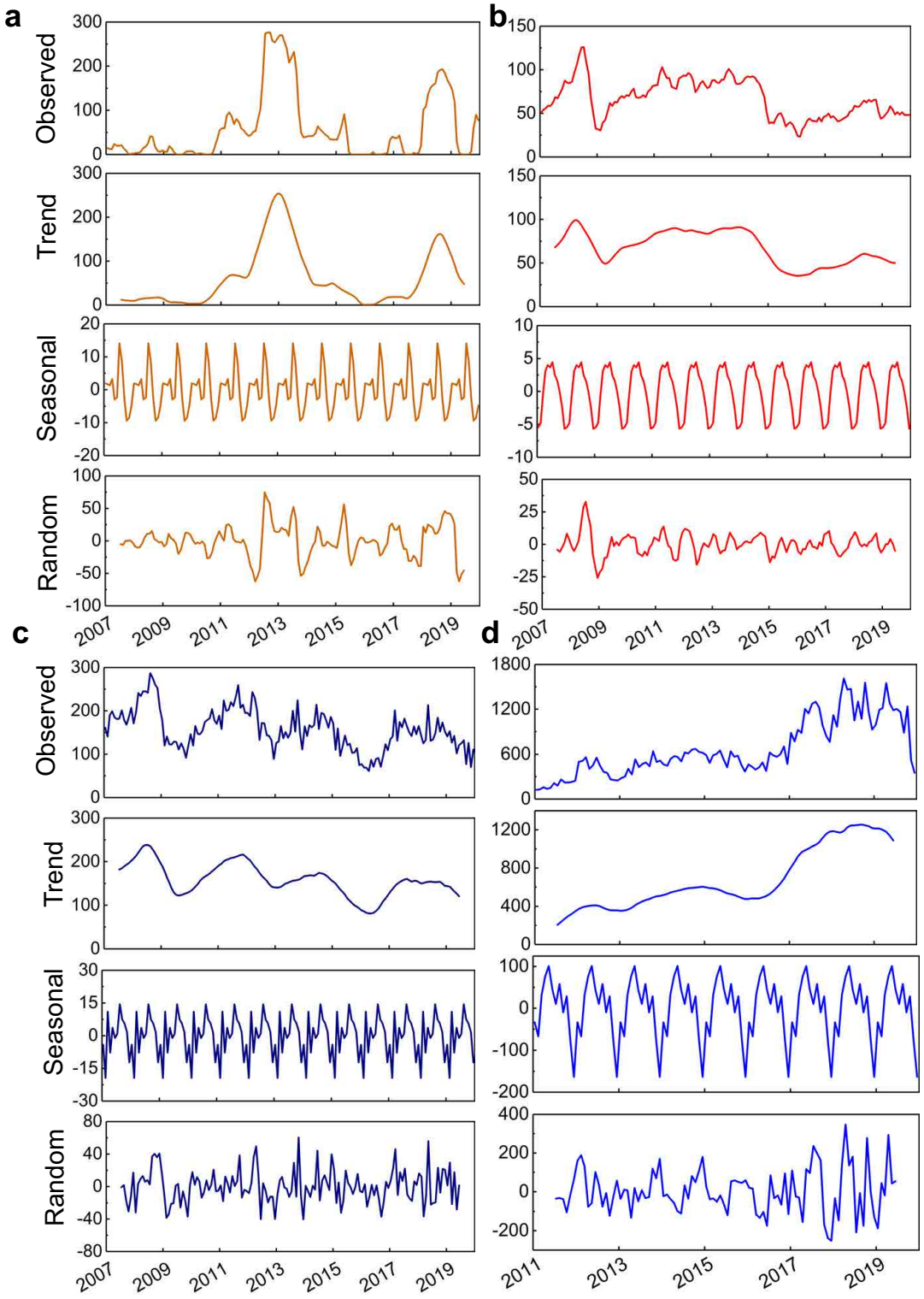

Figure A1. Decomposition of additive time series for monthly datasets of (a) DSCI, (b) crude oil price, (c) number of newly drilled wells, and (d) water consumption by HF.

Table A2. Correlations of DSCI or oil price with the number of newly drilled wells using data after removing the seasonal trend

Variable	Adjusted data after removing of seasonal trend					
	Pearson		Spearman		Kendall	
	r	p	r_s	p	τ	p
DSCI	0.01	0.9	0.21	0.007	0.14	0.012
Oil price	0.62	<0.001	0.61	<0.001	0.44	<0.001

As shown in Table A2, the correlation results after removing the seasonal components are consistent with those obtained by the above analyses, except that the Spearman and Kendall correlations become weaker between DSCI and the drilling activity. These analyses provide additional evidence that hydroclimate variation does not affect UOG activity, although the UOG industry is water consumptive.

We also performed the correlation analyses on the relationship between hydroclimate condition and water use by HF. As shown in Table A3, the DSCI shows no linear relationship with the water consumption by HF (the absolute value of Pearson's $r < 0.2$, and $p = 0.25$). However, a weakly negative monotonic correlation exists between DSCI and water consumption by HF with high significance, evidenced by both Spearman and Kendall correlations (the absolute values of r_s and $\tau < 0.3, p < 0.05$). Therefore, the water consumption by HF is slightly limited under high levels of drought climates, at least mathematically. In addition, the results after decomposition of time series are consistent with the above analyses (Table A4).

Table A3. Correlation coefficients of DSCI with the water consumption by hydraulic fracturing

Variables	**Raw Data**					
	Pearson		**Spearman**		**Kendall**	
	r	***p***	**r_s**	***p***	**τ**	***p***
DSCI	-0.15	0.25	-0.23	0.02	-0.16	0.014

Table A4. Correlations of DSCI with the water consumption by hydraulic fracturing after removing of the seasonal trend

Variables	**After removing of seasonal trend**					
	Pearson		**Spearman**		**Kendall**	
	r	***p***	**r_s**	***p***	**τ**	***p***
DSCI	-0.12	0.23	-0.25	0.009	-0.19	0.003

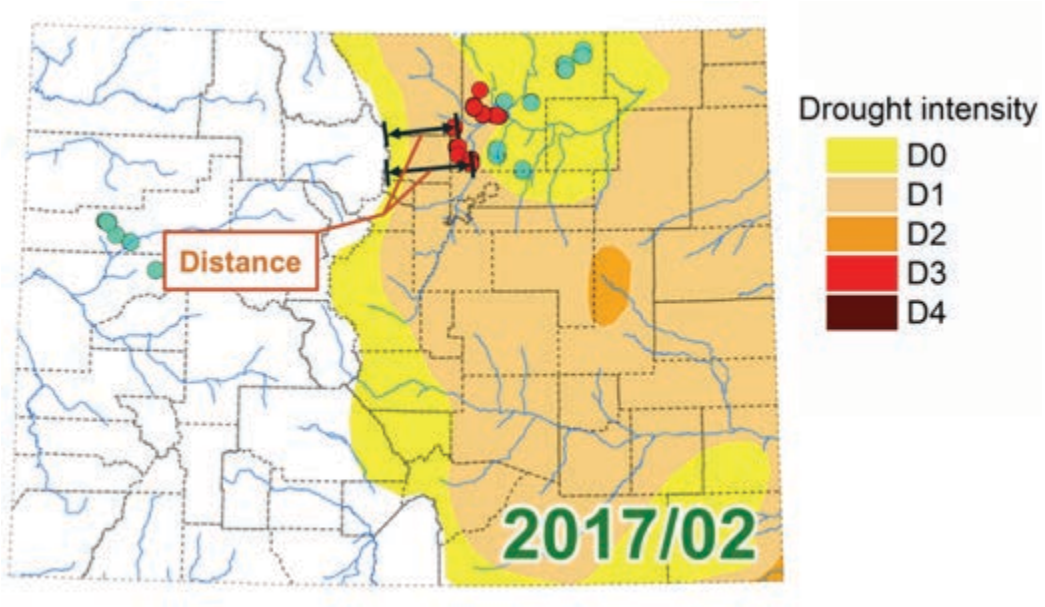

Figure A2. Schematic illustration of how the drought-escaping distance (d_{es}), which is defined as the distance between UOG wells (blue or red dots) located in drought area (D1-D4 drought categories, red dots) to the closest non-drought area (without any drought category), is calculated. Note that due to the size of the dots, one dot might cover more than one well.

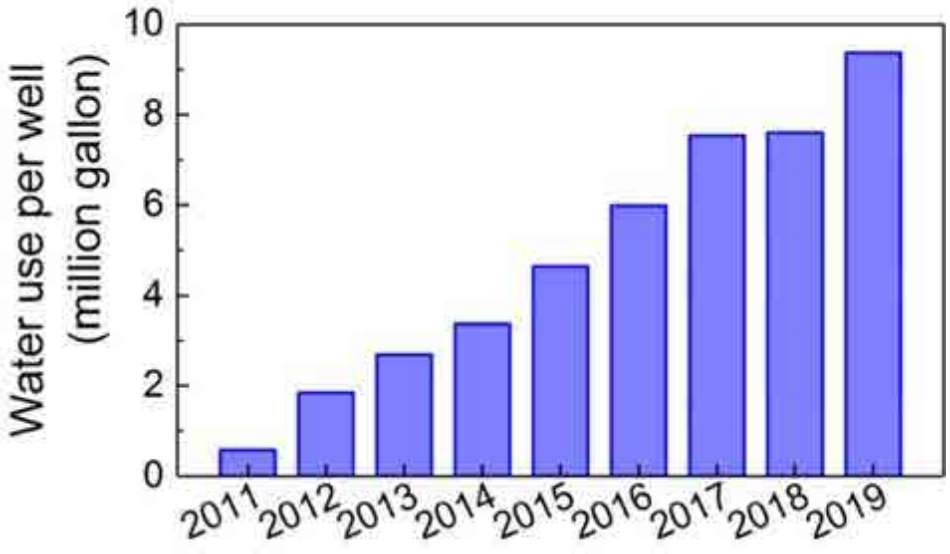

Figure A3. The annual average water use per well in Colorado between 2011 and 2019. The data are obtained from the FracFocus database.

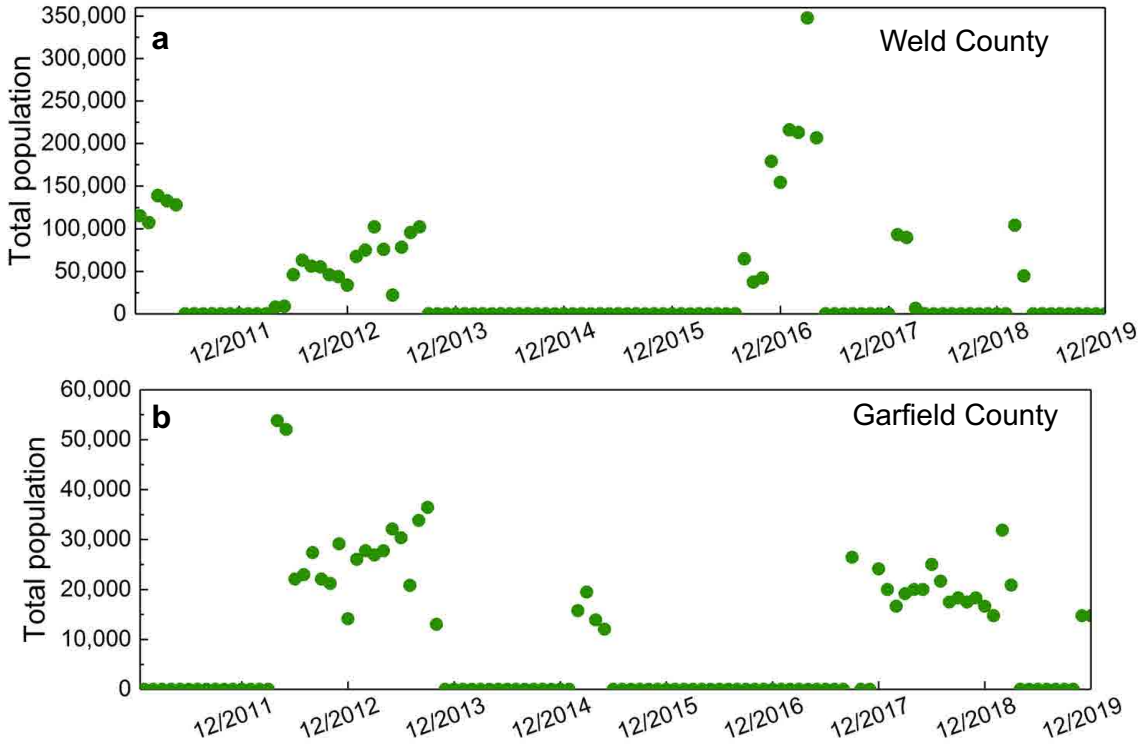

Figure A4. The population that would be sustained by water use of newly drilled UOG wells located in the drought areas (i.e., with drought categories of D1-D4) each month from 2011 to 2019 for (a) Weld County and (b) Garfield County.

References

1. Pearson, K.; Galton, F., The life, letters and labours of Francis Galton. *Cambridge University Press: Cambridge*, 1914.
2. Spearman, C., The proof and measurement of association between two things. 1961.
3. Kendall, M. G., Rank correlation methods. 1948.
4. Akoglu, H., User's guide to correlation coefficients. *Turkish journal of emergency medicine* 2018, 18, (3), 91-93.
5. Hemphill, J. F., Interpreting the magnitudes of correlation coefficients. 2003.
6. Hyndman, R.J., & Athanasopoulos, G. Forecasting: principles and practice, 2nd edition, OTexts: Melbourne, Australia. OTexts.com/fpp2. (Accessed on Spetember 13, 2020).

APPENDIX B

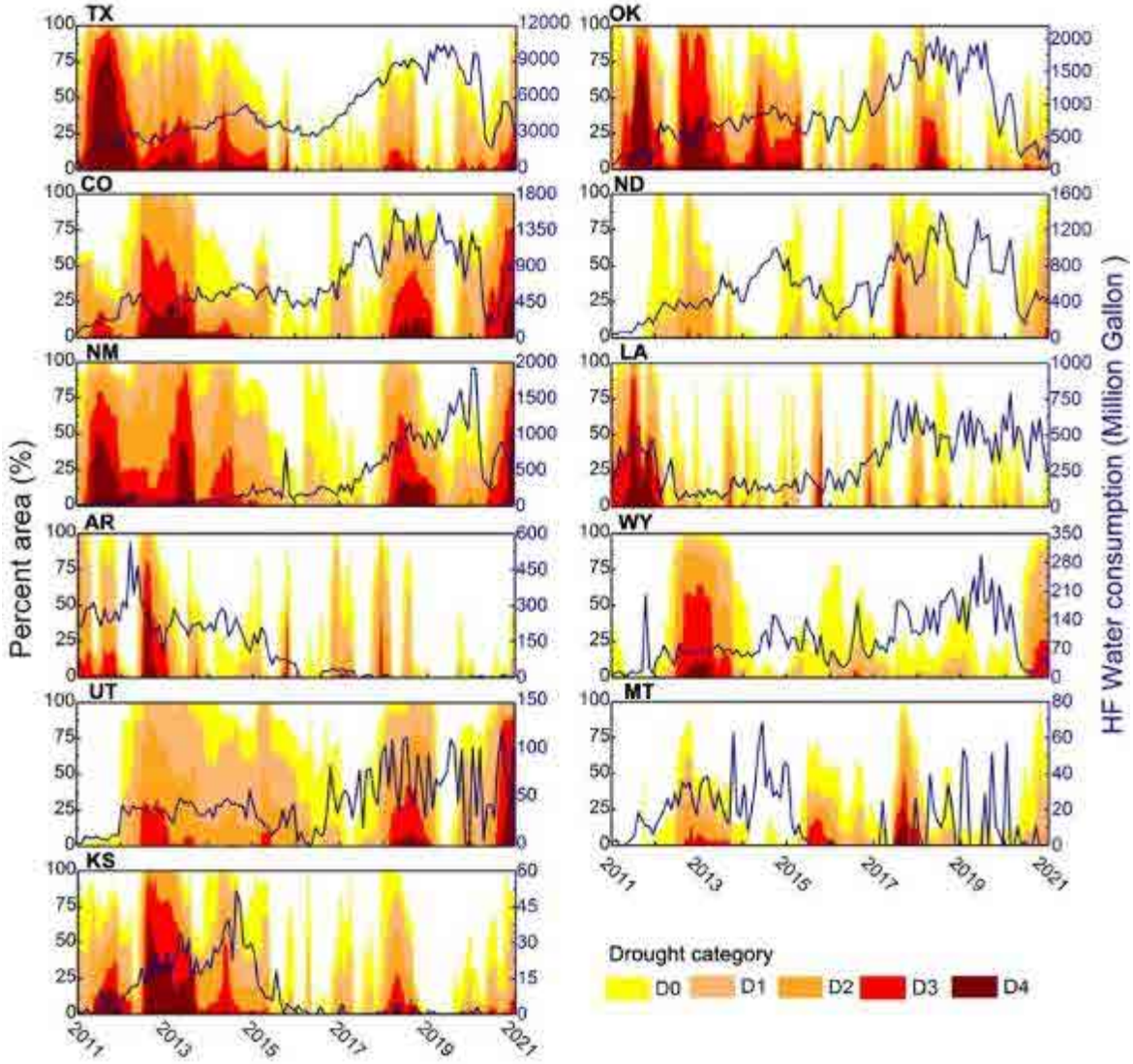

Figure B1. Time-series drought severity and coverage data and the corresponding water consumption of newly drilled wells by hydraulic fracturing (HF) each month (blue line) from 2011-2020 in 11 O&G-producing states. D0 to D4 refer to the area percentage under different drought categories as defined by the U.S. Drought Monitor.

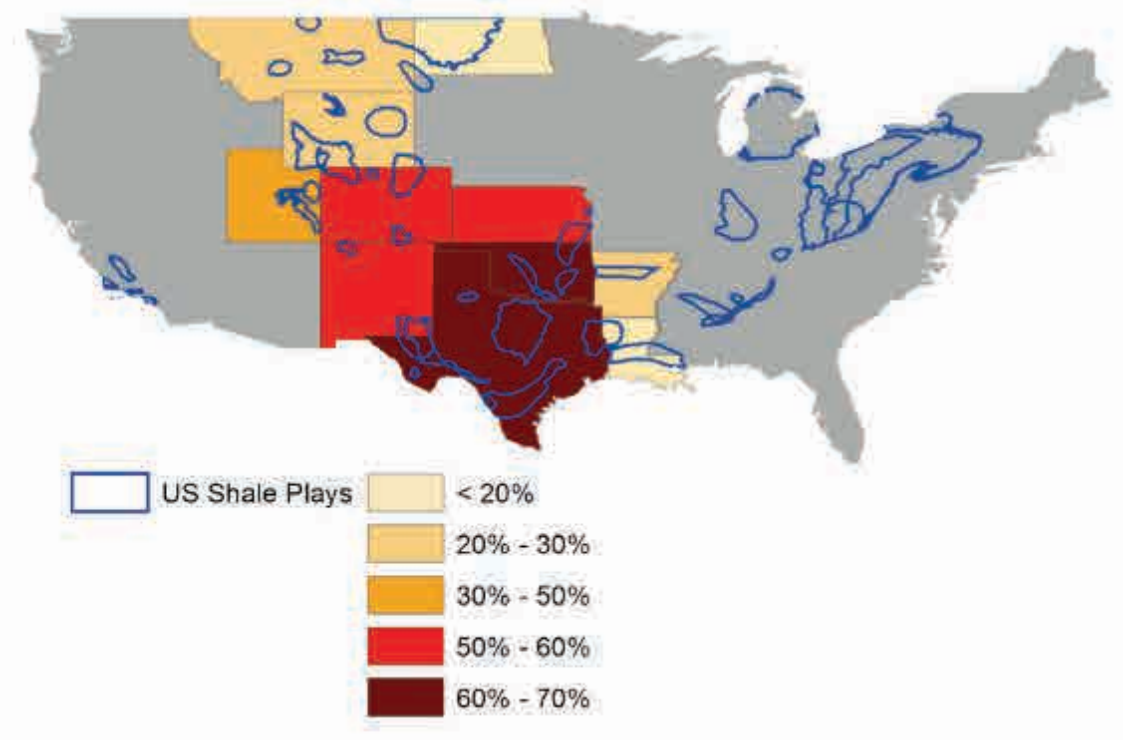

Figure B2. Map showing the time percentage when D3 or higher drought categories occurred within each of the 11 O&G-producing states during the period of 2011-2020.

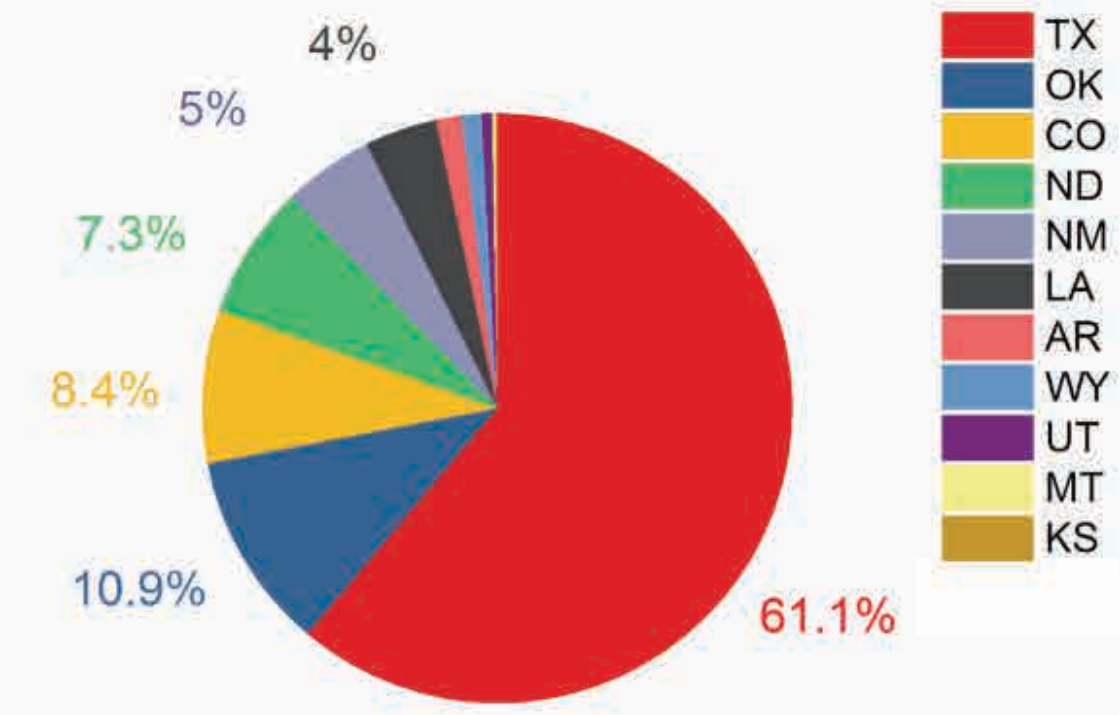

Figure B3. Percentage of total water use by HF activities for 11 O&G-producing states during the period of 2011-2020. The percentage values for the states of Texas, Oklahoma, Colorado, North Dakota, New Mexico, and Louisiana are indicated due to their major contributions.

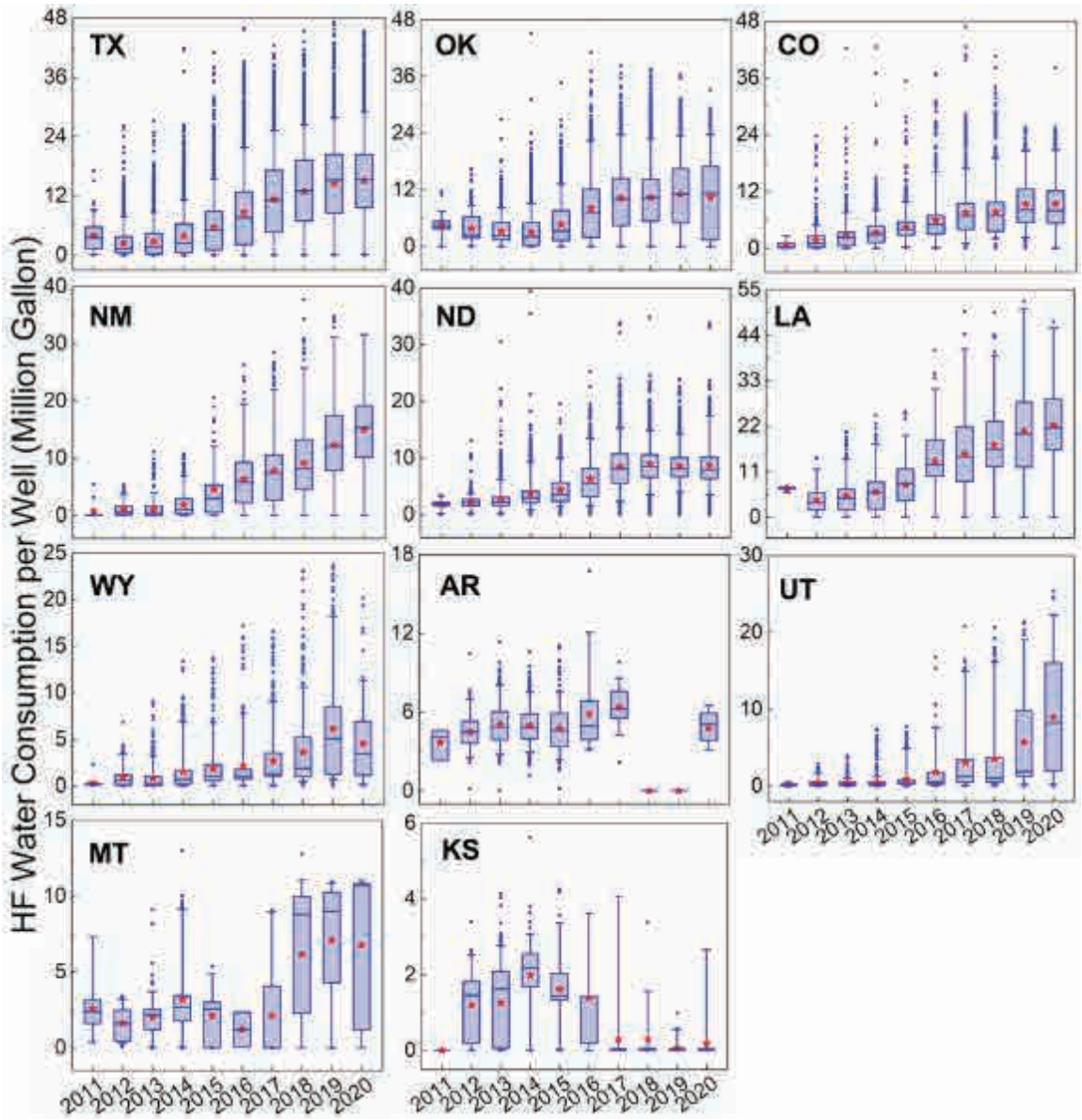

Figure B4. Boxplot of the HF water consumption per well from 2011 to 2020 in 11 investigated states. The central line of each box refers to the median value, while the top and bottom of each box represent the first and third quartile, respectively. Whiskers of the box plot represent the 95% bootstrap confidence intervals, while blue dots above the box plots show outliers in the data. Red stars show the annual average HF water consumption per well. The data are obtained from the Fracfocus database.[1]

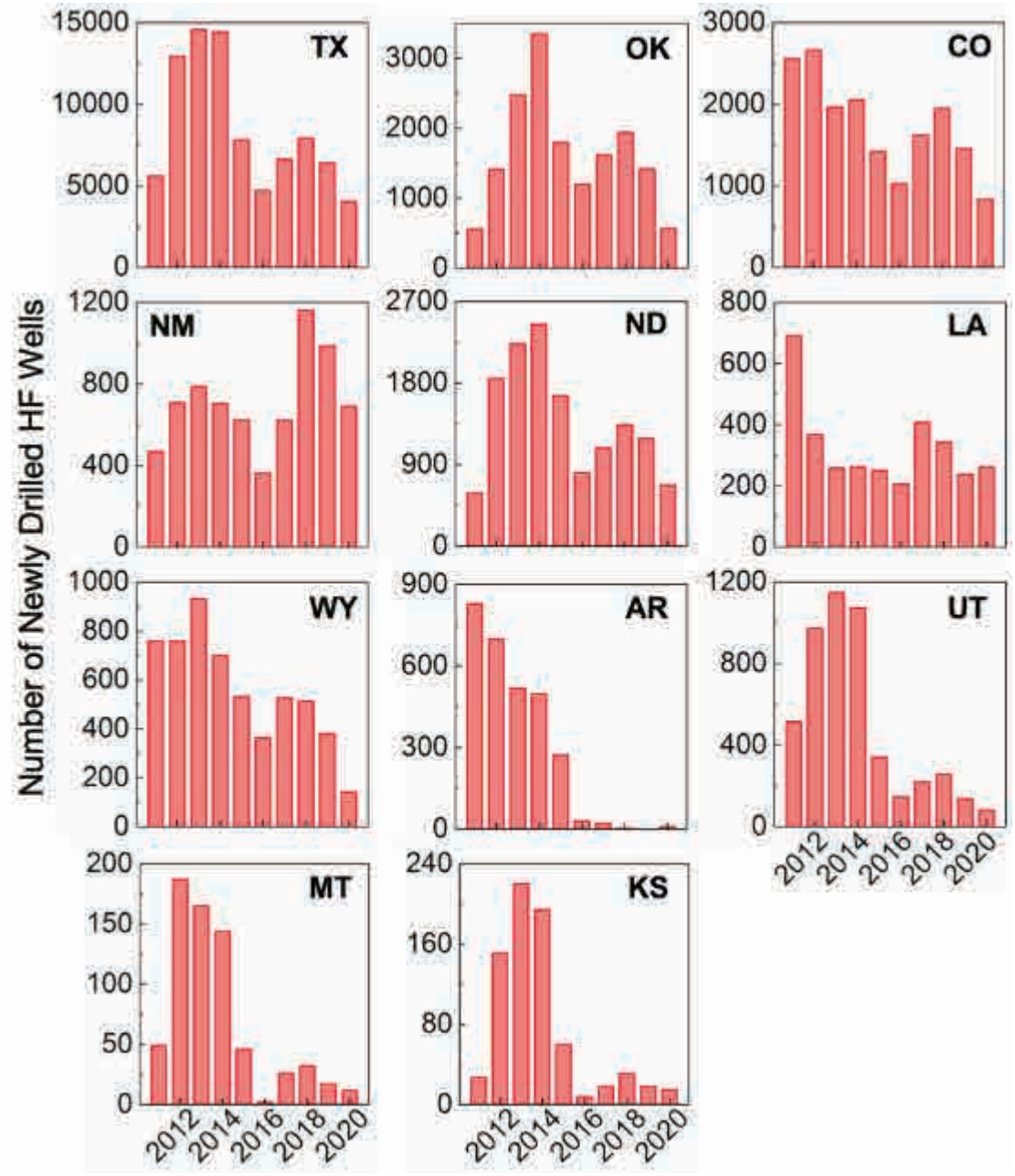

Figure B5. The annual number of newly drilled wells by HF in 11 O&G-producing states between 2011 and 2020. Data are obtained from the FracFocus database.[1]

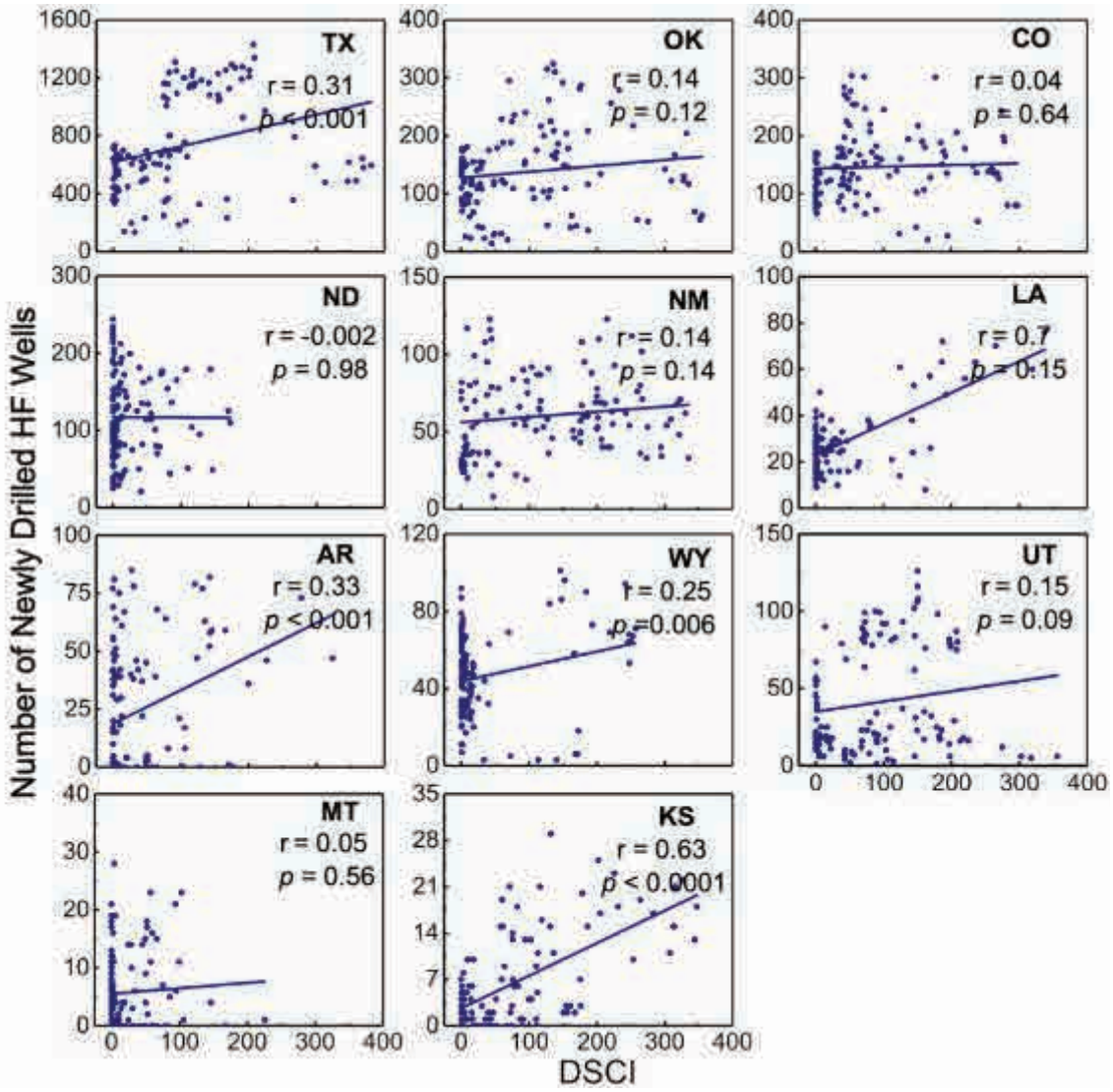

Figure B6. The correlation of the number of newly drilled wells by HF each month with the corresponding drought severity classification index (DSCI) from 2011 to 2020 in 11 O&G-producing states.

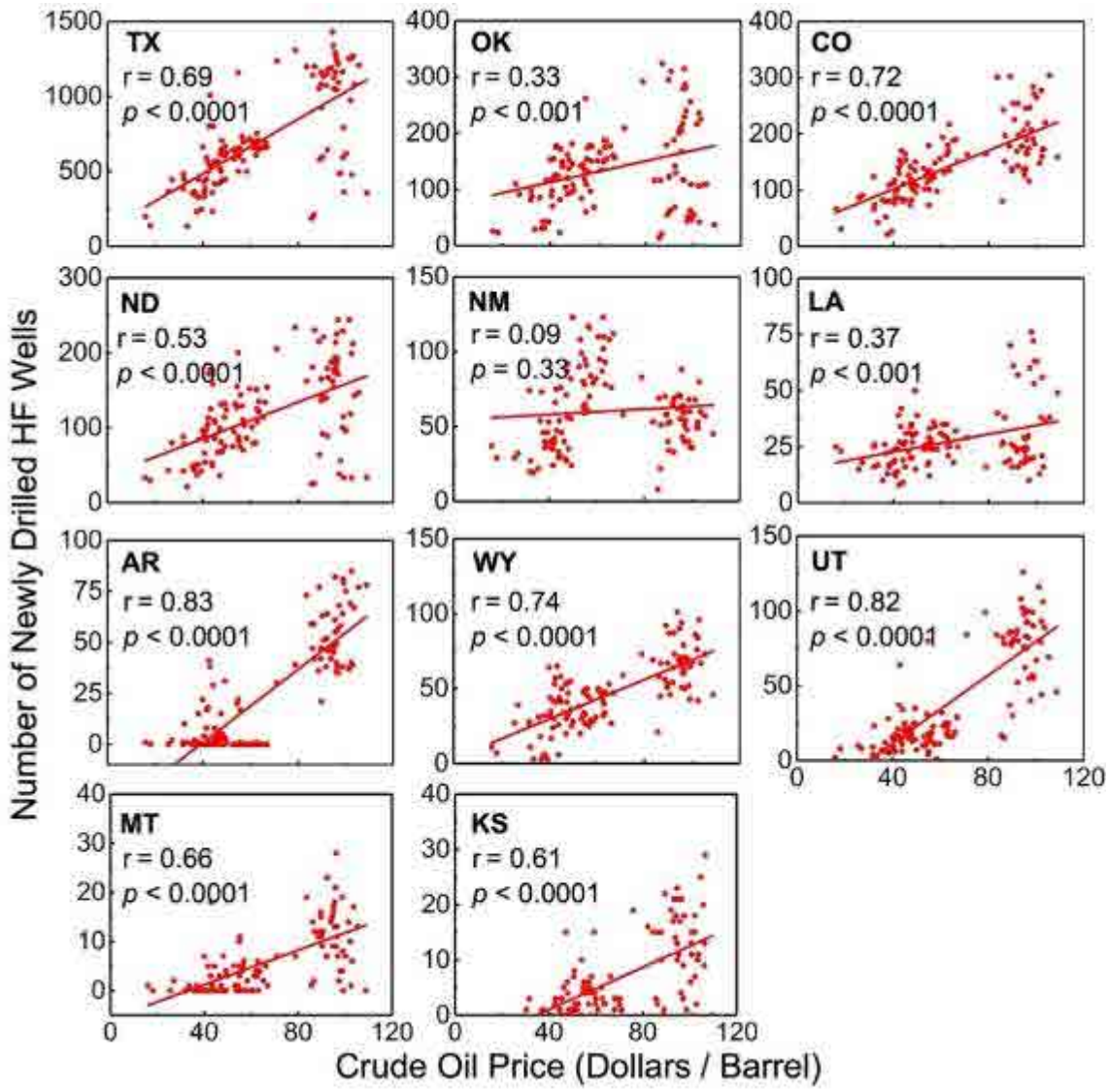

Figure B7. The correlation of the number of newly drilled wells by HF each month with the corresponding crude oil price from 2011 to 2020 in 11 O&G-producing states. The historical data of crude oil prices are obtained from the U.S. Energy Information Administration.[2]

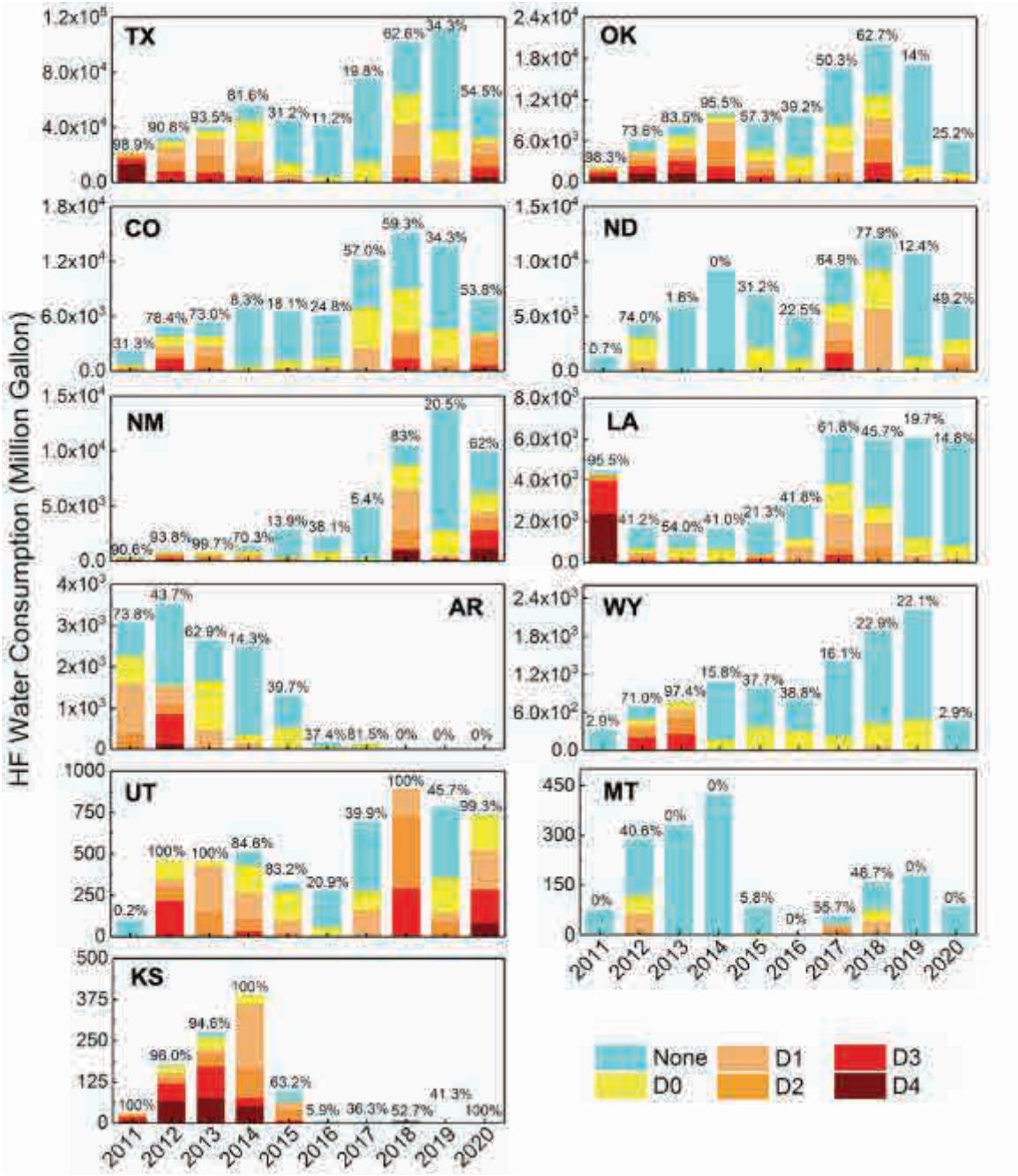

Figure B8. Annual water consumption of newly drilled wells by HF located in non-arid areas and areas under different drought categories between 2011 to 2020 in 11 O&G-producing states. The value above each bar indicates the percentage of water consumption occurred in arid areas under abnormally dry or drought (D0-D4) conditions.

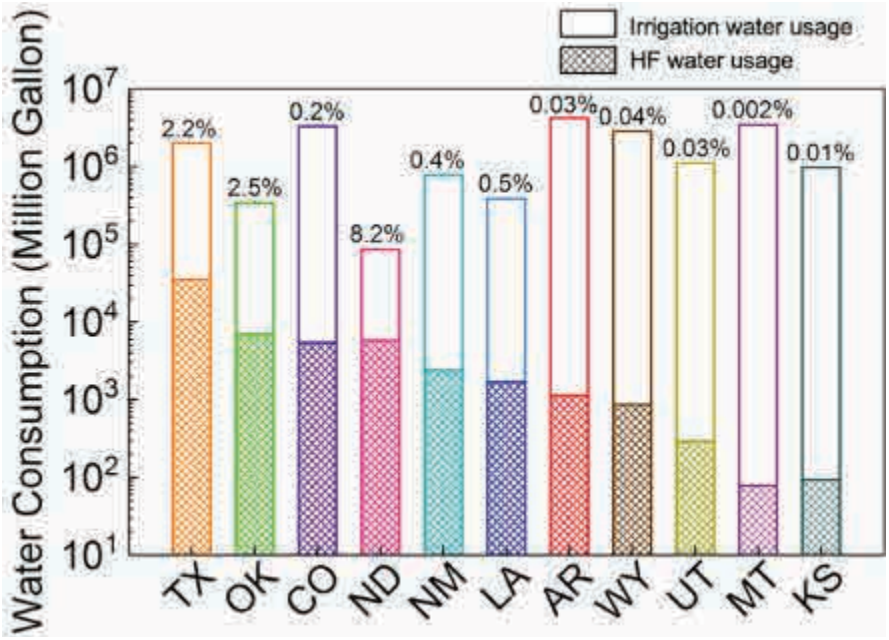

Figure B9. Comparison of water consumption between HF activities and irrigation in 11 O&G-producing states in 2015 (when the most recent data of irrigation water usage are available). The value above each bar indicates the volume ratio of HF water consumption to irrigation water usage.

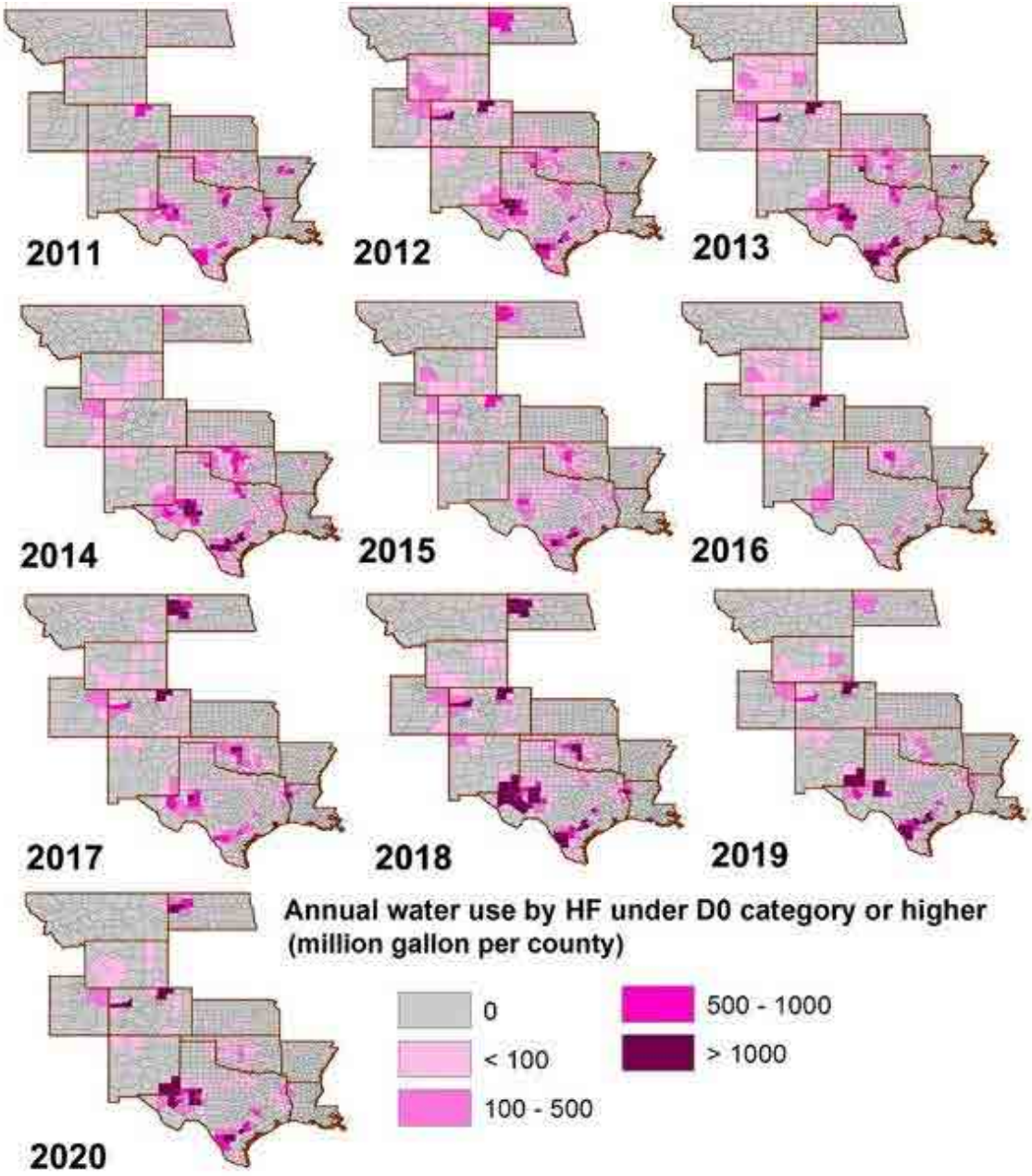

Figure B10. The density of annual HF water consumption under abnormally dry or drought (D0-D4) conditions at the county level from 2011 to 2020 in 11 O&G-producing states.

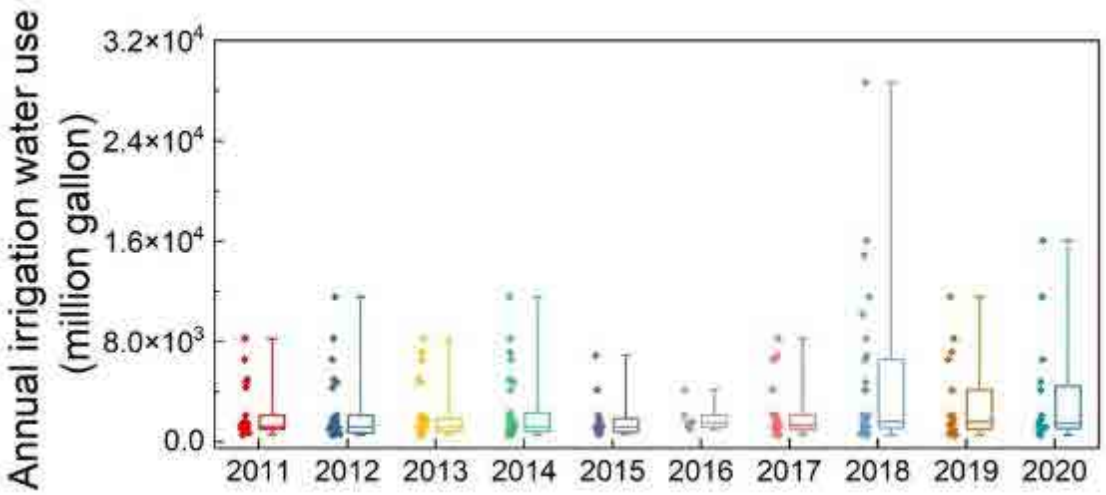

Figure B11. Box plot of annual irrigation water usage for the irrigation-active counties where the water usage ratios of HF under arid conditions to irrigation are ≥10%. The central line of each box refers to the median value, while the top and bottom of each box represent the first and third quartile, respectively. Whiskers of the box plot represent the minimum and maximum values, while dots on the left side of box plots show the distribution of irrigation water usage.

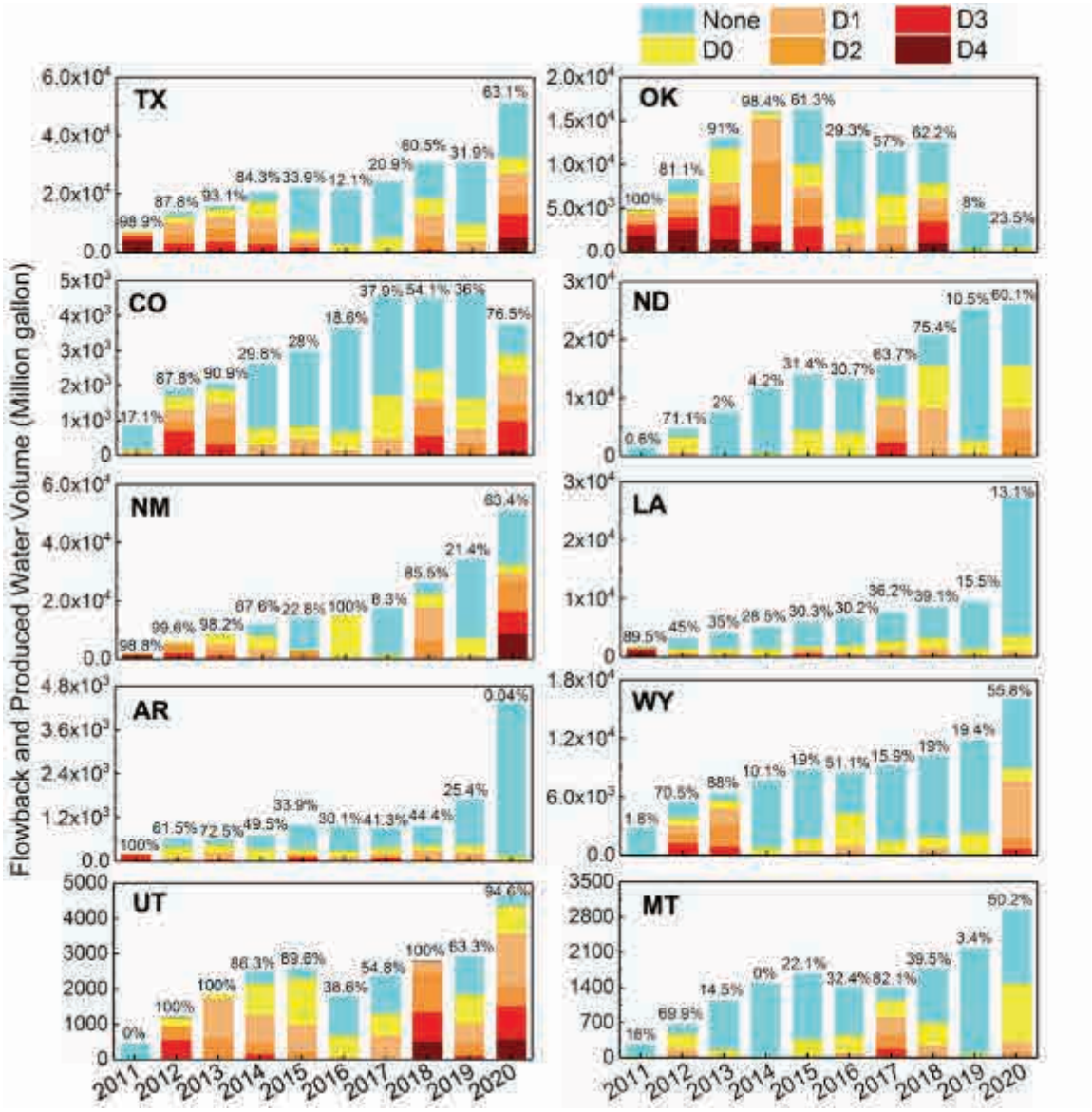

Figure B12. The volume of flowback and produced water generated under different hydroclimate conditions from 2011 to 2020 for 10 O&G-producing states. The data for Kansas are not available. The value above each bar indicates the percentage of flowback and produced water generated in arid areas under abnormally dry or drought (D0-D4) conditions.

References

1. FracFocus Chemical Disclosure Registry. Data Download. https://www.fracfocus.org/index.php?p=data-download (accessed July 10, 2021).
2. U.S. Energy Information Administration. Natural Gas Gross Withdrawals and Production. https://www.eia.gov/dnav/ng/ng_prod_sum_dc_NUS_mmcf_m.htm (accessed July 10, 2021).

APPENDIX C

Table C1. Chemical compositions of shale oil and gas produced waters used in the current study

Parameter	Sample 1	Sample 2	Unit
Alkalinity (as $CaCO_3$)	713	652	mg/L
Dissolved Aluminum	0.398	0.190	mg/L
Dissolved Barium	32.8	61.1	mg/L
Dissolved Calcium	1210	1070	mg/L
Chloride	23303	13551	mg/L
Dissolved Iron	0.189	0.076	mg/L
Dissolved Magnesium	141	83.4	mg/L
Dissolved Silica	39.5	34.5	mg/L
Dissolved Sodium	13900	7780	mg/L
Dissolved Strontium	103	97.0	mg/L
Sulfate	43.1	<0.05	mg/L
Total Dissolved Solids (TDS)	39650	40370	mg/L
Total Organic Carbon (TOC)	1460	700	mg/L
Oil and Grease	9.2	6.2	mg/L
Total Suspended Solids (TSS)	25	105	mg/L
Turbidity	43.2	291	NTU
GRO (TVPH)[a]	4.8	4.82	mg/L
Benzene	2.117	2.29	mg/L
Toluene	1.047	0.699	mg/L
Ethylbenzene	0.065	0.039	mg/L
Total Xylenes	0.271	0.104	mg/L
pH	7.25	6.17	

[a] GRO(TVPH) = Gas Range Organics (Total Volatile Petroleum Hydrocarbons)

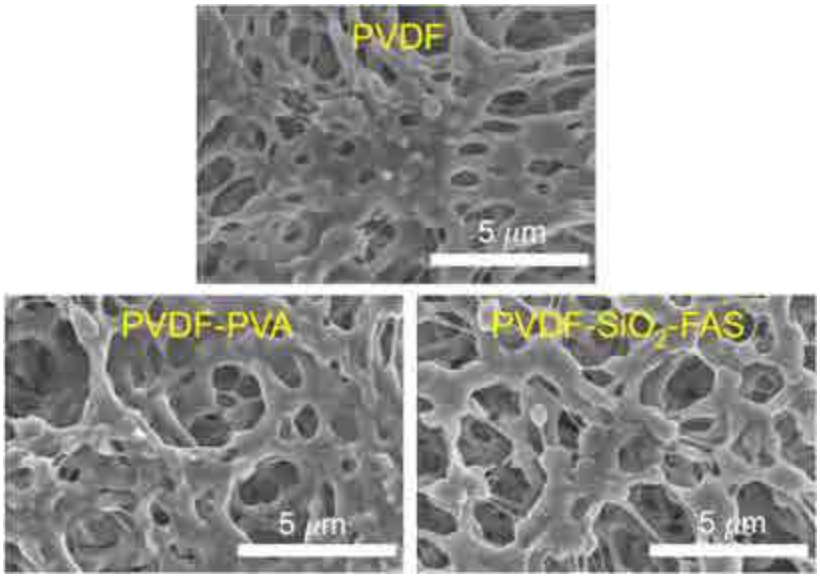

Figure C1. Top-view SEM observation of pristine and modified PVDF membranes (with magnification of 10000×).

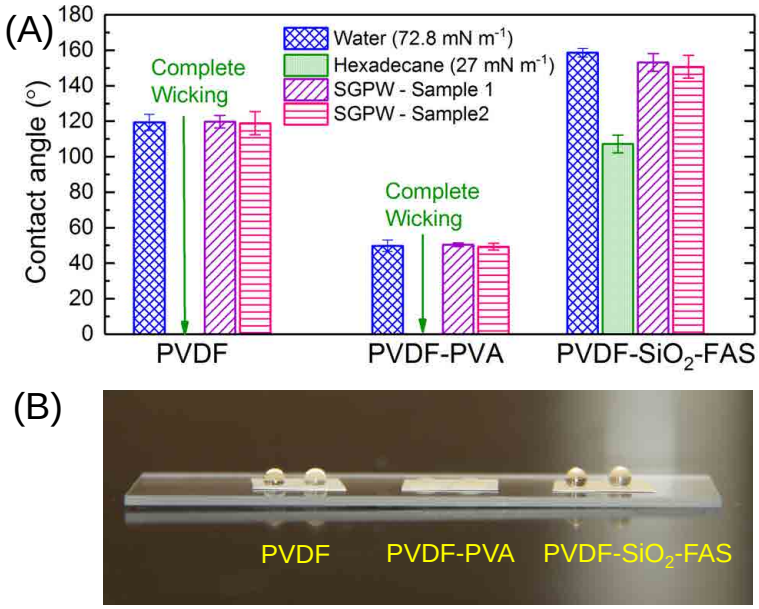

Figure C2. (A) Static contact angle of tested membranes measured with DI water, hexadecane, and shale gas produced water Sample 1 and Sample 2. (B) Photographs of the wetting behaviors of the tested membranes with shale gas produced water Sample 1 (the left drop) and Sample 2 (the right drop).

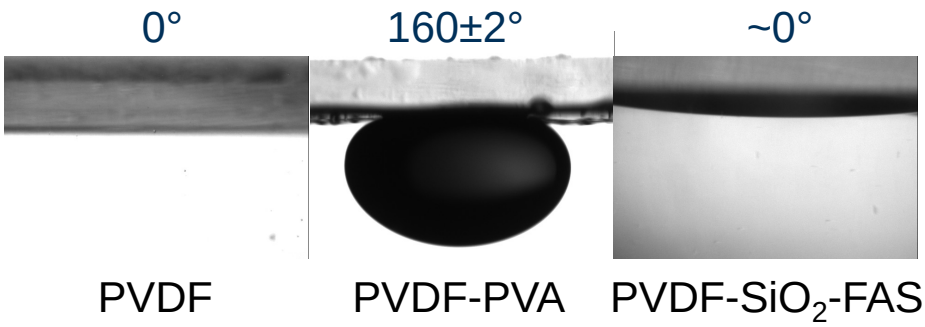

Figure C3. Underwater oil contact angles of the pristine and modified PVDF membranes. The data for the PVDF-PVA membrane are presented as average ± standard deviation (n = 3).

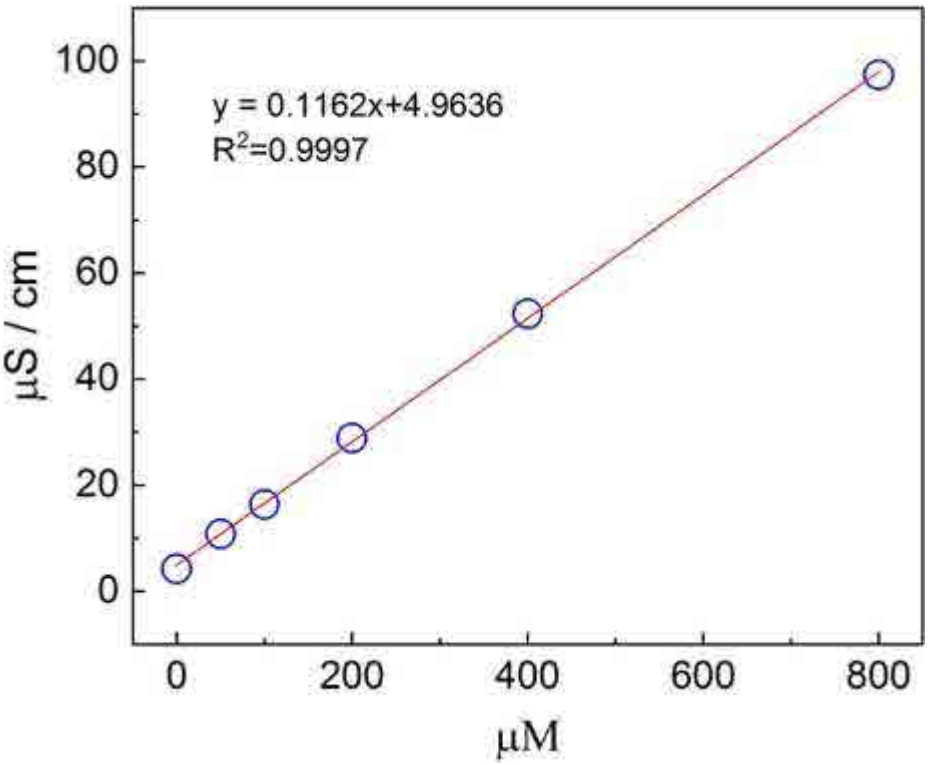

Figure C4. Calibration curve to calculate solution salinity (as expressed by µM of NaCl) from solution conductivity.

Membrane distillation of saline feed solutions containing surfacetants

The wetting resistance of the pristine PVDF membrane and PVDF-SiO_2-FAS membrane against surfactant sodium dodecyl sulfate (SDS) was evaluated with a custom-built direct contact membrane distillation (DCMD) system. The experimental setup and procedure have been described in Section 6.2.4. Instead of shale oil and gas produced water, saline solutions with 1M NaCl and varying concentrations of SDS were used as the DCMD feedwater. During the initial 90 min of MD desalination, 1 M NaCl solution at 60 °C was used as the feedwater. SDS was then introduced to the feed reservoir every 90 min to progressively increase the SDS concentration (meanwhile lowering the surface tension of the feed solution). The weight and conductivity of the solution in the distillate reservoir were monitored continuously to calculate the water vapor flux and assess membrane wetting.

The water vapor flux and salt rejection of the two membranes in the presence of SDS are presented in Figure C5. The pristine PVDF membrane was partially wetted by 0.05 mM SDS, evidenced by the increase of water flux and decrease of salt rejection rate. When the concentration of SDS reached 0.1 mM, the pristine PVDF membrane experienced a dramatic increase of water flux and concomitantly sharp drop of salt rejection. In contrast, the water flux and salt rejection of the superhydrophobic PVDF-SiO_2-FAS membrane were stable at a SDS concentration of 0.1 mM, indicating its improved wetting resistance in MD desalination. However, the PVDF-SiO_2-FAS membrane was still partially wetted by 0.2 mM SDS, which posed negligible impacts on the desalination performance of an omniphobic membrane reported in Boo et al.[1]

We attributed the varied wetting resistance against SDS observed between our PVDF-FAS-SiO_2 membrane and the omniphobic membrane of Boo et al. to the following reasons. In our study, the sizes of silica particles were ~20 nm, which were much smaller than those used in Boo et al. (~100 nm). According to the Cassie−Baxter theory, the wetting resistance of textured or hierarchically structured surfaces is determined by the geometry of the re-entrant structure (e.g.,

the size and inter-sphere spacing of the structure).[2,3] Therefore, the use of silica nanoparticles with different sizes, which introduced the re-entrant structure, was likely to result in membranes with varied omniphobicity. Also, due to the larger sizes of the silica particles, the pore sizes of the omniphobic membrane in Boo et al. were reduced and smaller than those of our PVDF-FAS-SiO_2 membrane (Figure C1 of our study versus Figure 2C of Boo et al.). Smaller pore sizes correspond to higher liquid breakthrough pressures (i.e., the pressure at which liquid transitions from the non-wetting Cassie-Baxter state to the wetted Wenzel state),[4] which could also contribute to better membrane wetting resistance. In addition, we performed fluorosilanization in liquid phase, whereas chemical vapor surface deposition was used in Boo et al.[1]

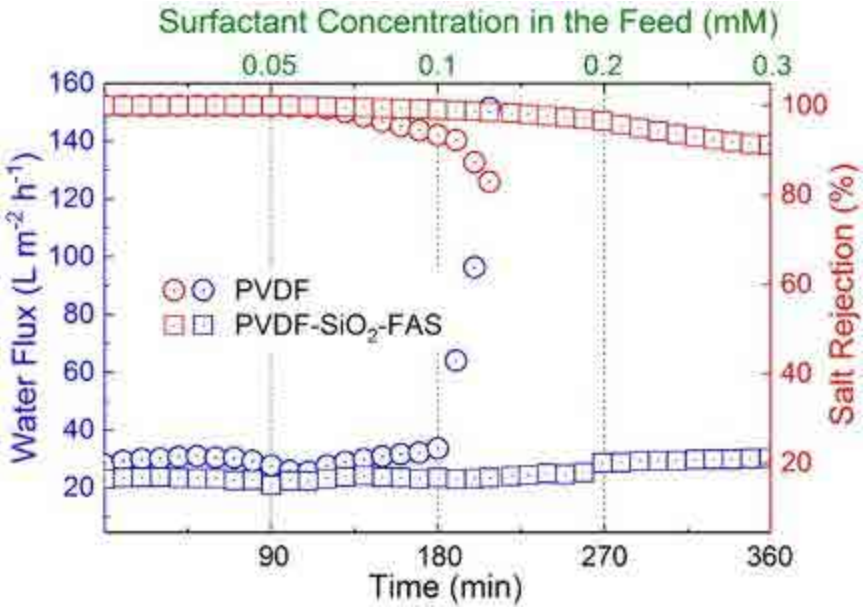

Figure C5. Water flux and salt rejection of the pristine PVDF membrane and PVDF-SiO_2-FAS membrane in DCMD experiments. NaCl solutions (1 M) with varying surfactant SDS concentrations were used as the feed solution, while DI water was used as the distillate solution. The feed and distillate temperatures were 60 °C and 20 °C, respectively.

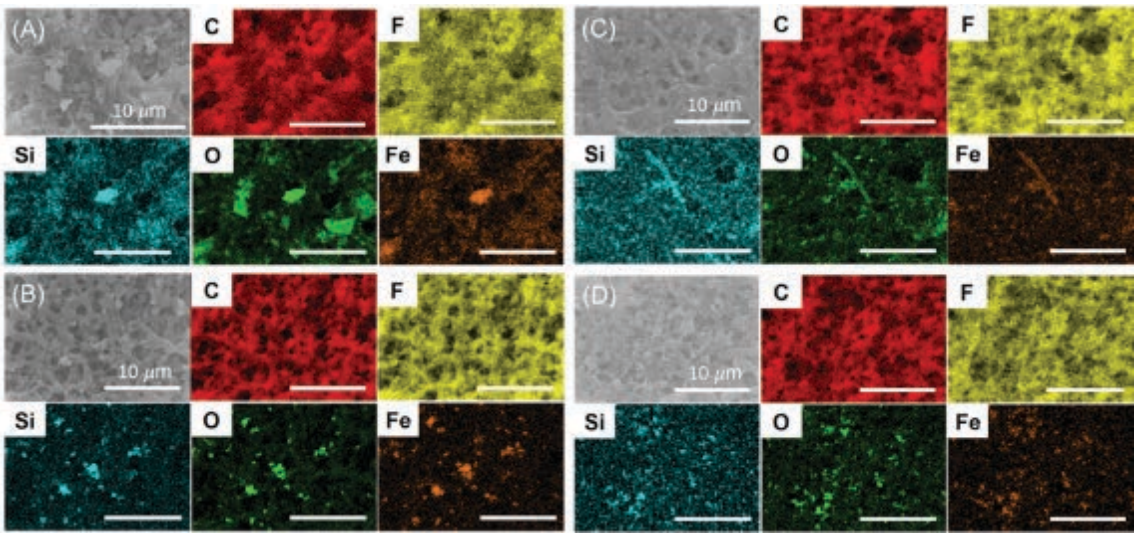

Figure C6.The elemental maps obtained by energy-dispersive X-ray spectroscopy for (A and B) the pristine PVDF and (C and D) PVDF-SiO_2-FAS membranes after the treatment of shale oil and gas produced water collected on (A and C) December 5th, 2017 (Sample 1) and (B and D) January 22nd, 2018 (Sample 2) in a single cycle. The scale bars represent 10 μm.

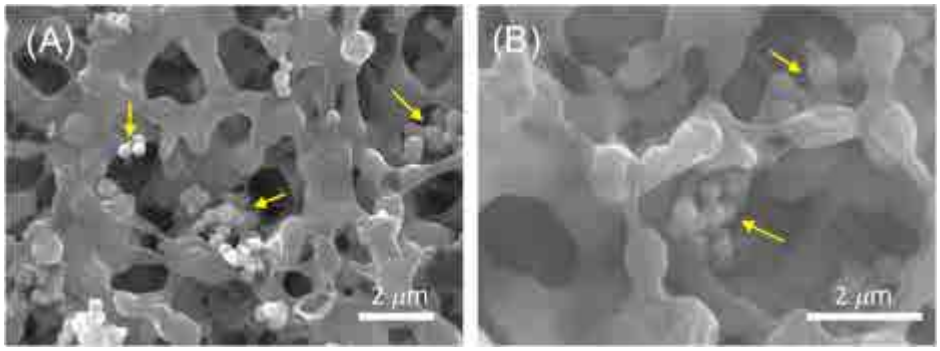

Figure C7. Spherical colloidal silica/silicate particles (indicated by the yellow arrows) located in the pores of (A) pristine PVDF membrane and (B) PVDF-SiO_2-FAS membrane after the treatment of shale gas produced water Sample 2 in a single cycle. The chemical composition of those particles was confirmed by EDX spectroscopy.

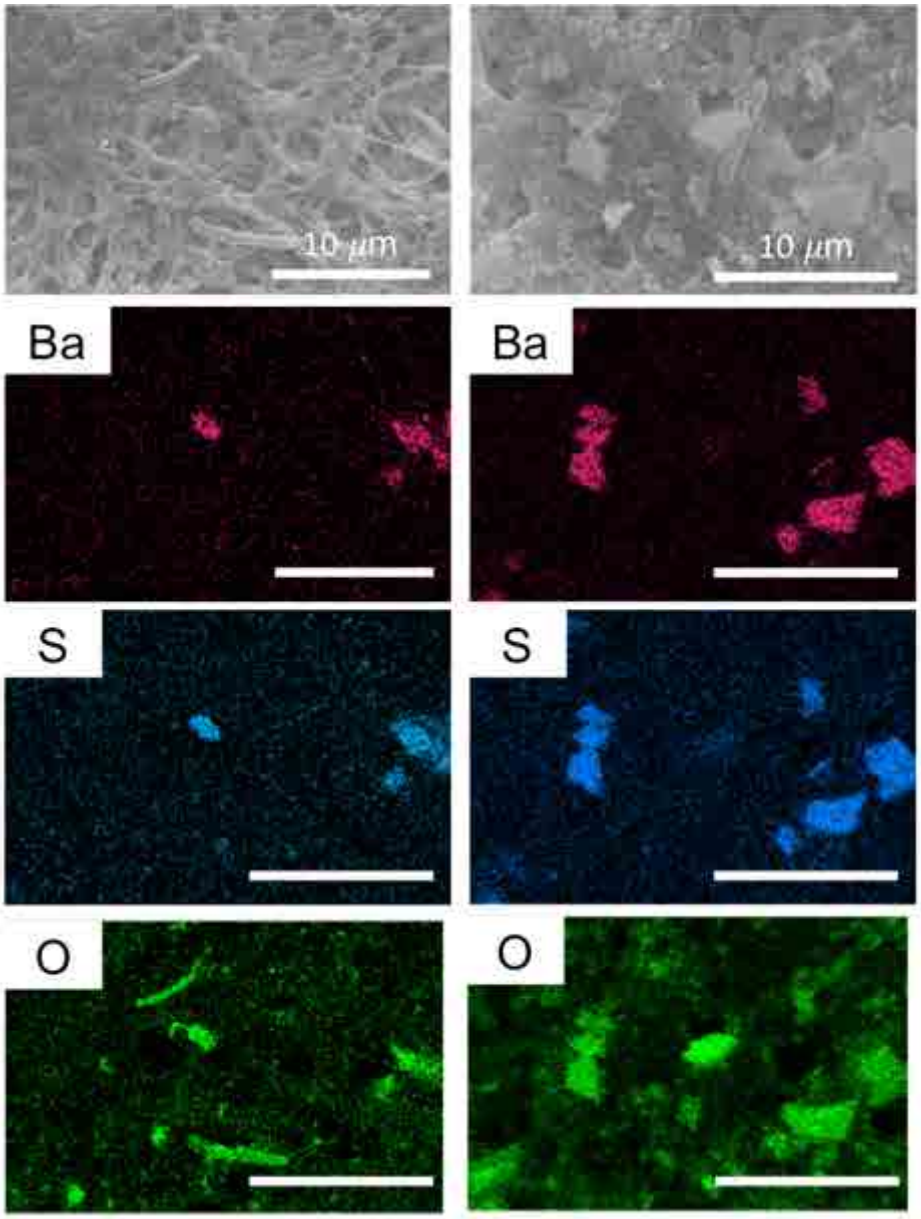

Figure C8. The presence of Barite ($BaSO_4$) on the MD membrane surface after the treatment of Sample 1 in a single cycle, which is indicated by the overlapping EDX signals from the elements Ba, S and O. The scale bars represent 10 μm.

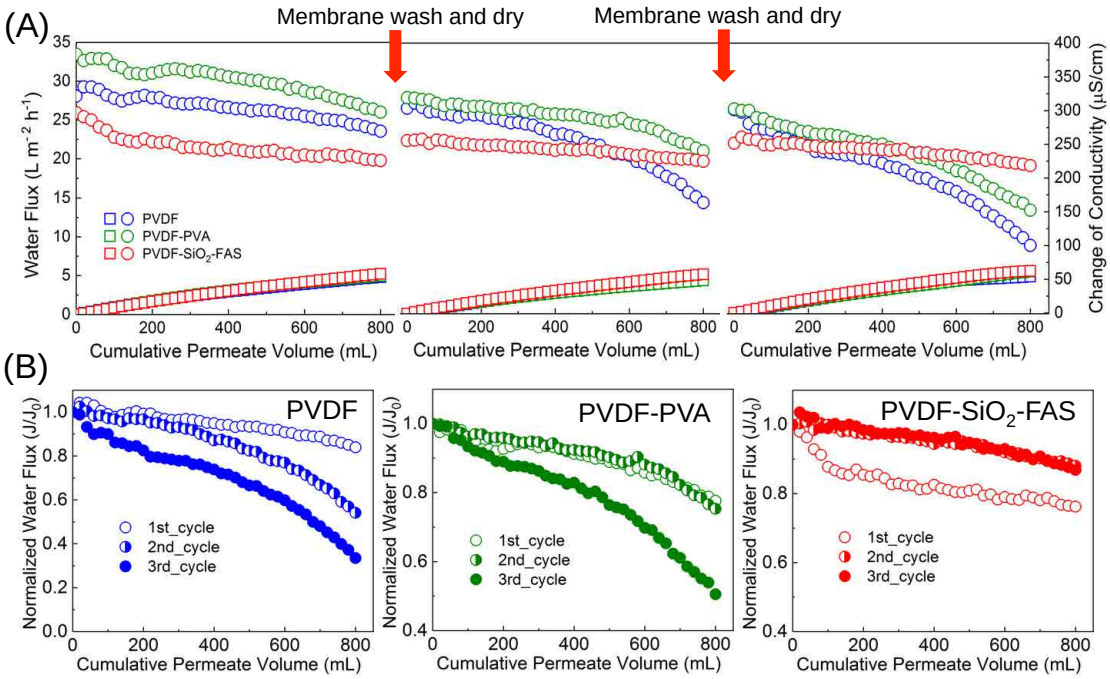

Figure C9. Fouling reversibility and membrane reusability during DCMD desalination of shale oil and gas produced water Sample 2 within three treatment cycles. (A) Absolute and (B) normalized water (vapor) fluxes for different tested membranes. The experimental condition of DCMD desalination was identical to that described in Figure 6-3. The red arrows indicate the time when the DCMD tests were terminated and the membrane coupons were subjected to physical cleaning followed by in-air drying. The dried membrane was then re-inserted into the DCMD unit to start another cycle of desalination with new shale oil and gas produced water.

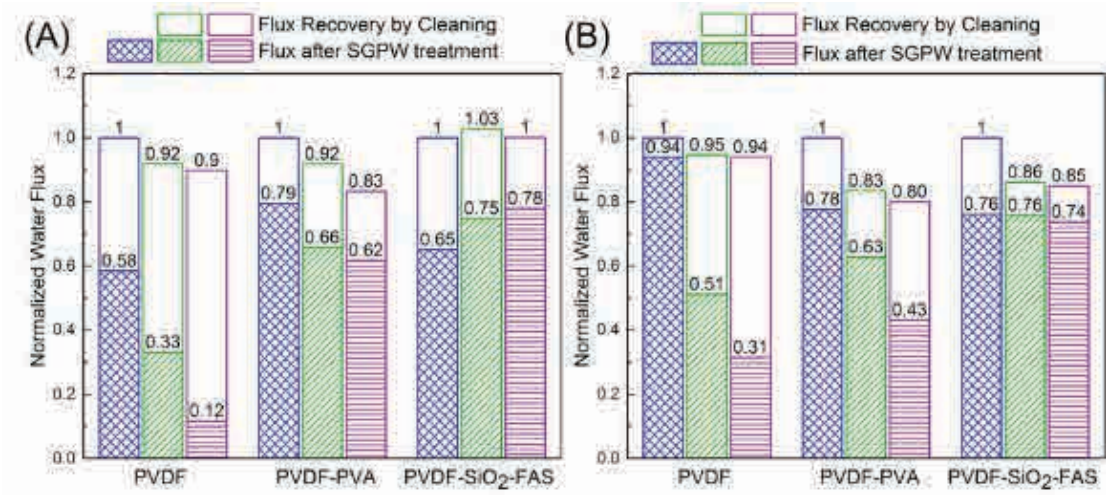

Figure C10. Water (vapor) flux recovery after physical membrane cleaning for the treatment of (A) Sample 1 and (B) Sample 2 by MD using different tested membranes. The initial water flux in treatment cycle 1 was set to one after normalization.

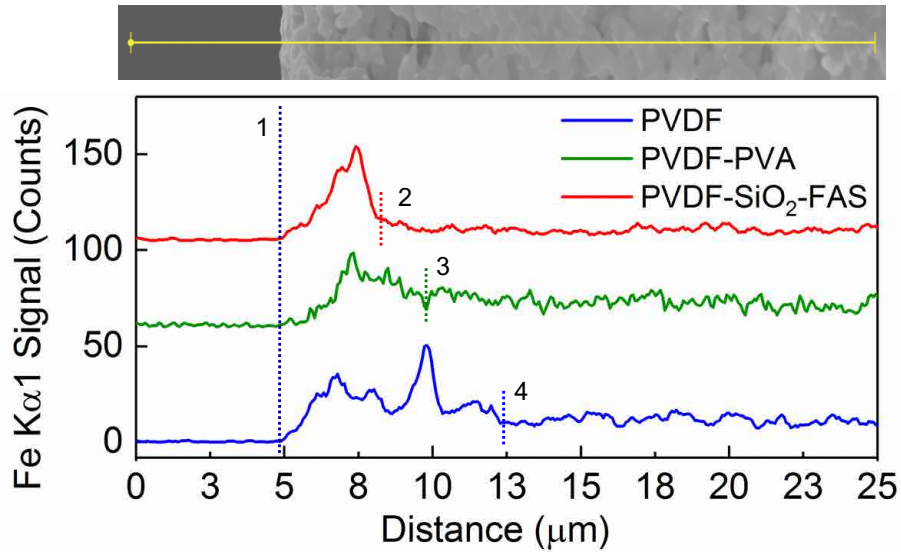

Figure C11. SEM-EDS line analysis of the cross-section of MD membranes after three treatment cycles for produced water Sample 2. The SEM image (only showing that of PVDF-PVA membrane as similar images were obtained for the other two membranes) indicates where the EDS line-scan was performed (yellow line). Fe kα1 signal was used as an indicator of foulant location due to the ubiquitous presence of Fe in the foulant layers.

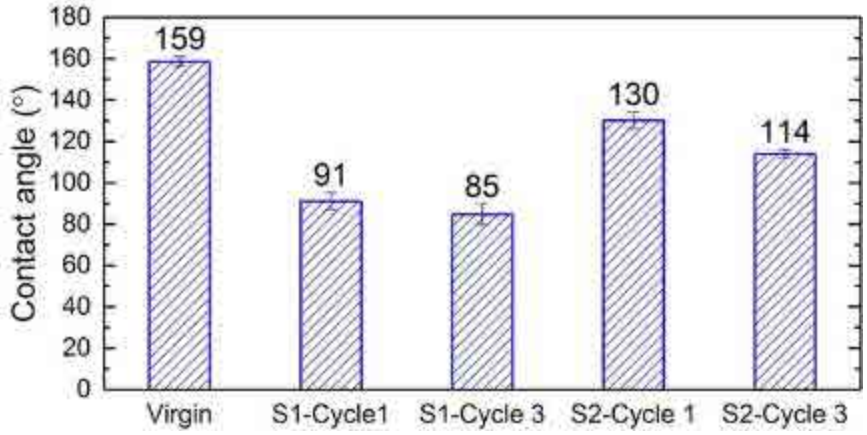

Figure C12. Water contact angles of PVDF-SiO_2-FAS membrane before and after fouled by shale oil and gas produced water. "S1-Cycle 1" represents PVDF-SiO_2-FAS membrane after the first treatment cycle for produced water Sample 1. The names of other samples follow the same rule.

References

1. C. Boo, J. Lee, M. Elimelech, Omniphobic polyvinylidene fluoride (PVDF) membrane for desalination of shale gas produced water by membrane distillation, *Environ Sci Technol*, 50 (2016) 12275-12282.
2. A.K. Kota, G. Kwon, A. Tuteja, The design and applications of superomniphobic surfaces, *NPG Asia Mater*, 6 (2014).
3. A. Tuteja, W. Choi, J.M. Mabry, G.H. McKinley, R.E. Cohen, Robust omniphobic surfaces, *P Natl Acad Sci USA*, 105 (2008) 18200-18205.
4. A.K. Kota, Y. Li, J.M. Mabry, A. Tuteja, Hierarchically structured superoleophobic surfaces with ultralow contact angle hysteresis, *Advanced Materials*, 24 (2012) 5838-5843.

APPENDIX D

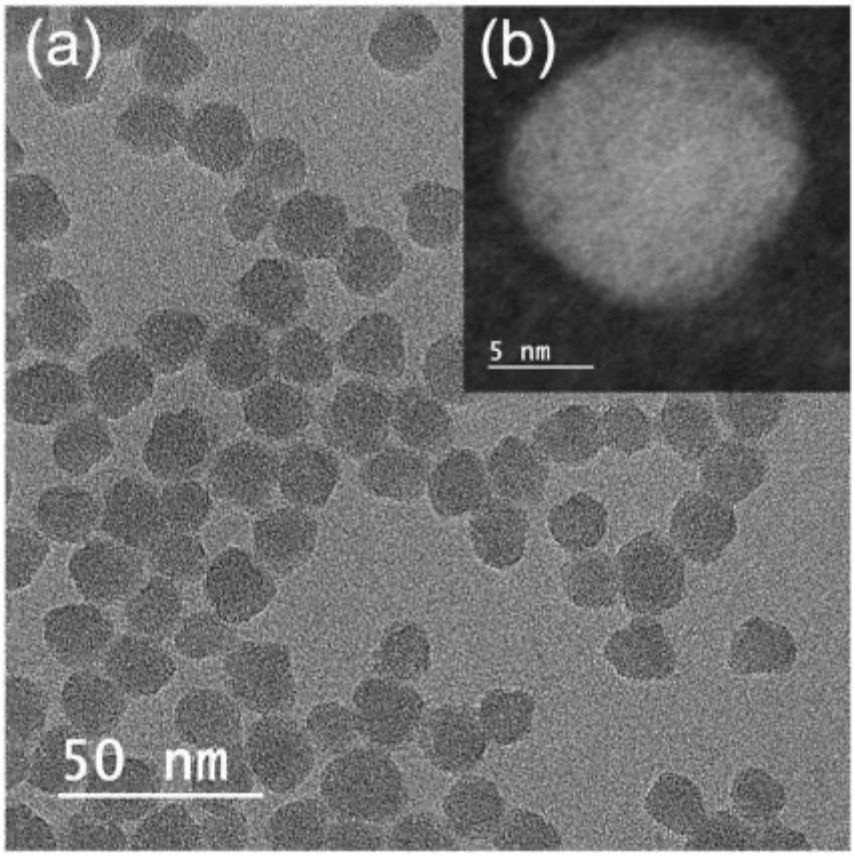

Figure D1. High-resolution (a) transmission electron microscope (TEM) and (b) scanning transmission electron microscope (STEM) images of 15 nm silica particles.

Table D1. Comparison of wetting resistance performances of omniphobic or wetting-resistant membranes for membrane distillation reported in this study and the literature. [a]

Omniphobic Membrane	Fluorocarbon Compounds		WCA (°)	DCMD Performance				Ref
	Name	Number of Fluorinated Carbons		Feed Solution	Temperature (F/P, °C)	Surface Tension (mN/m)	Rejection (%)	
PVDF-HPF/FAS-17/SiNPs coated GF membrane	FAS-17	8	~140	1 M NaCl with 0.4 mM SDS	60/20	~29	~100%	Lin[1]
PVDF-HPF/FAS-17/ZnO coated GF membrane	FAS-17	8	~152.8	1 M NaCl with 0.3 mM SDS	60/20	~31	~100%	Chen[2]
FDTS/SiNPs coated PVDF membrane	FDTS	8	~158	1 M NaCl with 0.2 mM SDS	60/20	~33	~100%	Boo-2016a[3]
FAS-17/SiNPs coated GF membrane	FAS-17	8	~150	1 M NaCl with 0.3 mM SDS	60/20	~31	~100%	Boo-2016b[4]
F-POSS/PVDF-HFP membrane	F-POSS	8	~154.5	1 M NaCl with 0.3 mM SDS	60/20	~31	~100%	Lu[5]
FDTS/PVDF membrane	FDTS	8	~149	1 M NaCl with 0.4 mM SDS	60/20	~29	~100%	Wang[6]
FDTS/SiNPs/PVDF-HFP/BTEAC membrane	FDTS	8	~150	1 M NaCl with 0.3 mM SDS	60/20	~31	~100%	Lee[7]
FDTS/SiNPs/PVDF-HFP membrane	FDTS	8	~151.5	3.5 wt% NaCl with 0.4 mM SDS	60/20	~30	~100%	Xu[8]
FAS-17/SiNPs/PVDF-HFP coated QF membrane	FAS-17	8	~151.5	1 M NaCl with 0.2 mM SDS	60/20	~33	~100%	Li-2019a[9]

FS/FAS-17/SiNPs coated PVDF membrane	FAS-17	8	~164.4	3.5 wt% NaCl with 0.4 mM SDS	70/20	~30	~99.99%	Li-2019b[10]
FDTS/PVDF-HFP membrane	FDTS	8	~154.1	3.5 wt% NaCl with 0.4 mM SDS	60/10	~30	~100%	Wu[11]
PFDT/AgNPs/PVDF membrane	PFDT	8	~164.5	3.5 wt% NaCl with 0.3 mM SDS	60/20	~32	~99.84%	Liao[12]
CTS/PFO/SiNPs coated CTAB/PVDF-HFP membrane	PFO	7	~156.9	0.4 mM SDS	60/20	~34.2	~100%	Huang[13]
PVDF/FTCS membrane	FTCS	10	~157.2	3.5 wt% NaCl with 0.1 mM SDS	60/20	~38	~100%	Deng[14]
PPFDA/PTFE coated PVDF HFM	PPFDA	8	~162	3.5 wt% NaCl with 0.4 mM SDS	70/22	~30	~100%	Ghaleni[15]
PVDF-120/15-FC4 membrane	FC-4	4	~158.3	1 M NaCl with 0.5 mM SDS	60/20	~27	~100%	This work
PVDF-120/15-FCB3 membrane	FC-B3	2	~141.3	1 M NaCl with 0.3 mM SDS	60/20	~31	~99.5%	This work
PVDF-120/15-FC1 membrane;	FC-1	1	~133.7	1 M NaCl with 0.1 mM SDS	60/20	~42	~100%	This work

[a] WCA: water contact angle; F/P: feed solution/permeate solution; FAS-17: (heptadecafluoro-1,1,2,2-tetrahydrodecyl)triethoxysilane; PVDF-HFP: polyvinylidene fluoride-co-hexafluoropropylene; GF: glass fiber; FDTS:1H,1H,2H,2H-perfluorodecyltrichlorosilane; F-POSS: fluorinated-decyl polyhedraloligomeric silsesquioxane; BTEAC: benzyltriethylammonium chloride; QF: quartz fiber; PFDT: 1H, 1H, 2H, 2H-perfluorodecanethiol; CTS: chitosan; PFO: perfluorooctanoate; CTAB: cetyltrimethylammonium bromide; FTCS: 1H, 1H, 2H, 2H-Perfluorododecyltrichlorosilane. PPFDA: poly(perfluorodecyl acrylate); HFM: hollow fiber membrane.

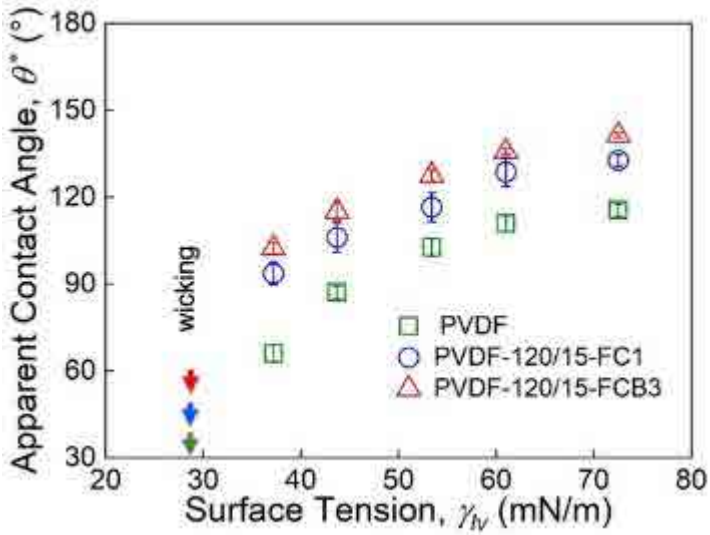

Figure D2. Apparent contact angles of liquids with different surface tensions on the membranes. Error bars represent standard deviation from three independent measurements. The green, red and blue arrows point to the surface tension at which liquid instantly wicked into pristine PVDF, PVDF-120/15-FCB3 and PVDF-120/15-FC1 membranes, respectively.

References

1. Lin, S.; Nejati, S.; Boo, C.; Hu, Y.; Osuji, C. O.; Elimelech, M., Omniphobic membrane for robust membrane distillation. *Environ Sci Tech Let* 2014, 1, (11), 443-447.
2. Chen, L.-H.; Huang, A.; Chen, Y.-R.; Chen, C.-H.; Hsu, C.-C.; Tsai, F.-Y.; Tung, K.-L., Omniphobic membranes for direct contact membrane distillation: effective deposition of zinc oxide nanoparticles. *Desalination* 2018, 428, 255-263.
3. Boo, C.; Lee, J.; Elimelech, M., Omniphobic Polyvinylidene Fluoride (PVDF) Membrane for Desalination of Shale Gas Produced Water by Membrane Distillation. *Environ Sci Technol* 2016, 50, (22), 12275-12282.
4. Boo, C.; Lee, J.; Elimelech, M., Engineering Surface Energy and Nanostructure of Microporous Films for Expanded Membrane Distillation Applications. *Environ Sci Technol* 2016, 50, (15), 8112-8119.
5. Lu, C.; Su, C.; Cao, H.; Ma, X.; Duan, F.; Chang, J.; Li, Y., F-POSS based omniphobic membrane for robust membrane distillation. *Mater Lett* 2018, 228, 85-88.
6. Wang, W.; Du, X.; Vahabi, H.; Zhao, S.; Yin, Y.; Kota, A. K.; Tong, T., Trade-off in membrane distillation with monolithic omniphobic membranes. *Nat Commun* 2019, 10, (1), 1-9.
7. Lee, J.; Boo, C.; Ryu, W.-H.; Taylor, A. D.; Elimelech, M., Development of omniphobic desalination membranes using a charged electrospun nanofiber scaffold. *Acs Appl Mater Inter* 2016, 8, (17), 11154-11161.
8. Xu, Y.; Yang, Y.; Fan, X.; Liu, Z.; Song, Y.; Wang, Y.; Tao, P.; Song, C.; Shao, M., In-situ silica nanoparticle assembly technique to develop an omniphobic membrane for durable membrane distillation. *Desalination* 2021, 499, 114832.
9. Li, C.; Li, X.; Du, X.; Tong, T.; Cath, T. Y.; Lee, J., Antiwetting and antifouling Janus membrane for desalination of saline oily wastewater by membrane distillation. *Acs Appl Mater Inter 2019*, 11, (20), 18456-18465.
10. Li, X.; Shan, H.; Cao, M.; Li, B., Facile fabrication of omniphobic PVDF composite membrane via a waterborne coating for anti-wetting and anti-fouling membrane distillation. *J Membrane Sci* 2019, 589, 117262.
11. Wu, X.-Q.; Wu, X.; Wang, T.-Y.; Zhao, L.; Truong, Y. B.; Ng, D.; Zheng, Y.-M.; Xie, Z., Omniphobic surface modification of electrospun nanofiber membrane via vapor deposition for enhanced anti-wetting property in membrane distillation. *J Membrane Sci* 2020, 606, 118075.
12. Liao, X.; Wang, Y.; Liao, Y.; You, X.; Yao, L.; Razaqpur, A. G., Effects of different surfactant properties on anti-wetting behaviours of an omniphobic membrane in membrane distillation. *J Membrane Sci* 2021, 634, 119433.
13. Huang, Y. X.; Wang, Z. X.; Jin, J.; Lin, S. H., Novel Janus Membrane for Membrane Distillation with Simultaneous Fouling and Wetting Resistance. *Environ Sci Technol* 2017, 51, (22), 13304-13310.
14. Deng, L.; Ye, H.; Li, X.; Li, P.; Zhang, J.; Wang, X.; Zhu, M.; Hsiao, B. S., Self-roughened omniphobic coatings on nanofibrous membrane for membrane distillation. *Sep Purif Technol* 2018, 206, 14-25.
15. Mohammadi Ghaleni, M.; Al Balushi, A.; Bavarian, M.; Nejati, S., Omniphobic hollow fiber membranes for water recovery and desalination. *ACS Applied Polymer Materials* 2020, 2, (8), 3034-3038.

APPENDIX E

Note E1. Characterization of surface chemical composition of pristine and etched PVDF membranes with XPS

In order to characterize the surface chemical composition of the pristine PVDF membrane and the etched PVDF membrane, we obtained the X-ray photon-electron spectroscopy (XPS) survey scans and high-resolution O1*s* spectra (see Figure E1). The etched PVDF membrane had a higher peak intensity ratio of C/F (~0.5) than pristine PVDF membrane (~0.18) based on the XPS survey scans. Compared to the pristine PVDF membrane, the etched PVDF membrane also possessed abundant oxygen-containing functional groups.

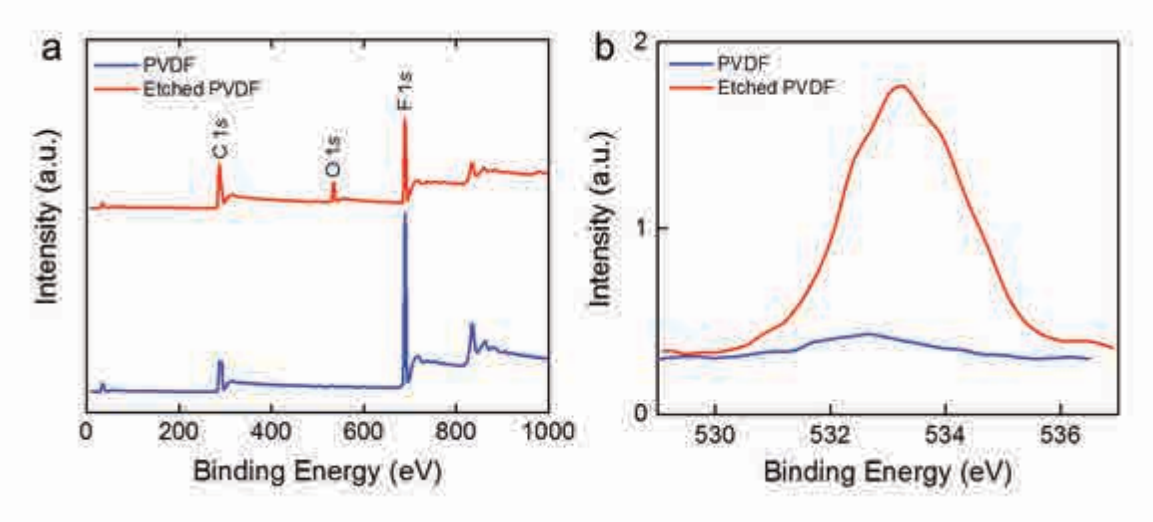

Figure E1. X-ray photon-electron spectroscopy (XPS) characterization of the pristine and etched polyvinylidene difluoride (PVDF) membranes. (a) XPS survey scans and (b) high-solution O1s XPS spectra of pristine PVDF membrane and etched PVDF membrane.

Note E2. Characterization of chemical composition of PVDF-FAS-5 and PVDF-FAS-60 membranes with XPS and FTIR

In order to characterize the surface chemical composition of PVDF-FAS-5 and PVDF-FAS-60 membranes, we obtained the XPS survey scans (see Figure E2a). Compared to pristine PVDF membrane that possesses only carbon and fluorine on the surface, the PVDF-FAS-5 and PVDF-FAS-60 membranes possess additional silicon and oxygen peaks due to the grafting of fluoroalkyl silane onto the membrane surface.

Further, Fourier-transform infrared spectroscopy (FTIR) was performed to characterize the functional groups of the membranes. The spectra of PVDF membranes were consistent with the literature (see Figure E2b).[1] For example, the absorbance peaks at approximately 833 cm^{-1}, 876 cm^{-1}, 1072 cm^{-1}, 1171/1232 cm^{-1}, and 1402 cm^{-1} correspond to crystal phase vibration, C-C skeleton vibration, crystal phase vibration, $-CF_2$ stretching vibration, and $-CH_2$ vibration, respectively.[1,2] As might be anticipated, no significant difference was observed among the FTIR spectra of the membranes due to the deeper penetration depth in FTIR spectroscopy.[3]

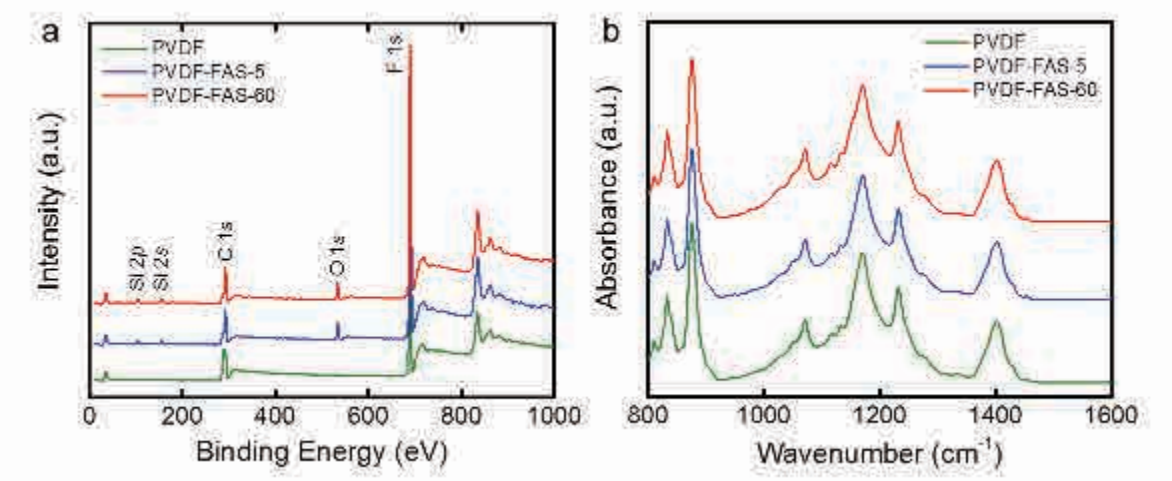

Figure E2. Membrane surface characterization. (a) XPS survey scans and (b) Fourier-transform infrared spectroscopy (FTIR) spectra of pristine PVDF membrane, PVDF-FAS-5 and PVDF-FAS-60 membranes. FAS refers to heptadecafluoro-1,1,2,2-tetrahydrodecyl trichlorosilane.

Note E3. Apparent surface pore size distributions of pristine and etched PVDF membranes

The surface morphology of the pristine and the processed PVDF membranes was characterized using a scanning electron microscope. The pristine and processed membranes consisted of interconnected micro-sized PVDF granules with a re-entrant texture (see Figure E3a-E3c). The apparent surface pore sizes as well as the feature sizes of the membranes were measured by analyzing the SEM images with ImageJ (National Institutes of Health). The grayscale SEM image (see Figure E3d) was first converted to a binary (i.e., black and white) image (see Figure E3e). The surface pores with irregular shapes were then automatically identified using ImageJ (see Figure E3f). For each surface pore, the Feret's diameter (i.e., the longest distance between any two points on the boundary of the surface pore) was measured as the apparent surface pore size. We used Feret's diameter to characterize the surface pore because the permeation of liquid into a pore with irregular shape depends on the largest dimension of the surface pore.[4-7] For each membrane, approximately 2000 individual pores obtained from 3 different SEM images were analyzed to obtain the apparent surface pore size distribution. The similar apparent surface pore size distributions (see Figure E3g-E3i) indicate that the morphology of the PVDF membranes remained unaltered after the etching and silanization processes.

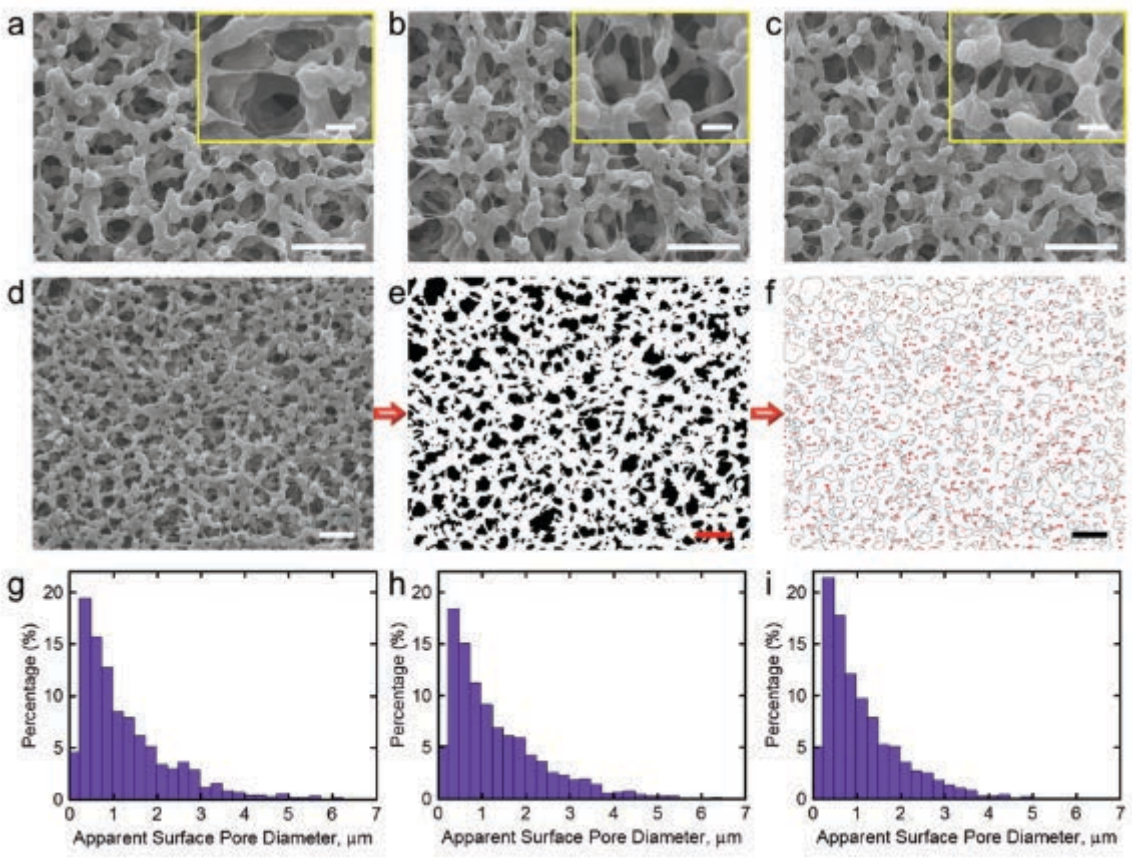

Figure E3. Scanning electron microscope (SEM) analysis of PVDF membranes. (a-c) SEM images of (a) pristine PVDF membrane, (b) PVDF-FAS-5 membrane, and (c) PVDF-FAS-60 membrane. The scale bars represent 5 μm and 1 μm (inset), respectively. (d-f) Grayscale SEM image (d) was converted to a binary image (e). The apparent surface pores (f) were then identified with ImageJ. The scale bars represent 5 μm. (g-h) Apparent surface pore size distribution of (g) pristine PVDF membrane, (h) PVDF-FAS-5 membrane, and (i) PVDF-FAS-60 membrane.

Note E4. Characterization of pristine and processed PVDF membranes with capillary flow porometry

The membranes were characterized with a capillary flow porometer (Model CFP-1100A) at Porous Materials Inc. to measure the membrane pore size and air permeability. The membrane mean pore sizes, measured with the wet/dry flow method, are 0.452 μm, 0.462 μm, and 0.456 μm for the pristine PVDF, PVDF-FAS-5, and PVDF-FAS-60 membranes, respectively. Also, all the tested membranes display similar membrane pore size distributions (see Figure E4a-E4c). These results indicate that the morphology of the processed PVDF membranes remains virtually unaltered compared to the pristine PVDF membrane. It is worth noting that the membrane pore size distributions measured with capillary flow porometry are narrower than the apparent surface pore size distributions (see Figure E3g-E3i) obtained from SEM image analysis. This is because the membrane pore size measured with capillary flow porometry represents the throat diameter (i.e., the most constricted/the smallest distance), along the pore.[8-10] Additionally, the air permeability measured at a wide range of pressures (see Figure E4d) indicates that our processed membranes do not display additional mass transfer resistance compared to the pristine PVDF membrane.

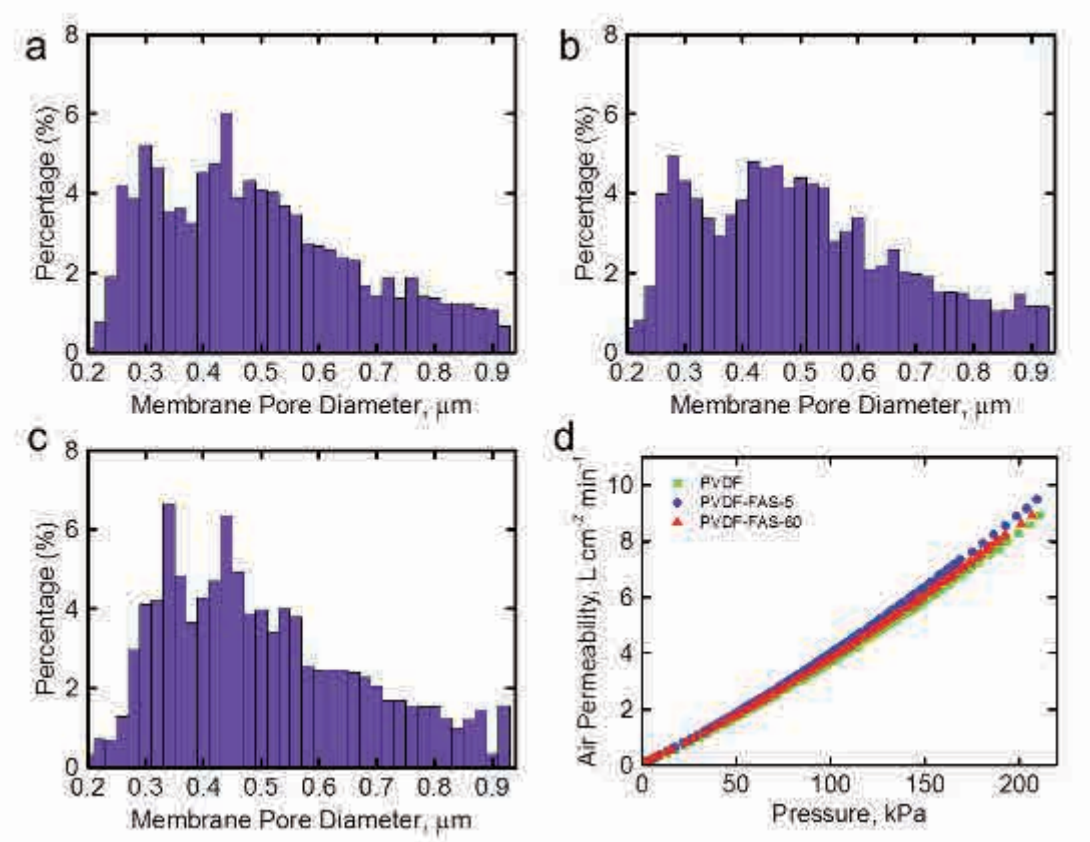

Figure E4. Membrane characterization with capillary flow porometry. (a-c) Membrane pore size distribution of (a) pristine PVDF membrane, (b) PVDF-FAS-5 membrane, and (c) PVDF-FAS-60 membrane. (d) Air permeability of the tested membranes measured at different pressures.

Note E5. Contact angles of different liquids

The apparent contact angles of ~8 μL droplets of liquids with different surface tensions on the pristine PVDF membrane and processed PVDF membranes with 5 min silanization (PVDF-FAS-5) and 1 h silanization (PVDF-FAS-60) are summarized in Table E1. It is worth noting that the PVDF-FAS-5 membrane was completely wetted by water+60% ethanol (γ_{lv} = 28.7 mN m^{-1}), water+80% ethanol (γ_{lv} = 24.5 mN m^{-1}) and 100% ethanol (γ_{lv} = 22.2 mN m^{-1}), which were polar liquids. However, it displayed good wetting resistance against non-polar liquids with lower surface tensions, such as hexadecane (γ_{lv} = 27.5 mN m^{-1}) and silicone oil (γ_{lv} = 21 mN m^{-1}). These results highlight the importance of using polar liquids with low surface tension to accurately assess the wetting resistance of MD membranes.

In addition to the three membranes discussed above, we also measured the apparent contact angles of liquids on another membrane designated as PVDF-FAS-E (E refers to extended immersion time in the etchant solution). This membrane was fabricated in the same way as PVDF-FAS-60 membrane, except that the immersion time in the etchant solution was extended to ~30 s. Our results indicate that the apparent contact angles of liquids on PVDF-FAS-60 membrane and PVDF-FAS-E membrane (see Table E1) are similar, indicating that the extended immersion time (~30 s) in the etchant solution did not alter the omniphobicity of the membrane.

Table E1. The apparent static contact angles θ^*, apparent advancing θ^*_{adv} and apparent receding θ^*_{rec} contact angles of various liquids on the pristine PVDF, PVDF-FAS-5, PVDF-FAS-60, and PVDF-FAS-E membranes. The errors in contact angle measurements were ≤ 3°.

		Pristine PVDF			PVDF-FAS-5			PVDF-FAS-60			PVDF-FAS-E		
Liquid	γ_{lv} (mN m^{-1})	θ^*	θ^*_{adv}	θ^*_{rec}	θ^*	θ^*_{adv}	θ^*_{rec}	θ^*	θ^*_{adv}	θ^*_{rec}	θ^*	θ^*_{adv}	θ^*_{rec}
Water	72.5	123°	138°	20°	139°	155°	45°	149°	160°	88°	150°	160°	87°
1.5 mM SDS	61	117°	130°	13°	138°	152°	14°	147°	155°	82°	147°	154°	80°
10% ethanol	53.4	113°	119°	8°	134°	148°	11°	145°	153°	43°	146°	153°	45°
20% ethanol	43.7	95°	99°	0°	127°	133°	9°	138°	149°	15°	138°	150°	13°
30% ethanol	37.2	0°	0°	0°	117°	122°	0°	131°	142°	10°	130°	140°	8°
60% ethanol	28.7	0°	0°	0°	0°	0°	0°	117°	128°	0°	119°	127°	0°
80% ethanol	24.5	0°	0°	0°	0°	0°	0°	103°	115°	0°	104°	115°	0°
100% ethanol	22.2	0°	0°	0°	0°	0°	0°	95°	100°	0°	93°	97°	0°
Hexadecane	27.5	0°	0°	0°	112°	118°	0°	117°	132°	0°	116°	129°	0°
Silicone oil	21	0°	0°	0°	99°	103°	0°	109°	115°	0°	109°	116°	0°

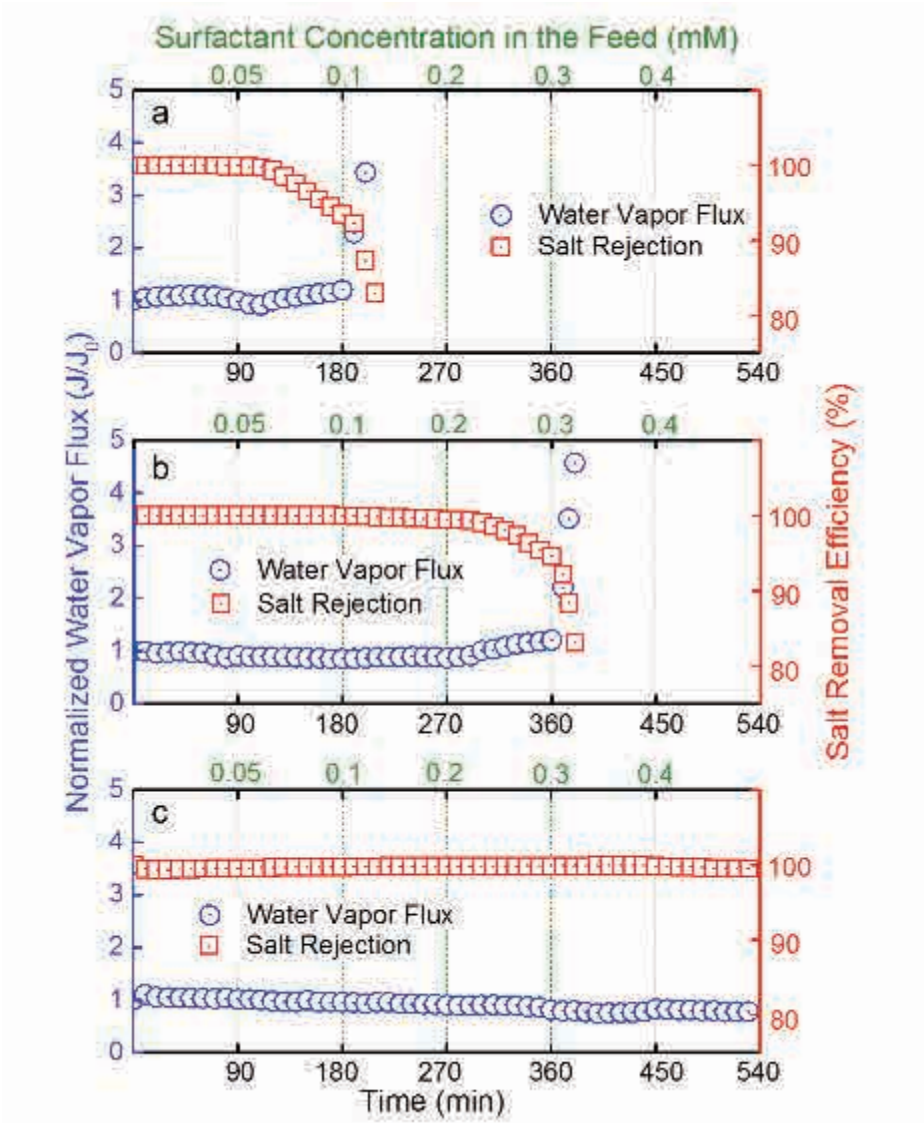

Figure E5. Membrane distillation (MD) performance of different PVDF membranes. Normalized water vapor flux (blue) and salt removal efficiency (red) of (a) pristine PVDF membrane, (b) PVDF-FAS-5 membrane, and (c) PVDF-FAS-60 membrane in direct contact membrane distillation (DCMD) desalination, based on sequential increasing doses of sodium dodecyl sulfate (SDS). The feed solution contained 1 M NaCl, supplemented with various concentrations of SDS. The feed and distillate temperatures were maintained at 60°C and 20°C, respectively. This figure serves as a replicate of the results presented in Figure 6-3.

Table E2. Comparison of water vapor permeability between omniphobic and hydrophobic membranes in MD desalination process. While the observed trade-off in prior studies could be attributed to altered membrane morphology (e.g., increased membrane thickness and decrease pore sizes), this cannot explain the trade-off observed in our monolithic membranes and indicates the importance of considering water vapor permeability in the membrane design for MD process.

Pristine Membrane		Omniphobic Membrane		Membrane Distillation Tests			Reference
Material	Water Contact Angle (°)	Fabricated Procedure	Water Contact Angle (°)	Feed Solution	Temp. (F/P [a], °C)	Initial Water Flux (F/P, L m^{-2} h^{-1})	
PVDF-HEP	136.4 ± 2.4	Grafting with fluorinated SiNPs [b]	156.9 ± 0.8	35 g/L NaCl	60/20	34.1/13.3	Huang[11]
PVDF-HEP	~130	Grafting with fluorinated SiNPs	~150	1 M NaCl	60/20	25/12.5	Lee[12]
PVDF	68.9 ± 2.3	Grafting with fluorinatedsilica aerogel via LBL [c] deposition	177.0 ± 0.4	RO brine from coal seam gas produced water	60/20	13.17/11.22	Woo[13]
PVDF	126.7± 1.4	Grafting with fluoribated hierarchical SiNPs@PS [d] spheres	176.5°± 0.1	An emulsion composed of SDS: hexadecane: NaCl = 240:2400:10000 (mg/L) in water	60/20	11/9	Zheng[14]
PVDF	~110	Grafting with fluorinated SiNPs	>150	1 M NaCl	60/20	23.5/13.6	Boo[1]
PVDF	124.2	Deposition of with fluorinated SiNPs	167.3	3.5 wt% NaCl solution	76/21	30/21	Lu-2017[15]
PVDF-HEP	132.1 ± 0.9	Electrospinning of PVDF-HEP and (F-POSS [e]) colloidal suspension solution.	154.5 ± 2.6	1 M NaCl	60/20	11/9	Lu-2018a[16]
PVDF	~117	Grafting with fluorinated SiNPs	~145	3.5 wt% NaCl solution	70/Liquid nitrogen (vacuum membrane	24.9/14.6	Lu-2018b[17]

					distillation)		
Glass fiber modified with 17-FAS [f]	~150	Grafting with fluorinated ZnO nanoparticles via chemical bath deposition	~154	1 M NaCl	60/20	12.5/11.4	Chen[18]
PVDF	119 ± 4	Grafting with fluorinated SiNPs	159 ± 2	Shale oil and gas produced water	60/20	30.2/24.8	Du[19]
PVDF	~123	Ecthing by FluoroEtch solvent, followed by silanization with FAS	~139	1M NaCl	60/20	29.2/25.3	This study
PVDF	~123	Ecthing by FluoroEtch solvent, followed by silanization with FAS	~149	1M NaCl	60/20	29.2/19.3	This study

[a] F/P: Feed solution/permeate solution; [b] SiNPs = silica nanoparticles; [c] LBL = layer-by-layer; [d] PS = polystyrene; [e] F-POSS = fluorinated-decyl polyhedraloligomeric silsesquioxane; [f] FAS = heptadecafluoro-1,1,2,2-tetrahydrodecyl trichlorosilane (or triethoxysilane).

Note E6. Estimation of breakthrough pressure

In order to determine the water breakthrough pressure P_b of individual pores within PVDF membranes, we assume that the membrane is composed of hexagonally arranged spherical features with diameter $2R$ and pore size (i.e., inter-feature spacing) $2D$ (see Figure E6). A force balance at the liquid-air interfaces gives:[20]

$$P_b \approx \frac{4\pi\gamma_{lv}(1-\cos\theta)}{R(2\sqrt{3}D^* - \pi)(\sqrt{D^*} - 1 + 2\sin\theta)} \qquad \text{(E1)}$$

Here, θ is the Young's contact angle, and the dimensionless parameter, $D^* = [(R+D)/R]^2$, is a measure of the air trapped underneath the liquid when it forms a composite interface with the textured surface. Using the particle diameters and pore sizes determined by analyzing the SEM images with ImageJ, the breakthrough pressure of each pore was estimated. When the breakthrough pressure of a specific pore is less than the transmembrane pressure (i.e., 1.2 kPa as measured by a low-pressure gauge), liquid water permeates into that pore.

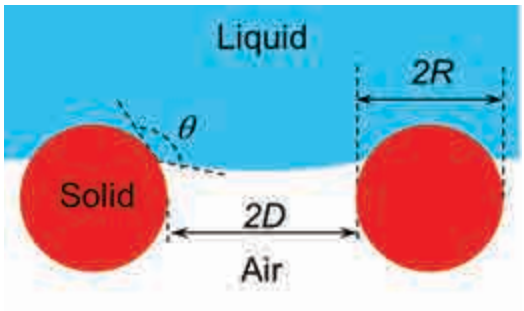

Figure E6. Schematic depicting the membrane surface texture with spherical features.

Note E7. Omniphobic membranes with a membrane pore size of 0.22 μm

In addition to the PVDF membranes with a membrane pore size of 0.45 μm described in the manuscript, we also fabricated omniphobic membranes using PVDF membranes with a membrane pore size of 0.22 μm (GVHP, Durapore) using the same method. The pristine membranes and the etched membranes after 5 min- and 1 h-silanization were designated as 0.22-PVDF, 0.22-PVDF-FAS-5 and 0.22-PVDF-FAS-60, respectively. The morphology of the processed PVDF membranes remained virtually unaltered compared to the pristine PVDF membranes, as evidenced by the SEM images (see Figure E7a-E7c). The omniphobic 0.22-PVDF-FAS-60 membrane possessed improved wetting resistance compared to pristine 0.22-PVDF membrane, as evidenced by the results of liquid repellency (see Figure E7d). Further, the results (see Figure E7e) of membrane distillation tests indicated that the 0.22-PVDF, 0.22-PVDF-FAS-5 and 0.22-PVDF-FAS-60 membranes displayed decreasing water vapor permeability with increasing wetting resistance, confirming the wetting resistance-water vapor permeability trade-off.

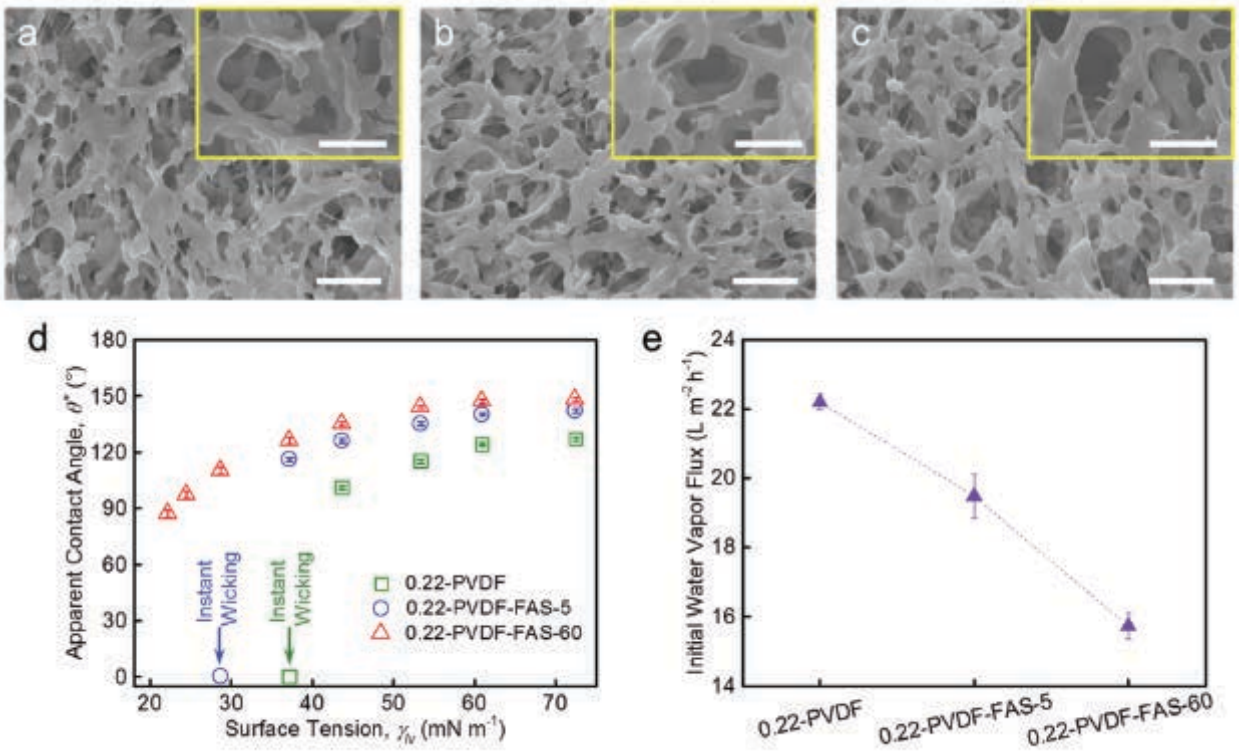

Figure E7. Monolithic omniphobic membranes with a membrane pore size of 0.22 μm. (a-c) SEM images of (a) pristine 0.22-PVDF membrane, (b) 0.22-PVDF-FAS-5 membrane, and (c) 0.22-PVDF-FAS-60 membrane. The scale bars represent 2 μm and 1 μm (inset), respectively. (d) Apparent contact angles of liquids with different surface tensions on the membranes. (e) The initial water vapor fluxes of different MD membranes. The water vapor flux decreases (e) with increasing wetting resistance (d). Error bars represent standard deviation from three independent measurements.

References

1. Boo, C.; Lee, J.; Elimelech, M., Omniphobic polyvinylidene fluoride (PVDF) membrane for desalination of shale gas produced water by membrane distillation. *Environ. Sci. Technol.* 2016, 50, (22), 12275-12282.
2. Deng, L.; Ye, H.; Li, X.; Li, P.; Zhang, J.; Wang, X.; Zhu, M.; Hsiao, B. S., Self-roughened omniphobic coatings on nanofibrous membrane for membrane distillation. *Sep. Purif. Technol.* 2018, 206, 14-25.
3. Tang, C. Y.; Kwon, Y.-N.; Leckie, J. O., Probing the nano-and micro-scales of reverse osmosis membranes—A comprehensive characterization of physiochemical properties of uncoated and coated membranes by XPS, TEM, ATR-FTIR, and streaming potential measurements. *J. Memb. Sci.* 2007, 287, (1), 146-156.
4. Bielinski, A. R.; Boban, M.; He, Y.; Kazyak, E.; Lee, D. H.; Wang, C.; Tuteja, A.; Dasgupta, N. P., Rational design of hyperbranched nanowire systems for tunable superomniphobic surfaces enabled by atomic layer deposition. *ACS Nano* 2016, 11, (1), 478-489.
5. Liu, T.; Kim, C.-J., Turning a surface superrepellent even to completely wetting liquids. *Science* 2014, 346, (6213), 1096-1100.
6. Papadopoulos, P.; Mammen, L.; Deng, X.; Vollmer, D.; Butt, H.-J., How superhydrophobicity breaks down. *Proc. Natl. Acad. Sci. U.S.A.* 2013, 110, (9), 3254-3258.
7. Wang, W.; Salazar, J.; Vahabi, H.; Joshi-Imre, A.; Voit, W. E.; Kota, A. K., Metamorphic superomniphobic surfaces. *Adv. Mater.* 2017, 29, (27), 1700295.
8. Manickam, S. S.; McCutcheon, J. R., Characterization of polymeric nonwovens using porosimetry, porometry and X-ray computed tomography. *J. Memb. Sci.* 2012, 407, 108-115.
9. Saffarini, R. B.; Mansoor, B.; Thomas, R.; Arafat, H. A., Effect of temperature-dependent microstructure evolution on pore wetting in PTFE membranes under membrane distillation conditions. *J. Memb. Sci.* 2013, 429, 282-294.
10. Islam, M. A.; Ulbricht, M., Microfiltration membrane characterization by gas-liquid displacement porometry: Matching experimental pore number distribution with liquid permeability and bulk porosity. *J. Memb. Sci.* 2019, 569, 104-116.
11. Huang, Y. X.; Wang, Z. X.; Jin, J.; Lin, S. H., Novel janus membrane for membrane distillation with simultaneous fouling and wetting resistance. *Environ. Sci. Technol*. 2017, 51, (22), 13304-13310.
12. Lee, J.; Boo, C.; Ryu, W. H.; Taylor, A. D.; Elimelech, M., Development of omniphobic desalination membranes using a charged electrospun nanofiber scaffold. *ACS Appl. Mater. Interfaces* 2016, 8, (17), 11154-11161.
13. Woo, Y. C.; Kim, Y.; Yao, M.; Tijing, L. D.; Choi, J. S.; Lee, S.; Kim, S. H.; Shon, H. K., Hierarchical composite membranes with robust omniphobic surface using layer-by-layer assembly technique. *Environ. Sci. Technol.* 2018, 52, (4), 2186-2196.
14. Zheng, R.; Chen, Y.; Wang, J.; Song, J. F.; Li, X. M.; He, T., Preparation of omniphobic PVDF membrane with hierarchical structure for treating saline oily wastewater using direct contact membrane distillation. *J. Memb. Sci.* 2018, 555, 197-205.
15. Lu, X. M.; Peng, Y. L.; Qiu, H. R.; Liu, X. R.; Ge, L., Anti-fouling membranes by manipulating surface wettability and their anti-fouling mechanism. *Desalination* 2017, 413, 127-135.

16. Lu, C.; Su, C.; Cao, H.; Ma, X.; Duan, F.; Chang, J.; Li, Y., F-POSS based omniphobic membrane for robust membrane distillation. *Mater. Lett.* 2018, 228, 85.
17. Lu, K. J.; Zuo, J.; Chang, J.; Kuan, H. N.; Chung, T. S., Omniphobic hollow-fiber membranes for vacuum membrane distillation. *Environ. Sci. Technol.* 2018, 52, (7), 4472-4480.
18. Chen, L. H.; Huang, A.; Chen, Y. R.; Chen, C. H.; Hsu, C. C.; Tsai, F. Y.; Tung, K. L., Omniphobic membranes for direct contact membrane distillation: Effective deposition of zinc oxide nanoparticles. *Desalination* 2018, 428, 255-263.
19. Du, X.; Zhang, Z.; Carlson, K.; Lee, J.; Tong, T. Z., Membrane fouling and reusability in membrane distillation of shale oil and gas produced water: Effects of membrane surface wettability. *J Membrane Sci* 2018, 567, 199-208.
20. Kota, A. K.; Li, Y.; Mabry, J. M.; Tuteja, A., Hierarchically structured superoleophobic surfaces with ultralow contact angle hysteresis. *Adv. Mater.* 2012, 24, (43), 5838-5843.